
En Pointe
Composing Novel Immunotherapy Strategies to Improve Systemic Anti-Tumor Immunity
Mandy van Gulijk

En Pointe:

Composing Novel Immunotherapy Strategies to Improve Systemic Anti-Tumor Immunity

Mandy van Gulijk

En Pointe: Composing Novel Immunotherapy Strategies to Improve Systemic Anti-Tumor Immunity

ISBN: 978-94-6483-984-5

Cover design and layout: © evelienjagtman.com
Print: Ridderprint, the Netherlands, www. Ridderprint.nl

Printing of this thesis was financially supported by: Erasmus MC, Department of Pulmonary Medicine | Leiden University Medical Center, Department of Medical Oncology | ChipSoft | IMAP Netherlands | Nutricia

IMAP
International Mergers and Acquisitions

The research in this thesis was financially supported by Stichting Asbestkanker - Rotary Rotterdam Zuid.

En Pointe:

Composing Novel Immunotherapy Strategies to Improve Systemic Anti-Tumor Immunity

En Pointe:
Het componeren van betere immuuntherapieën om
systemische anti-tumor immuniteit te versterken

Proefschrift

ter verkrijging van de graad van doctor aan de
Erasmus Universiteit Rotterdam
op gezag van de
rector magnificus

Prof.dr. A.L. Bredenoord

en volgens besluit van het college voor promoties.
De openbare verdediging zal plaatsvinden op

woensdag 12 juni 2024 om 13.00 uur

door

Mandy Larissa van Gulijk
geboren te Vlaardingen.

Erasmus University Rotterdam

Erasmus

Promotiecommissie:

Promotoren:	Prof.dr. J.G.J.V. Aerts
	Prof.dr. T. Van Hall
Overige leden:	Prof.dr. J.E.M.A. Debets
	Prof.dr. T.D. de Gruijl
	Prof.dr. K.E. de Visser
Copromotor:	Dr. F.H.W.P. Dammeijer

Table of contents

Chapter 1

General Introduction

General introduction

A diverse plethora of immune cells are involved in combatting tumor cells by orchestrating anti-tumor immunity in a delicately balanced manner. In-depth insights on the dynamic interactions between tumor cells and immune cells enabled the development and implementation of immunotherapy which created a paradigm shift in the treatment of patients with cancer. However, the majority of the patients does not respond durably and inevitably develops disease recurrence for reasons incompletely understood. This introductory chapter will highlight recent advances in the field of tumor immunology that are not restricted to the tumor site and are valuable in providing alternative therapeutic angles to improve efficacy of immunotherapy. Finally, the aim and outline of this thesis will be presented.

Seizing control: the continuous interaction between the immune system and tumor cells

Cancer has long been considered a cell-autonomous disease characterized by a multistep process of genetic alterations that results in deficits in normal regulatory pathways of cell proliferation and homeostasis. These genetic alterations in cancer cells were thought to be the main drivers of progressive transformation into malignant derivatives [1]. This reductionist view was challenged by observations in mice where the lack of critical effector molecules in T cells, such as interferon-gamma (IFNγ) or perforin, resulted in increased susceptibility to tumor development [2-6]. This supported the initial immunosurveillance theory by Burnet and Thomas, which proposed that the immune system acts as a tumor-extrinsic suppressor [7-9]. Later, it was discovered that immunological pressure not only suppresses tumor development but also functions as a dominant and selective force in sculpting clonal evolution of tumor cell variants capable of evading immunity [10,11]. Inverse relationships between the level of immune cell infiltration and tumor clonal diversity and corresponding neoantigen load in patient tumors illustrates the strong selection pressure of the immune system and signs of immunoediting [12-15]. As such, these continuous dynamic interactions between tumor cells and immune cells lead to the emergence of tumor cell clones progressively equipped with greater capability to evade immunological control. What are the mechanisms by which immunoedited tumor cell clones can evade immunological control?

Loss of control: tumor-cell mediated evasion of immunological control

Tumor cells acquire a variety of features to escape from immune attack. Anti-tumor immunity requires functional presentation of tumor antigens, preferably neoantigens, in class I and II human leukocyte antigens (HLA) for the recognition by T cell receptors and disruption to the antigen-presentation machinery in tumors could in turn facilitate immune escape. The integration of genomic, transcriptomic and epigenomic data has revealed neoantigen depletion during tumor evolution that occurs through mechanisms that span from genomic aberrations in the HLA locus (e.g. copy-number loss and loss of heterozygosity) to transcriptional repression of neoantigens [16,17]. Additionally, deficits in intracellular antigen processing, including TAP1

deficiencies, further contribute to impaired functional presentation of tumor antigens and immune evasion. Interestingly, these deficits can also give rise to a novel category of neoantigens, T cell epitopes associated with impaired peptide processing' (TEIPP) antigens, that can be presented by residual HLA class I molecules and activate cognate $CD8^+$ T cells [18-20]. Besides impaired tumor antigen presentation, rewiring of tumor cells on the (epi)genetic level, altered metabolism and disturbed intracellular signaling pathways influence the composition and functional state of the tumor microenvironment (TME) [21]. Alongside endothelial cells, fibroblasts and tumor cells, the TME is composed of a variety of immune cells. Hijacking the behavior of immune cells such as dendritic cells (DCs), tumor-associated macrophages (TAMs), neutrophils and regulatory T cells (Tregs) enables tumor cells to orchestrate a suppressive TME [22,23]. How are tumor cells modulating the behavior of immune cells in the TME and thereby facilitating tumor progression?

Suppressing immune cells that inhibit tumor growth: DC modulation in the TME

DCs are an important heterogeneous population of antigen presenting cells (APCs) that are able to infiltrate tumors and stimulate anti-tumor immunity. As such, $BATF3^+$ conventional DCs type 1 (cDC1), that excel in their cross-presentation capacity, were required for the rejection of immunogenic tumors and vaccination with tumor-associated antigen (TAA) loaded natural cDC1s reduced tumor growth [24,25]. Seminal discoveries suggested that APCs may be able to form intra-tumoral niches for infiltrating T cells, resembling the T cell zone of secondary lymphoid tissues. These niches can give progeny to a more terminally differentiated T cell population and maintain anti-tumor immunity while loss of these niches is associated with progression in patients with kidney cancer [26]. This highlights that compromised DC functionality predisposes the tumor site for impaired anti-tumor immunity. For example, the group of Gajewski found that reduced chemokine ligand 4 (CCL4) expression in tumors with active β-catenin resulted in lower cDC1 infiltration and increased tumor growth [27]. Mediators released by the tumor cells or other cells in the TME such as VEGF, TGFβ, IL-10, IL-6 and PGE2 can each inhibit DC differentiation, maturation and functionality. For example, TAM-derived IL-10 indirectly blunts $CD8^+$ T cell responses by restricting IL-12 production by intratumoral cDCs [28].

Promoting immune cells that support tumor growth: Regulatory T cell modulation in the TME

Besides the impairment of tumor-repressing immune cells, tumor cells extend their immune evasion mechanisms to the induction and/or recruitment of immunosuppressive cell types including TAMs, myeloid-derived suppressor cells (MDSCs) and Tregs. Tregs function as master regulators of the immune system and were shown to be crucial to prevent auto-immune diseases [29]. Shortly after, the involvement of Tregs in antitumor immunity was established by the observation that Treg depletion using anti-CD25 antibodies increased tumor rejection [30,31]. A range of different mechanisms are described by which Tregs can dampen the immune system either by directly impairing effector T cells or indirectly via APC modulation [32] (Fig. 1)**.** These

mechanisms are abundantly exerted in the TME as Tregs isolated from tumors express high levels of genes related to suppressive function and activation [33,34]. For example, DC modulation through transendocytosis of costimulatory molecules CD80 and CD86 by cytotoxic T-lymphocyte antigen 4 (CTLA-4) is a core mechanism of immunoregulation by Tregs at the tumor site [35,36]. Elegant experiments by the group of Mempel showed that this can blunt protective anti-tumor immunity by hampering effector T cell activation caused by destabilized contacts between DCs and effector T cells [37]. Interestingly, the modulation by Tregs also resulted in destabilization of their own contacts with DCs, thereby providing a negative feedback loop to calibrate their own function by regulating the level of costimulation they receive. This mechanism hinged on Tregs locally encountering antigens in the TME [37,38]. The dependence of local antigen stimulation aligns with findings that expanding neoantigen-specific Tregs were detected in melanoma patients and required continuous TCR signaling to exert their suppression function [39,40]. Due to the inherent suppressive functions of Tregs in the TME, a high ratio of Tregs to conventional T cells is associated with worse prognosis for a variety of cancer types [41]. Therefore, targeting Tregs is an attractive approach to enhance anti-tumor immunity. Nonetheless, effectively targeting Tregs in the clinical context remains a challenge. One extensively researched approach to target Tregs is through their depletion. However, depletion of the total Treg population using anti-CD25 antibodies (daclizumab and basiliximab) failed to deliver clinical responses [42,43]. A significant challenge in achieving effective depletion of Tregs is that potential targets, such as CD25, are shared between Tregs and effector T cells. By developing depleting anti-CD25 antibodies that preserve IL-2 signaling, the group of Quezada was able to effectively deplete Tregs without affecting the effector T cell compartment in preclinical models and are currently tested in clinical studies [44]. Additionally, there is the risk of autoimmune-related toxicities when indiscriminately depleting the entire Treg population [33]. For this reason, the potential of targeting chemotactic axes (CCR4 and CCR8) or transcription factors (BATF) that are specifically expressed on tumor-infiltrating Tregs are currently investigated as these approaches may preserve Treg functioning in other tissues [45-49]. Recently, CXCR3 has shown to be a critical chemokine receptor for the migration, accumulation and suppressive functions of Tregs at the tumor site by facilitating interactions with cDC1s, thereby offering a novel therapeutic tumor-directed Treg target [50].

Taken together, immune-edited tumor cells exert multiple local mechanisms to evade immune recognition and destruction. However, recent observations highlighted that these pertubations are not restricted to the tumor site as tumor cells alter the global immune landscape during tumor progression (Fig. 2) [51,52]. Therefore, to fully understand the immune response to tumor cells, the coordinated regulation of anti-tumor immunity spread across multiple tissues should be taken into account. What are the mechanisms by which tumor cells impact immunological control beyond the tumor site?

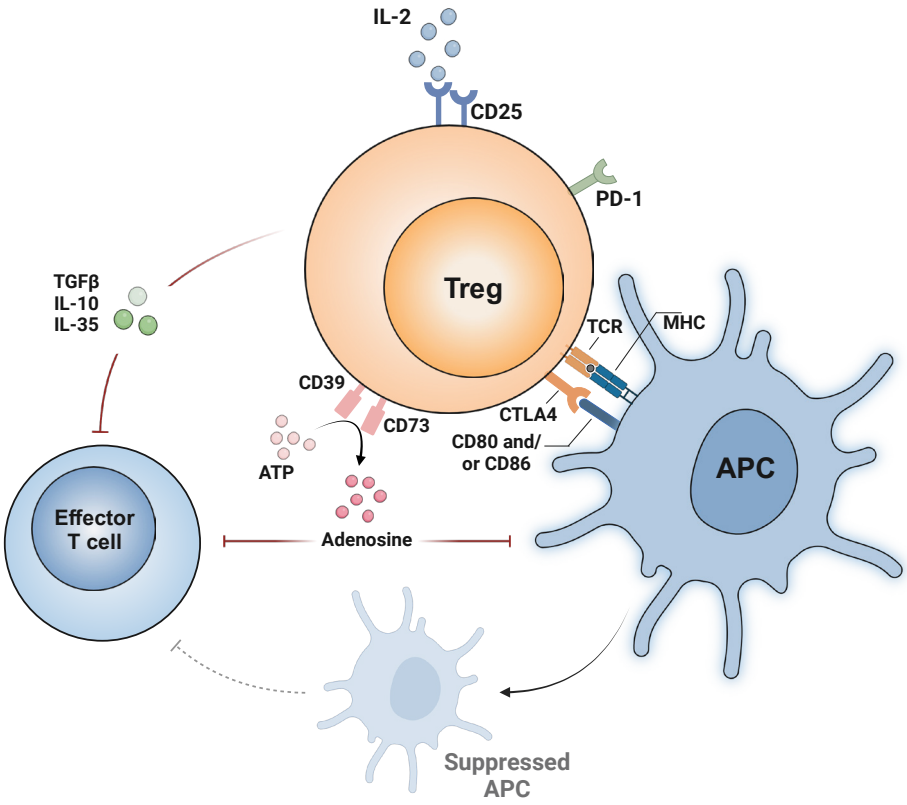

Figure 1: Variable mechanisms of Treg-mediated immunosuppression

Regulatory T cells (Tregs) express the IL-2 receptor subunit-α, also known as CD25, of the high-affinity heterotrimeric IL-2 receptor. Tregs are highly dependent on IL-2, and scavenge IL-2 from the environment by expressing CD25, thereby reducing the availability of this cytokine for other immune cells, including effector T cells. In addition, Tregs produce immunosuppressive cytokines, transforming growth factor-β (TGFβ), IL-10 and IL-35 that suppress the activity of effector T cells. Next to producing immunosuppressive cytokines, Tregs are able to convert ATP to adenosine by expressing CD39 and CD73 on their cell surface which transmits an immunosuppressive signal to both effector T cells and antigen presenting cells (APCs). By expressing cytotoxic T lymphocyte antigen (CTLA-4) on their cell surface, Tregs bind to CD80 and CD86 expressed on APCs, thereby suppressing their activity (solid arrow) and reducing their activating capacity of effector T cells (dashed arrow). CTLA-4 also directly inhibits effector T cell activation by inhibiting costimulation as CTLA-4 binds with higher affinity to CD80 and CD86 than CD28 In addition to CTLA-4, Tregs are known to express programmed death 1 (PD-1) to high levels.

A new holistic vantage point in dictating control: tumor immunology beyond the tumor microenvironment

Recent observations caused the formation of a new paradigm by highlighting the extension of tumor-imposed perturbations of the immune system to lymphoid organs including bone marrow, spleen and tumor-draining lymph node (TDLN) (Fig. 2). In bone marrow, cancer-imposed dysregulation of hematopoiesis resulted in excessive release of immature monocytes and neutrophils which

contribute to an immunosuppressive TME [53,54]. Also the spleen appeared to be a critical site of G-CSF and GM-CSF driven aberrant myelopoiesis at the cost of B- and T cells [55]. Next to dysregulated hematopoiesis, G-CSF reduced interferon regulatory factor-8 (IRF8) in cDC progenitors in the bone marrow, thereby driving reduced cDC1 development and maturation in patients with pancreatic and breast cancer [56]. These tumor-imposed effects on bone marrow can also extend to the T cell compartment as it was found that in patients and mice with intracranial tumors naïve T cells were sequestered in the bone marrow through regulation of the S1P1 axis, leading to lymphopenia [57]. Spearheaded by the groups of Wargo and Zitvogel, the impact of the gut microbiome on sculpting systemic anti-tumor immunity is beginning to unfold. Although the molecular mechanisms by which microbiomes are affecting systemic immune responses are incompletely understood, the gut microbiome is found to either promote or limit the development of multiple types of cancer. As such, gut dysbiosis by decreased diversity or composition is associated with cancer progression [58-60]. A central focus of recent research is the recognition of the TDLN as a vital orchestrator of systemic anti-tumor immunity. The tumor influences the structure and functioning of TDLNs connected to the tumor through a network of lymphatic vessels transporting fluid, soluble factors and cells. How is this affecting immune processes in the TDLN and consequently tumor control?

The central role of the TDLN in effective anti-tumor immunity

A series of sequential events must be initiated, allowed to proceed and expand iteratively for an anti-tumor immune response to effectively eliminate cancer cells. This series of carefully regulated events is summarized as the cancer immunity cycle proposed in 2013 by Chen en Mellman [61,62]. Critical steps of this cycle occur in the TDLN where tumor-derived antigens are captured and presented by DCs which, in the presence of appropriate signals, prime and activate cognate T cells that can subsequently infiltrate the TME to kill their target cells. Therefore, the immune contexture in the TDLN, especially the antigen presentation capacity, is important in dictating the nature, breadth and strength of anti-tumor immunity. CCR7-dependent migration of tumor-antigen loaded $CD103^+$ cDC1s to the TDLN and the hand-off of antigen to resident DCs were found to be requisites for driving $CD8^+$ T cell mediated anti-tumor immunity [63,64]. Subsequent studies by the same group highlighted the importance of migrating cDC2s to the TDLN in initiating anti-tumor $CD4^+$ T cell immunity [65]. Alternatively, altered phenotype and suppressed functionality of DCs in the TDLN were described to be associated with tumor progression by restricting T cell priming or induction of tolerance [66]. Suppressed priming by DCs in the TDLN is described to be linked to effects of intratumoral Tregs as well as to Tregs located in the TDLN. Intratumoral Tregs constrained cDC2 function and migration to the TDLN which resulted in restricted anti-tumor immunity due to suboptimal priming of helper $CD4^+$ T cells [65]. Recent findings also highlighted a prominent role for TDLN-located Tregs in restraining T cell priming by influencing DC functionality. More specifically, elevated IFNγ levels in the TDLN (e.g. mediastinal lymph node) driven by lung commensals increased the suppressive capacity of Tregs which resulted in suppressed costimulation and cytokines provided by cDC1 and subsequent dysfunctional $CD8^+$ T cell priming [67]. The ultimate aim of DC-T cell interactions in the TDLN is the priming and activation of tumor-reactive T cells. The TDLN appeared to be enriched for

tumor-specific T cells that displayed a progenitor exhausted phenotype (Tpex cells; Box 1) [68,69]. Deeper analysis on the architectural niche of Tpex cells in the TDLN of HNSCC patients using imaging revealed a primary localization in T cell zones [68]. Seminal discoveries using TCR sequencing highlighted the clonal relationship between Tpex cells in the TDLN and exhausted T cells in the TME suggesting a continuum of T cell differentiation from Tpex cells within the TDLN to a more exhausted state upon migration from the TDLN to the tumor [68,70,71]. Therefore, the TDLN is described to function as a reservoir by maintaining Tpex cells over time that seed the tumor to sustain anti-tumor immunity [69,72]. Indeed, elegant experiments by the group of Grogan showed that, across different types of cancer, intratumoral T cells are replenished by T cells from outside the tumor that are non-exhausted and the infiltration of TDLN-derived T cells could thereby provide an explanation for the paradoxical observation that tumor-specific T cells in the TME do not uniformly display a phenotypic exhaustion program [73]. While there is still much to be uncovered, these data are progressively revealing the pivotal role played by the TDLN in coordinating systemic anti-tumor immunity.

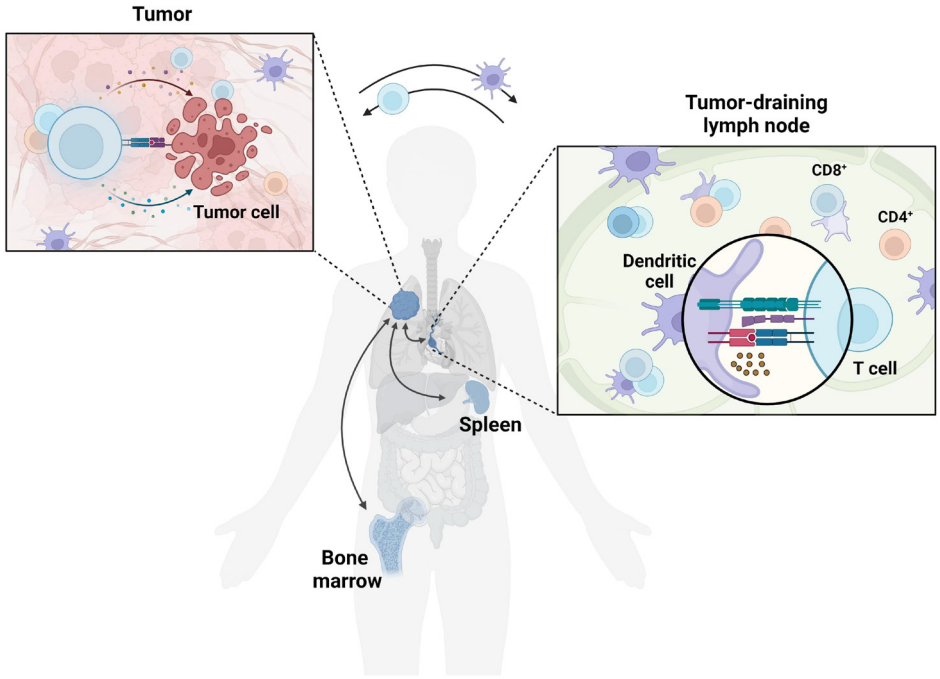

Figure 2: Systemic anti-tumor immunity is coordinated across multiple organs

For effective anti-tumor immunity, antigen-presenting cells (APCs) that migrate from the tumor microenvironment (TME) to the tumor-draining lymph node (TDLN) or are resident in the TDLN prime and activate T cells with a cognate T cell receptor. Following priming, licensed T cells migrate to the TME to kill tumor cells. The process of functional tumor cell killing by T cells is often impaired due to tumor-perturbations to the immune system in multiple tissues, including bone marrow, spleen and TDLN.

Box 1: T cell exhaustion

T cell exhaustion is described as a hypofunctional state driven mainly by chronic TCR signaling due to persistent antigen exposure in the context of chronic infections or cancer to limit immunopathology or autoreactivity [74,75]. In the tumor setting, an exhausted state is characterized by reduced cytokine production and functionality, a high expression of coinhibitory receptors, including PD-1, CTLA-4, LAG3 and CD39 and enrichment for tumor-reactive clones. Persistent stimulation of the TCR activates the transcription factor NFAT that, without the cooperation with AP-1 transcription factors, drives the expression of transcription factors related to the exhausted state [76,77]. The transcription factor TOX is predominantly described as an important regulator of exhaustion by epigenetically imprinting the dysfunctional program [78-80]. A spectrum of T cell exhaustion states exists, ranging from progenitor exhausted to terminally exhausted T cells that aligns with reduction in effector functions and recall expansion capacity. Progenitor exhausted T cells are characterized by an intermediate expression of coinhibitory receptors and expression of key transcription factor TCF-1 [81]. By self-renewal and proliferation, progenitor exhausted T cells give rise and maintain a more terminally exhausted T cell, creating a developmental hierarchy [82]. This progression of a progenitor to the terminally exhaustion state is defined by a gradual functional impairment and increase of the expression of coinhibitory receptors, loss of TCF-1 and gain of the transcription factor TOX, resulting in a epigenetically fixed exhausted state [83]. Although described as a hypofunctional state, terminally exhausted T cells retain a certain degree of effector functions as they express a broad spectrum of genes and proteins associated with effector functions [84,85]. Beyond the reduction of effector functions, the group of Delgoffe recently demonstrated that hypoxia within the TME can even drive the CD39-mediated acquisition of suppressive capacities by exhausted T cells [86].

Restoring control by immunotherapy: inducing durable anti-tumor immunity

Due to the importance of a functional immune system in combatting in tumor progression, the emergence of immunotherapy has made substantial impact on the treatment landscape for patients with cancer. Immune checkpoint blockade (ICB) has shown unparalleled success and the number of patients eligible for this type of immunotherapy continues to increase as this therapy positions itself as first or second line therapy for many types of cancer. Expression of checkpoints on T cells are evolutionarily conserved to prevent hyperactivation of the immune system and autoimmune diseases. The most-well described targets of ICB are programmed cell-death 1 (PD-1) and its ligand PD-L1 and CTLA-4. The mode of action is best understood for interference of the PD-1/PD-L1 axis in reviving existing T cell responses [87-91]. Instead of reviving T cell responses, vaccination strategies, including vaccination with DCs, primarily act to optimize the priming potential of APCs [92,93].

PD-1/PD-L1 biology and therapy

PD-1 was first discovered on T cells by the group of Nobel Prize winner Tasuka Honjo in 1991 and described to be involved in activation-induced cell death, hence the name programmed cell-death 1 [94,95]. Shortly after, PD-1 was found to be a negative regulator of the immune system as PD-1 knockout mice developed arthritis and nephritis [96]. The role of PD-1 in controlling the immune system was further emphasized when the ligands, PD-L1 and PD-L2, were discovered. Many cell types, including tumor cells, were able to bind PD-1 immunoglobulin Fc domain fusion proteins which resulted in impaired lymphocyte proliferation and cytokine production [97]. Seminal discoveries in the past 30 years has led to the central role of antibodies blocking the PD-1/PD-L1 axis in the treatment of patients with multiple types of cancer. The prevailing thought underlying this successful therapeutic approach is the revival of tumor-infiltrating T cells, more specifically by releasing the brake of PD-1$^+$ T cells, which are restrained by PD-L1 expression on tumor cells.

Given this prevailing thought, higher expression of PD-1 on T cells would reasonably positively correlate with the level of reinvigoration. Despite the highest expression of PD-1 on hypofunctional terminally exhausted T cells (Box 1), anti-PD-1/PD-L1 therapy is generally thought to be unable in functionally recovering terminally exhausted T cells in a durable manner. For example, transferred terminally exhausted T cells did not proliferate following anti-PD-1 treatment. Recent studies have shown that this unresponsiveness is regulated by robust epigenetic remodeling in exhausted T cells that is distinct from the epigenetic program in effector and memory T cells [75,83,98]. Instead, Tpex cells, expressing TCF-1 and CXCR5 and intermediate levels of PD-1, were found to be responsible for the proliferative burst following anti-PD-1/PD-L1 therapy in chronic infection and cancer [99-102]. Higher levels of TCF-1 protein in CD8$^+$ T cells associated with response to anti-PD1/PD-L1 therapy, suggesting that this subset may dictate therapeutic efficacy [101]. These data underscore that the expression of PD-1 does not strictly correlate with the capacity for T cell reinvigoration.

PD-1 expression is regulated by a multifaceted network of transcription factors induced by TCR signaling and various cytokine stimuli, such as IL-2 and type 1 interferons [95]. The cytoplasmic tail of PD-1 contains two intracellular motifs: the immunoreceptor tyrosine-based inhibitory motif (ITIM) and immunoreceptor tyrosine-based switch motif (ITSM) [103]. Mutational studies have shown that the inhibitory function of PD-1 mainly relies on ITSM which recruits Src homology region 2 domain-containing phosphatase (SHP-2) [104-106]. This recruitment results in downregulation of downstream TCR signaling pathways, with PI3K/AKT, mitogen activated protein kinase (MAPK) and mammalian target of rapamycin (mTOR) as prominent target pathways [107,108]. Although it was thought that SHP2 is the sole direct partner of PD-1, PD-1 inhibition retained efficacy in SHP2-deleted T cells, suggesting that additional PD-1 partners could be in play in downstream signaling [109]. Surprisingly, CD28 signaling appeared to be an important intracellular target of anti-PD-1/PD-L1 therapy besides direct TCR signaling in suppressing the TCR signalosome [110,111]. This discovery points to an important role for CD80 (B7-1) and CD86 (B7-2) expression on APCs in dictating anti-PD-1/PD-L1 therapy

efficacy. The role of APCs in dictating anti-PD-1/PD-L1 therapy efficacy is further supported by the observation that anti-PD-1/PD-L1 therapy remained effective in transplanted tumor models lacking PD-L1, thereby suggesting PD-L1 expressed on host cells, specifically myeloid cells, is essential in mediating anti-tumor immunity [112-114]. The role of PD-L1 on myeloid cells, mainly APCs, is further underlined as CD80 was described to be a second binding partner that is able to bind PD-L1 *in cis* which prevent ligation of PD-1 with PD-L1 *in trans*. Elegant experiments performed by the group of Hui showed that these *in cis* interactions prevent CD80 from binding to CTLA-4 *in trans* while persevering the binding of CD80 to CD28 [115]. This non-tumor cell centered view could also provide an explanation for the observation that some tumors failed to respond to anti-PD-1/PD-L1 therapy despite tumor positivity for PD-L1 [89]. These observations, together with data showing that novel T cell clones infiltrate the TME upon treatment, could indicate that anti-PD-1/PD-L1 therapy efficacy is determined by systemic immunity and not only restricted to the tumor site [116-118].

Therapeutic vaccination strategies

In addition to disruptions in the effector phase of the immune response, the initial priming phase of anti-tumor immunity is frequently impacted by perturbations induced by the tumor. These perturbations include compromised DC functionality, leading to a hindered activation of T cells by DCs. This initiated the field of therapeutic vaccination that typically boosts the immune system to eradicate tumor cells through various methods including injection of *ex-vivo* tumor-antigen loaded DCs and exogeneous administration of tumor antigens. Although there are other promising vaccination strategies developed or used in a clinical setting, the use of *ex-vivo* tumor-antigen loaded DCs and vaccination with neoantigens will be highlighted in this section to shed light on the impact of this treatment modality for cancer patients. For the use of *ex-vivo* tumor-antigen loaded DCs, DCs are directly obtained from blood or *ex-vivo* cultured from monocytes, exposed to tumor antigens and injected back into the patient. Once infiltrated in the lymph node, the DCs prime and activate vaccine-specific T cells that subsequently infiltrate the TME [119]. This therapeutic approach comes with the advantages of quality control and controlled adjuvant/antigen delivery and has shown to be able to induce clinical responses in a subset of patients [119-121]. As monocyte-derived DCs may not be the most optimal APCs to activate $CD8^+$ T cells, novel approaches using naturally occurring DC subsets, mainly cDC1s, could offer additional efficacy [122]. Although optimizing T cell priming capacities of DCs used for vaccination, immunosuppressive mechanisms could still restrain effective anti-tumor immunity in patients. Combinations with agents affecting these mechanisms have shown promising results as vaccination with DCs was only effective in an established pancreatic cancer mouse model when combined with anti-CD40 that modulates the suppressive TME [123]. A recently-described vaccination approach in resectable pancreatic cancer patients using individualized mRNA neoantigen vaccines appeared to be able to induce substantial and durable T cell responses in 50% of the patients, despite low mutation rates [124]. This approach was also described to be feasible and able to induce immunological responses in immune inflamed tumors, including melanoma, NSCLC and bladder cancer and offers a promising therapeutic vaccination approach [125,126].

Both blockade of PD-1/PD-L1 and therapeutic vaccination strategies have shown to be able to stimulate anti-tumor immunity and induce durable responses in a subset of patients. However, still the majority of the patients does not respond at all or only temporarily. What are the mechanisms that are underlying therapy resistance?

From restored control to rebound effect: immunotherapy resistance

Resistance to immunotherapy can be explained by a plethora of mechanisms. Often, mechanisms that are involved in evasion of immunological control in steady state are also involved in hampering efficacy of immunotherapy. When present prior to therapy, these mechanisms can prevent the induction of a meaningful immunological or clinical response following immunotherapy and are involved in primary resistance. Increased immunological pressure during therapy can also accelerate these mechanisms, thereby causing the acquirement of resistance and is often described as secondary resistance. Tumor-intrinsic pathways varying from lack of therapeutic target, for example PD-L1 on tumor cells, to deficits in antigen-processing and presentation machinery and loss of neoantigens through immunoediting are described to be related to therapy resistance [127-129]. For instance, by comparing pre- and post treatment tumor biopsies, 10% of patients with NSCLC were found to develop resistance to anti-PD-1 therapy through loss of neoantigen expression upon treatment [130]. Other mechanisms involve the upregulation of alternative coinhibitory molecules, including TIM3, CD39, TIGIT and LAG3, due to the increased activation state following reinvigoration by anti-PD-1/PD-L1 therapy. As such, high gene expression of CD39 and TIM3 in $CD8^+$ T cells was associated with non-responsiveness in patients with melanoma treated with anti-PD-1 [101]. Another important resistance mechanism is the preferred activation and attraction of immunosuppressive cells, including Tregs. Due to the inherent suppressive functions of Tregs, Tregs have shown to impede efficacy of anti-PD-1/PD-L1 therapy as Treg depletion using an optimized anti-CD25 antibodies synergized with anti-PD-1/PD-L1 therapy in preclinical murine models [44,131]. This synergy could be explained by data showing that oxidative-stress induced apoptotic Tregs abolished anti-PD-L1 efficacy as this subset displayed amplified suppressor capacity via the adenosine and A2a pathway. Transfer of apoptotic Tregs in the responsive MC38 model thwarted IFNγ and TNF production by $CD8^+$ T cells and translated into anti-PD-L1 resistance on tumor growth and survival [132]. On the contrary, IFNγ-mediated induction of Treg fragility, a plastic program with loss of suppressive functions, was required for anti-PD-1 therapy efficacy indicating, together with the other data, the importance of Treg functionality in dictating anti-PD-1/PD-L1 therapy efficacy [133]. Potentially the interaction of Tregs with cDC1s is important in impeding efficacy as Treg-specific knockout of CXCR3, which was found to facilitate this interaction, synergized with anti-PD-1 therapy in impairing tumor progression [50]. Despite the identification of these resistance mechanisms, efforts to translate these findings to biomarkers or novel therapeutic approaches have not shown able to substantially increase the subset of patients showing a durable response. To broaden the proportion of patients responsive to immunotherapy, a thorough understanding of known tumor-host immunological relationships and the discovery of new resistance pathways are imperative.

Aims and outline of this thesis

Cancer immunotherapy has significantly transformed cancer treatment, yet enduring success is confined to a minority of the patients for reasons incompletely understood. A deeper understanding of the prerequisites for effective immunotherapy and mechanisms that can thwart this efficacy are therefore crucial. For this deeper understanding, the systemic immune landscape beyond the tumor site should be considered as anti-tumor immunity is regulated across multiple tissues. By combining a wide range of translational preclinical mouse models and the clinical translation of the findings using patient-derived materials, the research presented in this thesis will improve this understanding and could provide novel therapeutic angles to improve immunotherapy efficacy.

Part A of this thesis focusses on the mode of action (*Chapter 2 and 3*) and resistance (*Chapter 4*) of ICB therapy. The prevailing thought is that efficacy of anti-PD-1/PD-L1 therapy is derived from the reinvigoration of T cells within the TME. However, data showed that PD-L1 expression on non-tumor cells is important in dictating response and, together with the restricted value of PD-L1 on tumor cells as biomarker and data showing infiltration with novel T cell clones following anti-PD-1/PD-L1 therapy, indicate that not only the TME is essential in dictating efficacy following anti-PD-1/PD-L1 therapy. As the TDLN has shown to have a central role in initiating anti-tumor immunity, the effects of anti-PD-1/PD-L1 therapy in the TDLN were studied in **Chapter 2**. Here, we assessed the presence of the PD-1/PD-L1 axis in the TDLN of multiple preclinical murine models and how this affected anti-tumor immunity by specifically blocking the axis at this site using a unique injection strategy. We then translated these findings to the clinical setting by assessing whether the level of PD-1/PD-L1 interactions in the TDLN of melanoma patients is associated with disease recurrence. Data presented in **Chapter 2** identified the PD-1/PD-L1 axis in the TDLN to be critical in dictating anti-PD-L1 therapy efficacy and to associate with recurrence in melanoma patients. A better understanding of the cells involved and their spatial localization in the TDLN would aid in deciphering how the TDLN is involved in recurrence in melanoma patients. To this end, in **Chapter 3**, we studied immune composition in the TDLN of stage III melanoma patients that either developed distant visceral organ metastasis or remained disease free for more than 5 years by using multiplexed gene expression analysis, digital spatial profiling and multi-color confocal imaging.

Besides identifying mechanisms related to response following anti-PD-1/PD-L1 therapy, identification of mechanisms that perturb this efficacy and are responsible for therapy resistance are vital for the design of therapeutic strategies that enhance anti-PD-1/PD-L1 efficacy. Suppression of the immune system is an inherent characteristic of Tregs and they appeared to have a dominant expression of PD-1 on their cell surface. Therefore, we aimed in **Chapter 4** to identify whether anti-PD-L1 therapy could have detrimental effects by activating Tregs, causing therapy resistance in the process. For this research question, we assessed the effect of anti-PD-L1 on Tregs (gene, protein and functional level) in therapy-responsive and –resistant tumor models and studied whether this was directly mediated via PD-1 on Tregs using bone marrow chimera experiments. We then attempted

to identify whether anti-PD-L1 mediated activation of Tregs actively promoted therapy resistance by depleting Tregs using anti-CD25 or by using diphtheria toxin in DEREG mice. The clinical relevance of these findings was evaluated using patient-derived tumor biopsies prior to and following anti-PD-1 therapy using published scRNA sequencing data[116,134] and peripheral blood of patients with lung cancer and mesothelioma.

Next to impaired T cell functionality, tumor-immune co-existence also negatively shapes the myeloid compartment of the immune system. Decreased functionality of DCs in tumor-burdened hosts sparked the interest of vaccination with exogenously cultured and loaded DCs. In **part B** of this thesis, we focused on combinatorial approaches with DC-based immunotherapy to improve efficacy which are reviewed in **Chapter 5**. As the PD-1/PD-L1 axis may be highly involved on DCs used for vaccination and induced T cells, sequential and concurrent combination of anti-PD-L1 with DC vaccination was evaluated in **Chapter 6.** To this end, efficacy of adjuvant anti-PD-1 therapy in DC-treated mesothelioma patients was assessed. Effects on systemic immunity in the setting of combination therapy were monitored by analyzing immune responses in blood and tumor and survival effects in a mesothelioma murine model.

T cell exhaustion could pose an additional hurdle in achieving effective cancer vaccine efficacy. Besides continuous TCR signaling, aberrant IL-2 signaling is implicated in driving T cell exhaustion[135,136]. In the effector phase, IL-2 is critical for the expansion and survival of T cells. However, excess IL-2 signaling in the priming phase impact the differentiation trajectory, with more effector T cells and exhaustion phenotype at the expense of memory formation. Therefore, excess IL-2 signaling could hamper vaccine efficacy. In **Chapter 7**, we combined vaccination strategies with targeting a key downstream target of IL2 signaling, JAK3, using a specific inhibitor (PF-06651600) that inhibits STAT5 signaling.

Finally, **Chapter 8** provides a general discussion of the data described in this thesis and how this can contribute to future research.

References

1. Hanahan, D. & Weinberg, R.A. The hallmarks of cancer. *Cell* **100**, 57-70 (2000).
2. Dighe, A.S., Richards, E., Old, L.J. & Schreiber, R.D. Enhanced in vivo growth and resistance to rejection of tumor cells expressing dominant negative IFN gamma receptors. *Immunity* **1**, 447-456 (1994).
3. Kaplan, D.H.*, et al.* Demonstration of an interferon gamma-dependent tumor surveillance system in immunocompetent mice. *Proc Natl Acad Sci U S A* **95**, 7556-7561 (1998).
4. Street, S.E., Cretney, E. & Smyth, M.J. Perforin and interferon-gamma activities independently control tumor initiation, growth, and metastasis. *Blood* **97**, 192-197 (2001).
5. van den Broek, M.E.*, et al.* Decreased tumor surveillance in perforin-deficient mice. *J Exp Med* **184**, 1781-1790 (1996).
6. Smyth, M.J.*, et al.* Perforin-mediated cytotoxicity is critical for surveillance of spontaneous lymphoma. *J Exp Med* **192**, 755-760 (2000).
7. Burnet, M. Cancer; a biological approach. I. The processes of control. *Br Med J* **1**, 779-786 (1957).
8. Dunn, G.P., Old, L.J. & Schreiber, R.D. The immunobiology of cancer immunosurveillance and immunoediting. *Immunity* **21**, 137-148 (2004).
9. Dunn, G.P., Bruce, A.T., Ikeda, H., Old, L.J. & Schreiber, R.D. Cancer immunoediting: from immunosurveillance to tumor escape. *Nat Immunol* **3**, 991-998 (2002).
10. Koebel, C.M.*, et al.* Adaptive immunity maintains occult cancer in an equilibrium state. *Nature* **450**, 903-907 (2007).
11. Baldwin, L.A.*, et al.* DNA barcoding reveals ongoing immunoediting of clonal cancer populations during metastatic progression and immunotherapy response. *Nat Commun* **13**, 6539 (2022).
12. Angelova, M.*, et al.* Evolution of Metastases in Space and Time under Immune Selection. *Cell* **175**, 751-765 e716 (2018).
13. Onkar, S.S.*, et al.* The Great Immune Escape: Understanding the Divergent Immune Response in Breast Cancer Subtypes. *Cancer Discov* **13**, 23-40 (2023).
14. Zhang, A.W.*, et al.* Interfaces of Malignant and Immunologic Clonal Dynamics in Ovarian Cancer. *Cell* **173**, 1755-1769 e1722 (2018).
15. Milo, I.*, et al.* The immune system profoundly restricts intratumor genetic heterogeneity. *Sci Immunol* **3**(2018).
16. Rosenthal, R.*, et al.* Neoantigen-directed immune escape in lung cancer evolution. *Nature* **567**, 479-485 (2019).
17. McGranahan, N.*, et al.* Allele-Specific HLA Loss and Immune Escape in Lung Cancer Evolution. *Cell* **171**, 1259-1271 e1211 (2017).
18. van Hall, T.*, et al.* Selective cytotoxic T-lymphocyte targeting of tumor immune escape variants. *Nat Med* **12**, 417-424 (2006).
19. Seidel, U.J., Oliveira, C.C., Lampen, M.H. & Hall, T. A novel category of antigens enabling CTL immunity to tumor escape variants: Cinderella antigens. *Cancer Immunol Immunother* **61**, 119-125 (2012).
20. van der Burg, S.H., Arens, R., Ossendorp, F., van Hall, T. & Melief, C.J. Vaccines for established cancer: overcoming the challenges posed by immune evasion. *Nat Rev Cancer* **16**, 219-233 (2016).
21. van Weverwijk, A. & de Visser, K.E. Mechanisms driving the immunoregulatory function of cancer cells. *Nat Rev Cancer* **23**, 193-215 (2023).
22. de Visser, K.E. & Joyce, J.A. The evolving tumor microenvironment: From cancer initiation to metastatic outgrowth. *Cancer Cell* **41**, 374-403 (2023).
23. Anderson, N.M. & Simon, M.C. The tumor microenvironment. *Curr Biol* **30**, R921-R925 (2020).
24. Hildner, K.*, et al.* Batf3 deficiency reveals a critical role for CD8alpha+ dendritic cells in cytotoxic T cell immunity. *Science* **322**, 1097-1100 (2008).
25. Wculek, S.K.*, et al.* Effective cancer immunotherapy by natural mouse conventional type-1 dendritic cells bearing dead tumor antigen. *J Immunother Cancer* **7**, 100 (2019).
26. Jansen, C.S.*, et al.* An intra-tumoral niche maintains and differentiates stem-like CD8 T cells. *Nature* **576**, 465-470 (2019).
27. Spranger, S., Bao, R. & Gajewski, T.F. Melanoma-intrinsic beta-catenin signalling prevents anti-tumour immunity. *Nature* **523**, 231-235 (2015).
28. Ruffell, B.*, et al.* Macrophage IL-10 blocks CD8+ T cell-dependent responses to chemotherapy by suppressing IL-12 expression in intratumoral dendritic cells. *Cancer Cell* **26**, 623-637 (2014).
29. Sakaguchi, S., Sakaguchi, N., Asano, M., Itoh, M. & Toda, M. Immunologic self-tolerance maintained by activated T cells expressing IL-2 receptor alpha-chains (CD25). Breakdown of a single mechanism of self-tolerance causes various autoimmune diseases. *J Immunol* **155**, 1151-1164 (1995).
30. Onizuka, S.*, et al.* Tumor rejection by in vivo administration of anti-CD25 (interleukin-2 receptor alpha) monoclonal antibody. *Cancer Res* **59**, 3128-3133 (1999).

31. Shimizu, J., Yamazaki, S. & Sakaguchi, S. Induction of tumor immunity by removing CD25+CD4+ T cells: a common basis between tumor immunity and autoimmunity. *J Immunol* **163**, 5211-5218 (1999).
32. Togashi, Y., Shitara, K. & Nishikawa, H. Regulatory T cells in cancer immunosuppression - implications for anticancer therapy. *Nat Rev Clin Oncol* **16**, 356-371 (2019).
33. Plitas, G.*, et al.* Regulatory T Cells Exhibit Distinct Features in Human Breast Cancer. *Immunity* **45**, 1122-1134 (2016).
34. De Simone, M.*, et al.* Transcriptional Landscape of Human Tissue Lymphocytes Unveils Uniqueness of Tumor-Infiltrating T Regulatory Cells. *Immunity* **45**, 1135-1147 (2016).
35. Onishi, Y., Fehervari, Z., Yamaguchi, T. & Sakaguchi, S. Foxp3+ natural regulatory T cells preferentially form aggregates on dendritic cells in vitro and actively inhibit their maturation. *Proc Natl Acad Sci U S A* **105**, 10113-10118 (2008).
36. Qureshi, O.S.*, et al.* Trans-endocytosis of CD80 and CD86: a molecular basis for the cell-extrinsic function of CTLA-4. *Science* **332**, 600-603 (2011).
37. Marangoni, F.*, et al.* Expansion of tumor-associated Treg cells upon disruption of a CTLA-4-dependent feedback loop. *Cell* **184**, 3998-4015 e3919 (2021).
38. Bauer, C.A.*, et al.* Dynamic Treg interactions with intratumoral APCs promote local CTL dysfunction. *J Clin Invest* **124**, 2425-2440 (2014).
39. Ahmadzadeh, M.*, et al.* Tumor-infiltrating human CD4(+) regulatory T cells display a distinct TCR repertoire and exhibit tumor and neoantigen reactivity. *Sci Immunol* **4**(2019).
40. Oliveira, G.*, et al.* Landscape of helper and regulatory antitumour CD4(+) T cells in melanoma. *Nature* **605**, 532-538 (2022).
41. Shang, B., Liu, Y., Jiang, S.J. & Liu, Y. Prognostic value of tumor-infiltrating FoxP3+ regulatory T cells in cancers: a systematic review and meta-analysis. *Sci Rep* **5**, 15179 (2015).
42. Jacobs, J.F.*, et al.* Dendritic cell vaccination in combination with anti-CD25 monoclonal antibody treatment: a phase I/II study in metastatic melanoma patients. *Clin Cancer Res* **16**, 5067-5078 (2010).
43. Rech, A.J.*, et al.* CD25 blockade depletes and selectively reprograms regulatory T cells in concert with immunotherapy in cancer patients. *Sci Transl Med* **4**, 134ra162 (2012).
44. Solomon, I.*, et al.* CD25-T(reg)-depleting antibodies preserving IL-2 signaling on effector T cells enhance effector activation and antitumor immunity. *Nat Cancer* **1**, 1153-1166 (2020).
45. Sugiyama, D.*, et al.* Anti-CCR4 mAb selectively depletes effector-type FoxP3+CD4+ regulatory T cells, evoking antitumor immune responses in humans. *Proc Natl Acad Sci U S A* **110**, 17945-17950 (2013).
46. Spranger, S.*, et al.* Up-regulation of PD-L1, IDO, and T(regs) in the melanoma tumor microenvironment is driven by CD8(+) T cells. *Sci Transl Med* **5**, 200ra116 (2013).
47. Kidani, Y.*, et al.* CCR8-targeted specific depletion of clonally expanded Treg cells in tumor tissues evokes potent tumor immunity with long-lasting memory. *Proc Natl Acad Sci U S A* **119**(2022).
48. Wang, T.*, et al.* CCR8 blockade primes anti-tumor immunity through intratumoral regulatory T cells destabilization in muscle-invasive bladder cancer. *Cancer Immunol Immunother* **69**, 1855-1867 (2020).
49. Itahashi, K.*, et al.* BATF epigenetically and transcriptionally controls the activation program of regulatory T cells in human tumors. *Sci Immunol* **7**, eabk0957 (2022).
50. Moreno Ayala, M.A.*, et al.* CXCR3 expression in regulatory T cells drives interactions with type I dendritic cells in tumors to restrict CD8(+) T cell antitumor immunity. *Immunity* **56**, 1613-1630 e1615 (2023).
51. Allen, B.M.*, et al.* Systemic dysfunction and plasticity of the immune macroenvironment in cancer models. *Nat Med* **26**, 1125-1134 (2020).
52. Spitzer, M.H.*, et al.* Systemic Immunity Is Required for Effective Cancer Immunotherapy. *Cell* **168**, 487-502 e415 (2017).
53. Wu, W.C.*, et al.* Circulating hematopoietic stem and progenitor cells are myeloid-biased in cancer patients. *Proc Natl Acad Sci U S A* **111**, 4221-4226 (2014).
54. Casbon, A.J.*, et al.* Invasive breast cancer reprograms early myeloid differentiation in the bone marrow to generate immunosuppressive neutrophils. *Proc Natl Acad Sci U S A* **112**, E566-575 (2015).
55. Steenbrugge, J., De Jaeghere, E.A., Meyer, E., Denys, H. & De Wever, O. Splenic Hematopoietic and Stromal Cells in Cancer Progression. *Cancer Res* **81**, 27-34 (2021).
56. Meyer, M.A.*, et al.* Breast and pancreatic cancer interrupt IRF8-dependent dendritic cell development to overcome immune surveillance. *Nat Commun* **9**, 1250 (2018).
57. Chongsathidkiet, P.*, et al.* Sequestration of T cells in bone marrow in the setting of glioblastoma and other intracranial tumors. *Nat Med* **24**, 1459-1468 (2018).
58. Park, E.M.*, et al.* Targeting the gut and tumor microbiota in cancer. *Nat Med* **28**, 690-703 (2022).
59. Helmink, B.A., Khan, M.A.W., Hermann, A., Gopalakrishnan, V. & Wargo, J.A. The microbiome, cancer, and cancer therapy. *Nat Med* **25**, 377-388 (2019).
60. Hanahan, D. Hallmarks of Cancer: New Dimensions. *Cancer Discov* **12**, 31-46 (2022).

61. Chen, D.S. & Mellman, I. Oncology meets immunology: the cancer-immunity cycle. *Immunity* **39**, 1-10 (2013).
62. Mellman, I., Chen, D.S., Powles, T. & Turley, S.J. The cancer-immunity cycle: Indication, genotype, and immunotype. *Immunity* **56**, 2188-2205 (2023).
63. Roberts, E.W.*, et al.* Critical Role for CD103(+)/CD141(+) Dendritic Cells Bearing CCR7 for Tumor Antigen Trafficking and Priming of T Cell Immunity in Melanoma. *Cancer Cell* **30**, 324-336 (2016).
64. Salmon, H.*, et al.* Expansion and Activation of CD103(+) Dendritic Cell Progenitors at the Tumor Site Enhances Tumor Responses to Therapeutic PD-L1 and BRAF Inhibition. *Immunity* **44**, 924-938 (2016).
65. Binnewies, M.*, et al.* Unleashing Type-2 Dendritic Cells to Drive Protective Antitumor CD4(+) T Cell Immunity. *Cell* **177**, 556-571 e516 (2019).
66. van den Hout, M.*, et al.* Melanoma Sequentially Suppresses Different DC Subsets in the Sentinel Lymph Node, Affecting Disease Spread and Recurrence. *Cancer Immunol Res* **5**, 969-977 (2017).
67. Zagorulya, M.*, et al.* Tissue-specific abundance of interferon-gamma drives regulatory T cells to restrain DC1-mediated priming of cytotoxic T cells against lung cancer. *Immunity* **56**, 386-405 e310 (2023).
68. Rahim, M.K.*, et al.* Dynamic CD8(+) T cell responses to cancer immunotherapy in human regional lymph nodes are disrupted in metastatic lymph nodes. *Cell* **186**, 1127-1143 e1118 (2023).
69. Connolly, K.A.*, et al.* A reservoir of stem-like CD8(+) T cells in the tumor-draining lymph node preserves the ongoing antitumor immune response. *Sci Immunol* **6**, eabg7836 (2021).
70. Prokhnevska, N.*, et al.* CD8(+) T cell activation in cancer comprises an initial activation phase in lymph nodes followed by effector differentiation within the tumor. *Immunity* **56**, 107-124 e105 (2023).
71. Pai, J.A.*, et al.* Lineage tracing reveals clonal progenitors and long-term persistence of tumor-specific T cells during immune checkpoint blockade. *Cancer Cell* **41**, 776-790 e777 (2023).
72. Gearty, S.V.*, et al.* An autoimmune stem-like CD8 T cell population drives type 1 diabetes. *Nature* **602**, 156-161 (2022).
73. Wu, T.D.*, et al.* Peripheral T cell expansion predicts tumour infiltration and clinical response. *Nature* **579**, 274-278 (2020).
74. Schietinger, A.*, et al.* Tumor-Specific T Cell Dysfunction Is a Dynamic Antigen-Driven Differentiation Program Initiated Early during Tumorigenesis. *Immunity* **45**, 389-401 (2016).
75. Blank, C.U.*, et al.* Defining 'T cell exhaustion'. *Nat Rev Immunol* **19**, 665-674 (2019).
76. Chow, A., Perica, K., Klebanoff, C.A. & Wolchok, J.D. Clinical implications of T cell exhaustion for cancer immunotherapy. *Nat Rev Clin Oncol* **19**, 775-790 (2022).
77. Martinez, G.J.*, et al.* The transcription factor NFAT promotes exhaustion of activated CD8(+) T cells. *Immunity* **42**, 265-278 (2015).
78. Khan, O.*, et al.* TOX transcriptionally and epigenetically programs CD8(+) T cell exhaustion. *Nature* **571**, 211-218 (2019).
79. Alfei, F.*, et al.* TOX reinforces the phenotype and longevity of exhausted T cells in chronic viral infection. *Nature* **571**, 265-269 (2019).
80. Mann, T.H. & Kaech, S.M. Tick-TOX, it's time for T cell exhaustion. *Nat Immunol* **20**, 1092-1094 (2019).
81. Chen, Z.*, et al.* TCF-1-Centered Transcriptional Network Drives an Effector versus Exhausted CD8 T Cell-Fate Decision. *Immunity* **51**, 840-855 e845 (2019).
82. Beltra, J.C.*, et al.* Developmental Relationships of Four Exhausted CD8(+) T Cell Subsets Reveals Underlying Transcriptional and Epigenetic Landscape Control Mechanisms. *Immunity* **52**, 825-841 e828 (2020).
83. Franco, F., Jaccard, A., Romero, P., Yu, Y.R. & Ho, P.C. Metabolic and epigenetic regulation of T-cell exhaustion. *Nat Metab* **2**, 1001-1012 (2020).
84. Tirosh, I.*, et al.* Dissecting the multicellular ecosystem of metastatic melanoma by single-cell RNA-seq. *Science* **352**, 189-196 (2016).
85. Bengsch, B.*, et al.* Epigenomic-Guided Mass Cytometry Profiling Reveals Disease-Specific Features of Exhausted CD8 T Cells. *Immunity* **48**, 1029-1045 e1025 (2018).
86. Vignali, P.D.A.*, et al.* Hypoxia drives CD39-dependent suppressor function in exhausted T cells to limit antitumor immunity. *Nat Immunol* **24**, 267-279 (2023).
87. Pardoll, D.M. Immunology beats cancer: a blueprint for successful translation. *Nat Immunol* **13**, 1129-1132 (2012).
88. Pardoll, D.M. The blockade of immune checkpoints in cancer immunotherapy. *Nat Rev Cancer* **12**, 252-264 (2012).
89. Ribas, A. & Wolchok, J.D. Cancer immunotherapy using checkpoint blockade. *Science* **359**, 1350-1355 (2018).
90. Wei, S.C., Duffy, C.R. & Allison, J.P. Fundamental Mechanisms of Immune Checkpoint Blockade Therapy. *Cancer Discov* **8**, 1069-1086 (2018).
91. Topalian, S.L., Drake, C.G. & Pardoll, D.M. Immune checkpoint blockade: a common denominator approach to cancer therapy. *Cancer Cell* **27**, 450-461 (2015).
92. Sellars, M.C., Wu, C.J. & Fritsch, E.F. Cancer vaccines: Building a bridge over troubled waters. *Cell* **185**, 2770-2788 (2022).

93. Saxena, M., van der Burg, S.H., Melief, C.J.M. & Bhardwaj, N. Therapeutic cancer vaccines. *Nat Rev Cancer* **21**, 360-378 (2021).
94. Ishida, Y., Agata, Y., Shibahara, K. & Honjo, T. Induced expression of PD-1, a novel member of the immunoglobulin gene superfamily, upon programmed cell death. *EMBO J* **11**, 3887-3895 (1992).
95. Chamoto, K., Yaguchi, T., Tajima, M. & Honjo, T. Insights from a 30-year journey: function, regulation and therapeutic modulation of PD1. *Nat Rev Immunol* **23**, 682-695 (2023).
96. Nishimura, H., Nose, M., Hiai, H., Minato, N. & Honjo, T. Development of lupus-like autoimmune diseases by disruption of the PD-1 gene encoding an ITIM motif-carrying immunoreceptor. *Immunity* **11**, 141-151 (1999).
97. Freeman, G.J*., et al.* Engagement of the PD-1 immunoinhibitory receptor by a novel B7 family member leads to negative regulation of lymphocyte activation. *J Exp Med* **192**, 1027-1034 (2000).
98. Pauken, K.E*., et al.* Epigenetic stability of exhausted T cells limits durability of reinvigoration by PD-1 blockade. *Science* **354**, 1160-1165 (2016).
99. Siddiqui, I*., et al.* Intratumoral Tcf1(+)PD-1(+)CD8(+) T Cells with Stem-like Properties Promote Tumor Control in Response to Vaccination and Checkpoint Blockade Immunotherapy. *Immunity* **50**, 195-211 e110 (2019).
100. Miller, B.C*., et al.* Subsets of exhausted CD8(+) T cells differentially mediate tumor control and respond to checkpoint blockade. *Nat Immunol* **20**, 326-336 (2019).
101. Sade-Feldman, M*., et al.* Defining T Cell States Associated with Response to Checkpoint Immunotherapy in Melanoma. *Cell* **175**, 998-1013 e1020 (2018).
102. Im, S.J*., et al.* Defining CD8+ T cells that provide the proliferative burst after PD-1 therapy. *Nature* **537**, 417-421 (2016).
103. Shinohara, T., Taniwaki, M., Ishida, Y., Kawaichi, M. & Honjo, T. Structure and chromosomal localization of the human PD-1 gene (PDCD1). *Genomics* **23**, 704-706 (1994).
104. Okazaki, T., Maeda, A., Nishimura, H., Kurosaki, T. & Honjo, T. PD-1 immunoreceptor inhibits B cell receptor-mediated signaling by recruiting src homology 2-domain-containing tyrosine phosphatase 2 to phosphotyrosine. *Proc Natl Acad Sci U S A* **98**, 13866-13871 (2001).
105. Chemnitz, J.M., Parry, R.V., Nichols, K.E., June, C.H. & Riley, J.L. SHP-1 and SHP-2 associate with immunoreceptor tyrosine-based switch motif of programmed death 1 upon primary human T cell stimulation, but only receptor ligation prevents T cell activation. *J Immunol* **173**, 945-954 (2004).
106. Yokosuka, T*., et al.* Programmed cell death 1 forms negative costimulatory microclusters that directly inhibit T cell receptor signaling by recruiting phosphatase SHP2. *J Exp Med* **209**, 1201-1217 (2012).
107. Patsoukis, N., Wang, Q., Strauss, L. & Boussiotis, V.A. Revisiting the PD-1 pathway. *Sci Adv* **6**(2020).
108. Sharpe, A.H. & Pauken, K.E. The diverse functions of the PD1 inhibitory pathway. *Nat Rev Immunol* **18**, 153-167 (2018).
109. Rota, G*., et al.* Shp-2 Is Dispensable for Establishing T Cell Exhaustion and for PD-1 Signaling In Vivo. *Cell Rep* **23**, 39-49 (2018).
110. Hui, E*., et al.* T cell costimulatory receptor CD28 is a primary target for PD-1-mediated inhibition. *Science* **355**, 1428-1433 (2017).
111. Kamphorst, A.O*., et al.* Rescue of exhausted CD8 T cells by PD-1-targeted therapies is CD28-dependent. *Science* **355**, 1423-1427 (2017).
112. Lau, J*., et al.* Tumour and host cell PD-L1 is required to mediate suppression of anti-tumour immunity in mice. *Nat Commun* **8**, 14572 (2017).
113. Kleinovink, J.W*., et al.* PD-L1 expression on malignant cells is no prerequisite for checkpoint therapy. *Oncoimmunology* **6**, e1294299 (2017).
114. Tang, H*., et al.* PD-L1 on host cells is essential for PD-L1 blockade-mediated tumor regression. *J Clin Invest* **128**, 580-588 (2018).
115. Zhao, Y*., et al.* PD-L1:CD80 Cis-Heterodimer Triggers the Co-stimulatory Receptor CD28 While Repressing the Inhibitory PD-1 and CTLA-4 Pathways. *Immunity* **51**, 1059-1073 e1059 (2019).
116. Yost, K.E*., et al.* Clonal replacement of tumor-specific T cells following PD-1 blockade. *Nat Med* **25**, 1251-1259 (2019).
117. Nagasaki, J*., et al.* PD-1 blockade therapy promotes infiltration of tumor-attacking exhausted T cell clonotypes. *Cell Rep* **38**, 110331 (2022).
118. Valpione, S*., et al.* Immune-awakening revealed by peripheral T cell dynamics after one cycle of immunotherapy. *Nat Cancer* **1**, 210-221 (2020).
119. Wculek, S.K*., et al.* Dendritic cells in cancer immunology and immunotherapy. *Nat Rev Immunol* **20**, 7-24 (2020).
120. Hegmans, J.P*., et al.* Consolidative dendritic cell-based immunotherapy elicits cytotoxicity against malignant mesothelioma. *Am J Respir Crit Care Med* **181**, 1383-1390 (2010).
121. Aerts, J*., et al.* Autologous Dendritic Cells Pulsed with Allogeneic Tumor Cell Lysate in Mesothelioma: From Mouse to Human. *Clin Cancer Res* **24**, 766-776 (2018).

122. Huber, A., Dammeijer, F., Aerts, J. & Vroman, H. Current State of Dendritic Cell-Based Immunotherapy: Opportunities for in vitro Antigen Loading of Different DC Subsets? *Front Immunol* **9**, 2804 (2018).
123. Lau, S.P*., et al.* Dendritic cell vaccination and CD40-agonist combination therapy licenses T cell-dependent antitumor immunity in a pancreatic carcinoma murine model. *J Immunother Cancer* **8**(2020).
124. Rojas, L.A*., et al.* Personalized RNA neoantigen vaccines stimulate T cells in pancreatic cancer. *Nature* **618**, 144-150 (2023).
125. Ott, P.A*., et al.* A Phase Ib Trial of Personalized Neoantigen Therapy Plus Anti-PD-1 in Patients with Advanced Melanoma, Non-small Cell Lung Cancer, or Bladder Cancer. *Cell* **183**, 347-362 e324 (2020).
126. Hu, Z*., et al.* Personal neoantigen vaccines induce persistent memory T cell responses and epitope spreading in patients with melanoma. *Nat Med* **27**, 515-525 (2021).
127. Vesely, M.D., Zhang, T. & Chen, L. Resistance Mechanisms to Anti-PD Cancer Immunotherapy. *Annu Rev Immunol* **40**, 45-74 (2022).
128. Dammeijer, F., Lau, S.P., van Eijck, C.H.J., van der Burg, S.H. & Aerts, J. Rationally combining immunotherapies to improve efficacy of immune checkpoint blockade in solid tumors. *Cytokine Growth Factor Rev* **36**, 5-15 (2017).
129. Sharma, P., Hu-Lieskovan, S., Wargo, J.A. & Ribas, A. Primary, Adaptive, and Acquired Resistance to Cancer Immunotherapy. *Cell* **168**, 707-723 (2017).
130. Anagnostou, V*., et al.* Evolution of Neoantigen Landscape during Immune Checkpoint Blockade in Non-Small Cell Lung Cancer. *Cancer Discov* **7**, 264-276 (2017).
131. Arce Vargas, F*., et al.* Fc-Optimized Anti-CD25 Depletes Tumor-Infiltrating Regulatory T Cells and Synergizes with PD-1 Blockade to Eradicate Established Tumors. *Immunity* **46**, 577-586 (2017).
132. Maj, T*., et al.* Oxidative stress controls regulatory T cell apoptosis and suppressor activity and PD-L1-blockade resistance in tumor. *Nat Immunol* **18**, 1332-1341 (2017).
133. Overacre-Delgoffe, A.E*., et al.* Interferon-gamma Drives T(reg) Fragility to Promote Anti-tumor Immunity. *Cell* **169**, 1130-1141 e1111 (2017).
134. Liu, B*., et al.* Temporal single-cell tracing reveals clonal revival and expansion of precursor exhausted T cells during anti-PD-1 therapy in lung cancer. *Nat Cancer* **3**, 108-121 (2022).
135. Liu, Y*., et al.* IL-2 regulates tumor-reactive CD8(+) T cell exhaustion by activating the aryl hydrocarbon receptor. *Nat Immunol* **22**, 358-369 (2021).
136. Beltra, J.C*., et al.* IL2Rbeta-dependent signals drive terminal exhaustion and suppress memory development during chronic viral infection. *Proc Natl Acad Sci U S A* **113**, E5444-5453 (2016).

Part 1

Novel perspectives on the mode of action and resistance of immune checkpoint blockade

Chapter 2

The PD-1/PD-L1-checkpoint restrains T cell immunity in tumor-draining lymph nodes

Mandy van Gulijk, Floris Dammeijer, Evalyn E Mulder, Melanie Lukkes, Larissa Klaase, Thierry van den Bosch, Menno van Nimwegen, Sai Ping Lau, Kitty Latupeirissa, Sjoerd Schetters, Yvette van Kooyk, Louis Boon, Antien Moyaart, Yvonne M. Mueller, Peter D Katsikis, Alexendar M. Eggermont, Heleen Vroman, Ralph Stadhouders, Rudi Hendriks, Jan von der Thüsen, Dirk J. Grünhagen, Cornelis Verhoef, Thorbald van Hall, Joachim Aerts

Cancer Cell 2020 Nov 9;38(5):685-700.e8

Abstract

PD-1/PD-L1-checkpoint blockade therapy is generally thought to relieve tumor-cell mediated suppression in the tumor microenvironment but PD-L1 is also expressed on non-tumor macrophages and conventional dendritic cells (cDCs). Here we show in mouse tumor models that tumor-draining lymph nodes (TDLNs) are enriched for tumor-specific PD-1$^+$ T cells which closely associate with PD-L1$^+$ cDCs. TDLN-targeted PD-L1-blockade induces enhanced anti-tumor T cell immunity by seeding the tumor site with progenitor-exhausted T cells, resulting in improved tumor control. Moreover, we show that abundant PD-1/PD-L1-interactions in TDLNs of nonmetastastic melanoma patients, but not those in corresponding tumors, associate with early distant disease recurrence. These findings point at a critical role for PD-L1 expression in TDLNs in governing systemic anti-tumor immunity, identifying high-risk patient groups amendable to adjuvant PD-1/PD-L1-blockade therapy.

Introduction

Drugs targeting the PD-1/PD-L1 pathway have revolutionized the treatment of multiple cancer types including non-small cell lung cancer, renal cancer and melanoma with a subset of patients experiencing durable responses. However, still a majority of patients and cancer types do not, or only temporarily respond to these immune checkpoint blocking (ICB) drugs [1,2]. PD-1/PD-L1 blocking antibodies are believed to act primarily in the tumor microenvironment (TME), by re-invigorating exhausted T cells and thereby reviving pre-existing anti-tumor immunity [2]. Based on this hypothesis, several theories have been proposed to explain the lack of ICB-efficacy in patients, such as a lack of PD-L1 expression or T cell infiltration in the TME and upregulation of other co-inhibitory receptors or suppressive molecules following ICB therapy [3,4]**.** However, the predictive value of these proposed biomarkers remains poor in the majority of tumors, while the relevance of PD-L1-expression at other sites remains unknown. Furthermore, results from recent trials evaluating combination therapy with anti-PD-(L)1 and other co-inhibitory pathways in the TME have been disappointing [5-8]. Therefore, a more comprehensive interrogation of the molecular and spatial mechanisms of anti-PD-1/PD-L1 therapy is needed to further boost immunotherapy efficacy.

Several recent insights exploring the biology of the PD-1 receptor and its corresponding ligand PD-L1 offer clues into what drives ICB efficacy. Besides tumor cells, myeloid cells expressing PD-L1 have been revealed to be essential for ICB efficacy as anti-PD-L1 antibodies remained effective in transplanted tumor cells lacking PD-L1 in a variety of models [9-12]. Furthermore, these seminal discoveries offer an explanation for the rather unexpected finding that PD-1 primarily acts by inhibiting signaling downstream of the CD28 costimulatory receptor following B7-ligation, proposedly by myeloid cells [13,14]. Where this interaction and therapeutic disruption in case of anti-PD-1/PD-L1 antibodies takes place, however, is still unknown as current genetic and pharmacologic interventions (e.g. with the S1PR-blocking agent FTY720) limit proper spatiotemporal analysis of ICB-induced anti-tumor immune responses [9,11,15]. Additional insights into these dynamics may improve ICB-response prediction and future immunotherapy development.

Recent investigations analyzing T cell receptor (TCR) clonotypes in mouse and patient tumors before and after anti-PD-1 therapy suggest the appearance of novel, previously non-existing clonotypes in ICB-treated tumors, and a limited expansion capacity of tumor-resident T cells following treatment [16,17]. In contrast to terminally differentiated tumor-resident T cells, T cell factor 1 (TCF-1)-expressing progenitor-exhausted T cells have recently been described to generate effector T cell progeny, however their exact origins remain unknown [18]. These findings, together with an abundance of B7-expressing antigen-presenting cells being exposed to draining tumor-antigens prompted us to investigate the role of tumor-draining lymph nodes (TDLNs) in efficacy of anti-PD-L1-therapy in multiple pre-clinical tumor mouse models. We find that TDLNs harbor significant proportions of tumor-specific PD-1^{+} T cells co-localizing with PD-L1 expressing myeloid cells including conventional

dendritic cells (cDCs). Selective targeting of PD-L1 only in the TDLN, reveals that TDLN-localized T cells are capable of mounting effective anti-tumor immune responses thereby demonstrating that TDLN-resident T cells are able to generate ICB-mediated immunity. Finally, we show the role of this PD-1/PD-L1 interaction in the TDLN of stage II melanoma patients, independent of known prognostic parameters. TDLNs in patients with early disease recurrence are enriched for PD-1/PD-L1 interactions which seem to primarily occur between T cells and $CD11c^+$ DCs. In patients without disease recurrence there are fewer PD-1/PD-L1 interactions in the TDLN. These results offer unexplored insights in the role of TDLNs in generating effective anti-tumor immunity and challenge the current dogma that PD-1/PD-L1-blockade occurs primarily at the tumor site.

Material and methods

Mouse models

Female 8- to 12-week-old CBA/J mice and C57BL/6 mice were purchased from Janvier and Envigo, respectively, and housed under specific pathogen-free conditions in individually ventilated cages at the animal care facility of the Erasmus MC, Rotterdam. All mouse experiments were controlled by the animal welfare committee (IvD) of the Erasmus MC and approved by the national central committee of animal experiments (CCD) under the permit number AVD101002017867, in accordance with the Dutch Acton Animal Experimentation and EU Directive 2010/63/EU.

Mouse tumor cell lines

The AC29 mesothelioma cell line was derived from tumors induced by crocidolite asbestos into CBA/J mice and was kindly provided by Prof. Bruce W.S. Robinson (Queen Elizabeth II Medical Centre, Nedlands, Australia). The OVA-transfected AE17 cell line was kindly provided by Prof. Delia J. Nelson (Curtin University, Perth, Australia). All mesothelioma cell lines were cultured in RPMI1640 medium containing 25 mmol/L HEPES, Glutamax, 50mg/mL gentamicin (all obtained from Gibco) and 5% fetal bovine serum (FBS) (Capricorn Scientific) in a humidified atmosphere and at 5% CO2, in air. For culturing AE17-OVA cells, the culture medium was supplemented with 50 mg/mL geneticin (Gibco). The MC38, B16F10, KPC3 and lentivirally transduced KPC3-OVA tumor cell lines were cultured in IMDM medium (Gibco) containing L-Glutamine, 25 mmol/L HEPES, 50mg/mL gentamicin and 8% FBS. Authentication of the cell lines was performed by short tandem microsatellite repeat analysis or by antigen-specific T cell recognition. For culture, either culture flasks or CellSTACKs (Corning Life Sciences) were used to reach the appropriate tumor cell frequencies for injection.

Melanoma patient cohort

For this study, cutaneous melanoma patients who underwent a sentinel lymph node biopsy (SLNB) at the Erasmus Medical Center (MC) Cancer Institute between 2005 and 2016 and had a *negative* SLN (i.e. no metastasis to the TDLN) were identified. From this cohort, two extreme populations

of patients were identified: 1) patients with a negative SLN with early (< 48 months) distant recurrence (with or without prior locoregional/regional lymph node recurrence); 2) patients with a negative SLN without recurrence (> 96 months). In an attempt to avoid confounding influences of prior malignant disease on TDLNs, patients who developed (prior) metastatic disease within the regional lymph nodes (similar to the SLN basin) within 9 months were excluded.

Histopathological information of the primary melanoma and SLN were retrieved from the pathology reports. Patient characteristics and follow-up data were obtained from the medical records. This study was approved by the Erasmus MC Ethics Committee (ref. no. MEC-2017-375). Human tissues and patient data were used according to "The Code for Proper Secondary Use of Human Tissue" and "The Code of Conduct for the Use of Data in Health Research" as stated by the Federation of Dutch Medical Scientific Societies.

According to aforementioned criteria, 40 patients were eligible. A pathologist from the Erasmus MC Cancer Institute a) assessed the presence of sufficient formalin-fixed paraffin-embedded (FFPE) SLN specimen, b) revised a hematoxylin and eosin (H&E) slide for each SLN confirming the absence of (micro)metastasis according to previously published protocols [19], c) selected one (of the) SLN(s) per patient. Eventually, sufficient and representative SLN material could be retrieved from 15 patients in group 1. Consequently, 15 cases from group 2 were randomly identified as well.

The median patient age was 50 years (interquartile range [IQR] 41 – 59), with a male predominance of 67% (20 males). Median duration to distant metastasis was 21.0 months (9.0 – 36.0). Further clinicopathological features and follow-up of all patients, and per subgroup, are summarized in table S1.

***In vivo* experiments in mouse tumor models**

For tumor inoculation, mice were i.p. injected with AC29 (10^7), AE17-OVA (10^6) or MC38 (2.5^5) tumor cells in 300 µL PBS. KPC3 (1.0^5), KPC3-OVA (1.0^5) or B16F10 (1.0^5) tumor cells were injected s.c. in 200 µL PBS in the flanks of mice that were briefly anesthetized using isoflurane. In case of non-TDLN and TDLN characterization, mice with established i.p. tumors (AC29, AE17-OVA and MC38) were killed when profoundly ill according to the body condition score, which was around day 20. Mice with established s.c. tumors (B16F10, KPC3 and KPC3-OVA) were euthanized when tumor size reached 1000-2000 mm^3 (measured by 0.52 x length x width x height). For B16F10 and KPC3 tumor models, this tumor size was reached around day 20 whereas this size was reached at ~ day 45 for the KPC3-OVA model. Mice were randomly assigned to experimental groups.

Anti-PD-L1 treatment. Dependent on treatment arm, mice with established peritoneal mesothelioma (AC29 or AE17-OVA) or peritoneal carcinomatosis (colon-carcinoma derived; MC38) were treated with either 200 µg isotype (clone 2A3, BioXCell), 2.5 µg anti-PD-L1 antibody

(clone MIH5, provided by L. Boon Bioceros) or 200 µg anti-PD-L1 antibody in 50 µL PBS when injected intravenously or, in case of intrapleural injection, in 200 µL PBS via injection in the pleural cavity of mice that were under short-term anesthesia.

FTY720 administration. To block lymphocyte trafficking, AC29 tumor-bearing mice received either vehicle or FTY720 (Sigma-Aldrich) from day 9 onwards via drinking water (2.5 µg/mL) and via daily oral gavage (2 µg/g body weight). Retention of lymphocytes in lymphoid organs was assessed on day 14 in peripheral blood by flow cytometry.

CEL treatment. In LN-macrophage depletion experiments, mice bearing AC29 mesothelioma tumors received 10 µL CEL (Clodrosome) dissolved in 190 µL PBS (5%) or 200 µL PBS i.pl., serving as a negative control.

Adoptive-cell transfer of OT-I and OT-II cells. For adoptive cell transfer of OT-I and OT-II cells, OT-I and OT-II CD45.1 (Ly5.1) were generated as reported previously (Hope, Front Immunol, 2019). LNs and spleens were harvested from 9-11 week-old female OT-I and OT-II CD45.1 transgenic mice after which OT-I and OT-II cells were isolated by negative selection, using EasySep magnetic nanoparticles (StemCell Technologies), according to manufacturer's protocol. Subsequently, CD45.1 OT-I and OT-II cells were labeled with Far Red Proliferation Dye (Thermo Fisher) according to the manufacturer's instructions, and injected i.v. (2.5^5-3.0^5 cells/mouse) into recipient mice.

Blood was collected at defined time points by tail vein incision to evaluate immune responses in peripheral blood. Mice were examined every 1-2 days for evidence of illness caused by overt tumor growth and euthanized at predefined endpoints or when mice were profoundly ill in case of survival analysis.

Preparation of single cell suspensions

Single-cell suspensions were generated from isolated interim blood, non-TDLN, TDLN and tumor tissue of mice from each group as previously reported [20]. Briefly, blood was collected in EDTA tubes (Microvette CB300, Sarstedt) after which the volume was determined. Subsequently, collected blood was lysed by erythrocyte lysis using osmotic lysis buffer (8.3% NH4Cl, 1% KHCO3, and 0.04% Na2EDTA in Milli-Q). Single-cell suspensions of non-TDLNs, TDLNs and spleens were generated by mechanically dispersing the lymph nodes through a 100-µM nylon mesh cell strainer (BD Biosciences) followed by osmotic lysis of erythrocytes in case of spleens. Tumors were collected, weighed in a microbalance and dissociated using a validated tumor dissociation system (Miltenyi Biotec) according to protocol. After dissociation, cell suspensions were filtered through a 100-µM nylon mesh cell strainer.

Flow cytometry

In order to measure cytokine production in lymphoid cells by flow cytometry, cells were restimulated for 4 hours at 37 °C using PMA and ionomycin (Sigma-Aldrich) supplemented with GolgiPlug (BD Biosciences). For cell surface staining, single cells were stained with antibodies together with anti-mouse 2.4G2 (anti-CD16/CD32) antibody (Provided by L. Boon, Bioceros; 1:300) for 30 minutes at 4°C. After this incubation period, cells were washed with FACS buffer (0.05% NaN3, 2% BSA in PBS), followed by a PBS wash and stained for viability using fixable LIVE/DEAD aqua cell stain (Thermo Fisher, 1:200) at 4°C for 15 minutes. After two washing steps with FACS buffer, cells were either directly measured or, in case of intracellular staining, fixated and permeabilized with Foxp3 / Transcription Factor Staining Buffer Set (Thermo Fisher) to stain nuclear factors. Intranuclear antibodies were incubated for 60 minutes at 4°C. A fixed number of counting beads (Polysciences Inc.) was added to the samples derived from blood prior to acquisition of the data to determine the absolute amount of cells.

In order to detect $OVA_{(257-264)}$ specific $CD8^+$ T cells in the AE17-OVA and KPC3-OVA models, PE-labeled tetramers of H-$2K^b$ major histocompatibility complex class I loaded with $OVA_{(257-264)}$ peptide were obtained [21]. Tetramer-binding to $CD4^+$ T cells was used to determine the level of background signal and to set cutoff limits. To assess the binding of *in vivo* administered anti-PD-L1, single cell suspensions of processed tissues were washed with FACS buffer and incubated with 5% normal donkey serum for 30 minutes on 4°C. After washing with FACS buffer, cells were counterstained using a donkey anti-rat IgG2A antibody labeled with either a Cy5-fluorochrome or a Alexa Fluor 488 fluorochrome (Jackson Immunoresearch) for 30 minutes on 4°C. Subsequently, cells were incubated for 10 minutes at 4°C with 5% rat serum in FACS buffer after washing with FACS buffer. Data were acquired using a LSR II flow cytometer equipped with three lasers and FACSDiva software (v.8.0.2) after compensation with UltraComp Compensation beads (Thermo Fisher). Acquired data were analyzed by using a licensed version of Flowjo (v.10.4.2). Immune cell subsets were characterized using the following set of markers following single cell, alive and $CD45^+$ cell selection: $CD8^+$ T cells ($CD3^+/CD4^-/CD8^+$), $CD4^+$ T-helper cells ($CD3^+/CD8^-/CD4^+/FoxP3^-$), Tregs ($CD3^+/CD8^-/CD4^+/FoxP3^+/CD25^{high}$). In the myeloid-cell panels, a lineage mix (CD3/CD19/CD335) was included. Subsets were characterized as: subcapsular sinus macrophages ($Lineage^-/Ly6C^{low}/Ly6G^-/CD169^+/F480^-$), medullary sinus macrophages ($Lineage^-/CD11b^+/Ly6C^{low}/Ly6G^-/CD169^+/F480^+$), granulocytes ($Lineage^-/CD11b^+/Ly6G^+$), conventional type 1 dendritic cells (cDC1: $lineage^-/CD11c^+/MHC\text{-}II^+/CD11b^-$), cDC2 ($lineage^-/CD11c^+/MHC\text{-}II^+/CD11b^+$). In the experiments performed in figure S3, CD172a and XCR1 were additionally included to characterize cDC2 and cDC1, respectively.

Multicolor confocal microscopy

TDLNs were embed in Tissue-TEK II optimum cutting temperature medium (Sakura), snap-frozen, and stored at -80°C. Tissue sections were cut at 16µm on a cryostat (Cryostar NX70, Thermo Fisher Scientific) and rehydrated in in 0.1 M Tris buffer for 30 minutes and blocked with blocking buffer

(0.1 M Tris buffer, 0.02% Triton X-100, 1% normal mouse serum, 1%BSA and 5% normal donkey serum) for 1 hour. After washing with 0,1 M Tris buffer, sections were stained with a donkey anti-rat antibody that would bind to the therapeutic antibody in blocking buffer for 6hours at 4°C followed by an incubation with 5% normal rat serum in blocking buffer for 10 minutes. Subsequently, sections were stained with directly labeled primary antibodies in Tris blocking buffer for 16 hours at 4°C and subsequently stained with streptavidin for 2 hours. After extensive washing with Tris buffer, nuclei were counterstained with JOJO-1 Iodide (Thermo Fisher) and tissue sections were mounted in Fluoromount-G (Thermo Fischer). Acquisition of whole cross-sections was performed on a Leica TCS SP8 confocal microscope with tunable white-light laser, 405 nm violet laser, and Leica PMT and HyD hybrid detectors. Acquisition was performed in 3 individual sequential acquisition steps, optimized tunable excitation and emission settings were defined experimentally using single stains, timed gating with the pulsed white light laser in combination with the HyD detector was applied with AF488, AF555, AF555, AF594 and AF647 dyes. Following acquisition, the tiled images were merged and compensated using the LAS X Merge and Channel Dye Separation module (using single stains under identical acquisition settings), respectively, after which the images were further analyzed using Imaris 9.2 (Bitplane). Following the histocytometry work flow as previously described, cellular identities were created to investigate co-localization. The channel for $CD8^+$ and $CD4^+$ cells was obtained by first creating a mask channel by selecting for $CD8^+$ $CD11c^-$ and $CD4^+$ $CD11c^-$ voxels, respectively. Next, a CD8 “T cell” and CD4 “T cell” expression channel was created by combining the $CD8^+$ or $CD4^+$ voxels on the $CD8^+$ $CD11c^-$ mask and $CD4^+$ $CD11c^-$ mask, respectively, to exclude $CD8^+$ $CD11c^+$ DCs and $CD4^+$ $CD11c^+$ DCs from this channel. In addition, channels for $CD169^+$ macrophages and $CD11c^+$ DCs that were bound by anti-PD-L1 were created by selecting $CD169^+$ anti-PD-$L1^+$ voxels or $CD11c^+$ anti-PD-$L1^+$ voxels, respectively. These channels, together with the $CD8^+$ $CD11c^-$ channel, were used to create surfaces with Imaris Surface Module (Bitplane) for figure representation. For publication and clarity purposes, we applied a gamma correction of 0.7 to the images, except for the surfaces.

TIL re-stimulation culture

Frozen single-cell suspensions generated from end-stage AE17-OVA tumors were thawed and stained with the CellTrace Far Red Cell Proliferation dye according to manufacturer's protocol. After labeling with the proliferation dye, cells were counted in trypane blue with a hemocytometer using the Bürker-Türk method. Subsequently, cells were resuspended in $2.0x10^6$ cells/mL culture medium consisting of IMDM containing L-Glutamine, Glutamax, 25 mmol/L HEPES, 50 mg/mL gentamicin, 50 mmol/L mercaptoethanol (Sigma-Aldrich), 10% FBS, 4 ng/mL IL-2, 4 ng/mL IL-7 4 ng/ml, 4 ng/mL IL-15 that was supplemented either with either 10 µg/mL isotype, 1 µg/mL $OVA_{(257-264)}$ peptide (provided by Anaspec) and 10 µg/mL isotype or with 1 µg/mL $OVA_{(257-264)}$ peptide and 10 µg/mL anti-PD-L1. Cells were incubated for three days in a humidified atmosphere and at 5% CO_2, in air, after which the cells were harvested and stained for extracellular and intracellular markers.

PLA and multiplex staining (cmIHC)

PLA and cmIHC was performed with an automated, validated and accredited staining system (Ventana Benchmark Discovery ULTRA, Ventana Medical Systems, Tucsen, AZ, USA). PLA was performed on 43 (34 TDLNs and 9 matched tumor samples) samples, in brief following deparaffinization and heat-induced antigen retrieval with CC1 (#950-500, Ventana Medical Systems) at 95°C for 64 minutes the tissue samples were co-incubated with anti-PD-L1 SP263 (#790-4905, Ventana Medical Systems) and anti-PD-1 NT105 (#760-4895, Cell Marque) at 37°C for 1 hour. Next, AP proximity detection (#253-5080 and #253-6037, Ventana Medical Systems) was performed for 16 minutes followed by pH buffer (#253-5083, Ventana Medical Systems) and proximity activator (#253-5082, Ventana Medical Systems) at 47°C for 12 minutes. Conjugating enzyme NP-HRP (#760-6038, Ventana Medical Systems) was added for 12 minutes followed by a DISC, amplified using TSA-HQ (#760-4519, Ventana Medical Systems) for 12 minutes and detected by using anti-HQ-HRP (#760-4820, Ventana Medical Systems) for 12 minutes. Visualization was performed using DAB (#760-159, Ventana Medical Systems) followed by hematoxylin II counter stain for 12 minutes and then a blue coloring reagent for 8 minutes according to the manufactures instructions (Ventana Medical Systems, Tucsen, AZ, USA).

PLA with cmIHC was performed on 6 additional slides, followed after PLA staining (see above) a CC2 (#950-123, Ventana Medical Systems) 100°C for 8 minutes stripping step was performed. CD68 KP1 (#790-2931, (#253-5083, Ventana Medical Systems) was incubated at 37°C for 32 minutes followed by secondary antibody, mouse omnimap HRP (#760-4310, Ventana Medical Systems) at 37°C for 24 minutes and visualized with purple (#760-229, Ventana Medical Systems) for 32 minutes. CC2 100°C for 8 minutes stripping step was performed and anti-CD8 (#790-4460, Ventana Medical Systems) was incubated at 37°C for 32 minutes followed by secondary antibody, rabbit omnimap HRP (#760-4311, Ventana Medical Systems) at 37°C for 24 minutes and visualized with Teal (#760-247, Ventana Medical Systems) for 32 minutes. CC2 100°C for 8 minutes stripping step was performed and anti-CD11c 5D11 (#111M-17, Cell Marque) was incubated at 37°C for 32 minutes followed by secondary antibody mouse-NP (#760-4816, Ventana Medical Systems) at 37°C for 32 minutes, enzyme conjugation was needed with NP-AP (#760-4827, Ventana Medical Systems) enzyme 37°C for 32 minutes visualized with Disc Yellow (#760-239, Ventana Medical Systems) for 44 minutes. Hematoxylin II counter stain for 8 minutes and then a blue coloring reagent for 4 minutes according to the manufactures instructions (Ventana Medical Systems).

Quantification of PLA and multiplex stainings

Scanned slides were viewed using NDP-viewing software (Hamamatsu) at 40× magnification and regions of interest were randomly selected from cortical regions, excluding germinal centers and captured and imported into ImageJ software (NIH). For enumeration of contacts, the number of contacts were manually counted per 40x high-power field (hpf) and the average of a total of 8 hpfs was included into analysis. A similar approach was taken to identify cells of origin in the multiplex

staining assay where PD-1/PD-L1-positivity was assessed on $CD8^+/CD8^-$ and $CD11c^+/CD68^+$/ $CD11c^+CD68^+/CD11c^-CD68^-$ -expressing cells, respectively. As a more objective and representative measure of total contacts, acquired 40x images were automatically quantified using a developed macro which includes 2 basic steps; the first step assessing total cell-surface area per hpf with the final step determining the percentage of PLA-positivity following color-dissection and thresholding (s*upplementary methods S1*). The percentage of PLA-assay positivity was then taken as a percentage of total cell-surface area and the average of 15 hpfs was included for analysis.

Statistical analysis

Data are expressed as means with the standard error of the mean (SEM). Comparisons between groups with independent samples were performed using the Mann-Whitney *U* test or independent t test whereas the Wilcoxon-signed rank test or paired t test were used to compare paired samples (see figure legends). In case of correlations, the Pearson correlation was used to test statistical significance. Survival data were plotted as Kaplan-Meier survival curves, using the log-rank test to determine statistical significance. P-value of 0.05 and below was considered significant (*), $p < 0.01$(**) and $p < 0.001$ (***) as highly significant. Data were analyzed using GraphPad Prism software (Graphpad, V5.01 and V8.0).

Results

TDLNs are enriched for $PD\text{-}1^+$ tumor-specific T cells

To gain insight into the activity of the PD-1/PD-L1-axis in LNs, we analyzed the frequencies and phenotype of tumor antigen-specific $CD8^+$ T cells in LNs of ovalbumin (OVA)-expressing AE17 mesothelioma tumors. AE17-OVA tumor cells were injected intraperitoneally and at late stage disease mediastinal LNs that drain tumors in the peritoneal cavity (TDLNs) and inguinal control LNs (non-TDLNs) were analyzed. We found higher frequencies of $OVA_{257\text{-}264}$-specific $CD8^+$ T cells in the TDLN, compared with a near absence of these cells in a non-TDLN (Fig. 1A, S1A). Tumor-specific $CD8^+$ T cells in the TDLN were highly proliferative, expressed PD-1 with higher frequencies and to higher levels than those in non-TDLNs (Fig. 1B). In the TDLN, the proportions of PD-1-expressing $CD8^+$ T cells strongly correlated with the frequency of tumor-specific $CD8^+$ T cells and could therefore serve as a marker for tumor-specificity (Fig. 1C, S1A). Therefore, we enumerated $PD\text{-}1^+$ $CD4^+$ and $CD8^+$ T cells in several solid tumor models and consistently found higher frequencies of $PD\text{-}1^+$ T cells in TDLNs compared with non-TDLNs, irrespective of cancer type, mouse genetic background, tumor localization or T cell subset, except for the KPC3 pancreatic cancer model (Fig. 1D). This difference in PD-1 expression did not appear to result from tumor metastasis to the TDLN, as the frequency of $CD45^-$ cells was equally low in both TDLNs and non-TDLNs (Fig. S1B). The poorly immunogenic KPC3 pancreatic cancer cell line did not induce $PD\text{-}1^+$ T cells in the TDLN, suggesting that PD-1 expression is related to immunogenicity of the tumor. In line with this hypothesis, introduction of

the immunogenic OVA-antigen in KPC3 recapitulated the results of the other tumor models (Fig. 1D). In addition to high PD-1 display, tumor antigen-specific CD8$^+$ T cells in TDLNs expressed other co-inhibitory receptors like TIM-3 and TIGIT, resembling T cells from the tumor site (Fig. 1E). In contrast to PD-1 expression, other parameters of lymphocyte activation such as proliferation were not consistently increased across different models (Fig. S1C), but absolute T cell numbers were enhanced (Fig. S1D).

To more comprehensively characterize both CD4$^+$ and CD8$^+$ PD-1$^+$ tumor-specific T cells in TDLNs and their dynamics, we infused naïve CD45.1$^+$ OT-I and OT-II cells in AE17-OVA-bearing CD45.2$^+$ mice and assessed their frequency and phenotype across tissues over time (Fig. 2A). As expected, CD45.1$^+$ cells initially accumulated in secondary lymphoid organs including the TDLN, followed by egress and migration in blood to finally infiltrate tumor tissue 6 days post-injection (Fig. 2B). Upon homing to TDLNs, CD45.1$^+$ T cells upregulated PD-1 and proliferated, suggesting PD-1 to be associated with activation rather than T cell exhaustion (Fig. 2C). Globally, PD-1$^+$ T cells further preferentially accumulated in TDLNs over time, where a subgroup of cells expressed effector molecules including IL-2, IFNγ and granzyme-B (Fig. 2D). In addition to increased expression of effector molecules, PD-1$^+$ CD4$^+$ and CD8$^+$ T cells expressed more CD28, CD44, CD69 and SLAMF6 (Ly108) compared with their PD-1$^-$ counterparts (Fig. S2) [22]. These results show initial activation of early-effector T cells in TDLNs, but not in non-TDLN, prior to PD-1 expression and migration to the tumor.

TDLNs contain abundant PD-L1^{high}- expressing myeloid cells including migratory cDC2s

Next, we set out to quantify and characterize the ligands of PD-1 on LN myeloid cells. LNs harbor a complex architecture of myeloid cells including CD11b$^+$ dendritic cells (DCs) and macrophages lining the subcapsular (CD169$^+$ SSM) and medullary sinuses (F4/80$^+$ MSM), type 1 and 2 conventional DCs (cDC1 and cDC2) and granulocytes interspersed between T cells in the paracortex [23-25]. TDLN-residing myeloid cells including SSMs and cDCs but not granulocytes expressed high levels of PD-L1, approaching levels found on their intratumoral counterparts (Fig. 3A). Interestingly, TDLN myeloid cells lacked or displayed low surface expression of PD-L2, whereas PD-L2 was strongly present on all investigated cells in the TME. PD-L1 expression and myeloid cell numbers were consistently higher in TDLNs compared with non-TDLNs in the investigated solid tumor models, paralleling PD-1 positivity on T cells (Fig. 3B-C). To evaluate which myeloid cells particularly expressed PD-L1 and therefore could be involved in suppressing PD-1-expressing T cells, we quantified PD-L1 on the aforementioned cell types and found especially high levels on cDC2s and both types of macrophages (SSM and MSM) in all tested tumor models (Fig. 3D). These findings were corroborated by multicolor confocal microscopy of TDLN tissue, where F4/80$^+$ MSMs in the medulla and CD11c$^+$ DCs in the LN cortex expressed the highest levels of PD-L1, whereas expression levels were negligible in granulocytes (Fig. 3E).

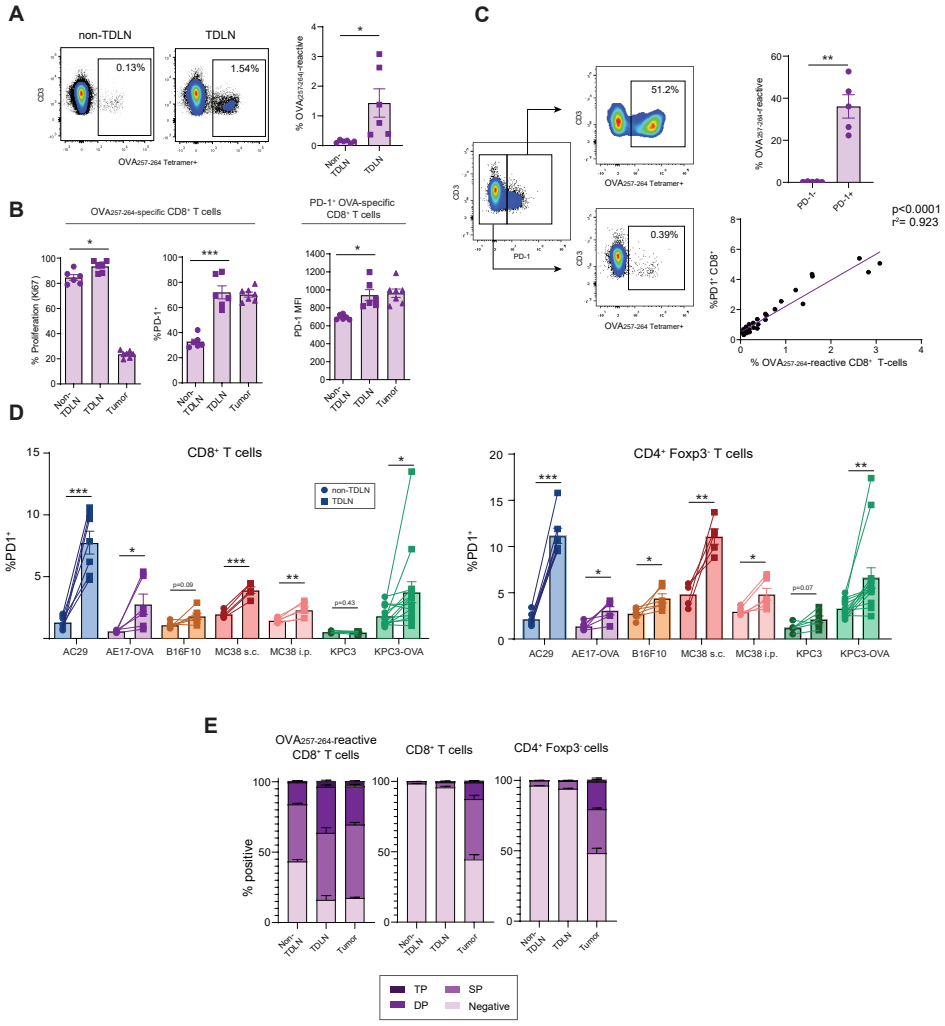

Figure 1: Tumor-draining lymph node harbor PD-1⁺ tumor-specific T cells

(A) Dot plots and quantification of CD8⁺ T cells in non-TDLNs and TDLNs showing percentages of OVA(257-264)-tetramer⁺ T cells. (B) Proliferation (Ki67) and PD-1-positivity were determined on ovalbumin (OVA) (257-264)-tetramer⁺ CD8⁺ T cells in non-TDLNs, TDLNs and tumor. Furthermore, PD-1-expression (MFI) was assessed on (PD-1⁺) OVA(257-264)-tetramer⁺ CD8⁺ T cells. (C) Tetramer-positivity of PD1⁺ and PD1⁻ CD8⁺ T cells in the TDLN. In addition, proportions of PD-1⁺ CD8⁺ T cells were plotted against proportions of OVA(257-264)-tetramer⁺ CD8⁺ T cells in the TDLN and a Pearson correlation coefficient was calculated (r^2). (D) Comparison of frequencies of PD-1⁺ CD8⁺ (left panel) and CD4⁺ Foxp3- T-helper (Th) cells (right panel) between TDLNs (circles) and non-TDLNs (squares) in different solid tumor models (different colors) transfected with/without OVA, or injected orthotopically (i.p.) or subcutaneously (s.c.) in CBA/J (AC29) or C57BL/6 mice (n = 6 to 7 mice per group, n = 14 in case of KPC3-OVA). (E) TIM-3, TIGIT and PD-1-single-postitivity and co-expression was assessed on T cells in different tissues (SP = single positive, DP = double positive, TP = triple positive). Means and standard error of the mean (SEMs) are shown, paired t tests were performed to determine statistical significance.

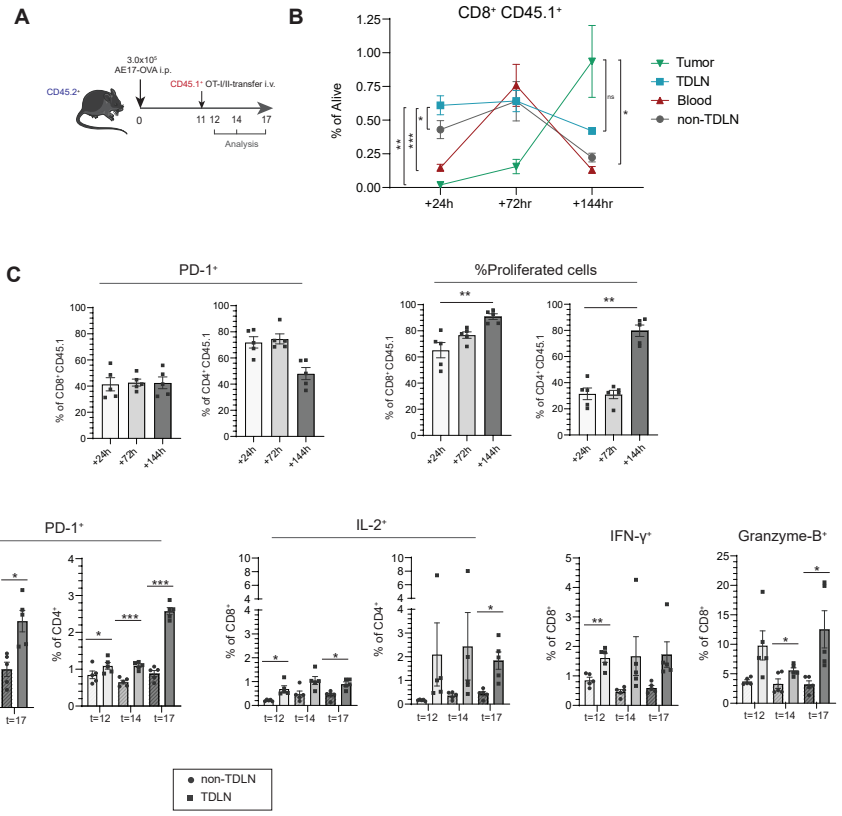

Figure 2: T cells are activated in TDLNs prior to migration and activation in the tumor

(A) Experimental design (n = 5 to 6 mice per group per time point). (B) Frequencies of CD45.1⁺ cells were determined in tumor, TDLN, blood and non-TDLN. (C) PD-1 positivity as well as the percentage of cells undergoing proliferation of CD8⁺CD45.1⁺ cells in the TDLN. (D) Percentages of PD-1⁺, IL-2⁺, IFN-γ⁺ and granzyme-B⁺ were compared for CD8⁺ T cells and CD4⁺ T cells in TDLN (circles) and non-TDLN (squares). Means and SEMs are shown, paired t tests were used to calculate statistical significance. * = $p < 0.05$, ** = $p < 0.01$, *** = $p < 0.001$. TDLN = tumor-draining lymph node, i.v. = intravenous, SEM = standard error of the mean, IL-2 = interleukin 2, IFN-γ = interferon-gamma.

DCs can be subdivided into migratory and resident subsets based on differential expression of CD11c and MHC-II (Fig. S3A) [26]. Based on this distinction, we detected a particularly strong increase in migratory cDC2s, especially in TDLNs (Fig. S3B). These cells expressed high levels of PD-L1 in addition to CD80 compared with cDC1s (Fig. S3C-D), which is in line with recent findings identifying migratory PD-L1⁺ DCs to predominantly present tumor-derived antigens in the TDLN [27]. These data indicate increased frequencies of PD-L1⁺ cells in TDLNs compared with non-TDLNs, especially for macrophages and cDC2s.

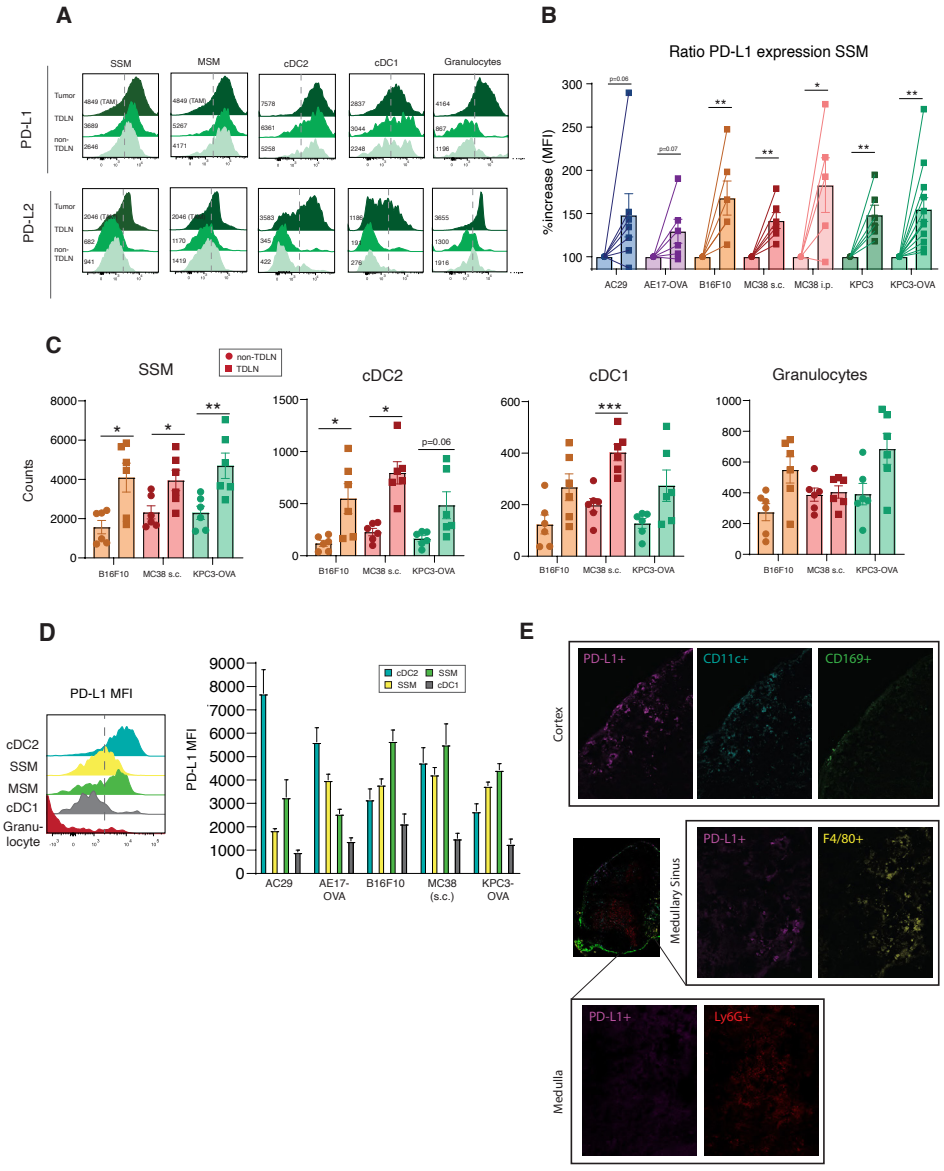
A
SSM
MSM
cDC2
cDC1
Granulocytes
PD-L1
PD-L2
Tumor
TDLN
non-TDLN
B
Ratio PD-L1 expression SSM
%increase (MFI)
AC29
AE17-OVA
B16F10
MC38 s.c.
MC38 i.p.
KPC3
KPC3-OVA
C
SSM
cDC2
cDC1
Granulocytes
non-TDLN
TDLN
Counts
D
PD-L1 MFI
cDC2
SSM
MSM
cDC1
Granu-locyte
PD-L1 MFI
AC29
AE17-OVA
B16F10
MC38 (s.c.)
KPC3-OVA
E
PD-L1+
CD11c+
CD169+
Cortex
Medullary Sinus
F4/80+
Medulla
Ly6G+

◂Figure 3: TDLN-myeloid cells express high levels of PD-L1 compared with non-TDLNs

(A) Expression of PD-L1 and PD-L2 (KPC3-OVA) on myeloid cells in the tumor, TDLN and non-TDLN at late-stage disease. (B) PD-L1 expression on subcapsular sinus macrophages (SSMs) was compared between TDLNs and non-TDLNs, with PD-L1 expression (MFI) on TDLN-macrophages divided over non-TDLN MFI multiplied x100 to indicate percentage increase of expression. (C) Absolute myeloid cell numbers in subcutaneous tumor models. Means and SEMs are shown and paired t tests were performed**.** (D) PD-L1 expression on $CD169^+$ SSMs, $F4/80^+$ medullary sinus macrophages (MSM), type 1 (cDC1) and 2 conventional dendritic cells (cDC2) and $Ly6G^+$ granulocytes from TDLNs. (E) Multicolor confocal microscopy of a representative TDLN section from an untreated mouse bearing AC29 tumor. Slides were stained for PD-L1, CD11c (DCs), CD169 (SSM and MSM), Ly6G (granulocytes) and F4/80 (MSM and medullary cord macrophages; MCM). A 3-dimensional composite image was created after spectral unmixing using single stains (lower left image). * = $p < 0.05$, ** = $p < 0.01$, *** = $p < 0.001$. TDLN = tumor-draining lymph node, SEM = standard error of the mean. paired t tests were performed to determine statistical significance.

Low-dose intrapleural PD-L1 antibody administration selectively targets TDLNs

In order to study the effect of selectively targeting the PD-1/PD-L1 axis in the TDLN on tumor progression we set up a system by which we selectively target TDLNs with therapeutic PD-L1 antibodies prohibited antibody availability in the tumor environment itself. We examined the option to administer ICB antibody via the intrapleural route. This location drains directly to mediastinal LNs which are the TDLNs of intraperitoneal tumors from where excess antibody continues to enter the blood via the thoracic duct [28]. Therapeutic anti-PD-L1 blocking antibodies were administered via intravenous (i.v.) or intrapleural (i.pl.) routes and dispersed tissues were counterstained with a fluorescently labeled anti-rat IgG2a antibody, thereby obviating the need to alter the therapeutic antibody itself potentially influencing drug pharmacokinetics (Fig. 4A). Irrespective of the route of administration, we could readily detect *in vivo* binding of the therapeutic PD-L1 antibody on tumor cells and TAMs by flow cytometry within 24 hours post-injection (Fig. 4B). The mediastinal TDLN SSMs, MSMs and cDC2s were similarly reached by i.v. as well as i.pl. administration and staining patterns paralleled those of direct *ex vivo* staining with PD-L1 antibodies (Fig. 4C). As expected from the previous findings showing decreased PD-L1 expression in non-TDLNs, binding of the PD-L1-antibody to myeloid cells was decreased in the absence of tumor (Fig. 4D). Interestingly, i.pl. injection appeared to especially reach TDLN subcapsular cells (SSMs & $CD11b^+$ cDC2s) more efficiently than the i.v. route in tumor-free animals in contrast to tumor-bearing mice in which antibody binding on these cells was largely similar between injection routes (Fig. 4D). This was not due to differences in PD-L1 expression on cells between treatment arms as PD-L1 expression (assessed in isotype treated animals, Fig. S4A) mirrored PD-L1 antibody binding in all the leukocyte subsets interrogated irrespective of injection route (Fig. 4E). These data suggest that antibody deposition in TDLNs is enhanced in the presence of tumor, possibly via secondary drainage of antibody from permeable tumor vasculature to afferent lymphatics, in addition to direct TDLN targeting (Fig. 4F). As we could now successfully target TDLNs via i.pl. injections we next examined the extent to which the efficacy of ICB depends on TDLNs and therefore titrated the i.pl.-administered anti-PD-L1-antibody dose to

a level that allowed selective blockade in the mediastinal TDLN, with no antibody drainage to the intraperitoneal tumor nor the circulation (Fig. S4B-C). At a near 100-fold lower anti-PD-L1-dosage of 2.5 µg, macrophages and cDCs in the TDLN still bound the antibody, albeit not completely, whereas the antibody did not reach non-TDLN nor tumor cells, TAMs or circulating monocytes and DCs (Fig. S4B-C).

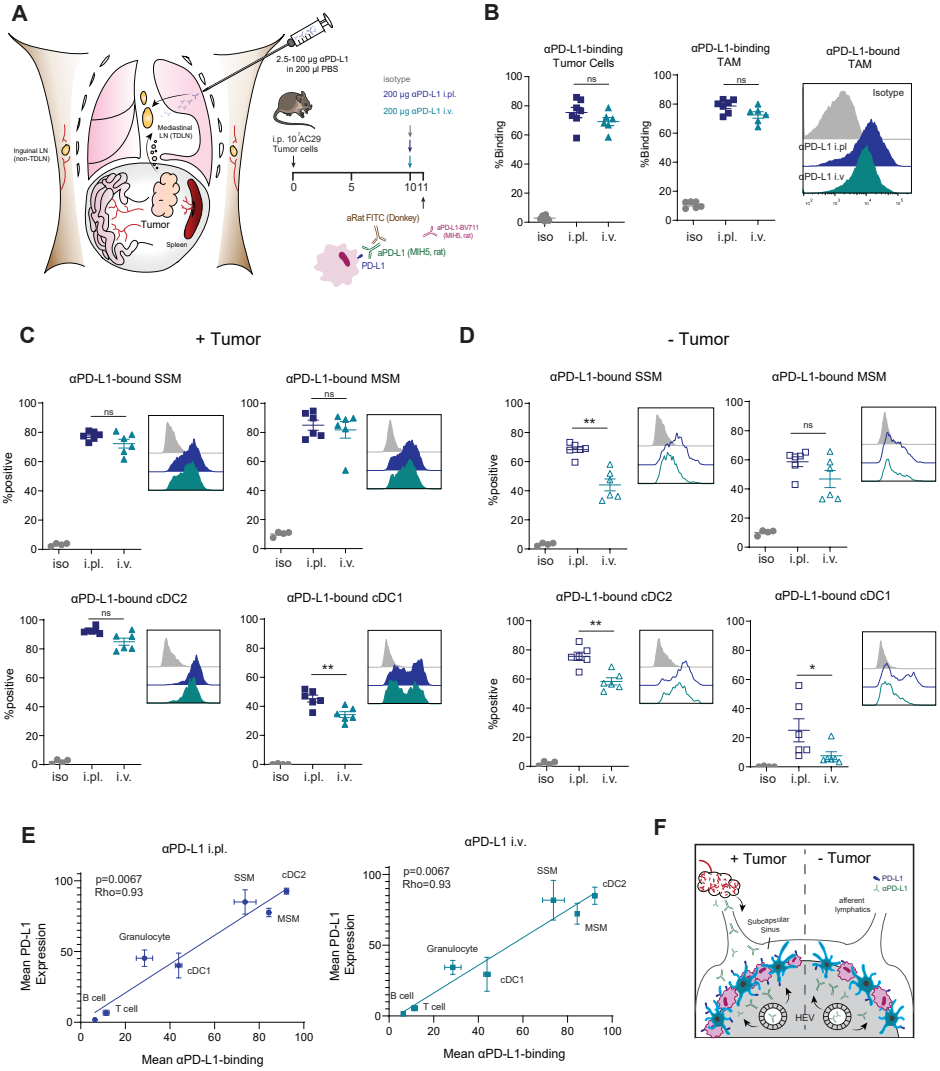

◂Figure 4: Systemically administered anti-PD-L1 antibodies bind to PD-L1 expressing cells in the TDLN

(A) Experimental setup (n = 6 to 7 mice per group) and mode of antibody administration. Tumor-bearing mice (filled symbols) were treated with 200 µg isotype (grey) intrapleurally (i.pl.) or alternatively with 200 µg anti-PD-L1 antibody i.pl (blue) or i.v. (turquoise) to target the TDLN directly or indirectly, respectively. (B) *In vivo* antibody expression was quantified on intratumoral cell types, and (C) on cells in the TDLN. Histograms showing PD-L1 expression patterns are displayed. (D) Quantification of antibody-binding on cells in mediastinal LNs in the absence of tumor (open squares and circles). (E) Mean PD-L1 expression on TDLN cells subsets derived from isotype treated animals (stained with the BV711-antibody) was correlated to anti-PD-L1 antibody binding (detected using the secondary anti-rat FITC-labeled antibody) for both i.pl. (left) and i.v. (right) injection routes. A Pearson correlation coefficient (Rho) was determined. (F) A graphical depiction of the proposed model showing that anti-PD-L1 antibodies reach TDLNs via intravascular and afferent lymphatics in the presence of tumor. Means and SEMs are shown and Mann-Whitney tests were performed indicating statistical significance. ns = not significant ($p \geq 0.05$), * = $p < 0.05$, ** = $p < 0.01$. i.p. = intraperitoneal, i.v. = intravenous, TDLN = tumor-draining lymph node, Ab = antibody, SSM = subcapsular sinus macrophages, MSM = medullary sinus macrophages, cDC = conventional dendritic cell, SEM = standard error of the mean.

TDLN-specific PD-L1 antibody elicits anti-tumor T cell immunity and tumor control

Using these established doses for local (2.5 µg i.pl.) TDLN targeting and for systemic (200 µg i.pl.) overall targeting of PD-L1, we examined the therapeutic effect of this ICB in two syngeneic tumor models, AC29 mesothelioma and MC38 colon carcinoma (Fig. 5A, S5A). Systemic targeting of PD-L1 as well as local TDLN targeting resulted in decreased tumor burden and increased survival (Fig. 5B, S5B). These therapeutic effects were quite strong, considering that not all PD-L1 molecules were blocked in TDLN at these low doses (Fig. S4B). $CD8^+$ tumor-infiltrating T cells (TILs) simultaneously expressing multiple co-inhibitory receptors were increased in MC38 tumor tissue, indicating a more exhausted phenotype which is in line with recent findings in the same tumor model [29]. Systemically administered anti-PD-L1 increased T cell proliferation in blood, whereas both TDLN targeted and systemic treatment caused elevated frequencies of $CD69^+$ cells (Fig. 5C). Whereas increased tumor infiltration of T cells was markedly induced by systemic anti-PD-L1 treatment, TDLN-targeted anti-PD-L1 specifically induced KLRG-1^+ effector T cell infiltration in the AC29 tumor model (Fig. 5C). In addition, while nearly all TILs were TOX-positive, TOX-MFI was significantly decreased in both treatment groups. Recent research has shown that tumors may harbor $TCF1^+$ $CD8^+$ T cells with a stem-like phenotype, giving rise to distinct populations, including terminally-differentiated exhausted T cells [18]. Similarly, we could identify a subset of TILs with a stem-like phenotype termed T_{EX}^{prog}, characterized by the surface marker $SLAMF6^+$ (Ly108), being a surrogate marker for TCF-1, displaying low Ki67, TIM-3 and CD39 (Fig. 5D-E, Fig. S5D-F) [30]. Intratumoral $CD8^+$ and $CD4^+$ T_{EX}^{prog} cells were increased by TDLN-targeted and systemic PD-L1 blockade with decreased levels of proliferation indicating preserved stemness following treatment (Fig. 5F).

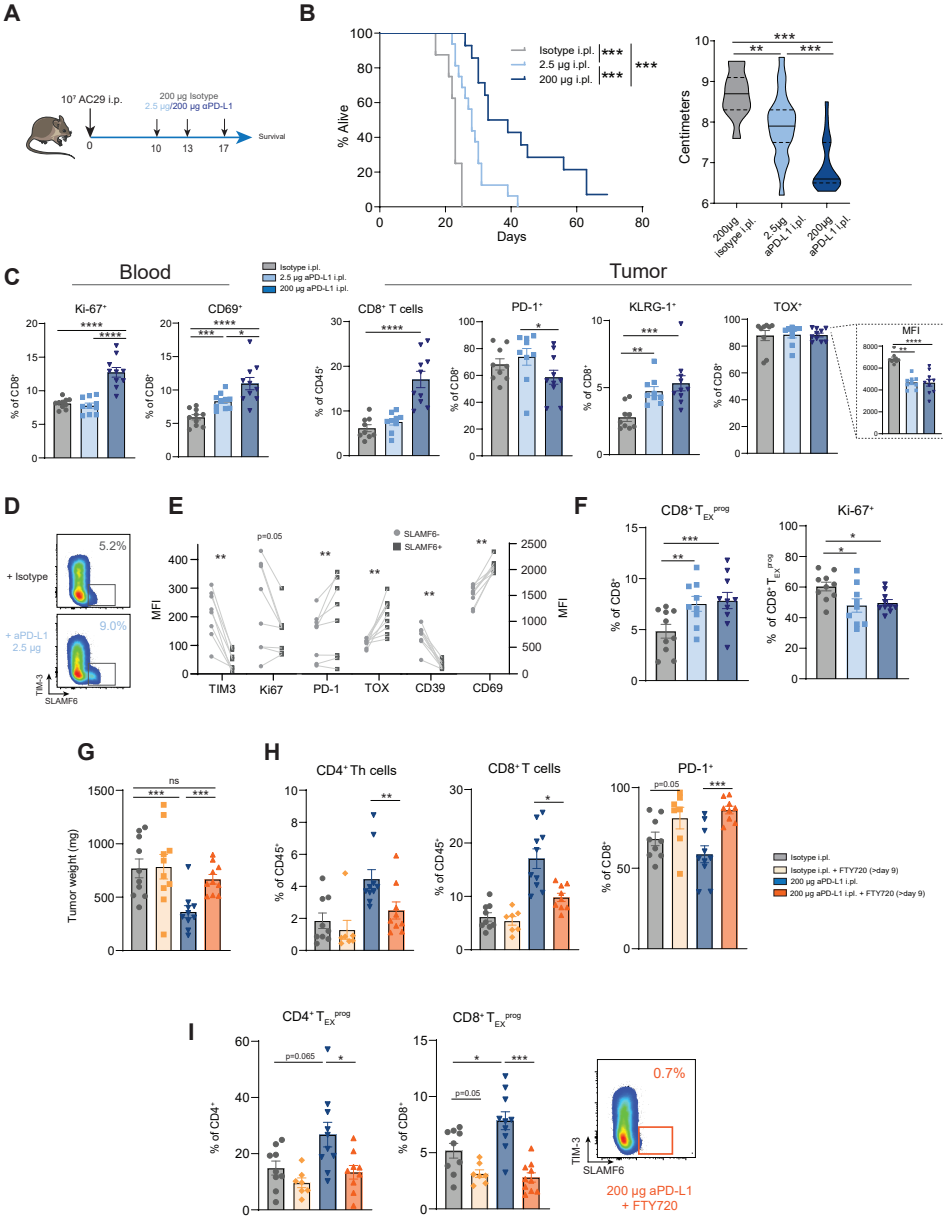
A
10⁷ AC29 i.p.
200 µg Isotype
2.5 µg/200 µg aPD-L1
Survival
0
10
13
17
B
% Alive
Days
Isotype i.pl.
2.5 µg i.pl.
200 µg i.pl.
Centimeters
200µg Isotype i.pl.
2.5µg aPD-L1 i.pl.
200µg aPD-L1 i.pl.
C
Blood
Tumor
Isotype i.pl.
2.5 µg aPD-L1 i.pl.
200 µg aPD-L1 i.pl.
Ki-67⁺
CD69⁺
CD8⁺ T cells
PD-1⁺
KLRG-1⁺
TOX⁺
MFI
D
+ Isotype
+ aPD-L1 2.5 µg
5.2%
9.0%
TIM-3
SLAMF6
E
SLAMF6-
SLAMF6+
MFI
TIM3
Ki67
PD-1
TOX
CD39
CD69
F
CD8⁺ T_EX^prog
Ki-67⁺
G
Tumor weight (mg)
ns
H
CD4⁺ Th cells
CD8⁺ T cells
PD-1⁺
Isotype i.pl.
Isotype i.pl. + FTY720 (>day 9)
200 µg aPD-L1 i.pl.
200 µg aPD-L1 i.pl. + FTY720 (>day 9)
I
CD4⁺ T_EX^prog
CD8⁺ T_EX^prog
0.7%
TIM-3
SLAMF6
200 µg aPD-L1
+ FTY720

◂Figure 5: Specific targeting of PD-L1 in the TDLN by low-dose intrapleural injection of anti-PD-L1 enhances clinical responses in the AC29 tumor model and is abrogated by FTY720 treatment

(A) Experimental setup (n = 8 to 15 mice per group) with mice being treated with either LN-local (2.5 µg) or systemic anti-PD-L1 antibodies (200 µg) i.pl. and survival was monitored. (B) Kaplan-Meier curve of the experiment in A showing tumor survival. Log-rank tests were used to determine statistical significance. In addition, abdominal circumferences (being a measure of ascites volume) were measured on t = 21 post tumor-cell injection and displayed as violin-plots. (C) Blood was isolated +4 days after first injection with anti-PD-L1 treatment and characterized by multicolor flow cytometry. Tumor infiltrating lymphocytes (TILs) were characterized by multicolor flow cytometry for frequencies as well as for positivity for PD-1, KLRG1 and TOX. (D) $CD8^+$ T_{EX}^{prog} cells in tumor tissue were characterized by positivity for SLAMF6 and further identified in (E) for expression of TIM3, Ki67, PD-1, TOX, CD39 and CD69. (F) Frequencies of tumor-infiltrating $CD8^+$ T_{EX}^{prog} cells and their level of proliferation ($Ki67^+$). (G) S1P receptor agonist FTY720 administration via drinking water and oral gavage at day 9-20 and isotype or anti-PD-L1 treatment (200 µg) i.p. at day 10, 13 and 17 (9 to 10 mice per group). (H) Frequencies of $CD4^+$ Th cells and $CD8^+$ T cells of $CD45^+$ T cells and PD-1 positivity on $CD8^+$ T cells were determined of TILs. (I) Frequency of $CD4^+$ and $CD8^+$ T_{EX}^{prog} cells was determined for total $CD4^+$ and $CD8^+$ TILs, respectively. Means and SEMs are shown and Mann-Whitney tests were performed indicating statistical significance. ns = not significant ($p \geq 0.05$), * = $p < 0.05$, ** = $p < 0.01$. i.p. = intraperitoneal, i.pl. = intrapleural, T_{EX}^{prog} = progenitor-exhausted T cells, SEM = standard error of the mean.

FTY720 abrogates systemic and TDLN-specific anti-PD-L1 immunotherapy efficacy

In order to confirm the role of the T cells activated in TDLN following PD-L1 treatment, we administered the S1P receptor agonist FTY720, which abrogates T cell egress from lymphoid organs [31] during anti-PD-L1 treatment. Retention of T cells in lymphoid organs was confirmed by decreased frequencies of T cells but not NK cells in peripheral blood (Figure S6A). FTY720-administration abrogated anti-PD-L1 treatment efficacy and prevented influx of $CD4^+$ Th- and $CD8^+$ TILs but retained T cells exhibiting increased PD-1 expression (Figure 5G-H). In addition, FTY720 administration neutralized both spontaneous and additional anti-PD-L1 mediated induction of tumor $CD4^+$ and $CD8^+$ T_{EX}^{prog} cells following local- and systemically administered anti-PD-L1 treatment (Fig. 5I, S6B). These results indicate that PD-L1 blockade not solely relies on re-invigoration of TME-localized T cells but in fact amplifies priming and activation of T cells, including T_{EX}^{prog}, from the TDLN.

PD-L1 antibody blockade amplifies T_{EX}^{prog} induction in TDLNs

To investigate the functional consequences of blocking the PD-1/PD-L1 axis in TDLNs on tumor-infiltrating T cells, we repeated the aforementioned experiment in the aggressive AE17 mesothelioma expressing the OVA model antigen allowing interrogation of tumor-specific T cells (Fig. S7A). $CD45.1^+$ T cell proliferation was enhanced in TDLNs compared with non-TDLN following anti-PD-L1 treatment (Fig. S7B). $CD45.1^+$ T cells were proliferating more and were more frequently present in TDLN compared with tumor early following systemic anti-PD-L1 while no significant differences between isotype-treated animals were found (Fig. S7C). Anti-PD-L1 treatment markedly increased endogenous $CD45.1^-$ T_{EX}^{prog} cells, starting in the TDLN after 24hrs, followed by blood and tumor on 72 and 144hrs, respectively (Fig. S7D). In an efficacy experiment, repeated dosing of

anti-PD-L1 locally in the TDLN and systemically resulted in decreased AE17-OVA-tumor burden (Fig. 6A-B), without overt increase in (tumor-specific) TILs (Fig. 6C). To assess the replicative potential and phenotype of TILs following anti-PD-L1 therapy, we developed an *ex vivo* T cell stimulation assay in which $CD8^+$ TILs were stimulated with cognate antigen in the presence of their original TME with or without blocking PD-L1 antibodies (Fig. 6D). Stimulation with SIINFEKL-peptide led to increased $CD8^+$ T cell activation in this assay, with profound upregulation of PD-1 following the addition of anti-PD-L1 *in vitro* (Fig. 6D). This induced activation system selectively triggered $CD8^+$ TILs and not $CD4^+$ TILs due to the lack of MHC-II binding OVA peptide. PD-L1 blockade in tumor cell cultures of mice treated with LN-targeted therapeutic ICB induced TIL activity to much higher extent than non-treated mice, as measured by increased cell frequencies, proliferation and decrease in PD-1 levels (Fig. 6E). These findings demonstrate that PD-L1 blockade in the TDLN alleviates the suppressive impact on intranodal tumor-specific T cells, resulting in trafficking to the tumor site where they display a much improved responsiveness to OVA tumor antigen.

Response to PD-L1-blockade occurs independent from TDLN macrophages

In order to investigate which PD-L1-expressing cells in the TDLN were most likely responsible for inhibiting T cell responses we made use of low dose i.pl. administrated clodronate encapsulated liposomes (CEL), which specifically deplete LN macrophages upon phagocytosis [32]. SSMs and MSMs, but not cDC2, were effectively depleted from the TDLN within 48 hours at a dose of 5% CEL, whereas macrophages in non-TDLNs and in the intraperitoneal tumor remained essentially unaltered (Fig. 7A-B). Importantly, repeated TDLN-localized CEL administration failed to abrogate anti-PD-L1 efficacy (Fig. 7C-D), demonstrating a negligible contribution of macrophages to anti-PD-L1 therapy in this model, which is in line with recently published data in genetically-modified models [29]. We then examined TDLNs using multicolor confocal microscopy to visualize co-localization of anti-PD-L1-expressed cDC2s with $CD8^+$ T cells. $CD8^+$ T cells did not co-localize with SSMs and MSMs in TDLNs, but we frequently found clusters of PD-L1 positive DCs and $CD8^+$ T cells (Fig. 7E). Together our data indicate an active role for TDLN in reinvigoration of tumor-specific T cells by ICB, most likely via PD-L1 expressing cDC(2)s, but not macrophages.

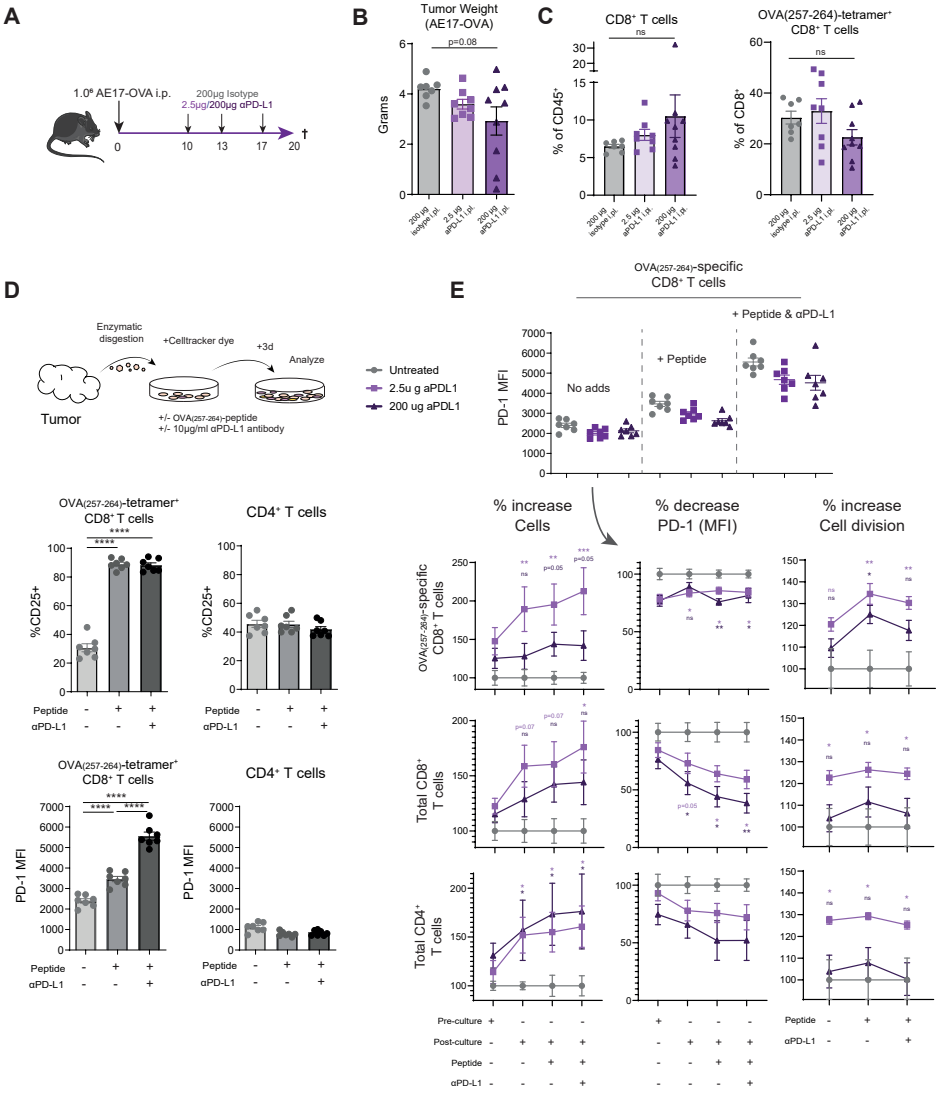

Figure 6: Specific targeting of PD-L1 in the TDLN elicits durable anti-tumor immune responses capable of re-invigoration *in vitro*

(A) Experimental design (n = 7 to 9 mice per group). (B) Tumor weights of the different treatment groups. (C) Frequencies of total CD8⁺ T cells and OVA(257-264)-specific CD8⁺ T cells in tumors as percentages of total alive CD45⁺ leukocytes or CD8⁺ T cells, respectively. (D) Design and validation of the *in vitro* culture system mimicking the tumor-microenvironment. Means and SEMs are depicted with paired t tests used for statistical analysis. (E) Tumor single cell suspensions from isotype (gray), anti-PD-L1 LN-specifically (pink) and anti-PD-L1 systemically (purple) treated mice were cultured as described in *D.* Means and SEMs are shown, Mann-Whitney tests were used to evaluate statistical significance For *E,* treatment arms were normalized to isotype treated animals and baseline and post-3 day culture values for the several conditions are shown.

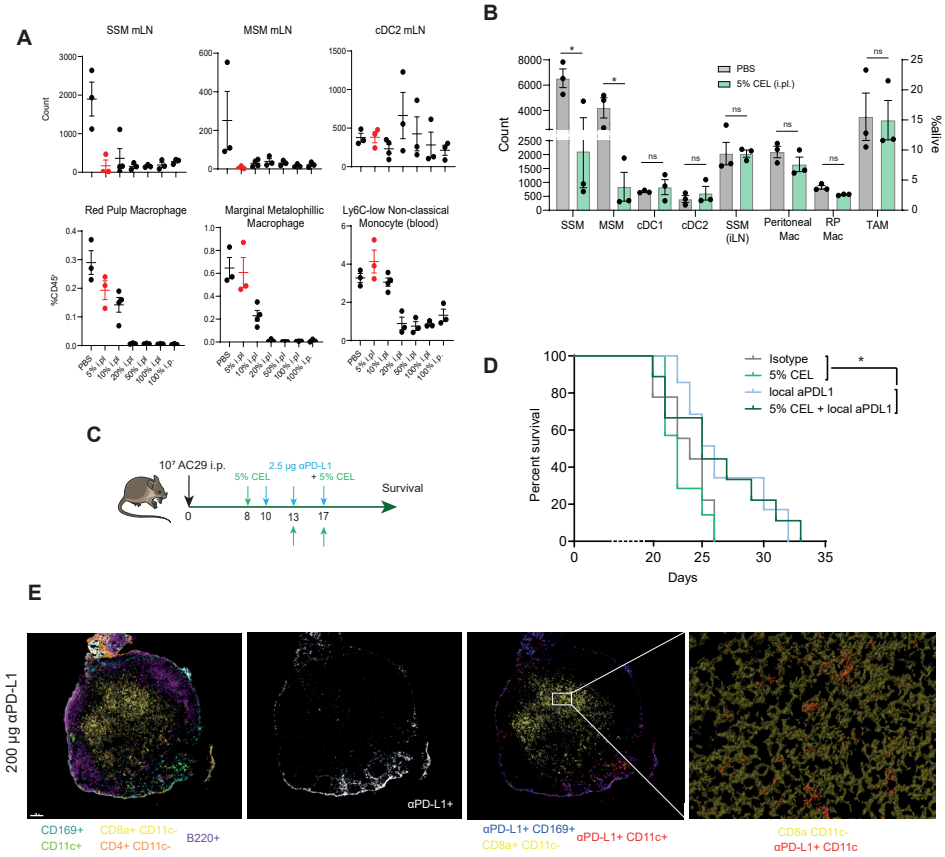

Figure 7: TDLN-local anti-PD-L1 treatment efficacy occurs independent of macrophages

(A-B) CBA/J (non-tumor bearing; A, and tumor-bearing; B) mice were treated with a range of clodronate-encapsulated liposomes (CEL) concentrations in PBS and myeloid cell subsets were analyzed 48 hours later. In red is the dose established for subsequent experiments (n = 3 to 4 mice per group). (C) Experimental setup (n = 7 to 8 mice per group). (D) KM-curve of the survival of the experiment described in C. As isotype/5%CEL and anti-PD-L1/combination treatment showed significant overlap, these groups were pooled and Log-rank tests were performed. (E) TDLN tissue 24 hours following systemic (200 µg) anti-PD-L1 antibody treatment allowing for visualizing of antibody binding to different myeloid cell subsets in the TDLN was assessed using 6-color confocal microscopy. I.pl. = intrapleural, anti-PD-L1 = anti-PD-L1 antibody. Ns = not significant ($p \geq 0.05$), * = $p < 0.05$,** = $p < 0.01$. i.p.= intraperitoneal, i.pl.= intrapleural, i.v.= intravenous, SSM = subcapsular sinus macrophages, MSM = medullary sinus macrophage, cDC = conventional dendritic cell, Mac = macrophage, TAM = tumor-associated macrophage, TDLN = tumor-draining lymph node, CEL = clodronate encapsulated liposome, SEM = standard error of the mean.

PD-1/PD-L1 interactions in TDLN but not in tumor TME correlate with prognosis in melanoma patients

As all the aforementioned data were derived from pre-clinical solid tumor models, it remained unclear whether PD-1/PD-L1 interaction takes place in patient TDLNs. Melanoma is a disease with a highly variable prognosis depending on the presence of distant and LN metastasis (stage III-IV), and in case of absence of distant metastasis (stage I-II); tumor characteristics including thickness (Breslow's-depth), tumor histology and presence of ulceration [33,34]. The melanoma setting is particularly suited for TDLN-characterization as these tissues are generally extracted for staging purposes with the aim of identifying patients that may benefit from adjuvant systemic (immuno-) therapy [35]. To identify whether melanoma TDLNs feature PD-1/PD-L1-axis activity in the absence of LN-metastasis, we stained for PD-1/PD-L1-interactions in TDLNs of systemic treatment-naive stage II melanoma using a proximity ligation assay (PLA, Fig 8A). We studied PD-1/PD-L1-positivity in TDLNs of stage II patients remaining disease free following surgery (n = 19) and patients with early distant disease recurrence (n = 15) (Table S1). As expected, known prognostic factors from the primary tumor such as Breslow's-depth, presence of ulceration and nodular histology were overrepresented in the short-RFS cohort compared with patients remaining long-term free of disease [33,36]. We detected a significantly higher PD-1/PD-L1-interaction density in patients with a short recurrence-free survival (RFS; < 48 months) compared with patients remaining disease free for more than 96 months (Fig. 8B), reflecting possible ineffective anti-tumor immune surveillance. Similar results were obtained when contacts were numerically quantified or alternatively calculated as percentage of total cell-surface area using automated software analysis (Methods S1). Interestingly, short RFS was associated with increased PD-1/PD-L1-contact density irrespective of the aforementioned prognostic factors, indicating that this process of PD-L1-mediated immune suppression arises independently of these primary tumor characteristics (Fig. 8C). To gain insight into which cells were involved in PD-1/PD-L1-interaction, we combined the PLA with multicolor immunofluorescence staining for CD8, CD11c and CD68. Using this method, we observed high PD-1/PD-L1-signalling in germinal centers largely devoid of $CD8^+$ T cells which is in line with previous data (containing primarily B cells and follicular T helper cells, *excluded from analysis in 8A-C* [37]). Also numerous interactions elsewhere in the LN-cortex were present (Fig. 8D). Similar to the murine data, these contacts were particularly established by $CD8^+$ (and to a lesser degree $CD8^-$) T cells and $CD11c^+$ DCs whereas $CD68^+$ macrophages barely associated with T cells (Fig. 8E). To investigate whether PD-1/PD-L1-interactions occur in melanoma tumors to a similar extend as in TDLNs, we performed PLA on matched primary tumor tissue of a subset of patients from whom material was available. Intriguingly, PD-1/PD-L1 interactions in tumor tissue of melanoma patients (n = 9) were scarce compared with the TDLN with the extent of the remainder of interactions not correlating with RFS (Fig. 8F). PD-L1 alone, however, was expressed in tumor tissue showing that the lack of PLA-positivity did not result from absence of PD-L1-expression (Fig. 8G). These findings support our initial findings in mice and highlight a previously unidentified role for PD-1/PD-L1-interactions in human TDLNs, possibly identifying high risk patient groups for adjuvant immunotherapy.

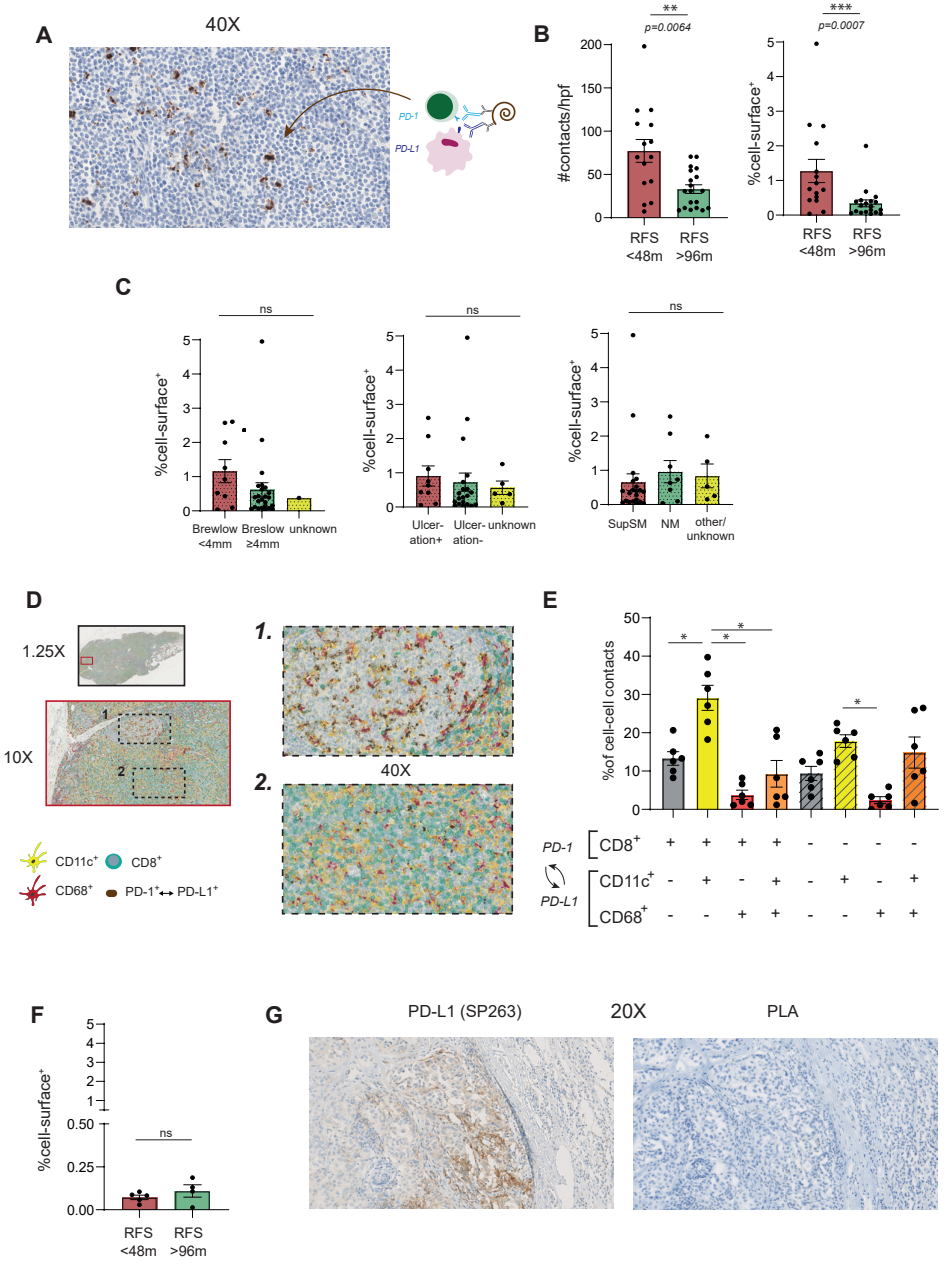
A
40X
PD-1
PD-L1
B
**
p=0.0064
#contacts/hpf
RFS <48m
RFS >96m
***
p=0.0007
%cell-surface+
C
ns
%cell-surface+
Brewlow <4mm
Breslow ≥4mm
unknown
Ulcer-ation+
Ulcer-ation-
SupSM
NM
other/ unknown
D
1.25X
10X
1.
2.
40X
CD11c+
CD8+
CD68+
PD-1+↔ PD-L1+
E
%of cell-cell contacts
PD-1
PD-L1
CD8+
CD11c+
CD68+
F
%cell-surface+
ns
RFS <48m
RFS >96m
G
PD-L1 (SP263)
20X
PLA

◂Figure 8: Stage II melanoma TDLNs harbor frequent PD-1/PD-L1 interactions which associates with early distant recurrence following surgery, and not in primary tumor tissue

(A) 40X magnified exemplary image of a stage II melanoma TDLN (sentinel node) displaying several PD-1/PD-L1-contacts stained using PLA. (B) Quantification of the average number of contacts, in patients with an early (< 48 months) recurrence of disease following surgery (n = 15) and no recurrence after 96 months (n = 19) either via manual (left) and automated (right) quantification analysis. Statistical significance was determined using Mann-Whitney tests and means plus SEMs ware depicted. (C) Using the outcome measure project in right panel *B,* patient tumors were divided according to Breslow's-depth (tumor-thickness), presence of tumor ulceration and histological subtype. (D-E) Multiplexed images from 6 patient TDLNs high in PD-1/PD-L1 contacts (5 short, 1 long RFS) were constructed combining the PLA with CD8 (green), CD11c (yellow) and CD68 (red), followed by counterstaining with hematoxylin (blue). 40X magnification images were acquired from cortical LN-regions showing germinal centers (1.) and surrounding area (2.) rich in PD-1/PD-L1-positivity. The latter images were used to identify the cells of origin establishing the contacts in E. (F) PD-1/PD-L1 interactions in primary tissue of stage II melanoma patients were stained using PLA (n = 9). The average number of contacts was enumerated from patients with an early recurrence (n = 5) and no recurrence after 96 months (n = 4). (G) A 20X magnified exemplary image of primary tumor tissue of stage II melanoma patients displaying PD-L1 expression (clone SP263; left) and PD-1/PD-L1 interactions using PLA (right). Means and SEMs are shown, Mann-Whitney tests were used to calculate statistical significance. TDLN = tumor-draining lymph node, RFS = recurrence-free survival, PLA = Proximity Ligation Assay, SupSM = Superficial spreading melanoma, NM = nodular melanoma, SEM = standard error of the mean.

Discussion

Our data formally establish a role for TDLNs in generating primary anti-tumor immune responses following anti-PD-L1 ICBs, a checkpoint that is generally regarded to act primarily at the TME [2]. These data could offer an explanation for the apparent clinical incongruences in which tumor PD-L1 negative tumors may still respond to anti-PD-1 blockade which has resulted in (chemo-) immunotherapy being first-line treatment in several metastatic cancer irrespective of PD-L1-positivity [35,38,39]. Although multiple mechanisms will likely define response to ICB therapy, alleviating immune suppression in the TDLN could propel systemic anti-tumor T cell immunity to effectively control distant tumor sites. Our data reveal a critical role of PD-L1 on cDCs in the TDLN, without negating the involvement of this inhibitory ligand in the TME.

Our data show that PD-1 expression on T cells in the TDLN seems to correlate with antigenicity of the tumor, which might explain the conflicting results from others showing a minor dependency on T cells from the TDLN [40]. Tumor-mutational burden has been identified as a predictive marker for ICB-efficacy in patients and our data strengthen the role of TDLNs as possible mediators of ICB-responses as these potentially immunogenic tumor-antigens are likely to drain or be transported to TDLNs for further T cell induction [41]. Others have previously hinted towards a role for LNs in generating anti-tumor immunity following PD-1/PD-L1 ICB in patients by describing several dysfunctional T

cell subsets arising following treatment [17,42]. Our data formally establish these notions and directly complement recent findings on TIL-clonality in patients treated with anti-PD-1 therapy, in which an extratumoral source of immunotherapy-elicited T cells was suggested [16].

TDLNs could therefore be pivotal in generating effective anti-tumor T cell responses following liberation by anti-PD-1/PD-L1 antibodies, as has been previously shown to be the case for other cancer immunotherapies [43]. Surgical removal of the TDLN in mouse tumor models revealed a contribution of TDLNs to ICB efficacy but as LNs are known to amplify direct anti-tumor effects of immunotherapy, formal assessment of their role in ICB therapy is lacking [15,43,44]. The role of TDLNs as main hubs in providing anti-tumor T cell immunity following ICB furthermore fits with recent insights into PD-1/PD-L1 biology showing that PD-1 inhibits CD28-B7 mediated T- co-stimulation, a process that takes place in a B7-rich environment such as LNs, and is less likely in the immune-suppressive tumor-microenvironment [13,14]. Furthermore, anti-tumor T cells in TDLN are less exhausted compared with TIL and thus may have a proliferative advantage with ICB [45].

Our tumor models evaluate the role of TDLN in a relatively early stage, at a time that T cell priming following tumor cell inoculation might still be occurring. The aggressiveness of the model prohibits treatment in later phases. TILs were not significantly decreased following FTY720-treatment on day 9, which suggests that initial priming has largely occurred in the preceding time window (Fig. 5H). Importantly, we do not exclude a role for PD-L1 blockade in the TME, but have technically not been able to selectively administer antibody to the i.pl. or s.c. located tumors in order to directly compare the importance of TDLN and TME to PD-L1 treatment efficacy. The exact contribution of TDLN versus TME during PD-1/PD-L1 checkpoint blockade therapy remains to be elucidated, however our data clearly unraveled the involvement of lymph nodes.

We identify PD-L1$^+$ cDCs, most likely cDC2s, as main targets of anti-PD-L1 antibodies in the TDLN, and not macrophages. Recently, *Oh* et al. showed that DC-specific genetic PD-L1-ablation phenocopied the effects of complete PD-L1-knock-out mice in bearing MC38 tumors, whereas macrophage-direct PD-L1-elimination did not [29]. However, as PD-L1 was ablated systemically via the CD11c promotor, analyses into the site and preferred mechanism of PD-L1-PD-1-blockade mediated anti-tumor rejection remained elusive. Classically, a division of labor has been proposed with cDC2s predominantly inducing CD4$^+$ T cell activation and cDC1s priming CD8$^+$ T cells [46]. We show however that cDC2s are significantly more PD-L1-positive and frequent in TDLNs compared with cDC1s and co-localize with CD8$^+$ T cells in the TDLN cortex, challenging the current dogma. In agreement with our findings are recent publications by different groups showing cDC2s to be efficient CD8$^+$ T cell stimulators in the context of solid cancer and viral infection, in addition to their well-described role in activating CD4$^+$ T cells [47,48]. Moreover,

comprehensive analysis of tumor- and TDLN-DCs by *Maier* et al. shows that both cDC1s and cDC2s adopt a regulatory phenotype upon apoptotic tumor-cell ingestion and upregulate PD-L1 thereby preventing proper T cell induction [27]. These combined findings provide a rationale for manipulating cDC2s for the benefit of cancer immunotherapy.

Our analysis of PD-1/PD-L1-axis activity in non-metastatic TDLNs of melanoma patients complements our findings in murine solid tumor models by identifying a subset of patients with high PD-1/PD-L1 interaction density which was associated with early disease relapse following surgery. Although these early stage (II) patients generally have a favorable prognosis following primary resection, a minor subset eventually presents with distant recurrences bearing a poor prognosis [36,49]. It is tentative to speculate that PD-L1-mediated suppression of anti-tumor T cell responses in the TDLNs of these patients is involved in the development or progression of distant metastasis, and future research will likely shed more light on the validity of this hypothesis. An ancillary observation supporting this hypothesis is the fact that the two patients who received primary anti-PD-1 antibodies at disease recurrence resulting in durable complete responses were the second and third-highest expressers of PD-1/PD-L1 in the TDLN (Fig. S8). Although the TDLNs bearing these high-density contacts were excised at primary disease presentation, it is likely that distant micrometastases bearing a similar genetic and TME-makeup would be susceptible to later anti-PD1 ICB therapy.

Perhaps unexpectedly, we found PD-1/PD-L1-interactions to occur sporadically in primary melanoma tumors compared with corresponding TDLNs. Moreover, PD-L1 expression in melanoma tumors has been variably linked to favorable prognosis while its predictive value is limited [50-52]. Our data suggest that PD-1/PD-L1-axis activity in TDLNs rather than the tumor itself could be a primary target for PD-1/PD-L1 checkpoint blocking antibodies, thereby amplifying anti-tumor T cell induction. As PD-1 ICB is currently being administered adjuvant to surgery in stage IIIB-C disease, it will be of interest to assess the validity of PD-1/PD-L1 expression in the TDLN of these patients. A different approach currently being investigated is the neo-adjuvant administration of anti-PD-1 which shows early encouraging results [53]. This is in line with our hypothesis claiming that targeting the PD-1/PD-L1 checkpoint when the TDLN is still *in situ* could harness effective anti-tumor immunity. Further evidence supporting this notion comes from neo-adjuvant and metastatic PD-1-blockade studies showing increased proliferation of activated $CD8^+$ $PD\text{-}1^+$/$HLA\text{-}DR^+$ T cells in peripheral blood early after start of ICB treatment, followed by increased T cell infiltrates in the tumor [53,54].

In summary, our findings implicate TDLNs as key orchestrators of anti-tumor T cell immune responses which can be induced following blockade of PD-L1 in the TDLN. These data challenge the current dogma that PD-1/PD-L1-checkpoint act primarily at the effector (tumor) site and offers additional avenues for biomarker and combination-immunotherapy discovery.

References

1. Dammeijer, F., Lau, S.P., van Eijck, C.H.J., van der Burg, S.H. & Aerts, J. Rationally combining immunotherapies to improve efficacy of immune checkpoint blockade in solid tumors. *Cytokine & growth factor reviews* (2017).
2. Ribas, A. & Wolchok, J.D. Cancer immunotherapy using checkpoint blockade. *Science* **359**, 1350-1355 (2018).
3. Nishino, M., Ramaiya, N.H., Hatabu, H. & Hodi, F.S. Monitoring immune-checkpoint blockade: response evaluation and biomarker development. *Nature reviews. Clinical oncology* **14**, 655-668 (2017).
4. Koyama, S.*, et al.* Adaptive resistance to therapeutic PD-1 blockade is associated with upregulation of alternative immune checkpoints. *Nature communications* **7**, 10501 (2016).
5. Havel, J.J., Chowell, D. & Chan, T.A. The evolving landscape of biomarkers for checkpoint inhibitor immunotherapy. *Nature reviews. Cancer* **19**, 133-150 (2019).
6. Ready, N.*, et al.* First-Line Nivolumab Plus Ipilimumab in Advanced Non-Small-Cell Lung Cancer (CheckMate 568): Outcomes by Programmed Death Ligand 1 and Tumor Mutational Burden as Biomarkers. *Journal of clinical oncology : official journal of the American Society of Clinical Oncology* **37**, 992-1000 (2019).
7. Long, G.V.*, et al.* Epacadostat plus pembrolizumab versus placebo plus pembrolizumab in patients with unresectable or metastatic melanoma (ECHO-301/KEYNOTE-252): a phase 3, randomised, double-blind study. *The Lancet. Oncology* **20**, 1083-1097 (2019).
8. Hellmann, M.D.*, et al.* Nivolumab plus Ipilimumab in Advanced Non-Small-Cell Lung Cancer. *The New England journal of medicine* (2019).
9. Lau, J.*, et al.* Tumour and host cell PD-L1 is required to mediate suppression of anti-tumour immunity in mice. *Nat Commun* **8**, 14572 (2017).
10. Tang, H.*, et al.* PD-L1 on host cells is essential for PD-L1 blockade-mediated tumor regression. *J Clin Invest* **128**, 580-588 (2018).
11. Lin, H.*, et al.* Host expression of PD-L1 determines efficacy of PD-L1 pathway blockade-mediated tumor regression. *The Journal of clinical investigation* **128**, 1708 (2018).
12. Kleinovink, J.W.*, et al.* PD-L1 expression on malignant cells is no prerequisite for checkpoint therapy. *Oncoimmunology* **6**, e1294299 (2017).
13. Hui, E.*, et al.* T cell costimulatory receptor CD28 is a primary target for PD-1-mediated inhibition. *Science* **355**, 1428-1433 (2017).
14. Kamphorst, A.O.*, et al.* Rescue of exhausted CD8 T cells by PD-1-targeted therapies is CD28-dependent. *Science* **355**, 1423-1427 (2017).
15. Chamoto, K.*, et al.* Mitochondrial activation chemicals synergize with surface receptor PD-1 blockade for T cell-dependent antitumor activity. *Proceedings of the National Academy of Sciences of the United States of America* **114**, E761-E770 (2017).
16. Yost, K.E.*, et al.* Clonal replacement of tumor-specific T cells following PD-1 blockade. *Nat Med* **25**, 1251-1259 (2019).
17. Sade-Feldman, M.*, et al.* Defining T Cell States Associated with Response to Checkpoint Immunotherapy in Melanoma. *Cell* **175**, 998-1013.e1020 (2018).
18. Jansen, C.S.*, et al.* An intra-tumoral niche maintains and differentiates stem-like CD8 T cells. *Nature* **576**, 465-470 (2019).
19. van der Ploeg, A.P.*, et al.* EORTC Melanoma Group sentinel node protocol identifies high rate of submicrometastases according to Rotterdam Criteria. *European journal of cancer* **46**, 2414-2421 (2010).
20. Dammeijer, F.*, et al.* Depletion of Tumor-Associated Macrophages with a CSF-1R Kinase Inhibitor Enhances Antitumor Immunity and Survival Induced by DC Immunotherapy. *Cancer immunology research* **5**, 535-546 (2017).
21. Zhao, M.*, et al.* Rapid in vitro generation of bona fide exhausted CD8+ T cells is accompanied by Tcf7 promotor methylation. *PLOS Pathogens* **16**, e1008555 (2020).
22. Kurtulus, S.*, et al.* Checkpoint Blockade Immunotherapy Induces Dynamic Changes in PD-1(-)CD8(+) Tumor-Infiltrating T Cells. *Immunity* **50**, 181-194 e186 (2019).
23. Gray, E.E. & Cyster, J.G. Lymph node macrophages. *Journal of innate immunity* **4**, 424-436 (2012).
24. Eisenbarth, S.C. Dendritic cell subsets in T cell programming: location dictates function. *Nature reviews. Immunology* **19**, 89-103 (2019).
25. Glodde, N.*, et al.* Reactive Neutrophil Responses Dependent on the Receptor Tyrosine Kinase c-MET Limit Cancer Immunotherapy. *Immunity* **47**, 789-802.e789 (2017).
26. Ohl, L.*, et al.* CCR7 governs skin dendritic cell migration under inflammatory and steady-state conditions. *Immunity* **21**, 279-288 (2004).
27. Maier, B.*, et al.* A conserved dendritic-cell regulatory program limits antitumour immunity. *Nature* **580**, 257-262 (2020).

28. Kool, M., *et al.* Alum adjuvant boosts adaptive immunity by inducing uric acid and activating inflammatory dendritic cells. *The Journal of experimental medicine* **205**, 869-882 (2008).
29. Oh, W., Cheung, Navarro, Xiong, Cubas,Totpal, Chiu, Wu, Comps-Agrar, Leader, Merad, Roose-Germa, Warming, Yan, Kim, Rutz, Mellman PD-L1 expression by dendritic cells is a key regulator of T-cell immunity in cancer. *Nature Cancer* (2020).
30. Beltra, J.C., *et al.* Developmental Relationships of Four Exhausted CD8(+) T Cell Subsets Reveals Underlying Transcriptional and Epigenetic Landscape Control Mechanisms. *Immunity* **52**, 825-841 e828 (2020).
31. Yanagawa, Y., *et al.* FTY720, a novel immunosuppressant, induces sequestration of circulating mature lymphocytes by acceleration of lymphocyte homing in rats. II. FTY720 prolongs skin allograft survival by decreasing T cell infiltration into grafts but not cytokine production in vivo. *Journal of immunology (Baltimore, Md. : 1950)* **160**, 5493-5499 (1998).
32. van Rooijen, N. & Hendrikx, E. Liposomes for specific depletion of macrophages from organs and tissues. *Methods Mol Biol* **605**, 189-203 (2010).
33. Schadendorf, D., *et al.* Melanoma. *Nature reviews. Disease primers* **1**, 15003 (2015).
34. Verver, D., *et al.* Risk stratification of sentinel node-positive melanoma patients defines surgical management and adjuvant therapy treatment considerations. *European journal of cancer* **96**, 25-33 (2018).
35. Eggermont, A.M.M., Robert, C. & Ribas, A. The new era of adjuvant therapies for melanoma. *Nature reviews. Clinical oncology* **15**, 535-536 (2018).
36. Verver, D., *et al.* Development and validation of a nomogram to predict recurrence and melanoma-specific mortality in patients with negative sentinel lymph nodes. *The British journal of surgery* **106**, 217-225 (2019).
37. Shi, J., *et al.* PD-1 Controls Follicular T Helper Cell Positioning and Function. *Immunity* **49**, 264-274.e264 (2018).
38. Gandhi, L., *et al.* Pembrolizumab plus Chemotherapy in Metastatic Non-Small-Cell Lung Cancer. *The New England journal of medicine* **378**, 2078-2092 (2018).
39. Paz-Ares, L., *et al.* Pembrolizumab plus Chemotherapy for Squamous Non-Small-Cell Lung Cancer. *The New England journal of medicine* **379**, 2040-2051 (2018).
40. Siddiqui, I., *et al.* Intratumoral Tcf1(+)PD-1(+)CD8(+) T Cells with Stem-like Properties Promote Tumor Control in Response to Vaccination and Checkpoint Blockade Immunotherapy. *Immunity* **50**, 195-211 e110 (2019).
41. Samstein, R.M., *et al.* Tumor mutational load predicts survival after immunotherapy across multiple cancer types. *Nature Genetics* **51**, 202-206 (2019).
42. Li, H., *et al.* Dysfunctional CD8 T Cells Form a Proliferative, Dynamically Regulated Compartment within Human Melanoma. *Cell* **176**, 775-789 e718 (2019).
43. Spitzer, M.H., *et al.* Systemic Immunity Is Required for Effective Cancer Immunotherapy. *Cell* **168**, 487-502.e415 (2017).
44. Fransen, M.F., *et al.* Tumor-draining lymph nodes are pivotal in PD-1/PD-L1 checkpoint therapy. *JCI insight* **3**(2018).
45. Hope, J.L., *et al.* Microenvironment-Dependent Gradient of CTL Exhaustion in the AE17sOVA Murine Mesothelioma Tumor Model. *Frontiers in immunology* **10**, 3074 (2019).
46. Wculek, S.K., *et al.* Dendritic cells in cancer immunology and immunotherapy. *Nat Rev Immunol* **20**, 7-24 (2020).
47. Ruhland, M.K., *et al.* Visualizing Synaptic Transfer of Tumor Antigens among Dendritic Cells. *Cancer cell* **37**, 786-799 e785 (2020).
48. Bosteels, C., *et al.* Inflammatory Type 2 cDCs Acquire Features of cDC1s and Macrophages to Orchestrate Immunity to Respiratory Virus Infection. *Immunity* **52**, 1039-1056 e1039 (2020).
49. von Schuckmann, L.A., *et al.* Risk of Melanoma Recurrence After Diagnosis of a High-Risk Primary Tumor. *JAMA dermatology* **155**, 688-693 (2019).
50. Morrison, C., *et al.* Predicting response to checkpoint inhibitors in melanoma beyond PD-L1 and mutational burden. *Journal for immunotherapy of cancer* **6**, 32 (2018).
51. Hodi, F.S., *et al.* Nivolumab plus ipilimumab or nivolumab alone versus ipilimumab alone in advanced melanoma (CheckMate 067): 4-year outcomes of a multicentre, randomised, phase 3 trial. *The Lancet. Oncology* **19**, 1480-1492 (2018).
52. Daud, A.I., *et al.* Programmed Death-Ligand 1 Expression and Response to the Anti-Programmed Death 1 Antibody Pembrolizumab in Melanoma. *Journal of clinical oncology : official journal of the American Society of Clinical Oncology* **34**, 4102-4109 (2016).
53. Huang, A.C., *et al.* A single dose of neoadjuvant PD-1 blockade predicts clinical outcomes in resectable melanoma. **25**, 454-461 (2019).
54. Herbst, R.S., *et al.* Predictive correlates of response to the anti-PD-L1 antibody MPDL3280A in cancer patients. *Nature* **515**, 563-567 (2014).

Supplementary data

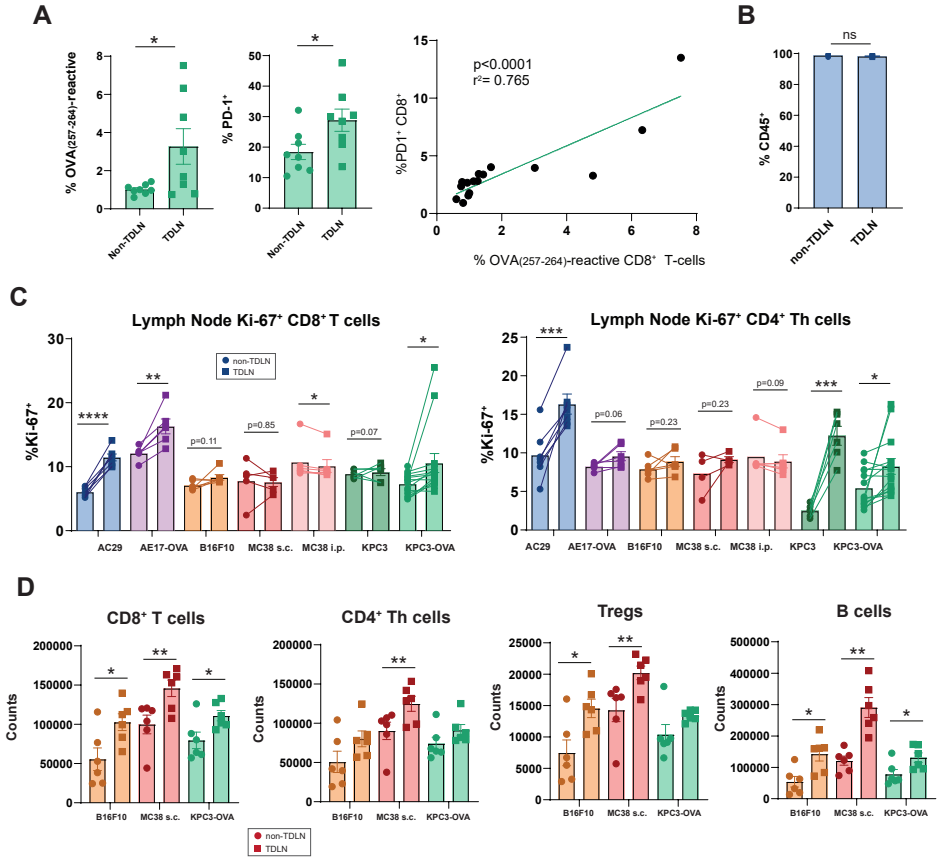

Figure S1. (A) Similar to Fig.1A, TDLNs and non-TDLNs from end-stage disease KPC3-OVA-bearing mice were harvested and stained for PD-1-positivity and OVA(257-264)-reactive $CD8^+$ T cells using tetramers. Medians and SEM are shown and a Wilcoxon matched-pairs signed rank test was used to calculate statistical significance. In addition, total PD-1^+ $CD8^+$ T cells were plotted against OVA(257-264)-$tetramer^+$ $CD8^+$ T cells in the TDLN and a correlation was made and a Pearson correlation coefficient was calculated (r^2). (B) Graphs showing $CD45^-$ cell frequencies in TDLN and non-TDLN. (C) $CD8^+$ and $CD4^+$ Th-cell proliferation was assessed in TDLNs (squares) versus non-TDLNs (circles) by intra-nuclear Ki67-staining using flow cytometry. (D) Absolute lymphocyte cell numbers were quantified in subcutaneous tumor models allowing for ipsi- (tumor draining) and contralateral (non-tumor draining) LN extraction and evaluation. Means and SEMs are shown and paired t-tests were performed. Means and SEMs are shown, including p-values determined by ratio paired t tests. * = $p < 0.05$, ** = $p < 0.01$, *** = $p < 0.001$. SSM = subcapsular sinus macrophages, Treg = Regulatory T cell, SEM = standard error of the mean.

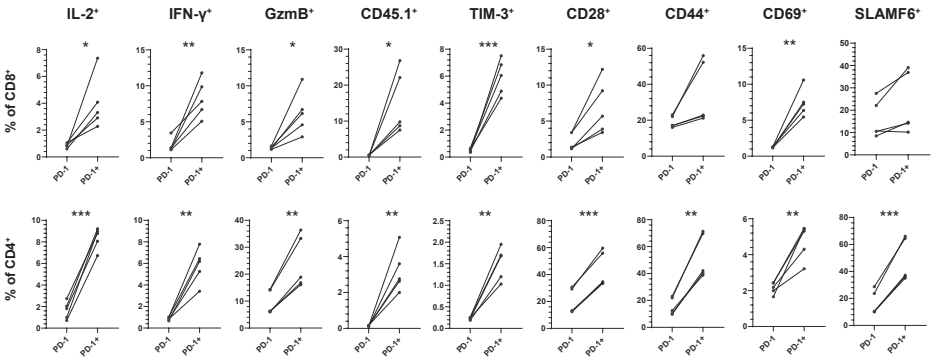

Figure S2. Levels of IL-2, IFN-γ, granzyme-B, CD45.1, TIM-3, CD28, CD44, CD69 and SLAMF6 were determined for PD-1$^-$ and PD-1$^+$ CD4$^+$ and CD8$^+$ T cells isolated from TDLN 17 days after AE17-OVA tumor inoculation. Means and SEMs are shown, paired t tests were used to calculate statistical significance. * = $p < 0.05$, ** = $p < 0.01$, *** = $p < 0.001$.

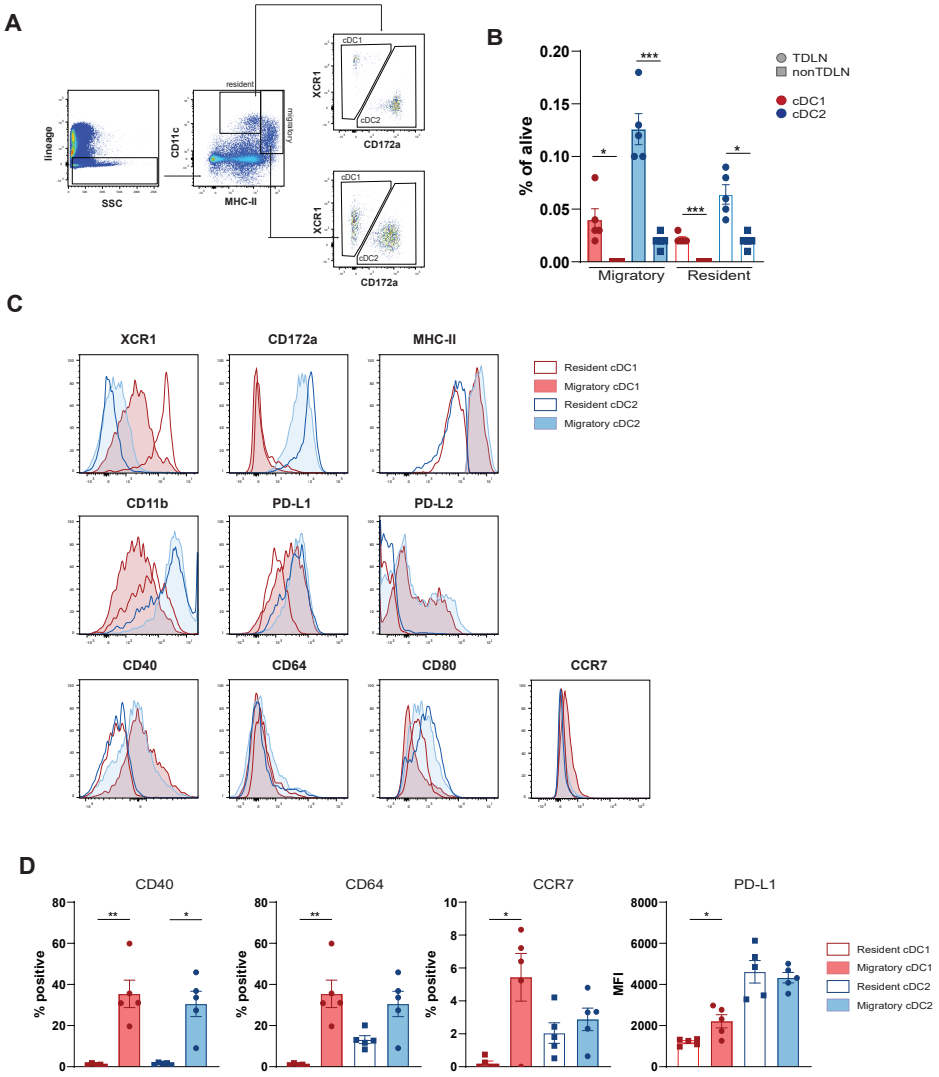

Figure S3. (A) Gating strategy of resident and migratory conventional dendritic cell type 1 and 2 (cDC1s and cDC2s) in TDLNs and non-TDLNs isolated from AE17-OVA tumor-bearing mice 12 days after tumor inoculation. (B) Frequencies of migratory and resident cDC1s (red) and cDC2s (blue) of alive were determined in TDLN (circles) and non-TDLNs (squares). (C) Histograms showing level of expression of XCR1, CD172a, MHC class II, CD11b, PD-L1, PD-L12, CD40, CD62, CD80 and CCR7 on resident (open) and migratory (closed) cDC1s (red) and cDCs (blue) in the TDLN. (D) Histograms demonstrating frequencies of CD40, CD64, CCR7 and MFI for PD-L1 for resident (open) and migratory (closed) cDC1s (red) and cDC2s (blue). Means and SEMs are shown, paired t tests were used to calculate statistical significance. * = $p < 0.05$, ** = $p < 0.01$, *** = $p < 0.001$. TDLN = tumor-draining lymph node.

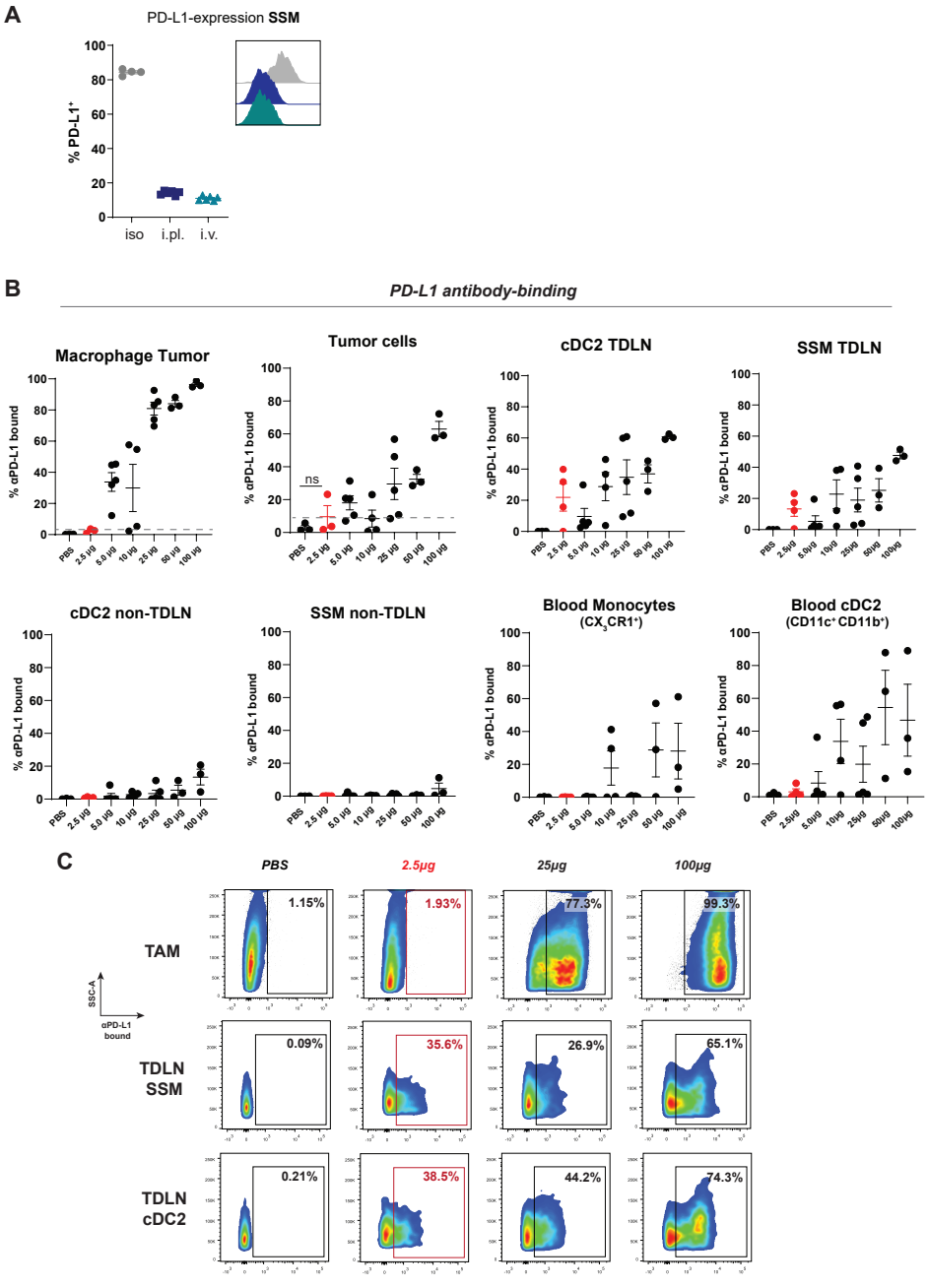
A
PD-L1-expression SSM
% PD-L1+
iso
i.pl.
i.v.
B
PD-L1 antibody-binding
Macrophage Tumor
Tumor cells
cDC2 TDLN
SSM TDLN
cDC2 non-TDLN
SSM non-TDLN
Blood Monocytes
(CX3CR1+)
Blood cDC2
(CD11c+CD11b+)
% αPD-L1 bound
ns
PBS
2.5 µg
5.0 µg
10 µg
25 µg
50 µg
100 µg
C
PBS
2.5µg
25µg
100µg
TAM
TDLN SSM
TDLN cDC2
SSC-A
αPD-L1 bound
1.15%
1.93%
77.3%
99.3%
0.09%
35.6%
26.9%
65.1%
0.21%
38.5%
44.2%
74.3%

◂**Figure S4**. (A) Representative graph showing PD-L1 expression as assessed by the *ex vivo* anti-PD-L1 BV711 antibody. PD-L1-expression (used in Fig. 4E, y-axis) could be assessed in isotype-treated mice whereas binding was limited due to *in vivo* PD-L1 binding of the therapeutic antibody (B) In order to specifically target the TDLN while leaving other sites unaffected, a method was developed whereby low-dose anti-PD-L1 was injected i.pl., whereby only TDLN-resident cells were targeted (SSM and cDC2 are shown) but cells in the tumor were not (in red the selected dose used in subsequent experiments). Wildtype AC29-tumor bearing mice (+10 days post-tumor cell injection) were treated with increasing doses of anti-PD-L1 antibodies administered intrapleurally or with PBS as a control. 24 hours later, tissues were harvested and cells were counterstained as illustrated in Fig. 4A. Indicated in red (2.5 µg) is the selected dose in subsequent experiments, dotted lines indicate background staining level. (C) Representative FACS plots of A. Means and SEM are indicated. cDC2 = conventional type 2 dendritic cells, TDLN = tumor-draining lymph node, SSM = subcapsular sinus macrophage.

Figure S5. (A) C57/Bl6 mice were inoculated with $2.5x10^6$ MC38 tumor cells i.p. and treated with either isotype, 2.5 µg of anti-PD-L1 (local) or 200 µg of anti-PD-L1 (systemic) i.pl. at day 8, 11 and 15. Mice were euthanized 19 days following tumor injection (4 days after the last treatment) and (B) tumors weights were quantified. (C) Tumors were enzymatically digested and stained for flow cytometry to assess $CD4^+$ and $CD8^+$ TIL-phenotype. In addition to sole expression of individual co-inhibitory checkpoints on $CD8^+$ T cells, mean co-expression of receptors was evaluated with SP indicating receptor single positivity. DP = double positive, TP = triple positive and QP = quadruple positive for the investigated checkpoints. Inside the circle, statistical significance is indicated for QP-cells between the different treatment groups. (D) Phenotype of $SLAMF6^+CD8^+$ T cells was compared with $SLAMF6^-CD8^+$T cells and $CD3^-$ lymphocytes in tumor tissue of AC29 tumor-bearing mice isolated 20 days after tumor inoculation. (E) Expression level of TCF-1 was determined in $SLAMF6^+CD8^+$ T cells versus $SLAMF6^-CD8^+$T cells. (F) Representative dotplots showing expression of TCF1 and SLAMF6 (left plot) and TCF1 and CD39 (right plot) in $CD8^+$ TILs. Means and SEMs are shown and Mann-Whitney tests were performed in case of tumor analysis, whereas unpaired t tests were used for interim blood analyses. Ns = not significant ($p \geq 0.05$), * = $p < 0.05$, ** = $p < 0.01$, *** = $p < 0.001$, **** = $p < 0.0001$. anti-PD-L1 = anti-PD-L1 antibody i.p. = intraperitoneal, i.pl.= intrapleural, i.v.= intravenous, TDLN = tumor-draining lymph node, Th cells = T-helper cells.▸

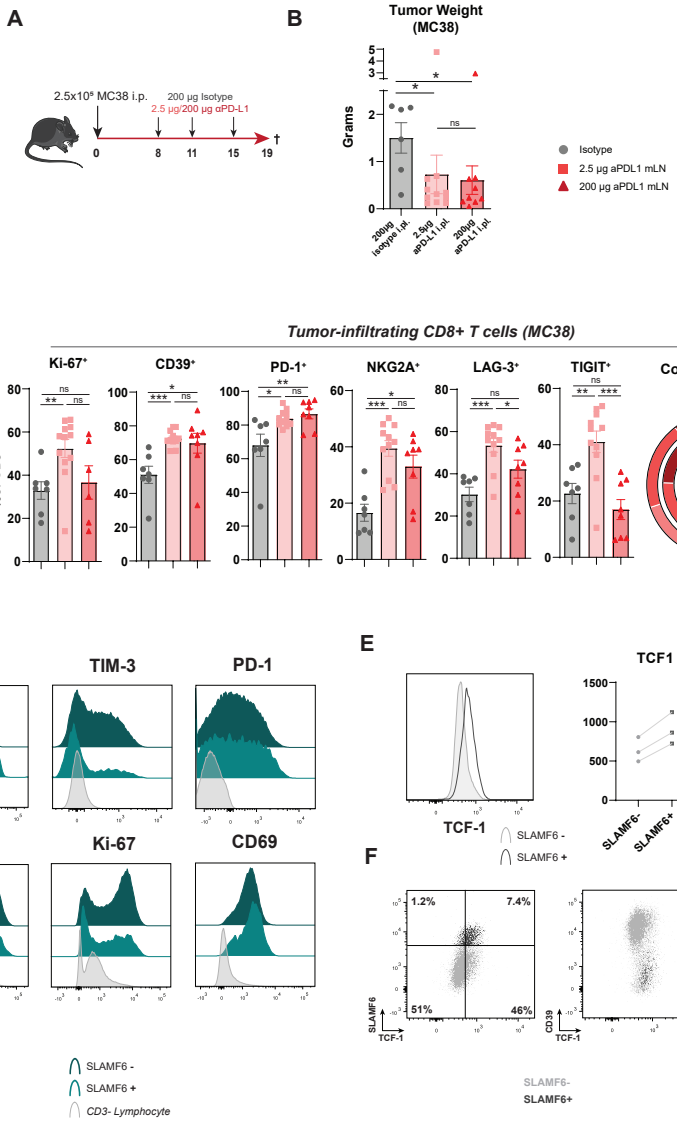
A
2.5x10⁵ MC38 i.p.
200 µg Isotype
2.5 µg/200 µg αPD-L1
0
8
11
15
19
†
B
Tumor Weight (MC38)
Grams
Isotype
2.5 µg aPDL1 mLN
200 µg aPDL1 mLN
C
Tumor-infiltrating CD8+ T cells (MC38)
Ki-67+ CD4+ cells
%of Foxp3- CD4+
Ki-67+
CD39+
PD-1+
NKG2A+
LAG-3+
TIGIT+
Co-expression
%of CD8+
Neg
SP
DP
TP
QP
D
TOX
TIM-3
PD-1
CD39
Ki-67
CD69
SLAMF6 -
SLAMF6 +
CD3- Lymphocyte
E
TCF1
TCF-1
SLAMF6 -
SLAMF6 +
SLAMF6-
SLAMF6+
F
1.2%
7.4%
51%
46%
SLAMF6
TCF-1
CD39
TCF-1
SLAMF6-
SLAMF6+

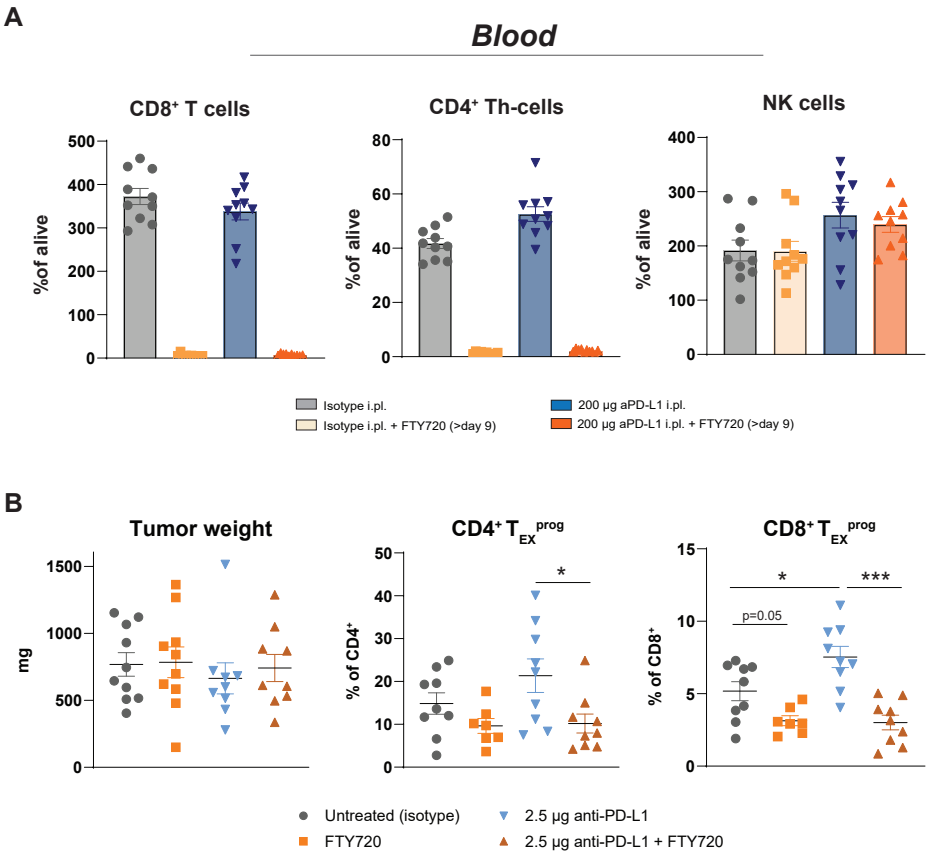

Figure S6. (A) Comparison of frequencies of CD8⁺ T cells, CD4⁺ Th-cells and NK cells in peripheral blood of AC29 tumor-bearing mice isolated at day 14 (4 days after first anti-PD-L1 treatment (200µg i.p.) and 5 days after start FTY720). (B) AC29 tumor-bearing mice received S1P receptor agonist FTY720 via drinking water and oral gavage at day 9-20 and isotype or TDLN-local anti-PD-L1 treatment (2.5 µg) i.p. at day 10, 13 and 17. Mice were sacrificed at day 20 followed by tumor isolation, enzymatic digestion and staining of tumor tissue for flow cytometry. Tumor weight was determined after isolation. Frequency of CD4⁺ and CD8⁺ T_{EX}^{prog} cells was determined for total CD4/8⁺ TILs. Means and SEMs are shown. Mann-Whitney tests were performed. ns = not significant ($p \geq 0.05$), * = $p < 0.05$, *** = $p < 0.001$, i.pl. = intrapleural, SEM = standard error of the mean.

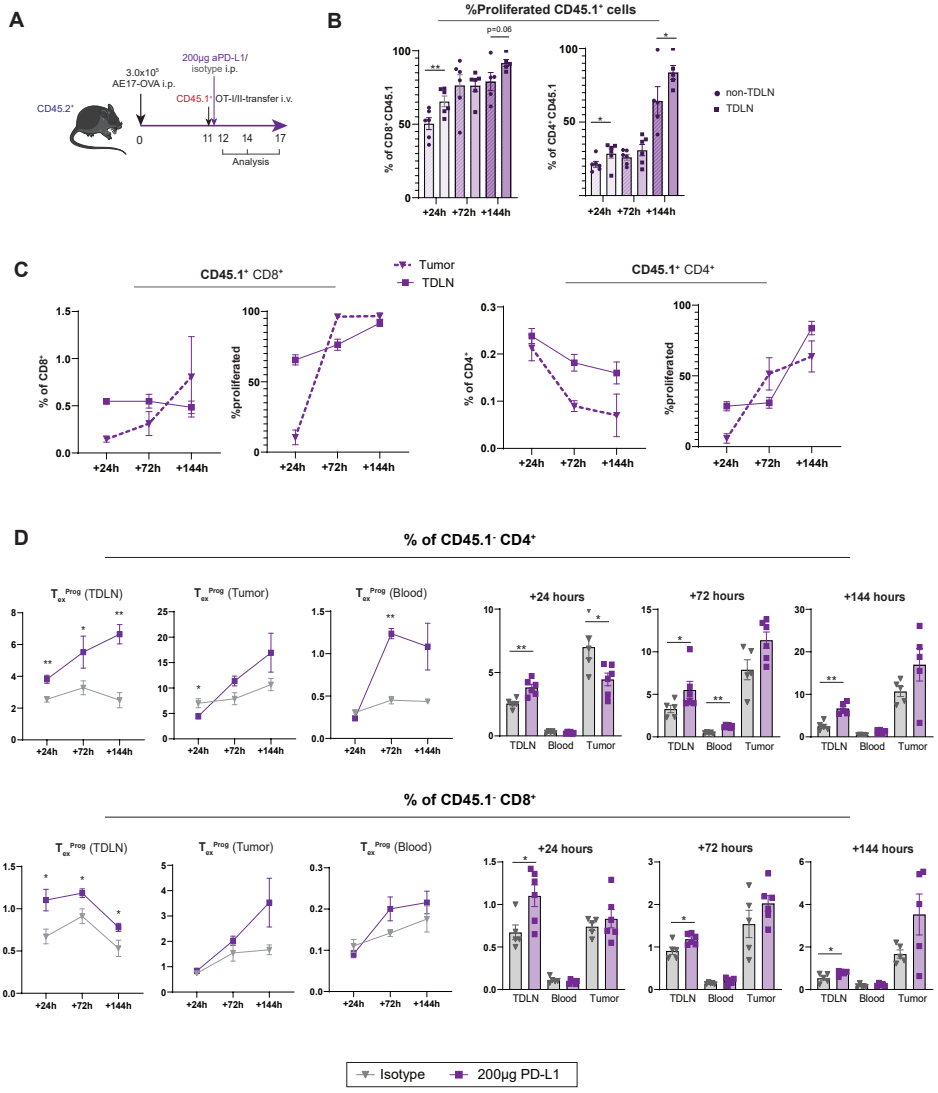

Figure S7. (A) Wildtype CD45.2⁺ congenic mice injected i.p. with AE17-OVA tumor cells received cell-trace labeled CD45.1⁺ OT-I and OT-II cells i.v. at day 11 followed by i.p. injection of isotype or anti-PD-L1 therapy (200 µg) at day 11 and mice were sacrificed (n = 5 to 6 mice per group per time point) at day 12, 14 and 17. (B) Percentage of proliferated CD45.1⁺ cells of the CD45.1⁺ CD8⁺ T cell population in and CD45.1⁺ CD4⁺ T cell population in TDLN and non-TDLN. (C) Graphs showing frequencies of CD45.1⁺ cells of CD8⁺ and CD4⁺ T cells and percentage of proliferated CD45.1⁺ CD4/8⁺ T cells isolated from TDLN and tumor (dotted line) at indicated time points in anti-PD-L1 treated animals. (D) Endogenous (CD45.1⁻) T_{EX}^{prog} CD4⁺ (above) and CD8⁺ (below) cells in TDLN, blood and tumor 24, 72 and 144 hours post a one-time systemically administered dose of anti-PD-L1 (200 µg) visualized through time (left) or per tissue (right). * = $p < 0.01$, T_{EX}^{prog} = progenitor-exhausted T cells. i.v. = intravenous, i.p. = intraperitoneal, i.pl. = intrapleural, TDLN = tumor-draining lymph node.

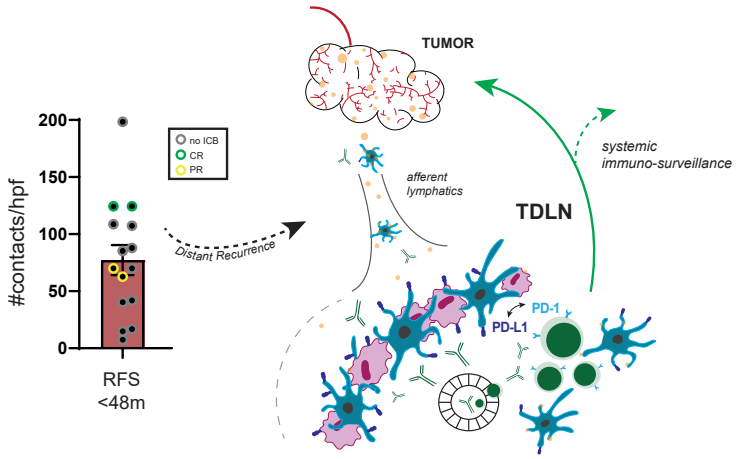

Figure S8. Graphical abstract including patients not receiving immunotherapy at distant disease recurrence (gray) and those experiencing complete response (CR, green) or partial response (PR, yellow) following PD-1 (-containing) immunotherapy are highlighted from the graph in Fig. 8A.

Table S1. Clinicopathological descriptives of all samples, and per subgroup (recurrence < 48 months vs. no recurrence > 96 months), n (%) or median (IQR).

Characteristics	All patients (n=30)	Recurrence <48mo (n=16)	No recurrence >96mo (n=15)	P value
Patient characteristics				
Age	**50** (41 – 59)	**55** (49 – 63)	**43** (35 – 52)	0.006
Sex				0.005
Male	**20** (67)	**14** (93)	**6** (40)	
Female	**10** (33)	**1** (7)	**9** (60)	
Tumor characteristics				
Breslow, mm	**2.4** (1.8 – 4.9)	**3.7** (2.3 – 6.0)	**2.0** (1.3 – 2.6)	0.002
Ulceration				0.003
Absent	**17** (68)	**6** (43)	**11** (100)	
Present	**8** (32)	**8** (57)	**0**	
Unknown	**5**	**1**	**4**	
Histology				0.001
SSM	**18** (67)	**6** (40)	**12** (100)	
NM	**8** (30)	**8** (53)	**0**	
Other	**1** (4)	**1** (7)	**0**	
Unknown	**3**	**0**	**3**	

Table S1. Continued

Characteristics Patient characteristics	All patients (n=30)	Recurrence <48mo (n=16)	No recurrence >96mo (n=15)	P value
Location				0.324
Arm	**6** (20)	**3** (20)	**3** (20)	
Leg	**7** (23)	**2** (13)	**5** (33)	
Trunk	**16** (53)	**10** (67)	**6** (40)	
Head & Neck	**1** (3)	**0**	**1** (7)	
SLN surgical removal				
No. of SNs	**1.0** (1.0 – 2.0)	**1.0** (1.0 – 2.0)	**1.0** (1.0 – 2.0)	0.233
SN Region				0.245
Axillar	**20** (67)	**12** (80)	**8** (53)	
Inguinal-iliac	**9** (30)	**3** (20)	**6** (40)	
Cervical	**1** (3)	**0**	**1** (7)	
Outcome				
Time to distant metastasis, months		21 (9-36)	N/A	-
Status* [median time to status, months]				-
NED		N/A	**15** (100) [108.0]	
CR		**2** (13) [21.0]	N/A	
AWD		**2** (13) [57.5]	N/A	
DOD		**11** (73) [25.0]	N/A	
Site(s) of first distant recurrence			N/A	-
One metastatic organ				
Lung only		**4** (27)		
Brain only		**2** (13)		
Other		**1** (7)		
Multiple metastatic organs		**8** (53)		

** No evidence of disease (NED), Complete response (CR), Alive with disease (AWD), Dead of disease (DOD)*

Methods S1. Automatic quantification of PLA on melanoma sentinel lymph nodes using ImageJ software and corresponding macros. PLA = proximity ligation assay

The following macro scripts were designed and used to quantify PD-1/PD-L1 interaction density at TDLN slides of at 40X magnification. A total of 15 images per TDLN were randomly selected from the LN cortex, excluding images containing germinal centers. These images were then loaded into ImageJ software (ImageJ, V1.52, Fuji platform) and the macros below were run, with the results from 2, being taken as a percentage of 1, establishing the percentage of cell surface area positive for PD-1/PD-L1.

Macro 1

```
run("Color Threshold...");
// Color Thresholder 2.0.0-rc-69/1.52s
// Autogenerated macro, single images only!
min=newArray(3);
max=newArray(3);
filter=newArray(3);
a=getTitle();
run("HSB Stack");
run("Convert Stack to Images");
selectWindow("Hue");
rename("0");
selectWindow("Saturation");
rename("1");
selectWindow("Brightness");
rename("2");
min[0]=0;
max[0]=255;
filter[0]="pass";
min[1]=0;
max[1]=255;
filter[1]="pass";
min[2]=205;
max[2]=255;
filter[2]="stop";
for (i=0;i<3;i++){
  selectWindow(""+i);
  setThreshold(min[i], max[i]);
  run("Convert to Mask");
  if (filter[i]=="stop")  run("Invert");
}
imageCalculator("AND create", "0","1");
imageCalculator("AND create", "Result of 0","2");
for (i=0;i<3;i++){
  selectWindow(""+i);
  close();
}
selectWindow("Result of 0");
close();
```

```
selectWindow("Result of Result of 0");
rename(a);
// Colour Thresholding----------
run("Measure");
```

Macro 2

```
rename("test.jpg");
run("Split Channels");
selectWindow("test.jpg (blue)");
setAutoThreshold("Default");
//run("Threshold...");
setThreshold(0, 195);
setThreshold(0, 108);
run("Measure");
```

Chapter 3

Immune suppression in the tumor-draining lymph node corresponds with distant disease recurrence in patients with melanoma

Anneloes van Krimpen, Mandy van Gulijk, Vivian I. V. Gerretsen, Evalyn E.A.P. Mulder, Thierry P.P. van den Bosch, Jan von der Thusen, Dirk J. Grünhagen, Cornelis Verhoef, Dana Mustafa, Joachim G. Aerts, Ralph Stadhouders, Floris Dammeijer

Cancer Cell 2022 Aug 8;40(8):798-799

Immune checkpoint blockade (ICB) using anti-PD-1/PD-L1 and anti-CTLA-4 antibodies significantly enhances survival in metastatic melanoma patients and has recently been shown to prolong relapse-free survival in stage III and high-risk stage II melanoma patients [1-3]. However, a significant proportion of patients does not respond to ICB prior to or following surgery for reasons incompletely understood. We and others recently identified tumor-draining lymph nodes (TDLNs) to be critically involved in anti-PD-L1 treatment efficacy in preclinical tumor models [4,5]. Furthermore, we found that abundant PD-1 and PD-L1 interactions in TDLNs of patients with non-metastatic melanoma at presentation were associated with distant disease recurrence suggesting that immune suppression in TDLNs might prevent a durable and effective systemic anti-tumor immune response. However, it remains incompletely understood which cells and pathways - including their spatial tissue localization - within TDLNs promote disease recurrence in melanoma. Here, we address these issues by analyzing the immune composition in TDLNs of stage III melanoma patients using multiplexed gene expression analysis, digital spatial profiling (DSP) and multi-color confocal imaging.

We selected 20 stage III melanoma patients who underwent surgical resection of the primary tumor and the TDLN (sentinel lymph node procedure), consisting of 10 patients with distant visceral organ metastasis within 24 months after surgery (Recurrence group) and 10 patients who were disease-free after a minimal follow-up of 5 years (No Recurrence group) (Fig. S1A, Table S1A). We performed Nanostring whole-slide gene expression analysis (n = 730 genes) of TDLNs following microscopic excision of metastases to exclude tumor-infiltrating leukocytes. Differential gene expression analysis identified a total of 94 differentially expressed genes, of which 74 were upregulated in the No Recurrence group (Fig. S1B). Genes upregulated in patients without recurrence were associated with lymphocyte activation (Fig. S1C-D), suggesting that increased T cell activation in TDLNs could be involved in anti-tumor immune control. In contrast, a type II interferon response signature was upregulated in patients with recurrence, which has previously been associated with immune suppression in TDLNs and ICB-resistance in preclinical models [6,7] (Fig. S1C-D).

As lymph nodes are functionally and architecturally heterogeneous, site-specific immune processes are obscured by bulk tissue analyses. Therefore, we performed digital spatial profiling (DSP) on TDLNs from a subset of the patients (Fig. S1A, Table S1B), all with macrometastasis in the TDLN, according to the Rotterdam criteria [8]. Breslow depths and the presence of ulceration were comparable. A targeted 58-protein immunology-oncology marker panel was quantified within regions of interest (ROIs) within the TDLN at the invasive tumor margin ('proximal', n = 3 per patient) or at unaffected ('distant', n = 2 per patient) areas. These ROIs were selected based on CD11c, CD3 and S100B immunofluorescence signals (Fig. S1E-F). Principal component analysis revealed significant clustering of proximal and distant ROIs irrespective of patient outcome (Fig. S1G), suggesting distinct immune activity occurring throughout different regions of the TDLN. Most variation in protein expression between patient groups, however, occurred in distant interfollicular areas of the TDLN (Fig. S1G-H). Notably, patients with disease recurrence demonstrated increased

expression of key effector T cell suppressive proteins including CTLA-4, IDO1, PD-L1 and FOXP3 (Fig. S1I-J). Collectively, these data suggest that disease recurrence is associated with immune suppression distant from tumor metastases within the TDLN of melanoma patients.

To evaluate whether the upregulated lymphocyte activation gene signature detected by whole-slide bulk analysis (Fig. S1C) is related to decreased immune suppression, specifically in distant ROIs, we correlated both bulk and spatial measurements from the same patients (Fig. S1K). Whereas several myeloid cell markers (e.g. CD68, CD14, CD11c) and the immune-stimulatory protein STING were strongly associated with lymphocyte activation, immune-suppressive proteins increased in distant ROIs from patients with recurrence (e.g. CTLA-4, PD-L1, IDO1) were inversely correlated with the lymphocyte activation gene module from our bulk analysis (Fig. S1K). Notably, we observed significant downregulation of these inhibitory proteins in the distant regions of patients without recurrence (Fig. S1L). To confirm these findings and identify the cellular origins of these TDLN immune-suppressive molecules, we performed multi-color confocal imaging focused on IDO1 or PD-L1 expression on different immune cells from our DSP ROIs and used machine learning to quantify cell type-specific expression. We observed increased frequencies of $IDO1^+$ and $PD\text{-}L1^+$ cells in distant regions of TDLNs from patients with recurrence, involving different types of immune cells (Fig. S1M-N). $PD\text{-}L1^+$ DCs in TDLNs have been found to limit anti-tumor immunity [4,9]. We found $PD\text{-}L1^+$ DCs to be significantly increased in distant areas of TLDNs from patients developing distant disease recurrence (Fig. S1N-P). Importantly, these cells frequently interacted with $CD8^+$ T cells (Fig. S1Q), confirming anti-tumor immune suppression occurring in regions of the melanoma TDLN that are spatially distant from the tumor itself.

We hypothesized that differences in immune contexture of TDLNs would underlie the presence of effective anti-tumor immunity and hence influence the risk of developing distant disease recurrence in melanoma. Our experiments indicate that disease recurrence is not dictated by an immune response in perimetastatic regions of the TDLN, but is rather driven by lymphocyte activation or suppression in distant areas of the TDLN. These data confirm and complement recent findings by Reticker-Flynn *et al.* demonstrating that murine melanoma cells shape the TDLN immune environment resulting in not only local TDLN immune suppression but also promoting distant organ metastasis[7]. Intriguingly, they could detect a type II interferon signature driving increased suppression of T cells in TDLNs through upregulation of PD-L1, which is strikingly analogous to our findings in melanoma patient tissues. Although we could not analyze distant visceral organ metastasis material in our melanoma patient cohort, our data support increased immune suppression within the TDLN - specifically in regions segregated from the metastatic part of the node- as a potential mediator of failed systemic anti-tumor immunity. Together, these observations suggest that the interaction between the primary tumor and the TDLN determines systemic anti-tumor immunity and risk of distant metastasis formation, thus impacting patient survival.

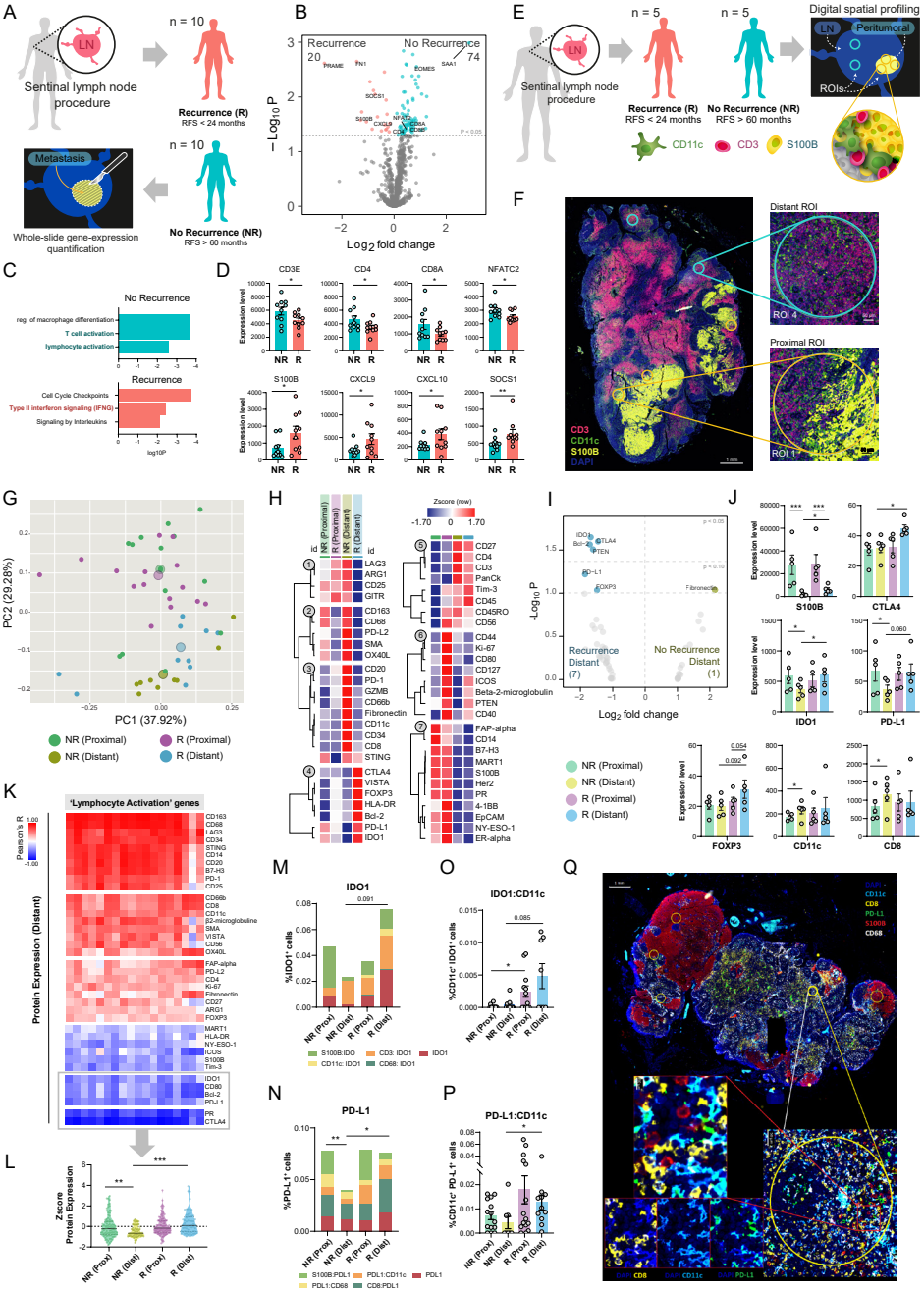
A
Sentinal lymph node procedure
LN
n = 10
Recurrence (R)
RFS < 24 months
n = 10
No Recurrence (NR)
RFS > 60 months
Metastasis
Whole-slide gene-expression quantification
B
Recurrence
No Recurrence
20
74
PRAME
FN1
TOMM5
SAA1
SOCS1
S100B
CXCL9
NFATC2
CXCL10
CD8A
CD4
CD3E
SMA
P = 0.05
−Log10 P
Log2 fold change
C
No Recurrence
reg. of macrophage differentiation
T cell activation
lymphocyte activation
Recurrence
Cell Cycle Checkpoints
Type II interferon signaling (IFNG)
Signaling by Interleukins
log10P
D
CD3E
CD4
CD8A
NFATC2
S100B
CXCL9
CXCL10
SOCS1
Expression level
NR
R
E
Sentinal lymph node procedure
LN
n = 5
n = 5
Recurrence (R)
RFS < 24 months
No Recurrence (NR)
RFS > 60 months
CD11c
CD3
S100B
Digital spatial profiling
LN
Peritumoral
ROIs
F
CD3
CD11c
S100B
DAPI
Distant ROI
ROI 4
Proximal ROI
ROI 11
G
PC2 (29.28%)
PC1 (37.92%)
NR (Proximal)
R (Proximal)
NR (Distant)
R (Distant)
H
Zscore (row)
-1.70
0
1.70
id
LAG3
ARG1
CD25
GITR
CD163
CD68
PD-L2
SMA
OX40L
CD20
PD-1
GZMB
CD66b
Fibronectin
CD11c
CD34
CD8
STING
CTLA4
VISTA
FOXP3
HLA-DR
Bcl-2
PD-L1
IDO1
CD27
CD4
CD3
PanCk
Tim-3
CD45
CD45RO
CD56
CD44
Ki-67
CD80
CD127
ICOS
Beta-2-microglobulin
PTEN
CD40
FAP-alpha
CD14
B7-H3
MART1
S100B
Her2
PR
4-1BB
EpCAM
NY-ESO-1
ER-alpha
I
IDO1
Bcl-2
CTLA4
PTEN
PD-L1
FOXP3
Fibronectin
Recurrence
Distant
(7)
No Recurrence
Distant
(1)
-Log10 P
Log2 fold change
NR (Proximal)
NR (Distant)
R (Proximal)
R (Distant)
J
S100B
CTLA4
IDO1
PD-L1
FOXP3
CD11c
CD8
Expression level
K
'Lymphocyte Activation' genes
Pearson's R
Protein Expression (Distant)
CD163
CD68
LAG3
CD34
STING
CD14
CD20
B7-H3
PD-1
CD25
CD66b
CD8
CD11c
β2-microglobuline
SMA
VISTA
CD56
OX40L
FAP-alpha
PD-L2
CD4
Ki-67
Fibronectin
CD27
ARG1
FOXP3
MART1
HLA-DR
NY-ESO-1
ICOS
S100B
Tim-3
IDO1
CD80
Bcl-2
PD-L1
PR
CTLA4
L
Zscore Protein Expression
NR (Prox)
NR (Dist)
R (Prox)
R (Dist)
M
IDO1
%IDO1+ cells
S100B:IDO
CD3: IDO1
IDO1
CD11c: IDO1
CD68: IDO1
O
IDO1:CD11c
%CD11c+ IDO1+ cells
N
PD-L1
%PD-L1+ cells
S100B:PDL1
PDL1:CD11c
PDL1
PDL1:CD68
CD8:PDL1
P
PD-L1:CD11c
%CD11c+ PD-L1+ cells
Q
CD11c
CD8
PD-L1
S100B
CD68
DAPI
DAPI CD8
DAPI CD11c
DAPI PD-L1

◂Figure 1: Stage III melanoma patients with distant metastasis show increased immune suppression within the tumor-draining lymph node in areas segregated from the metastatic site

(A) Experimental set-up of NanoString whole-slide targeted gene expression profiling (PanCancer Immune Profiling panel, n = 730 genes) of TDLNs (metastases were removed) from patients that either developed recurrence (R) (RFS < 24 months, n = 10) or remained long-term disease-free (no recurrence, NR) (RFS > 60 months, n = 10). (B) Volcano plot showing differentially expressed genes (P < 0.05) in TDLNs from patients with or without recurrence. (C) Pathway enrichment analysis of differentially expressed genes from panel B. (D) Normalized expression levels of selected genes, displayed as mean +/- SEM. (E) Experimental setup for Nanostring digital spatial profiling (DSP) analysis of TDLNs from patients that either developed recurrence (R) (RFS < 24 months, n = 5) or remained long-term disease-free (no recurrence, NR) (RFS > 60 months, n = 5). Regions of interest (ROIs) were selected using morphological markers CD11c, CD3, S100B and DAPI. For each patient, regions proximal to metastasis (n = 3) and distant to metastasis (n = 2) were selected. (F) Representative image of TDLN tissue used for DSP analysis stained with morphological markers CD11c (green), CD3 (magenta), S100B (yellow) and DAPI (blue) to select ROIs. (G) Principal Component Analysis of normalized protein expression levels (n = 58 markers) measured by DSP. Larger circles denote median expression values of the four indicated ROI groups. (H) Heatmap of median normalized protein expression levels measured by DSP clustered hierarchically. Numbers indicate different clusters identified. (I) Volcano plot of differentially expressed proteins measured by DSP (P < 0.10 or P < 0.05 thresholds are indicated). (J) Median expression levels of selected proteins from proximal and distant ROIs, displayed as mean +/- SEM. (K) Pearson's R correlation plot of gene expression values of 'lymphocyte activation' genes (whole-slide gene expression profiling, panel C, n = 18 genes) with protein expression data (DSP) of matched patients (Recurrence, R, n = 4; no recurrence, NR, n = 2). (L) Scaled (z-score) expression levels of proteins negatively correlated with 'lymphocyte activation' genes (panel K, Pearson's R≤-0.6, n = 6). Individual dots represent expression of one protein of one patient within the associated group. (M-N) TDLN tissue was stained for IDO1, CD3, CD11c, S100B and CD68 (panel M) or for PD-L1, CD8, CD11c, S100B and CD68 (panel N) and visualized using confocal imaging (Recurrence, R, n = 5; no recurrence, NR, n = 4 or 5). The number of cells expressing each marker was quantified and visualized as a percentage of total nuclei inside an ROI, matched with its original location in the DSP analysis. Statistical significance was determined on the total number of IDO1 (panel M) or PD-L1 (panel N) expressing cells. (O-P) Percentage of $CD11c^+$ IDO1+ (panel O) or $CD11c^+$ $PD\text{-}L1^+$ (panel P) cells compared with total nuclei quantified inside an ROI. Shown are mean +/- SEM. (Q) Representative TDLN section of a patient with recurrent disease showing co-localization of PD-L1+ $CD11c^+$ cells (green, blue) and $CD8^+$ T cells (yellow) within a distant ROI. Linear Mixed Model (LMM) tests as implemented by nSolver Analysis Software (v4.0) and the Advanced Analysis module (v2.0) (Nanostring Technologies) were used to determine statistical significance in panels B-D and I-J). Statistical significance in panels L and M-P was determined using a Mann Whitney U test. * = p < 0.05, ** = p < 0.01, *** = p < 0.001.

References

1. Robert, C.*, et al.* Nivolumab in previously untreated melanoma without BRAF mutation. *The New England journal of medicine* **372**, 320-330 (2015).
2. Eggermont, A.M.M.*, et al.* Adjuvant Pembrolizumab versus Placebo in Resected Stage III Melanoma. *New England Journal of Medicine* **378**, 1789-1801 (2018).
3. Luke, J.J.*, et al.* Pembrolizumab versus placebo as adjuvant therapy in completely resected stage IIB or IIC melanoma (KEYNOTE-716): a randomised, double-blind, phase 3 trial. *Lancet* **399**, 1718-1729 (2022).
4. Dammeijer, F.*, et al.* The PD-1/PD-L1-Checkpoint Restrains T cell Immunity in Tumor-Draining Lymph Nodes. *Cancer cell* **38**, 685-700.e688 (2020).
5. Fransen, M.F.*, et al.* Tumor-draining lymph nodes are pivotal in PD-1/PD-L1 checkpoint therapy. *JCI insight* **3**(2018).
6. Benci, J.L.*, et al.* Tumor Interferon Signaling Regulates a Multigenic Resistance Program to Immune Checkpoint Blockade. *Cell* **167**, 1540-1554.e1512 (2016).
7. Reticker-Flynn, N.E.*, et al.* Lymph node colonization induces tumor-immune tolerance to promote distant metastasis. *Cell* **185**, 1924-1942 e1923 (2022).
8. van Akkooi, A.C., de Wilt, J.H., Verhoef, C. & Eggermont, A.M. The Rotterdam criteria for sentinel node tumor load: the simplest prognostic factor? *Journal of clinical oncology : official journal of the American Society of Clinical Oncology* **26**, 6011; author reply 6012 (2008).
9. Maier, B.*, et al.* A conserved dendritic-cell regulatory program limits antitumour immunity. *Nature* **580**, 257-262 (2020).

Supplementary data

Table 1A. Whole-slide gene expression analysis: baseline patient & tumor characteristics; n (%) or median (interquartile range)

Characteristics	All patients (n=20)	Recurrence <24mo (n=10)	No recurrence >60mo (n=10)	P value
Patient characteristics				
Age	54 (46-63)	49 (45-62)	54 (47 – 66)	0.920
Sex				0.739
Male	9 (45)	4 (40)	5 (50)	
Female	11 (55)	6 (60)	5 (50)	
Tumor characteristics				
Breslow, mm	3.80 (2.53-4.83)	4.10 (3.07-5.50)	2.60 (1.38-4.38)	0.851
Location				0.436
Leg	7 (35)	5 (50)	2 (20)	
Trunk	12 (60)	4 (40)	8 (80)	
Head & Neck	1 (5)	1 (10)	0 (0)	
Histology				0.912
SSM	6 (30)	4 (40)	2 (20)	
NM	12 (60)	4 (40)	8 (80)	
ALM	2 (10)	2 (20)	0 (0)	
Ulceration				0.739
Absent	9 (45)	4 (40)	5 (50)	
Present	11 (55)	6 (60)	5 (50)	
BRAF status				0.280
Negative	17 (85)	7 (70)	10 (100)	
Positive	2 (10)	2 (20)	0 (0)	
Unknown	1 (5)	1 (10)	0 (0)	
No of positive SNs	1.00 (1.00-2.00)	1.00 (1.00-2.00)	1.50 (1.00-2.25)	0.280
Tumor burden, mm	1.30 (0.73-2.00)	2.00 (1.43-5.85)	0.76 (0.38-1.10)	0.000
Rotterdam criteria				0.002
<0.1mm	1 (5)	0 (0)	1 (10)	
≥0.1mm ≤ 1.0 mm	7 (35)	0 (0)	7 (70)	
>1.0 mm	12 (60)	10 (100)	2 (20)	
DEWAR				0.853
Subcap	5 (25)	2 (20)	3 (30)	
Combined	8 (40)	5 (50)	3 (30)	
Parenchymal	3 (15)	1 (10)	2 (20)	
Multifocal	2 (10)	0 (0)	2 (20)	

Table 1A. Continued

Characteristics	All patients (n=20)	Recurrence <24mo (n=10)	No recurrence >60mo (n=10)	P value
Extensive	2 (10)	2 (20)	0	
Time				
Time from primary excision to SN (months)	2 (1-2)	1.5 (1-2)	2 (1-3)	0.481
Time from SN procedure to first Metastatic recurrence (months)	12 (7-16)	12 (7-16)	>64	X

Abbreviations: SN*, sentinel node*

Table 1B. Digital spatial profiling (DSP) analysis: clinicopathological features of all samples, and per subgroup (recurrence <24 months vs. no recurrence >60 months), n (%) or median (IQR).

Characteristics	All patients (n=10)	Recurrence <24mo (n=5)	No recurrence >60mo (n=5)	P value
Patient characteristics				
Age	54 (31-66)	61 (47-64)	60 (43-62)	0.691
Sex				>0.999
Male	4 (40)	2 (40)	2 (40)	
Female	6 (60)	3 (60)	3 (60)	
Tumor characteristics				
Breslow, mm	3.2 (2.4-4.1)	3.1 (2.5 – 4.2)	3.2 (2.3-3.8)	>0.999
Tumor Burden. mm	6.8 (2.0 – 7)	6.8 (2.0-7)	6.0 (2.0-7.0)	>0.999
Ulceration				0.665
Absent	2 (20)	1 (20)	1 (20)	
Present	8 (80)	4 (80)	4 (80)	
Unknown				
Histology				0.879
SSM	5 (50)	4 (80)	1 (20)	
NM	4 (40)	1 (20)	3 (60)	
Other	0 (0)	0 (0)	0 (0)	
Unknown	1 (10)	0 (0)	1 (20)	
Location				>0.999
Arm	1 (10)	1 (20)	0 (0)	
Leg	3 (30)	1 (20)	2 (40)	
Trunk	5 (50)	2 (40)	3 (60)	
Head & Neck	1 (10)	1 (20)	0 (0)	
SLN surgical removal				

Table 1B. Continued

Characteristics	All patients (n=10)	Recurrence <24mo (n=5)	No recurrence >60mo (n=5)	P value
SN Region				0.822
Axillar		3 (60)	3 (60)	
Inguinal-iliac		1 (20)	2 (40)	
Cervical		1 (20)	0 (0)	
Outcome				
Time to distant metastasis, months		12 (7 – 16)	N/A	-
Status* [median time to status, months]				-
NED	5 (50)	0 (0)	5 (100)	
DOD	5 (50)	5 (100)	0 (0)	
Site(s) of first distant recurrence				-
Multiple metastatic organs		5 (100)	0 (0)	
Lymph node		4 (80)	-	
Lung		5 (100)	-	
Bone		1 (20)	-	
Liver		2 (40)	-	
Other		1 (20)	-	

Abbreviations: SSM, superficial spreading melanoma; NM, nodular melanoma, NED, no evidence of disease; DOD, dead of disease

Methods

Patient selection

From patients who underwent a sentinel lymph node procedure at the Erasmus MC Cancer Institute between 2005 and 2017, individuals with nodal metastasis (i.e. positive tumor-draining lymph nodes (TDLN)) were identified. For comparative purposes, we selected patients that either presented with early (< 24 months) distant disease recurrence or that did not develop disease recurrence for at least 60 months following sentinel lymph node procedure. In an attempt to avoid including a false negative TDLN, we only included patients with a negative TDLN who developed (prior) metastatic disease within the regional lymph nodes (similar to the TDLN basin) after ≥ 9 months.

Ethics approval

This study was approved by the Erasmus MC Ethics Committee (MEC-2017-375). All patients provided written informed consent and human tissues and patient data were used according to 'The Code for Proper Secondary Use of Human Tissue' and 'The Code of Conduct for the Use of Data in Health Research' as stated by the Federation of Dutch Medical Scientific Societies.

Tissue samples

Formalin-fixed paraffin-embedded (FFPE) lymph node samples were retrieved from the Erasmus MC Pathology department. The study was designed as a case-control study, each group consisted of ten samples of lymph nodes. Hematoxylin-Eosin (H&E) stained 5µm sections from each sample were evaluated by an experienced pathologist. For targeted gene expression profiling, tumor infiltrated areas were excluded from RNA isolation. For Digital Spatial Profiling, five lymph nodes were selected for each patient group.

RNA isolation and quality control

Depending on the size of the lymph nodes, 10-15 sections of 10µm FFPE samples were used to isolate RNA. Sections were deparaffinized using Xylene, after which they were washed using series dilutions of ethanol and finally washed with water. The total RNA was isolated using the RNeasy Plus Micro Kit (Qiagen) according to the manufacturer's protocol. RNA quality and quantity was determined using the Agilent 2100 Bio-analyzer (Agilent, CA, USA), after which the concentration was adjusted for use in NanoString technology.

Targeted gene expression profiling using NanoString® Technology

The PanCancer Immune Profiling panel of NanoString® technology was used to profile the samples. The panel consists of 730 immune-related genes and 40 housekeeping (HK) genes. A total of 300 ng/ 5µl of good quality RNA (≥300 bp fractions) were hybridized for 17 hours at 65°C overnight. The nCounter FLEX platform was used to wash away the excess of unhybridized probes following the manufacturer's recommendations. Genes were counted by scanning 490 Fields-Of-View (FOV). Gene expression values were normalized using nSolver® software (version 4.0) and differential expression analysis was performed using the the Advanced Analysis module (version 2.0) of NanoString (NanoString, Seattle, WA, USA).

Nanostring GeoMX Digital Spatial Profiling (DSP)

TDLN slides were stained and analysed on the Nanostring GeoMx® Digital Spatial Profiling (DSP) platform. Regions of interest were selected using morphological markers CD11c, CD3 and S100B. Regions were selected either peritumorally (proximal, n = 3) or distant of the metastasis (distant, n = 2) and assessed by an experienced pathologist. The protein panel consisted of Nanostring modules 'Immuno-Oncology (IO) Drug Targeting', 'Immune Cell Activation Status' and 'Immune Cell Typing' (n= 58 markers). Slides were processed as per manufacturer's instructions. Antibody barcodes were counted on the nCounter® platform as per manufacturer's instructions and External RNA Controls Consortium (ERCC) QC were performed in the DSP analysis suite prior to outputting data for bioinformatic analysis. Data was normalized using S6 and GAPDH as positive controls, as well region size and nuclei count. Differential expression analysis was performed using a Linear Mixed Model test as implemented by nSolver® (version 4.0) and the Advanced Analysis module (version 2.0) of NanoString (NanoString, Seattle, WA, USA).

Bioinformatic Analysis and Visualisation

Volcanoplots were generated using 'EnhancedVolcano'(v1.10.0) [10] in R (v4.1.2). Pathways enrichment analysis was performed using the online tool Metascape(v3.5) [11] against a custom background consisting of all genes included in the Nanostring® PanCancer Immune Profiling panel. The Principal Component Analysis was performed using the package 'ggfortify'(v4.14) [12]. Heatmaps were generating using web-based tool Morpheus [13] and clustered hierarchically using the Pearson's minus One correlation setting.

Correlation of Nanostring and DSP data

Expression of genes belonging to the 'Lymphocyte activation' pathway (n = 18 genes) were correlated with protein-expression of patients of whom we had matching gene- and protein-expression data (Recurrence: n = 4; No-Recurrence: n = 2) using Pearson's R calculated by the 'Hmisc' R package (v4.6-0) [14]. Z-scores were calculated for proteins negatively correlated with the 'lymphocyte activation' signature ($R \leq -0.6$) and visualised using Prism GraphPad®.

Automated Multiplex Immunofluorescent Staining and celltype quantification

5-plex staining with 2 different panels was done by automated multiplex IF using the Ventana Benchmark Discovery (Ventana Medical Systems Inc.). In brief for Panel 1, following deparaffinization and heat-induced antigen retrieval with CC1 (#950-500, Ventana) for 32 minutes at 97°C, the tissue samples were incubated firstly with CD8 for 32 minutes at 37˚C followed by detection with omnimap anti-rabbit HRP (#760-4311, Ventana) for 16 minutes followed by visualization with R6G (#760-244, Ventana) for 4 minutes. Antibody denature step was performed using CC2 (#950-123, Ventana) for 20 minutes at 100˚C. Secondly, CD11c was incubated for 60 minutes at 37˚C followed by detection with omnimap anti-mouse HRP (#760-4310, Ventana) for 16 minutes followed by visualization with DCC for 8 minutes (#760-240, Ventana). Antibody denature step was performed using CC2 (#950-123, Ventana) for 20 minutes at 100˚C. Thirdly, S100 was incubated for 32 minutes at 37 ˚C followed by detection with omnimap anti-rabbit HRP (#760-4311, Ventana) for 16 minutes followed by visualization with Red610 for 8 minutes (#760-235, Ventana). Antibody denature step was performed using CC2 (#950-123, Ventana) for 20 minutes at 100˚C. Fourthly, CD68 was incubated for 60 minutes at 37˚C followed by detection with omnimap anti-mouse HRP (#760-4310, Ventana) for 16 minutes followed by visualization with Cy5 for 8 minutes (#760-238, Ventana). Antibody denature step was performed using CC2 (#950-123, Ventana) for 8 minutes at 100˚C. Lastly, PDL1 SP263 was incubated for 60 minutes at 37˚C followed by detection with omnimap anti-rabbit HRP (#760-4311, Ventana) followed by visualization with FAM (#760-243, Ventana) for 4 minutes.

In brief for Panel 2, following deparaffinization and heat-induced antigen retrieval with CC1 (#950-500, Ventana) for 32 minutes at 97°C the tissue samples were incubated firstly with CD11c was incubated for 60 minutes at 37˚C followed by detection with omnimap anti-mouse HRP (#760-4310, Ventana) for 16 minutes followed by visualization with DCC for 8 minutes (#760-240, Ventana).

Antibody denature step was performed using CC2 (#950-123, Ventana) for 20 minutes at 100˚C. Secondly, IDO1 was incubated for 32 minutes at 37˚C followed by detection with omnimap anti-rabbit HRP (#760-4311, Ventana) followed by visualization with R6G (#760-244, Ventana) for 4 minutes. Antibody denature step was performed using CC2 (#950-123, Ventana) for 20 minutes at 100˚C. Thirdly, S100 was incubated for 32 minutes at 37 ˚C followed by detection with omnimap anti-rabbit HRP (#760-4311, Ventana) for 16 minutes followed by visualization with Red610 for 8 minutes (#760-235, Ventana). Antibody denature step was performed using CC2 (#950-123, Ventana) for 20 minutes at 100˚C. Fourthly, CD68 was incubated for 60 minutes at 37˚C followed by detection with omnimap anti-mouse HRP (#760-4310, Ventana) for 16 minutes followed by visualization with Cy5 for 8 minutes (#760-238, Ventana). Antibody denature step was performed using CC2 (#950-123, Ventana) for 8 minutes at 100˚C. Lastly, CD3 was incubated for 32 minutes at 37˚C followed by detection with omnimap anti-rabbit HRP (#760-4311, Ventana) followed by visualization with FAM (#760-243, Ventana) for 4 minutes. Slides were incubated in PBS with DAPI for 15 minutes and covered with anti-fading medium (DAKO, S3023).

Images were acquired using a Zeiss Axio Imager II Fluorescence microscope. For the quantification of cells, QuPath version 0.3.2 was used[15]. Cell detection was performed using the built-in cell detection tool. Cells were classified positive or negative for each marker independently based on a single intensity threshold. A single combined classifier was created using the composite object classifier tool and applied to all cells in the ROIs. Quintuple positive cells were excluded from analysis.

Supplemental References

10. Blighe K, R.S., Lewis M. EnhancedVolcano: Publication-ready volcano plots with enhanced colouring and labeling. R package version 1.10.0. (2022).
11. Zhou, Y*., et al.* Metascape provides a biologist-oriented resource for the analysis of systems-level datasets. *Nat Commun* **10**, 1523 (2019).
12. Yuan Tang, M.H., and Wenxuan Li. ggfortify: Unified Interface to Visualize Statistical Results of Popular R Packages. *The R Journal* **8**(2016).
13. Morpheus. Vol. 2022.
14. Harrell, F. Hmisc. Vol. 2022 (2004).
15. Bankhead, P*., et al.* QuPath: Open source software for digital pathology image analysis. *Sci Rep* **7**, 16878 (2017).

Chapter 4

PD-L1 checkpoint blockade promotes regulatory T cell activity that underlies therapy resistance

Mandy van Gulijk, Anneloes van Krimpen, Sjoerd Schetters, Mike Eterman, Marit van Elsas, Joanne Mankor, Larissa Klaase, Marjolein de Bruijn, Menno van Nimwegen, Tim van Tienhoven, Wilfred van Ijcken, Louis Boon, Johan van der Schoot, Martijn Verdoes, Ferenc Scheeren, Sjoerd H. van der Burg, Bart N. Lambrecht, Ralph Stadhouders, Floris Dammeijer, Joachim Aerts, Thorbald van Hall

Science Immunology 2023 May 19;8(83):eabn6173

Abstract

Despite the clinical success of immune checkpoint blockade (ICB), in certain cancer types, most patients with cancer do not respond well. Furthermore, in patients for whom ICB is initially successful, this is often short-lived due to the development of resistance to ICB. The mechanisms underlying primary or secondary ICB resistance are incompletely understood. Here, we identified preferential activation and enhanced suppressive capacity of regulatory T cells (Tregs) in anti-PD-L1 therapy resistant solid-tumor bearing mice. Treg depletion reversed resistance to anti-PD-L1 with concomitant expansion of effector T cells. Moreover, we found that tumor-infiltrating Tregs in human skin cancer patients, and in patients with non-small cell lung cancer, upregulated a suppressive transcriptional gene program after ICB treatment, which correlated with lack of treatment response. Anti-PD-1/PD-L1 induced PD-1^{+} Treg activation was also seen in peripheral blood of patients with lung cancer and mesothelioma, especially in nonresponders. Together, these data reveal that treatment with anti-PD-1 and anti-PD-L1 unleashes the immunosuppressive role of Tregs, resulting in therapy resistance, suggesting that Treg targeting is an important adjunct strategy to enhance therapeutic efficacy.

Introduction

Immune checkpoint blockade (ICB) using inhibitors to programmed cell death protein 1 or programmed death-ligand 1 (anti-PD-1/PD-L1) has revolutionized cancer therapy by unleashing T cell mediated anti-tumor immunity, resulting in clinical responses in multiple cancer types, including melanoma and non-small cell lung cancer (NSCLC) [1]. However, most patients with certain tumor types, including mesothelioma and small cell lung cancer (SCLC), do not experience durable clinical benefit from anti-PD-1/PD-L1 therapy for reasons largely unknown [2-4]. Therefore, identification of the mechanisms responsible for therapy resistance remains essential to further boost efficacy of ICB therapy.

Regulatory T cells (Tregs) represent a major barrier to successful anti-tumor immunity as they are potent suppressors of effector T cells in the tumor microenvironment (TME) and lymphoid organs [5]. Accordingly, the high abundance of Tregs relative to effector T cells in the TME is associated with poor prognostic outcomes in multiple solid cancers [6,7]. In contrast, the absence of Tregs or genetic/pharmacological depletion of Tregs results in improved anti-tumor immunity and delayed tumor growth in multiple murine models [8-10]. Tregs exert these immunosuppressive effects through multiple contact-dependent and soluble signaling mechanisms. These mechanisms include the scavenging of interkleukin-2 (IL-2) through constitutive expression of the high affinity IL-2 receptor, containing the CD25 subunit; secretion of immunosuppressive molecules such as IL-10; and expression of inhibitory cell surface receptors like cytotoxic T lymphocyte associated protein 4 (CTLA-4) that impair effective costimulation of effector T cells by antigen-presenting cells (APCs) [5,11,12]. Besides CTLA-4, Tregs express high levels of PD-1, but the functional consequence of anti-PD-1/PD-L1 therapy in this context remains incompletely understood [13-15]. Recently, increased PD-1 expression in tumor-infiltrating Tregs compared with $CD8^+$ T cells before anti-PD-1 treatment accurately predicted resistance to anti-PD-1/PD-L1 therapy and correlated with hyperprogressive disease (HPD) in patients with gastric cancer [16,17]. However, whether anti-PD-1/PD-L1 treatment-mediated activation of Tregs occurs beyond the rare phenomenon and is involved in therapy resistance remains largely unknown. Therefore, identifying the role and site of action of anti-PD-1/PD-L1 treatment on Tregs in the context of anti-PD-1/PD-L1 resistance could guide identification of targets aimed at rewiring Tregs and thus improve anti-PD-1/PD-L1 therapy efficacy.

In the present study, we found that anti-PD-L1 treatment preferentially activated Tregs in therapy-resistant tumor models but not effector T cells in both the TME and secondary lymphoid organs. Anti-PD-L1 increased the suppressive capacity of Tregs, whereas Treg depletion, in turn, sensitized both primary and secondary resistant tumor models to anti-PD-L1 treatment. Analysis of single-cell RNA sequencing (scRNA seq) data of Tregs isolated from tumor biopsies before and after anti-PD-1 treatment revealed elevated expression of immune suppressive genes after anti-PD-1 treatment, specifically in nonresponding patients. Importantly, $PD\text{-}1^+$ Tregs in peripheral blood of SCLC, NSCLC

and mesothelioma patients showed increased proliferation after anti-PD-1/PD-L1 treatment, specifically in nonresponding patients. These results indicate that Tregs are not mere bystanders but can be activated by anti-PD-1/PD-L1 treatment which associates with therapy resistance. This offers insights in the mechanisms underlying anti-PD-1/PD-L1 resistance and provides avenues for anti-PD-1/PD-L1 ICB biomarker and combination immunotherapy discovery.

Material and methods

Study design

The objective of this study was to investigate the effect of ICB using anti-PD-1/PD-L1 on Tregs and the association with treatment resistance. In order to investigate this, we used various mouse solid tumor models treated with ICB alone or in combination with Treg depleting agents anti-CD25 and DT in case of DEREG mice. Impact on tumor outgrowth was measured together with *in vitro* suppression assays, flow cytometry profiling of TME, and RNA sequencing. Patient-derived peripheral blood mononuclear cells (PBMCs) on ICB treatment were analyzed by flow cytometry, and publicly available scRNA sequencing data were reanalyzed from site-matched tumor biopsies for clinical relevance. The sample size and number of biological replicates are indicated in each of the figure legends. No data were excluded from the study. In all *in vivo* experiments shown in the study, animals were randomized and assigned to experimental groups on the basis of sex and age. Tumor measurements were performed by a researcher blinded to each animal's treatment group. Sampling replicates are indicated in figure legends. Data collection in all mouse experiments was performed until the humane or experimental end point was reached, predetermined and approved by the national central committee of animal experiments (CCD). Data was reported according to Animal Research: Reporting of In Vivo Experiment (ARRIVE) guidelines.

Mouse models

In general, female 8- to 12-week-old C57BL/6 mice were purchased from Envigo. For the RNA sequencing experiment and the *in vitro* suppression assay, 10- to 12-week old female and male FoxP3^{RFP} reporter mice were used which were obtained by in-house breeding of GATIR mice (*Gata3* knock-in reporter mice) [18] and FoxP3^{RFP} mice [19]. Female and male DEREG mice were purchased from Jackson Laboratory (catalog no. 032050), bred in house (IRC VIB, Ghent, Belgium) and used for experiments at 7 to 14 weeks of age. For the bone marrow chimera experiments, donor female and male 8 week-old PD-1^{KO} were purchased from Jackson Laboratory (catalog no. 028276), bred in house (Center for Inflammation Research (IRC) of the Flemish Institute of Biotechnology (VIB), Ghent, Belgium) and used in experiment at 14 weeks of age. In experiments where both female and male mice were used, the experimental treatment groups were sex-balanced. For the mixed chimera experiments, bone marrow from donors was sex matched with the recipients. All mice were housed under specific pathogen-free conditions in individually ventilated cages at the animal

care facility of the Erasmus MC, Rotterdam, The Netherlands or at the animal facility at the IRC, Ghent University, Belgium. All mouse experiments were controlled by the animal welfare committee (IvD) of the Erasmus MC and approved by the CCD under the permit number AVD101002017867. Experiments performed at the IRC, Belgium were approved under national license LA1400019.

Mouse tumor cell lines

The OVA-transfected AE17 tumor cell line was kindly provided by D. J. Nelson (Curtin University, Perth, Australia). The AC29 mesothelioma cell line was derived from tumors induced by crocidolite asbestos into CBA/J mice and was kindly provided by B. W. S. Robinson (Queen Elizabeth II Medical Centre, Nedlands, Australia). The AE17-OVA and AC29 cell lines were cultured in RPMI-1640 medium containing HEPES (25 mmol/liter), Glutamax, gentamicin (50 mg/ml; all obtained from Gibco), geneticin (50 mg/ml Gibco) and either 5% fetal bovine serum (FBS) (Capricorn Scientific) for AC29 tumor cells or 10% FBS for AE17-OVA tumor cells in a humidified atmosphere and at 5% CO2 air. The MC38 and B16F10 tumor cell lines were cultured in IMDM medium (Gibco) containing L-Glutamine, HEPES (25 mmol/liter), gentamicin (50 mg/ml) and 8% FBS. Authentication of the cell lines was performed by short tandem microsatellite repeat analysis or by antigen-specific T cell recognition.

SCLC, NSCLC and mesothelioma patient cohorts

Patients with advanced malignant pleural mesothelioma, stage IV SCLC and stage IV NSCLC in this study were enrolled in the MULTOMAB study (Netherlands Trial Registry: NTR7015; local ethics board study number MEC16–011). The study was approved by the institutional review board of the Netherlands Cancer Institute and in accordance with the Declaration of Helsinki. All patients provided written informed consent before enrolment. In case of NSCLC, adenocarcinoma patients harboring an actionable driver mutation (EGFR, no NTRK, ROS, RET, MET of BRAF were present in this study) were excluded as these respond differently to anti-PD-1 therapy [20,21]. Mutations in the KRAS oncogene were permitted. In summary, 21 stage patients with IV NSCLC and 15 patients with mesothelioma were treated with either nivolumab (240 mg flat dose every 2 weeks) or pembrolizumab (200 mg every 2 weeks). Response to PD-(L)1 inhibitors was evaluated according to Response Evaluation Criteria in Solid Tumors (RECIST) criteria (version 1.1) and modified RECIST-criteria were used for pleural malignant mesothelioma [22]. All patients received at least one CT scan every 6 weeks in total to assess true disease progression and pseudoprogression followed by response or ongoing response. For NSCLC, responders were defined as having a radiological response (partial response (PR) according to RECIST) after 6 weeks whereas for mesothelioma, patients with either radiological response after 6 weeks or stable disease for longer than 12 months were classified as a responder. Clinical and pathological characteristics of all patients are summarized in supplementary table 1.

***In vivo* tumor inoculation**

For tumor inoculation, mice were intraperitoneally (i.p.) injected with AE17-OVA ($3x10^5$) or AC29 ($10x10^6$) in 300 µl of phosphate-buffered saline (PBS) or subcutaneously with MC38 ($5x10^5$) or B16F10 ($1x10^5$) tumor cells in 200 µl of PBS. Subsequently, mice were randomly assigned to experimental groups. Mice with established intraperitoneal tumors were euthanized at indicated time points for immune cell profiling or when profoundly ill according to the body condition score for therapy efficacy experiments. For subcutaneous tumors, mice were euthanized at indicated time points for immune cell profiling or when the tumor reached a volume of 1500 mm^3 for therapy efficacy experiments.

***In vivo* treatments**

Anti-PD-L1 treatment. Mice with established mesothelioma (AE17-OVA) were treated with either 200 µg isotype (clone 2A3, BioXCell) or 200 ug anti-PD-L1 (clone MIH5) in 300 µl PBS i.p. at indicated time points. For mice with established subcutaneous MC38 tumors (colon-carcinoma derived), mice were treated with isotype (clone MPC-11, BioXCell) or 200 ug anti-PD-L1 (clone 10F.9G2, BioXCell) in 100 µl PBS i.p. at day 5, 8 and 11.

DT treatment. Tregs were depleted in DEREG mice using i.p. injections of 1 µg of DT (Enzo Life Sciences; BML-G135-0001) at days 8, 9 and 12.

Anti-CD25 treatment. Tregs were depleted using i.p. injections of 200 µg anti-CD25-mIgG2a PC-61.5.3 (AE17-OVA: Absolute Antibody; MC38: isotype switched PC-61 hybridoma by CRISPR/HDR engineering [23] at days 7 and 9 for the AE17-OVA model and at days 5 and 7 for MC38 model. As a control, mice were treated with isotype (AE17-OVA: Anti-hapten 4-hydroxy-3-nitrophenyl acetyl (NP) clone B1-8 (Absolute Antibody); MC38: clone C1.18.4 (BioXCell)).

Preparation of single cell suspensions from mouse tissues

Single-cell suspensions were generated from isolated blood, spleen, non-TDLN, TDLN, bone marrow, and tumor tissue of mice from each group as previously reported [24]. Briefly, blood was collected in EDTA tubes (Microvette CB300, Sarstedt) after which the volume was determined. Subsequently, collected blood was lysed by erythrocyte lysis using osmotic lysis buffer (8.3% NH_4Cl, 1% $KHCO_3$, and 0.04% Na_2EDTA in Milli-Q). Single-cell suspensions of non-TDLNs, TDLNs, bone marrow, and spleens were generated by mechanically dispersing the lymph nodes through a 100-µM nylon mesh cell strainer (BD Biosciences) followed by osmotic lysis of erythrocytes in case of spleens. Tumors were collected, weighed in a microbalance, and dissociated using a validated tumor dissociation system (Miltenyi Biotec) according to protocol. After dissociation, cell suspensions were filtered through a 100-µm nylon mesh cell strainer.

***In vitro* suppression assay**

For *in vitro* suppression assay with tumor-derived Tregs, AE17-OVA bearing mice were treated with isotype or anti-PD-L1 at days 10 and 14. At day 17, mice were sacrificed and $CD4^+RFP^+$ cells were sorted from AE17-OVA tumors. Splenic $CD4^+CD25^+RFP^+$ cells were sorted at day 13, 3 days after treatment with either isotype or anti-PD-L1 at day 10. Splenic naïve $CD8^+$ T cells from wildtype mice (responder cells, T_{resp}) were isolated using negative magnetic labeling (Miltenyi) and were labeled with CellTrace Far Red Cell Proliferation dye (Thermo Fisher Scientific). For APCs, wild-type splenocytes were T cell depleted (CD90.2 microbeads; Miltenyi Biotec) and treated with mitomycin-c (Sigma-Aldrich) to prevent the proliferation of APCs, which could influence the readout of the assay. Responder cells ($1x10^4$), APCs ($16.7x10^3$) and titrated numbers of Tregs were activated with 0.5 ug/ml anti-CD3 (BD Biosciences) in a 96-well round bottom plate with 200 µl IMDM supplemented with gentamycin (50 mg/ml), 50 mM β-ME and 10% FBS for 3 days. Suppression was calculated as previously described [25]. Briefly, cells were acquired by BD Symphony, and the division index of responder cells was analyzed using FlowJo based on the division of CellTrace FarRed. Suppression was then calculated with the formula % Suppression = (1-DITregs/DICtrl) × 100% (DITregs stands for the division index of responder cells with Tregs, and DICtrl stands for the division index of responder cells activated without Tregs).

RNA sequencing

RNA was isolated from sorted tumor-derived Tregs. Tumor-derived Tregs were isolated from AE17-OVA tumor bearing $FoxP3^{RFP}$ mice treated with isotype or with anti-PD-L1 3 days after treatment at day 10. For the isolation of Tregs, tumor samples were stained with antibodies listed in table S3 and subsequently sorted using a FACSAria III sorter with a purity ≥ 98% (number of sorted $PD\text{-}1^{+/-}$ Tregs ranged between 900 and 7000 cells). RNA was isolated using the RNeasy Micro kit (Qiagen) according to the manufacturer's instruction. Library preparation was based on the Smart-seq2 protocol [26]. Samples were sequenced in accordance to the Illumina TruSeq Rapid v2 protocol on an Illumina HiSeq2500 to obtain 50-bp single-end reads. Reads were aligned to the mm10 (GRCm38) mouse genome using HISAT2 [27]. To identify DEGs, DESeq2 was used as implemented in HOMER [28,29] and read alignment was performed to the murine genome mm10 (GRCm38). Sample scaling and statistical analysis were performed using the R package DESeq2. DEGs were determined by >1.0 absolute log2 fold change and an adjusted P-value < 0.05. Standard reads per kilobase per million (RPKM) values were used as an absolute measure of gene expression. Genes with an RPKM <1 in 50% of replicates in one condition were excluded. To assess sample quality, principal components analysis was conducted on using log-transformed RPKM values using the prcomp function from the ggfortify (0.4.11) package in R (executed from R Studio v1.1.383). K-means clustering was performed using Past3 software. Heatmaps were produced using web-based tool Morpheus (https://software.broadinstitute.org/morpheus). Pathway enrichment was performed using web-based tool Metascape [30].

Bone marrow chimeras

CD45.1.2 host mice were administered a single total body gamma radiation 8 Gy. Donor CD45.1 wild-type mice and CD45.2 PD-1^{KO} mice were euthanized by cervical dislocation, and femurs were harvested and collected in RPMI. Bone marrow cells were isolated in a sterile environment by flushing the femur with a 20 G needle using PBS and 2% FBS. Red blood cells were lysed using RBC lysis buffer (eBioscience; 00-4333-57) and washed using PBS. Harvested cells were filtered through a 40-µm cell filter and counted. Donor mixes were prepared by mixing CD45.1 and CD45.2 cells in a 1:1 ratio in sterile PBS. From both CD45.1 and CD45.2 bone marrow cells, 3.0x10^6 were transplanted via the tail vein in a total volume of 100 µl. After 8 weeks of reconstitution, transplanted hosts were bled via the tail vein to confirm chimerism and assess circulating lymphocyte populations. On the same day, host mice were i.p. injected with AE17-OVA tumor cells. Host mice were treated with either isotype or anti-PD-L1 10 days post tumor inoculation and sacrificed at day 13, and bone marrow, spleen, blood, non-TDLN, TDLN and tumor were harvested for characterization of Tregs.

Reanalysis of scRNA sequencing data

scRNAseq data analysis. Publicly available scRNAseq data were analyzed using the Seurat (4.0.0) package. Predefined Treg clusters were isolated and processed for downstream analysis. We excluded cells in which fewer than 500 genes were detected and those that had a mitochondrial DNA content greater than 10%. Next, we used a zero-inflated negative binomial model implemented by the DESingle package (v1.10.0) in R to identify DEGs [31]. Genes with an absolute $\log_2$ fold change > 0.5 and an adjusted P-value [false discovery rate (FDR)] < 0.05 were deemed significantly differentially expressed.

scRNAseq data visualization. Violin plots were generated using log-normalized counts with a scaling factor of 10.000 using the Seurat package. Unweighted pathway enrichment analysis was performed using web-based tool Metascape [30]. Weighted pathway enrichment analysis was performed via GSEA using the ClusterProfiler (v3.18.1) package in R. Genes with an absolute $\log_2$ fold change > 0.5 were included in the analysis. Genesets included in 'biological process' were selected from MsigDB (http://software.broadinstitute.org/gsea/msigdb). GSEA was ran with a minimum geneset size of 10 and nPermSimple = 100.000. GSEA plots were superimposed in Adobe Illustrator and plotted with the normalized enrichment score (NES) and P-value. Heatmaps were created using the R package Pheatmap (v1.0.12) using the normalized mean expression per cell as calculated by DESingle.

Patient-derived peripheral blood processing

Peripheral blood was collected at day 1 of cycle 1 (before start of therapy; baseline) and at day 1 of cycle 2. About 50 mL of blood was collected in EDTA tubes, and PBMCs were isolated by density gradient centrifugation using Ficoll-hypaque (GE Healthcare). Cells were cryopreserved in 10% dimethylsulfoxide (Sigma-Aldrich), 40% FCS, and RPMI for later reconstitution and analysis.

Flow cytometry

Murine samples. For cell surface staining, single cells were stained with antibodies for 30 minutes at 4°C . After this incubation period, cells were washed with fluorescence-activated cell sorting (FACS) buffer (0.05% NaN3, 2% bovine serum albumin in PBS), followed by a PBS wash, and stained for viability using fixable LIVE/DEAD aqua cell stain (Thermo Fisher, 1:200) at 4°C for 15 min. After two washing steps with PBS and FACS buffer, cells were fixated and permeabilized with Foxp3 / Transcription Factor Staining Buffer Set (Thermo Fisher Scientific) to stain nuclear factors. Intranuclear antibodies were incubated for 60 min at 4°C. A fixed number of counting beads (Polysciences Inc.) was added to the samples derived from blood before acquisition of the data to determine the absolute number of cells. Data were acquired using a FACSymphony flow cytometer equipped with four lasers and FACSDiva software (v.8.0.2) after compensation with UltraComp Compensation beads (Thermo Fisher Scientific). Acquired data were analyzed by using a licensed version of Flowjo (v.10.4.2).

Human samples. To assess PD-1 expression in peripheral blood isolated from ICB-treated patients by flow cytometry, cells were preincubated with either nivolumab or pembrolizumab (depending on *in vivo* treatment) for 20 min at 4°C [32]. Subsequently, cells were stained with a biotinylated anti-IgG4 antibody (Sigma-Aldrich, 1:100) that specifically binds to nivolumab and pembrolizumab. Last, cells were incubated with streptavidin that specifically binds to the anti-IgG4 antibody. Extracellular staining with other antibodies of interest, fixation and permeabilization, and subsequent intracellular staining was according to the protocol for murine samples. Data were acquired using a FACSymphony flow cytometer equipped with four lasers and FACSDiva software (v.8.0.2) after compensation with UltraComp Compensation beads (Thermo Fisher Scientific). Acquired data were analyzed by using a licensed version of Flowjo (v.10.4.2).

Statistical analysis

Data are expressed as means with the SEM. Comparisons between two groups with independent samples were performed using unpaired t test whereas the paired t test were used to compare paired samples (see figure legends). In case of multiple comparisons, one-way or two-way analysis of variance (ANOVA) was used with Sidak's post-test or Tukey's post-test, respectively. Survival data were plotted as Kaplan-Meier survival curves using the log-rank test to determine statistical significance. A P-value of 0.05 and below was considered significant (*), $p < 0.01$(**) and $p < 0.001$ (***) were considered highly significant. Statistical approaches were verified per figure. All DEG analyses were Benjamini Hochberg-corrected for false discovery rate (FDR < 0.05). Data were analyzed using GraphPad Prism software (Graphpad, V5.01 and V8.0).

Results

Anti-PD-L1 therapy induces preferential activation and proliferation of Tregs in treatment-resistant murine tumor models

To gain insight into the mechanisms responsible for ICB resistance, we studied the intraperitoneal AE17-OVA mesothelioma tumor model which is refractory to anti-PD-L1 therapy, because anti-PD-L1 treatment did not prolong survival, even when initiated early at day 5 (Fig. 1A-B). T cell phenotype and activation status were measured in tumor-draining lymph nodes (mediastinal lymph node; TDLN), non-TDLN (inguinal LN), spleen, blood, and tumor at several time points before and after anti-PD-L1 treatment (Fig. 1C). $CD8^+$ T cells were only marginally activated after treatment in these tissues with minor temporal upregulation of co-stimulatory (e.g. 4-1BB, CD25, ICOS and OX40) and coinhibitory markers (e.g. CD39, NKG2A, PD-1, LAG3, TIGIT and CTLA-4) (Fig. 1D, Fig. S1 and Fig. S2A). The same pattern was observed for the proliferation marker Ki67, which did not increase after anti-PD-L1 treatment in total $CD8^+$ T cells or ovalbumin (OVA)-specific $CD8^+$ T cells (Fig. S2B). $CD4^+$ T cells, however, displayed a more activated phenotype after treatment, including sustained expression of Ki67 and the exhaustion-program driver TOX. When discriminating between $CD4^+$ T-helper cells ($CD4^+$ Th) and Tregs based on FoxP3 expression (Fig. S2C-D), the observed effect could largely be assigned to anti-PD-L1-induced activation of Tregs with induction of CTLA-4, Ki67, PD-1 and TOX 3 days after treatment (day 13). Proliferation was more profoundly induced in Tregs after anti-PD-L1 treatment compared with $CD8^+$ T cells in the AE17-OVA model, whereas the opposite was observed in the anti-PD-L1-responsive MC38 tumor model (Fig. 1E-F). Inclusion of a second therapy-responsive model (mesothelioma; AC29) and therapy-resistant model (melanoma; B16F10) showed the same pattern with stronger induced proliferation in $CD8^+$ T cells or Tregs in the responsive and resistant tumor models, respectively (Fig. 1G). Because checkpoint blockade may also impact immunity via myeloid cells, we examined alterations in these subsets after anti-PD-L1 treatment [33]. Anti-PD-L1 treatment appeared to have effects on myeloid cells that were less substantial compared with Tregs (Fig. S3). Together, these results indicate that anti-PD-L1 could activate Tregs in the setting of primary therapy unresponsiveness.

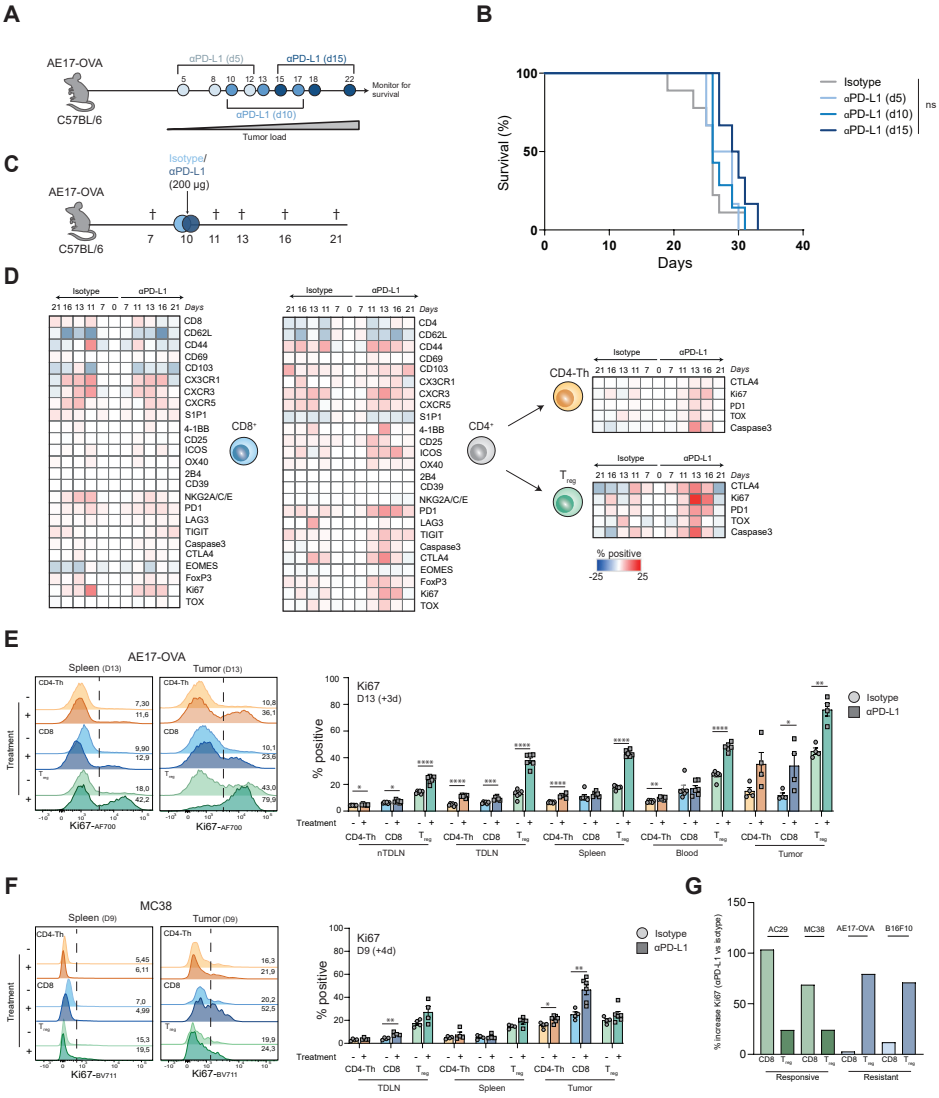
A
AE17-OVA
C57BL/6
αPD-L1 (d5)
αPD-L1 (d15)
αPD-L1 (d10)
Monitor for survival
Tumor load
B
Survival (%)
Days
Isotype
αPD-L1 (d5)
αPD-L1 (d10)
αPD-L1 (d15)
ns
C
Isotype/ αPD-L1 (200 µg)
AE17-OVA
C57BL/6
D
CD8+
CD4+
CD4-Th
Treg
% positive
E
AE17-OVA
Spleen (D13)
Tumor (D13)
Ki67 D13 (+3d)
nTDLN
TDLN
Spleen
Blood
Tumor
F
MC38
Spleen (D9)
Tumor (D9)
Ki67 D9 (+4d)
G
% increase Ki67 (αPD-L1 vs Isotype)
AC29
MC38
AE17-OVA
B16F10
Responsive
Resistant

◂Figure 1: Anti-PD-L1 treatment specifically induces rapid activation of Tregs with marginal activation of CD8⁺ T cells and CD4⁺ Th cells in a therapy-resistant mesothelioma murine model

(A-B) Experimental setup (n = 3 to 7 mice per group) with mice being treated with systemic isotype or anti-PD-L1 antibodies i.p. starting from day 5, day 10 or day 15 onwards and monitored for survival. Log rank tests were used to determine statistical significance. (C) Experimental setup (n = 5 or 6 mice per group) with mice being treated with systemic isotype or anti-PD-L1 antibodies i.p. at day 10 and euthanized at different time points before and after isotype and anti-PD-L1 treatment. (D) Protein expression of costimulatory, coinhibitory and transcription factors were compared between isotype- and anti-PD-L1-treated mice at each indicated time point (days post tumor inoculation) by flow cytometry and displayed in heatmaps. Differences in percentage positive compared with day 0 (tumor-free mice) for each individual marker were displayed for spleen. (E-F) Representative histograms and quantification displaying Ki67 expression in spleen and tumor for CD4⁺ Th cells (orange), CD8⁺ T cells (blue) and Tregs (green) of isotype- (-) and anti-PD-L1- (+) treated AE17-OVA tumor bearing mice (d13) (E) and MC38 tumor bearing mice (d9) (F). (G) Bar graphs displaying differences in Ki67 expression in treated mice versus untreated mice for the AC29 mesothelioma (n = 7) and MC38 colon adenocarcinoma (n = 5 to 7; responsive models) and the AE17-OVA mesothelioma (n = 6) and B16F10 melanoma model (n = 8; resistant models) in peripheral blood at day 13, 3 days after treatment. Means and SEMs are shown and unpaired t tests were performed, indicating statistical significance. * = $p < 0.05$, ** = $p < 0.01$, *** = $p < 0.001$, **** = $p < 0.0001$. i.p. = intraperitoneal, TDLN = tumor-draining lymph node.

Anti-PD-L1 therapy amplifies the immunosuppressive phenotype and activity of Tregs

To comprehensively examine the effect of anti-PD-L1 treatment on Treg phenotype, we investigated a wide variety of markers associated with the immunosuppressive function of Tregs in TDLN, non-TDLN, spleen, blood and tumor material 3 days after anti-PD-L1 treatment. In spleen, expression levels of key molecules associated with suppressive capacity of Tregs (ICOS, CTLA-4, CD39 and PD-1) were significantly elevated in anti-PD-L1 treated mice compared with those given isotype treatment (Fig. 2A). This coincided with a tended increase in absolute Treg numbers, whereas this was not observed for CD4⁺ Th cells or CD8⁺ T cells (Fig. S4A). The pattern of enhanced expression of key suppressive molecules was also apparent in TDLN, non-TDLN, blood and tumor, despite already higher basal expression levels on intratumoral Tregs (Fig. S4B). We further assessed the effects of anti-PD-L1 treatment on tumor-derived Tregs in an unbiased manner by performing RNA sequencing. Pathway analysis of genes differentially expressed in anti-PD-L1-treated PD-1⁺ Tregs versus isotype-treated PD-1⁺ Tregs revealed enrichment for genes involved in T cell activation and apoptosis whereas these pathways were not enriched in PD-1⁻ Tregs or CD4⁺ Th cells (Fig. 2B, S5A). More specifically, anti-PD-L1-treated PD-1⁺ Tregs showed enhanced expression of key signature genes related to suppressive function such as *Il10, Tigit* and *Icos* but also *Fgl2, Tsc1* and *Ets1,* which were previously reported to mediate Treg suppressive activity [34-38] (Fig. 2C, S5B). The up-regulation of genes related to suppressive function was less robust in PD-1⁻ Tregs and CD4⁺ Th cells, indicating a greater effect on the PD-1⁺ subpopulation (Fig. S5C). In addition, anti-PD-L1 treatment induced a proapoptotic gene signature specifically in PD-1⁺ Tregs as anti-apoptotic genes, including *Bcl2,* were down-regulated whereas proapoptotic genes, such as *Bcl2l11* (encoding for BIM), were up-regulated

(Fig. 2C, S5B). The decreased Bcl2/BIM ratio was confirmed at the protein level and coincided with increased expression of activated caspase 3 (Fig. S5D). Ki67 expression was higher in $Bcl2^-$ Tregs compared with their $Bcl2^+$ counterparts (Fig. S5E). These data are in line with a recent report showing apoptotic Tregs to be superior in mediating immunosuppression compared with nonapoptotic Tregs [39]. Therefore, these data indicate that Tregs, in particular PD-1^+ Tregs, acquire a more immunosuppressive transcriptional signature after treatment.

Next, we examined whether anti-PD-L1-treated Tregs were also functionally more suppressive. To this end, we isolated Tregs from tumors and spleens by flow sorting from tumor-bearing $FoxP3^{RFP}$ reporter mice treated with either isotype or anti-PD-L1. Tregs were subsequently cultured with naïve prelabeled responder $CD8^+$ T cells in the presence of anti-CD3 monoclonal antibody and mitomycin-treated APCs (Fig. 2D, S5F). Whereas $CD8^+$ T cells proliferated vigorously in the absence of Tregs, this proliferation was reduced by addition of isotype-treated Tregs. Anti-PD-L1 treatment resulted in tumor-derived Tregs with significantly more potent suppressive function than after isotype treatment (Fig. 2D). This anti-PD-L1-induced suppression was more marked in tumor-derived Tregs compared with spleen-derived Tregs (Fig. S5F). Together, these data show that anti-PD-L1 treatment increases the suppressive capacity of Tregs *in vivo*.

PD-1 exerts an important function in modulating Treg phenotype after checkpoint blockade

To pinpoint whether the effect of anti-PD-L1 treatment is directly mediated via PD-1 expressed on Tregs, we performed a bone marrow chimera experiment, in which sub-lethally irradiated C57BL/6-CD45.1.2 recipient mice were reconstituted with a 1:1 mix of PD-1^{WT} CD45.1 and PD-1^{KO} CD45.2 donor bone marrow cells, allowing for donor reconstitution to be tracked and quantified using allele-specific CD45 antibodies. After reconstitution, recipient mice were inoculated with AE17-OVA tumor cells and treated with either isotype or anti-PD-L1 (Fig. 3A-B). This setup allowed us to assess within the same animal whether anti-PD-L1 treatment enhanced Treg proliferation by direct PD-1 uncoupling in Tregs or via Treg-independent effects of anti-PD-L1 treatment. In accordance with our previous observations, basal levels of Ki67 expression were elevated in PD-1^{KO} Tregs as compared with PD-1^{wt} Tregs in isotype treated animals (Fig. 3B-C). Anti-PD-L1 treatment significantly increased Treg proliferation in PD-1^{WT} Tregs (up to 2- to 3 fold) and this appeared to be less in PD-1^{KO} Tregs (1- to 1.5 fold), pointing to an important cell intrinsic role for PD-1 on Tregs in modulating Treg phenotype.

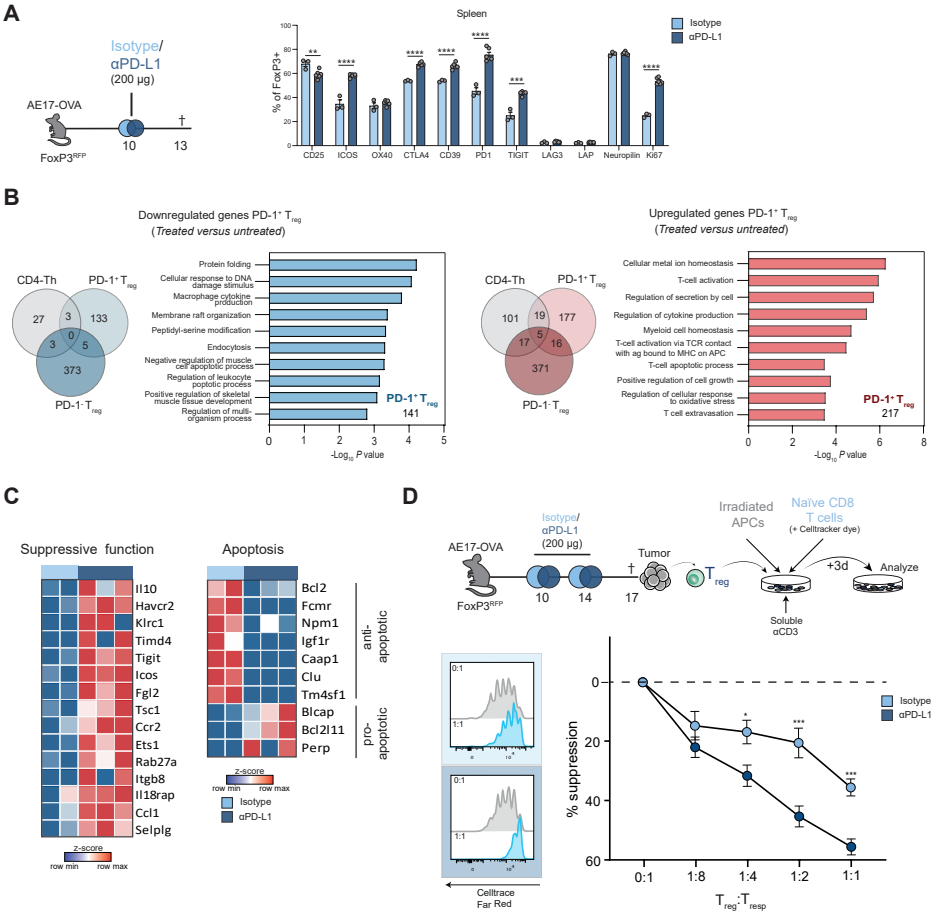
A
Isotype/
αPD-L1
(200 μg)
AE17-OVA
FoxP3RFP
10
13
†
Spleen
Isotype
αPD-L1
% of FoxP3+
CD25
ICOS
OX40
CTLA4
CD39
PD1
TIGIT
LAG3
LAP
Neuropilin
Ki67
B
Downregulated genes PD-1+ Treg
(Treated versus untreated)
CD4-Th
PD-1+ Treg
PD-1- Treg
27
3
133
0
3
5
373
Protein folding
Cellular response to DNA damage stimulus
Macrophage cytokine production
Membrane raft organization
Peptidyl-serine modification
Endocytosis
Negative regulation of muscle cell apoptotic process
Regulation of leukocyte apoptotic process
Positive regulation of skeletal muscle tissue development
Regulation of multi-organism process
PD-1+ Treg
141
-Log10 P value
Upregulated genes PD-1+ Treg
(Treated versus untreated)
101
19
177
5
17
16
371
Cellular metal ion homeostasis
T-cell activation
Regulation of secretion by cell
Regulation of cytokine production
Myeloid cell homeostasis
T-cell activation via TCR contact with ag bound to MHC on APC
T-cell apoptotic process
Positive regulation of cell growth
Regulation of cellular response to oxidative stress
T cell extravasation
PD-1+ Treg
217
-Log10 P value
C
Suppressive function
Apoptosis
Il10
Havcr2
Klrc1
Timd4
Tigit
Icos
Fgl2
Tsc1
Ccr2
Ets1
Rab27a
Itgb8
Il18rap
Ccl1
Selplg
z-score
row min
row max
Bcl2
Fcmr
Npm1
Igf1r
Caap1
Clu
Tm4sf1
Blcap
Bcl2l11
Perp
anti-apoptotic
pro-apoptotic
z-score
row min
row max
Isotype
αPD-L1
D
Isotype/
αPD-L1
(200 μg)
AE17-OVA
FoxP3RFP
10
14
17
†
Tumor
Treg
Irradiated APCs
Naïve CD8 T cells
(+ Celltracker dye)
+3d
Analyze
Soluble αCD3
0:1
1:1
Celltrace Far Red
% suppression
0
20
40
60
Isotype
αPD-L1
0:1
1:8
1:4
1:2
1:1
Treg:Tresp

◂Figure 2: Anti-PD-L1 treatment enhances suppressive phenotype and capacity of Tregs

(A) Experimental setup (n = 3 to 6 mice per group) of AE17-OVA bearing mice treated with isotype or anti-PD-L1 antibodies i.p. at day 10 and sacrificed at day 13 (left). Expression of markers associated with suppressive capacity of Tregs were assessed by flow cytometry and compared between isotype- and anti-PD-L1-treated mice in spleen (right). (B) Venn diagrams depicting overlap of genes ($PD1^+$ Tregs, $PD1^-$ Tregs and CD4 T helper cells) and pathways analysis ($PD1^+$ Tregs) down-regulated (blue) or up-regulated (red) of DEGs in anti-PD-L1 versus isotype treatment (n = 2 to 3 mice). Number in corners indicate the number of DEGs. (C) Heatmaps displaying DEGs in anti-PD-L1-treated versus isotype-treated PD-1^+ Tregs (shown as z scores of RPKM levels with row min-max based on all three T cell subsets) associated with suppressive function and apoptosis. (D) Experimental setup of AE17-OVA-bearing $FoxP3^{RFP}$ reporter mice treated with either isotype or anti-PD-L1 antibodies i.p. at days 10 and 14 and euthanized at day 17. RFP^+CD4^+ T cells were sorted from tumors and cultured for 3 days with labeled naive $CD8^+$ T cells, mitomycin-irradiated T cell depleted splenocytes (APCs) and soluble anti-CD3 for 3 days. Proliferation of naive $CD8^+$ T cells was assessed with different T_{reg}:T_{resp} ratios with Tregs from either isotype or anti-PD-L1-treated mice (n = 8 to 12) and depicted in histograms. Percent suppression was calculated as described in Materials and Methods. Means and SEMs are shown and unpaired t tests were performed, indicating statistical significance. * = $p < 0.05$, ** = $p < 0.01$, *** = $p < 0.001$, **** = $p < 0.0001$. i.p. = intraperitoneal, APCs = antigen-presenting cells, DEGs = differentially expressed genes.

Systemic depletion of Tregs reverts anti-PD-L1 resistance and improves immunotherapy efficacy

Although anti-PD-L1 treatment induced a more activated and immune suppressive phenotype of Tregs in the therapy-resistant AE17-OVA murine tumor model, it remained unclear whether this actively promoted therapy resistance. To this end, we treated $FoxP3^{DTR}$ mice with diphtheria toxin (DT) to deplete Tregs, followed by isotype or anti-PD-L1 treatment (Fig. 4A). DT treatment alone resulted in decreased tumor burden. When Treg depletion was combined with anti-PD-L1 treatment, tumor burden was further reduced to near absence that was accompanied by an overt increase in memory tumor-infiltrating lymphocytes (TILs), demonstrating that Tregs are involved in therapy resistance (Fig. 4B). As a more translational approach, we then systemically depleted Tregs using an Fc-optimized anti-CD25 antibody in the therapy-resistant AE17-OVA tumor model[8,23] (Fig. 4C). First, we could confirm that anti-CD25 treatment effectively decreased Tregs at multiple sites including secondary lymphoid organs and especially tumors rapidly after treatment, resulting in enhanced $CD8^+$ T cell/Treg ratios (Fig. 4D, S6A-B). Second, anti-CD25 treatment before anti-PD-L1 treatment led to a synergistic induction of $CD8^+$ and $CD4^+$ Th-cell proliferation and activation in peripheral blood after immunotherapy, which was also observed in the therapy-resistant B16F10 tumor model (Fig. 4E-G, S6C). Last, Treg depletion sensitized AE17-OVA tumors for anti-PD-L1 treatment as observed by prolonged survival and decreased tumor weight (day 17), although all mice eventually succumbed due to progressive tumor growth (Fig. 4H). A similar effect was induced in the B16F10 model, with half of the mice showing prolonged survival and delayed tumor growth (Fig. 4I, S6D). Although MC38-bearing mice were initially responsive to anti-PD-L1 treatment with reduced tumor growth (Fig. 4J, inset), mice eventually relapsed because of acquired resistance and did not show prolonged

survival. Combination treatment, however, induced long-term survival in most of the mice (Fig. 4J). Whether anti-PD-L1 treatment exacerbates Treg induced immunosuppression in this model as compared with the primary resistant models remains to be investigated. These data show that Tregs are involved in both primary and secondary therapy resistance to anti-PD-L1 treatment in preclinical solid mouse tumor models.

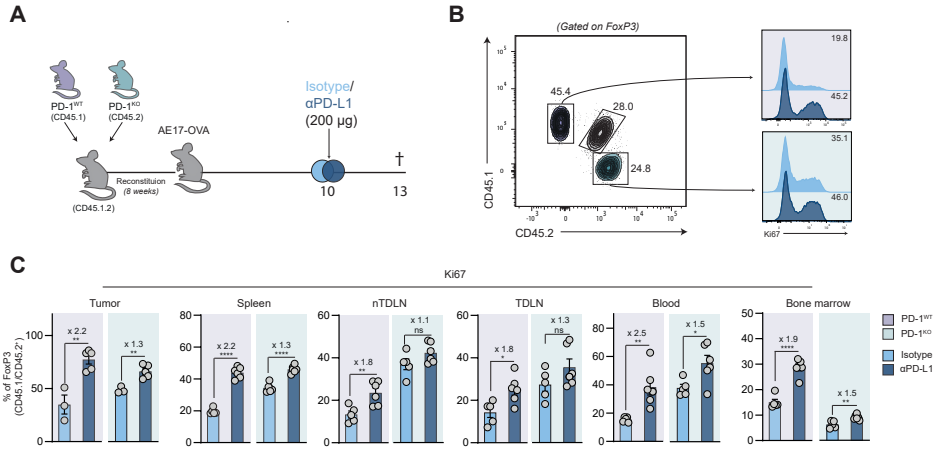

Figure 3: PD-1 exerts an important function in mediating checkpoint-blockade induced effects on Tregs

(A) Experimental design with sublethally irradiated CD45.1.2 recipient mice being reconstituted with CD45.1 PD-1^{WT} and (purple) CD45.2 PD-1^{KO} (green) bone marrow cells followed by AE17-OVA inoculation and treatment with either isotype (n = 5) or anti-PD-L1 (n = 6). Mice were euthanized at day 13 and proliferation of PD-1^{WT} and PD-1^{KO} Tregs was evaluated in multiple tissues. (B) Proportions of CD45.1/CD45.2 Treg populations and their level of proliferation, as depicted in histograms of intracellular Ki67 levels, at day 13 in spleen (3 days after treatment). (C) Percentage of Tregs (PD-1^{WT} and PD-1^{KO}) positive for Ki67 after isotype or anti-PD-L1 treatment in multiple tissues at day 13. Means and SEMs are shown and unpaired t tests were performed, indicating statistical significance. *= $p < 0.05$, ** = $p < 0.01$, *** = $p < 0.001$, **** = $p < 0.0001$. TDLN = tumor-draining lymph node, non-TDLN = non-tumor draining lymph node, SEM = standard error of the mean.

Treg activation in patient tumor biopsies and peripheral blood after ICB treatment is associated with poor treatment response

Although we observed robust treatment-induced augmentation of Treg effector functions in preclinical murine models, effects of anti-PD-1/PD-L1 treatment on Tregs in a clinical setting and its association with treatment response remain unclear. We therefore assessed the effects of anti-PD-1 treatment on tumor-infiltrating Tregs in publicly available scRNA-seq data from site-matched tumor biopsies of responding and nonresponding patients with nonmelanoma skin cancer (BCC) or NSCLC before and after anti-PD-1 treatment (Fig. 5A) [40,41]. Phenotypically similar Tregs were extracted from these datasets and gene expression was compared before and after treatment in both responders and nonresponders (Table S1, Fig. S7A-B). Nonresponding patients with BCC and

NSCLC shared 64 up-regulated genes in Tregs after treatment as compared with before treatment, including *PDCD1* encoding PD-1, while little to no overlap was seen for responding patients after treatment or in pretreatment comparisons (Fig. 5B, S7C-F). Pathway enrichment analysis of the differentially expressed genes (DEGs) up-regulated after treatment revealed genes significantly associated with (the regulation of) cell activation and apoptosis, specifically in nonresponding patients with BCC and NSCLC (Fig. 5C). In agreement, gene set enrichment analysis (GSEA) showed significant enrichment of genes involved in the 'Negative regulation of α/β T-cell activation' pathway among genes up-regulated after treatment only in nonresponders (Fig. 5C-D). When comparing Treg transcriptomes after treatment between responding and nonresponding patients with BCC and NSCLC, we observed a shared signature of treatment-induced genes involved in cell activation and enhanced suppressive capacity of Tregs (Fig. 5E-H). These included genes related to Treg-mediated suppression (e.g. *PDCD1, CTLA4, HAVCR2*, and *CD38*), T cell receptor signaling (e.g. JUN/FOS, LAT) and the cell cycle (*MKI67*), which were expressed at higher average levels and at greater frequencies in Tregs from nonresponders (Fig. 5H-I). Only few genes were up-regulated in responders after treatment, showing no overlap between both tumor types and no functional links with Treg activation or suppressive capacity (Fig. S7G-H). Together, these data suggest that anti-PD-1 treatment induces an immunosuppressive activation program specifically in Tregs from nonresponding patients.

To assess whether differences in the Treg phenotype at baseline could be linked to therapy resistance, we compared nonresponding and responding patients before treatment for both tumor types. BCC and NSCLC Tregs showed fewer overlapping gene expression signatures before treatment as compared with after treatment (80 DEGs versus 776 DEGs respectively, see Fig. 5E, S8A-D), suggesting that shared therapy resistance mechanisms could be acquired during treatment or are more tumor-specific at baseline. Pathway enrichment analysis of the (largely unique) pretreatment DEGs from both tumor types did indicate a more activated Treg phenotype specifically in nonresponding patients with BCC and NSCLC (Fig. S8B). These data suggest that Tregs are already more activated at baseline in patients that subsequently experience therapy resistance after anti-PD-1 treatment.

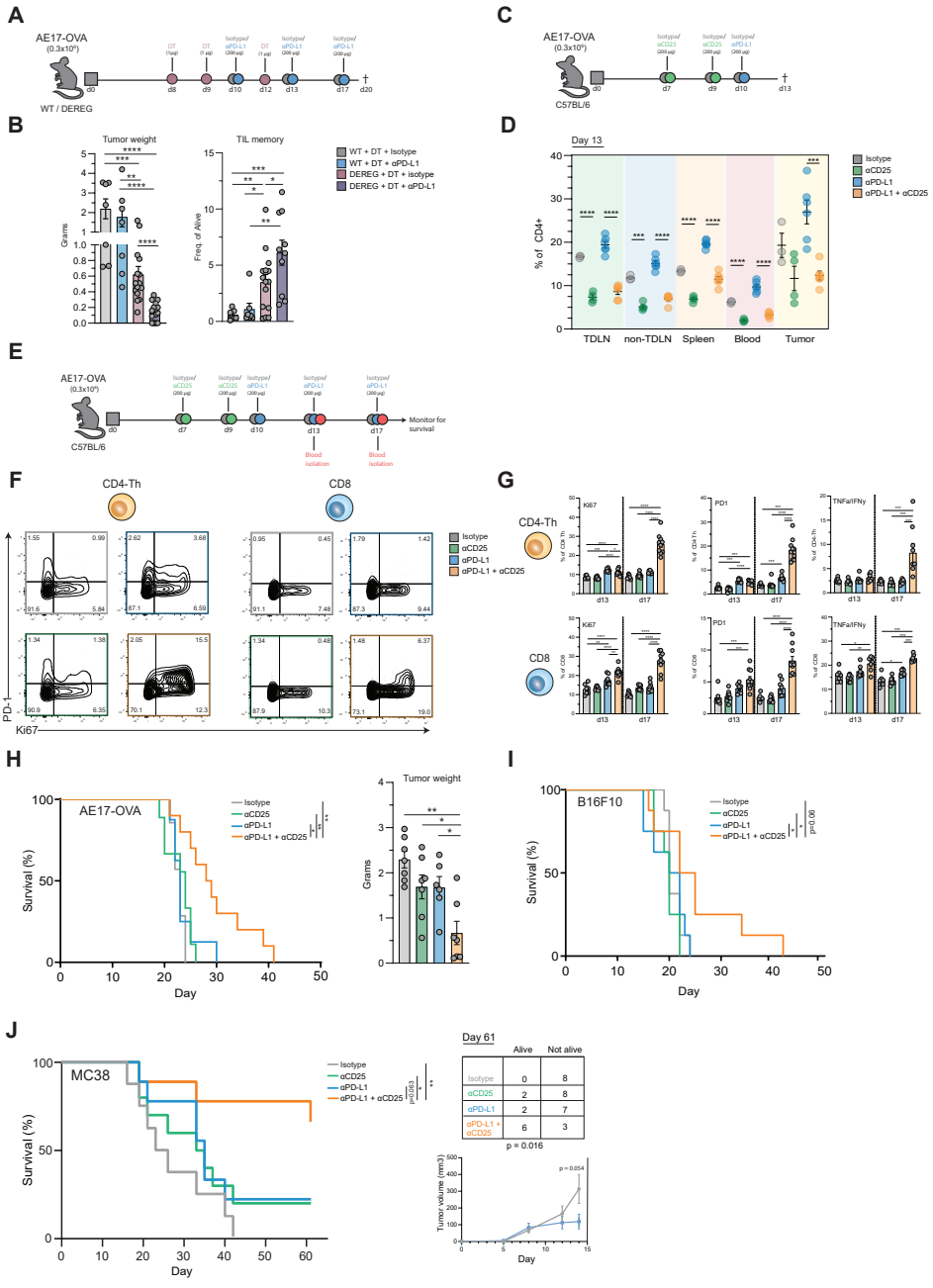
A
AE17-OVA
(0.3x10⁶)
WT / DEREG
B
Tumor weight
TIL memory
Grams
Freq. of Alive
WT + DT + Isotype
WT + DT + αPD-L1
DEREG + DT + isotype
DEREG + DT + αPD-L1
C
AE17-OVA
(0.3x10⁶)
C57BL/6
D
Day 13
% of CD4+
Isotype
αCD25
αPD-L1
αPD-L1 + αCD25
TDLN
non-TDLN
Spleen
Blood
Tumor
E
AE17-OVA
(0.3x10⁶)
C57BL/6
Monitor for survival
Blood isolation
F
CD4-Th
CD8
PD-1
Ki67
G
CD4-Th
CD8
Ki67
PD1
TNFa/IFNγ
H
AE17-OVA
Survival (%)
Day
Tumor weight
Grams
I
B16F10
Survival (%)
Day
J
MC38
Survival (%)
Day
Day 61
Alive
Not alive
Isotype 0 8
αCD25 2 8
αPD-L1 2 7
αPD-L1 + αCD25 6 3
p = 0.016
Tumor volume (mm3)
p = 0.054

◂Figure 4: **Anti-PD-L1 therapy resistance is reverted by Treg depletion by improving anti-tumor immunity and survival**

(A) Experimental design where wild-type or DEREG mice (n = 7 to 16 mice per group) were treated with DT followed by either isotype or anti-PD-L1 treatment at days 10, 13 and 17. Mice were euthanized at day 20. (B) Bar graphs displaying tumor weights (left) and the percentage of memory $CD8^+$ T cells infiltrating the tumor (right) for the different treatment groups at day 17. (C) Experimental design during which mice bearing AE17-OVA tumors (n = 8 to 10 mice per group) were treated with isotype or anti-CD25 mIgG2a Treg-depleting antibody at days 7 and 9 followed by anti-PD-L1 treatment at day 10. (D) Mice were euthanized at day 13 to assess Treg cell frequencies in TDLNs, non-TDLNs, spleens, blood, and tumors. (E) Immunotherapeutic protocol of anti-PD-L1 treatment at days 10, 13 and 17 in the presence of Treg depleting antibody at days 7 and 9. Peripheral blood was isolated from the tail vein at days 13 and 17 and mice were monitored for survival. (F) Representative flow cytometry plots displaying level of proliferation (Ki67) for different treatment groups in$CD4^+$ Th cells and $CD8^+$ T cells in peripheral blood at day 17. (G) Quantification of level of proliferation (Ki67), PD-1 expression and expression of TNFα and IFNγ at days 13 and 17 for both $CD4^+$ Th cells and $CD8^+$ T cells in peripheral blood. (H) Kaplan-Meier curves of the experiment in E showing tumor survival and bargraphs displaying tumor weights at day 17 (n = 7 mice per group). (I) Kaplan-Meier curves of checkpoint-resistant B16F10-bearing mice treated with the same protocol as AE17-OVA bearing mice in E. (J) Kaplan-Meier curves of checkpoint-sensitive MC38-bearing mice treated with anti-CD25 mIgG2a at days 5 and 7 and anti-PD-L1 treatment at days 5, 8 and 11 (n = 8 to 10 mice per group). Log rank tests were used to determine statistical significance. Chi-square test was performed to assess the association of treatment and survival at day 61. Tumors were measured for 14 days after inoculation in mice treated with isotype and anti-PD-L1. Means and SEMs are shown and for comparisons between two groups, unpaired t test was used. For comparisons between multiple groups, one-way (G and H) or two-way (B) ANOVA was used with multiple-comparison tests.*= $p < 0.05$, ** = $p < 0.01$, *** = $p < 0.001$, **** = $p < 0.0001$. TDLN = tumor-draining lymph node, non-TDLN = non-tumor draining lymph node, SEM = standard error of the mean.

To further explore whether ICB-induced Treg activation and proliferation is related to clinical therapy efficacy, we characterized Tregs in paired pre- and posttreatment peripheral blood samples of three independent cohorts: anti-PD-L1-resistant stage IV SCLC patients, patients with mesothelioma, and patients with stage IV NSCLC (Table S2). Advanced SCLC tumors bear among the highest tumor mutational burdens but are considered largely refractory to anti-PD-(L)1 monotherapy, with only limited additional benefit when combined with first-line combination chemotherapy [42,43]. For all three tumor types, we observed a greater increase in proliferation after anti-PD-1/PD-L1-containing treatment in $PD\text{-}1^+$ Tregs but not in $PD\text{-}1^-$ Tregs, suggesting a direct effect of treatment via PD-1 on Tregs (Fig. 6A). Because we could dissect responding (R), including complete responses and partial responses, and nonresponding patients (NR) for NSCLC and mesothelioma, we examined whether the impact of anti-PD-1/PD-L1 treatment in $PD\text{-}1^+$ Tregs correlated with response to treatment in these patient cohorts. We detected significantly enhanced levels of proliferation after treatment in $PD\text{-}1^+$ Tregs, but not in $PD\text{-}1^-$ Tregs in nonresponding patients with NSCLC and mesothelioma (Fig. 6B-C, S9A-B). This effect appeared to be enriched in nonresponding patients because $PD\text{-}1^+$ Tregs proliferated less robustly in patients with clinical response to anti-PD-1/PD-L1 treatment. No clear correlations

with response were found in the PD-1^{+} and PD-1^{-} effector CD4^{+} and CD8^{+} T cell populations (Fig. S9C-H). These data indicate that anti-PD-1/PD-L1 treatment affects PD-1^{+} Treg proliferation in patients with cancer and that this associates with resistance to anti-PD-1/PD-L1 therapy.

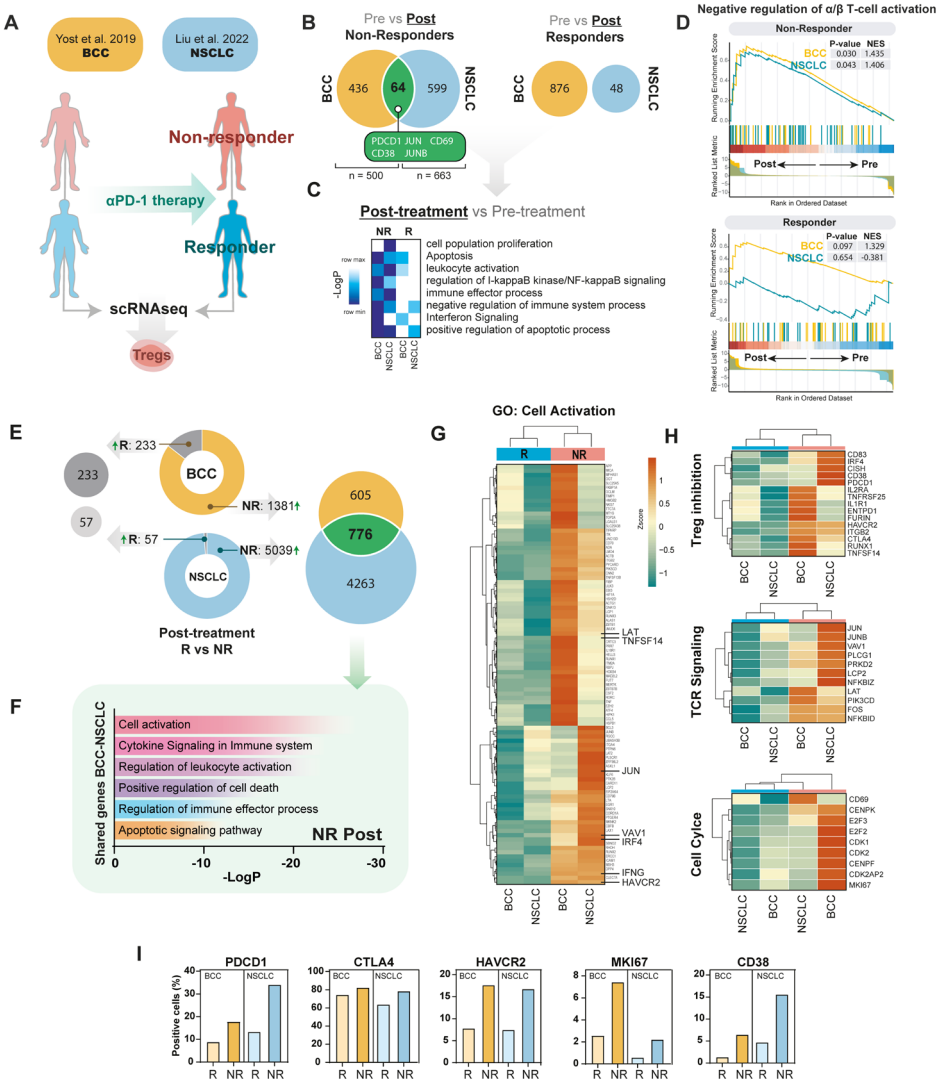

◂Figure 5: Tregs in the TME of anti-PD-1 resistant patients with cancer up-regulate a transcriptional program linked to enhanced immunosuppression after treatment

(A) Predefined Treg clusters were isolated from published BCC and NSCLC tumor scRNA seq datasets in which biopsies were taken before (pre) and after (post) treatment with anti-PD1 therapy (pembrolizumab). Patients were classified as either responders or nonresponders based on RECIST v1.1. (B) Venn diagrams displaying overlap in genes up-regulated after treatment (as compared with pretreatment samples) from comparisons of Tregs in either nonresponder (left) or responder (right) BCC and NSCLC patients. Genes of interest in the overlap are highlighted. (C) Pathway enrichment analysis displaying overlap in biological pathways associated ($P < 0.05$) with significantly up-regulated genes after versus before treatment in BCC and NSCLC Tregs (input genes are shown in panel B), separated by therapy response (NR = non-responder, R = responder). Strength of association is visualized by a Z-score of the $-Log_{10}$ transformed P-values. (D) GSEA plots (including genes with an absolute log_2 fold change > 0.5) comparing Treg transcriptomes before versus after treatment of nonresponders (top) and responders (bottom) from BCC and NSCLC for the 'Negative Regulation of alpha/beta T-cell activation' pathway (GO:0046636). (E) Donut plot of up- and down-regulated genes comparing responder with nonresponder patients after treatment. The arrows indicate the number of up-regulated genes per indicated patient group. Venn diagrams display the overlap in up-regulated genes between the BCC and NSCLC datasets of responders and nonresponders. (F) Pathway enrichment analysis of genes up-regulated in nonresponders compared with responders after treatment that are shared between the BCC and NSCLC datasets. The association strength of pathways is displayed by $-log_{10}$ transformed P-values. (G) Hierarchically clustered heatmap displaying scaled expression levels of genes included in the 'Cell Activation' pathway (GO:0001775). (H) Hierarchically clustered heatmaps showing scaled expression levels for selected genes relevant for the indicated biological functions. (I) Percentage of positive cells (i.e. displaying a transcript count > 0) for selected genes. (B and C and E to I) Adjusted P-value (FDR) < 0.05 and absolute log_2 fold change > 0.5 BCC = basal cell carcinoma; DEG = Differentially Expressed Genes, GSEA = Gene Set Enrichment Analysis; NSCLC = non-small cell lung cancer.

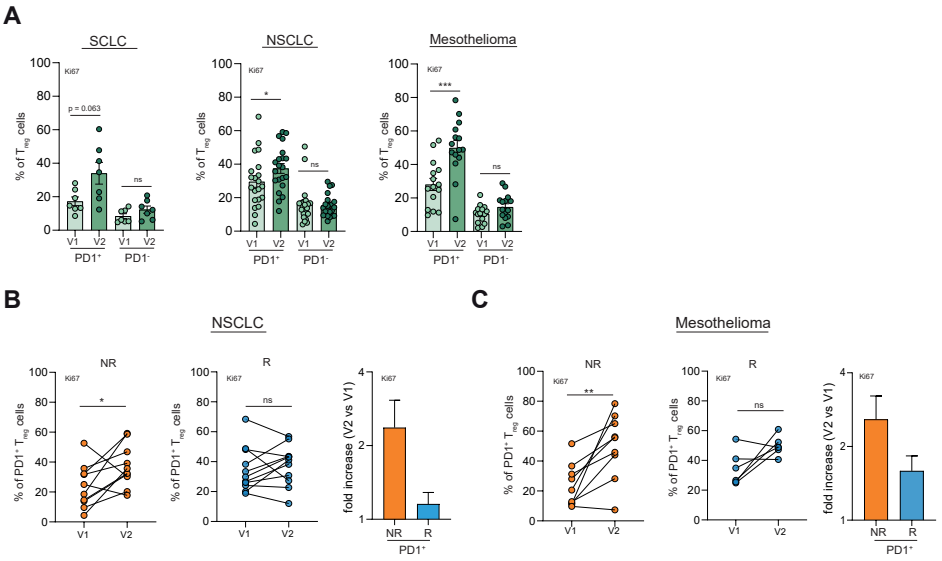

Figure 6: Increased proliferation of PD-1⁺ Tregs in peripheral blood after anti-PD-1/PD-L1 treatment is associated with treatment resistance

(A) Level of proliferation (Ki67) was assessed in PD-1⁺ and PD-1⁻ Tregs at baseline (V1) and 2 weeks after start of anti-PD-1/PD-L1 treatment (V2) in peripheral blood of patients with SCLC, NSCLC, and mesothelioma. Increased proliferation after treatment start was determined in PD-1⁺ and PD-1⁻ T_{reg} cells and expressed as fold change in nonresponding (NR) and responding (R) NSCLC patients (B) and mesothelioma patients (C). Means and SEMs are shown and paired t tests were performed indicating statistical significance. * = $p < 0.05$, ** = $p < 0.01$, *** = $p < 0.001$, **** = $p < 0.0001$. SCLC = small-cell lung cancer, NSCLC = non-small-cell lung cancer.

Discussion

In this study, we show that Tregs are not just exerting their known immunosuppressive role in cancer as a default characteristic but that this suppression is itself regulated by cell-intrinsic PD-1 engagement. Clinical use of anti-PD-1/PD-L1 unleashes this form of regulation, leading to enhanced Tregs immunosuppression and underlying therapy resistance. The data underline the importance of rational combination immunotherapy designs to specifically induce effector antitumor T cell populations without concomitant immune suppression through ICB-activated Tregs.

Recently, Kamada et al. reported that increased Treg activity after anti-PD-1 treatment in patients with gastric cancer was associated with HPD [17]. In addition, Kumagai et al. demonstrated that the balance of PD-1 expression on CD8⁺ T cells and Tregs before treatment in the TME predicted immunotherapy efficacy in NSCLC and gastric cancer. We elaborated on these findings, showing that the undesirable effect of anti-PD-1/PD-L1 treatment on Tregs could be more widespread, as

evidenced by a significant subset of nonresponding patients showing increased Treg proliferation after anti-PD-1/PD-L1 treatment. A small subset of responding patients displayed increased PD-1^{+} Treg proliferation, not necessarily in parallel with increased effector T cell proliferation, suggesting that alternative mechanisms underlying anti-PD-1/PD-L1-response are at play, as documented by others [44].

In addition to enhanced expression of genes related to immunosuppression by Tregs after treatment, we show that Tregs also acquire a more proapoptotic gene expression program. These data confirm earlier findings in a graft-versus-host disease model demonstrating superior immunosuppressive activity after PD-1 blockade by apoptotic Tregs compared with their nonapoptotic counterparts [39]. Apoptotic Tregs abolished anti-PD-L1 efficacy in various tumor models [39,45]. However, data obtained in claudin-low murine breast cancer, commonly linked to triple-negative breast cancer, suggest that anti-PD-1 treatment can promote the survival of Tregs [46]. Factors such as timing, tumor model and antibody used could account for this discrepancy. Future efforts should confirm whether, upon excess stimulation, Tregs indeed benefit from an apoptotic phenotype and whether reverting Treg apoptosis could improve efficacy of anti-PD-1/PD-L1 therapy.

Our data indicate that PD-1 exerts an important function in directly modulating Treg phenotype after anti-PD-L1 treatment. These findings align with recent data showing PD-1-deficient Tregs to be superior immunosuppressors compared with their wildtype counterparts [17,47-49]. The direct effect mitigated via PD-1 expressed on Tregs appeared not to be exclusive, and it is tempting to speculate that besides direct effects, also indirect effects mediated via mechanisms such as the modulation of APCs are also at play. Future research in anti-PD-1/PD-L1-resistant tumor-bearing mice and in models with a Treg-specific PD-1 deficiency could shed further light on this hypothesis. However, because genetic deletion of PD-1 on Tregs will likely mimic anti-PD-1/PD-L1 antibody-mediated Treg activation, therapeutic efficacy may already be compromised.

How PD-1 blockade could affect downstream receptor signaling in Tregs remains incompletely understood. In line with its impact on effector T cells, PD-1 signaling in Tregs decreased phosphatidylinositol 3-kinase (PI3K)-AKT signaling whereas antibody-mediated blockade or genetic ablation enhanced suppressive capacity in a murine tumor model [16]. These data are in sharp contrast with data derived from an autoimmune encephalomyelitis model where PD-1 deficiency in Tregs resulted in diminished PI3K-AKT signaling, whereas an AKT activator reduced suppressive activity [48]. These contrasting effects of PD-1 signaling in Tregs may be explained by different disease settings or specific rewiring of Tregs depending on the metabolic milieu. For example, lactic acid in the TME is important for Treg immune suppressive function and the resultant efficacy of anti-CTLA-4 therapy [50-53]. Therefore, context-specific adjustments in Tregs may profoundly influence the net effect of PD-1 signaling on Tregs.

Our temporal analysis across multiple organs indicates that anti-PD-1/PD-L1-mediated effects on Tregs are systemically mediated. Others have previously indicated the importance of peripheral lymphoid tissues in generating effective anti-PD-1/PD-L1 efficacy and we have recently demonstrated a critical role for TDLNs in generating progenitor exhausted T cells after ICB that subsequently seed the tumor [54-56]. Tregs in the TDLN have already been shown to mediate a role in anti-tumor immunity by restraining tumor invasion in patients with breast cancer whereas Tregs in tumors were dysfunctional [57]. In the context of anti-PD-1/PD-L1 resistance, durable therapy resistance may therefore not only depend on anti-PD-1/PD-L1 mediated activation of Tregs in the TME but also on activation of Tregs peripheral lymphoid tissues, including the TDLN, that are recruited to the tumor. Selective PD-L1 blockade or Treg depletion in TDLNs could provide clues to the location and mechanisms of Treg mediated T cell suppression.

To date, clinical efficacy of manipulation of Treg number or function by CD25-directed antibodies is restricted. Development of novel CD25-depleting antibodies that preserves CD25 signaling in the effector T cell compartment offers opportunities [58]. In addition, the discovery and clinical investigation of targets increased by checkpoint blockade, such as TIGIT, or recently identified Tregs targets, including endoglin, MCT1 and BATF, could offer avenues in attenuating ICB-mediated Treg activation [59-61]. However, not all nonresponding patients showed increased Treg activity after treatment, indicating that other resistance mechanisms are in play and that careful selection of eligible patients is essential.

Although we were able to show activation of Tregs upon anti-PD-L1 treatment in mouse models of primary and acquired resistance to therapy, we did not selectively ablate PD-1 on Tregs to determine a direct causal relation of this inhibitory molecule with therapy resistance. Furthermore, the responses of Tregs in patients with cancer under treatment were measured retrospectively and would ideally be taken from cancer lesions instead of peripheral blood.

In summary, our findings implicate anti-PD-1/PD-L1-mediated activation of Tregs as an important mediator of therapy resistance. These data offer avenues for further research into the underlying mechanisms, identification of biomarkers and treatment-induced Treg-specific targets that could reverse anti-PD-1/PD-L1 resistance.

References

1. Yarchoan, M., Hopkins, A. & Jaffee, E.M. Tumor Mutational Burden and Response Rate to PD-1 Inhibition. *N Engl J Med* **377**, 2500-2501 (2017).
2. Dammeijer, F., Lau, S.P., van Eijck, C.H.J., van der Burg, S.H. & Aerts, J. Rationally combining immunotherapies to improve efficacy of immune checkpoint blockade in solid tumors. *Cytokine Growth Factor Rev* **36**, 5-15 (2017).
3. Ribas, A. & Wolchok, J.D. Cancer immunotherapy using checkpoint blockade. *Science* **359**, 1350-1355 (2018).
4. van Elsas, M.J., van Hall, T. & van der Burg, S.H. Future Challenges in Cancer Resistance to Immunotherapy. *Cancers (Basel)* **12**(2020).
5. Togashi, Y., Shitara, K. & Nishikawa, H. Regulatory T cells in cancer immunosuppression - implications for anticancer therapy. *Nat Rev Clin Oncol* **16**, 356-371 (2019).
6. Shang, B., Liu, Y., Jiang, S.J. & Liu, Y. Prognostic value of tumor-infiltrating FoxP3+ regulatory T cells in cancers: a systematic review and meta-analysis. *Sci Rep* **5**, 15179 (2015).
7. Sharma, P., Hu-Lieskovan, S., Wargo, J.A. & Ribas, A. Primary, Adaptive, and Acquired Resistance to Cancer Immunotherapy. *Cell* **168**, 707-723 (2017).
8. Arce Vargas, F.*, et al.* Fc-Optimized Anti-CD25 Depletes Tumor-Infiltrating Regulatory T Cells and Synergizes with PD-1 Blockade to Eradicate Established Tumors. *Immunity* **46**, 577-586 (2017).
9. Penaloza-MacMaster, P.*, et al.* Interplay between regulatory T cells and PD-1 in modulating T cell exhaustion and viral control during chronic LCMV infection. *J Exp Med* **211**, 1905-1918 (2014).
10. Liu, J.*, et al.* Assessing Immune-Related Adverse Events of Efficacious Combination Immunotherapies in Preclinical Models of Cancer. *Cancer Res* **76**, 5288-5301 (2016).
11. Vignali, D.A., Collison, L.W. & Workman, C.J. How regulatory T cells work. *Nat Rev Immunol* **8**, 523-532 (2008).
12. Wing, K.*, et al.* CTLA-4 control over Foxp3+ regulatory T cell function. *Science* **322**, 271-275 (2008).
13. Okazaki, T., Chikuma, S., Iwai, Y., Fagarasan, S. & Honjo, T. A rheostat for immune responses: the unique properties of PD-1 and their advantages for clinical application. *Nat Immunol* **14**, 1212-1218 (2013).
14. Flies, D.B., Sandler, B.J., Sznol, M. & Chen, L. Blockade of the B7-H1/PD-1 pathway for cancer immunotherapy. *Yale J Biol Med* **84**, 409-421 (2011).
15. Riley, J.L. PD-1 signaling in primary T cells. *Immunol Rev* **229**, 114-125 (2009).
16. Kumagai, S.*, et al.* The PD-1 expression balance between effector and regulatory T cells predicts the clinical efficacy of PD-1 blockade therapies. *Nat Immunol* **21**, 1346-1358 (2020).
17. Kamada, T.*, et al.* PD-1(+) regulatory T cells amplified by PD-1 blockade promote hyperprogression of cancer. *Proc Natl Acad Sci U S A* **116**, 9999-10008 (2019).
18. Rao, T.N.*, et al.* Novel, Non-Gene-Destructive Knock-In Reporter Mice Refute the Concept of Monoallelic Gata3 Expression. *J Immunol* **204**, 2600-2611 (2020).
19. Wan, Y.Y. & Flavell, R.A. Identifying Foxp3-expressing suppressor T cells with a bicistronic reporter. *Proc Natl Acad Sci U S A* **102**, 5126-5131 (2005).
20. Mazieres, J.*, et al.* Immune checkpoint inhibitors for patients with advanced lung cancer and oncogenic driver alterations: results from the IMMUNOTARGET registry. *Ann Oncol* **30**, 1321-1328 (2019).
21. Gainor, J.F.*, et al.* EGFR Mutations and ALK Rearrangements Are Associated with Low Response Rates to PD-1 Pathway Blockade in Non-Small Cell Lung Cancer: A Retrospective Analysis. *Clin Cancer Res* **22**, 4585-4593 (2016).
22. Tsao, A.S.*, et al.* A practical guide of the Southwest Oncology Group to measure malignant pleural mesothelioma tumors by RECIST and modified RECIST criteria. *J Thorac Oncol* **6**, 598-601 (2011).
23. van Elsas, M.J.*, et al.* Regulatory T Cell Depletion Using a CRISPR Fc-Optimized CD25 Antibody. *Int J Mol Sci* **23**(2022).
24. Dammeijer, F.*, et al.* Depletion of Tumor-Associated Macrophages with a CSF-1R Kinase Inhibitor Enhances Antitumor Immunity and Survival Induced by DC Immunotherapy. *Cancer Immunol Res* **5**, 535-546 (2017).
25. McMurchy, A.N. & Levings, M.K. Suppression assays with human T regulatory cells: a technical guide. *Eur J Immunol* **42**, 27-34 (2012).
26. Picelli, S.*, et al.* Smart-seq2 for sensitive full-length transcriptome profiling in single cells. *Nat Methods* **10**, 1096-1098 (2013).
27. Kim, D., Langmead, B. & Salzberg, S.L. HISAT: a fast spliced aligner with low memory requirements. *Nat Methods* **12**, 357-360 (2015).
28. Love, M.I., Huber, W. & Anders, S. Moderated estimation of fold change and dispersion for RNA-seq data with DESeq2. *Genome Biol* **15**, 550 (2014).

29. Heinz, S.*, et al.* Simple combinations of lineage-determining transcription factors prime cis-regulatory elements required for macrophage and B cell identities. *Mol Cell* **38**, 576-589 (2010).
30. Zhou, Y.*, et al.* Metascape provides a biologist-oriented resource for the analysis of systems-level datasets. *Nat Commun* **10**, 1523 (2019).
31. Miao, Z., Deng, K., Wang, X. & Zhang, X. DEsingle for detecting three types of differential expression in single-cell RNA-seq data. *Bioinformatics* **34**, 3223-3224 (2018).
32. Zelba, H.*, et al.* Accurate quantification of T-cells expressing PD-1 in patients on anti-PD-1 immunotherapy. *Cancer Immunol Immunother* **67**, 1845-1851 (2018).
33. Strauss, L.*, et al.* Targeted deletion of PD-1 in myeloid cells induces antitumor immunity. *Sci Immunol* **5**(2020).
34. Shalev, I.*, et al.* Targeted deletion of fgl2 leads to impaired regulatory T cell activity and development of autoimmune glomerulonephritis. *J Immunol* **180**, 249-260 (2008).
35. Chruscinski, A.*, et al.* Role of Regulatory T Cells (Treg) and the Treg Effector Molecule Fibrinogen-like Protein 2 in Alloimmunity and Autoimmunity. *Rambam Maimonides Med J* **6**(2015).
36. Park, Y.*, et al.* TSC1 regulates the balance between effector and regulatory T cells. *J Clin Invest* **123**, 5165-5178 (2013).
37. Mouly, E.*, et al.* The Ets-1 transcription factor controls the development and function of natural regulatory T cells. *J Exp Med* **207**, 2113-2125 (2010).
38. Polansky, J.K.*, et al.* Methylation matters: binding of Ets-1 to the demethylated Foxp3 gene contributes to the stabilization of Foxp3 expression in regulatory T cells. *J Mol Med (Berl)* **88**, 1029-1040 (2010).
39. Maj, T.*, et al.* Oxidative stress controls regulatory T cell apoptosis and suppressor activity and PD-L1-blockade resistance in tumor. *Nat Immunol* **18**, 1332-1341 (2017).
40. Yost, K.E.*, et al.* Clonal replacement of tumor-specific T cells following PD-1 blockade. *Nat Med* **25**, 1251-1259 (2019).
41. Liu, B.*, et al.* Temporal single-cell tracing reveals clonal revival and expansion of precursor exhausted T cells during anti-PD-1 therapy in lung cancer. *Nat Cancer* **3**, 108-121 (2022).
42. Horn, L.*, et al.* First-Line Atezolizumab plus Chemotherapy in Extensive-Stage Small-Cell Lung Cancer. *N Engl J Med* **379**, 2220-2229 (2018).
43. Antonia, S.J.*, et al.* Nivolumab alone and nivolumab plus ipilimumab in recurrent small-cell lung cancer (CheckMate 032): a multicentre, open-label, phase 1/2 trial. *Lancet Oncol* **17**, 883-895 (2016).
44. Nishino, M., Ramaiya, N.H., Hatabu, H. & Hodi, F.S. Monitoring immune-checkpoint blockade: response evaluation and biomarker development. *Nat Rev Clin Oncol* **14**, 655-668 (2017).
45. Asano, T.*, et al.* PD-1 modulates regulatory T-cell homeostasis during low-dose interleukin-2 therapy. *Blood* **129**, 2186-2197 (2017).
46. Vick, S.C., Kolupaev, O.V., Perou, C.M. & Serody, J.S. Anti-PD-1 Checkpoint Therapy Can Promote the Function and Survival of Regulatory T Cells. *J Immunol* **207**, 2598-2607 (2021).
47. Zhang, B., Chikuma, S., Hori, S., Fagarasan, S. & Honjo, T. Nonoverlapping roles of PD-1 and FoxP3 in maintaining immune tolerance in a novel autoimmune pancreatitis mouse model. *Proc Natl Acad Sci U S A* **113**, 8490-8495 (2016).
48. Tan, C.L.*, et al.* PD-1 restraint of regulatory T cell suppressive activity is critical for immune tolerance. *J Exp Med* **218**(2021).
49. Perry, J.A.*, et al.* PD-L1-PD-1 interactions limit effector regulatory T cell populations at homeostasis and during infection. *Nat Immunol* **23**, 743-756 (2022).
50. Overacre-Delgoffe, A.E.*, et al.* Interferon-gamma Drives Treg Fragility to Promote Anti-tumor Immunity. *Cell* **169**, 1130-1141 e1111 (2017).
51. Wang, H.*, et al.* CD36-mediated metabolic adaptation supports regulatory T cell survival and function in tumors. *Nat Immunol* **21**, 298-308 (2020).
52. Watson, M.J.*, et al.* Metabolic support of tumour-infiltrating regulatory T cells by lactic acid. *Nature* **591**, 645-651 (2021).
53. Lim, S.A.*, et al.* Lipid signalling enforces functional specialization of Tregs in tumours. *Nature* **591**, 306-311 (2021).
54. Li, H.*, et al.* Dysfunctional CD8 T Cells Form a Proliferative, Dynamically Regulated Compartment within Human Melanoma. *Cell* **176**, 775-789 e718 (2019).
55. Sade-Feldman, M.*, et al.* Defining T Cell States Associated with Response to Checkpoint Immunotherapy in Melanoma. *Cell* **175**, 998-1013 e1020 (2018).
56. Dammeijer, F.*, et al.* The PD-1/PD-L1-Checkpoint Restrains T cell Immunity in Tumor-Draining Lymph Nodes. *Cancer Cell* **38**, 685-700 e688 (2020).
57. Nunez, N.G.*, et al.* Tumor invasion in draining lymph nodes is associated with Treg accumulation in breast cancer patients. *Nat Commun* **11**, 3272 (2020).
58. Solomon, I.*, et al.* CD25-Treg-depleting antibodies preserving IL-2 signaling on effector T cells enhance effector activation and antitumor immunity. *Nat Cancer* **1**, 1153-1166 (2020).

59. Schoonderwoerd, M.J.A., *et al.* Targeting Endoglin-Expressing Regulatory T Cells in the Tumor Microenvironment Enhances the Effect of PD1 Checkpoint Inhibitor Immunotherapy. *Clin Cancer Res* **26**, 3831-3842 (2020).
60. Kumagai, S., *et al.* Lactic acid promotes PD-1 expression in regulatory T cells in highly glycolytic tumor microenvironments. *Cancer Cell* **40**, 201-218 e209 (2022).
61. Itahashi, K., *et al.* BATF epigenetically and transcriptionally controls the activation program of regulatory T cells in human tumors. *Sci Immunol* **7**, eabk0957 (2022).

Supplementary data

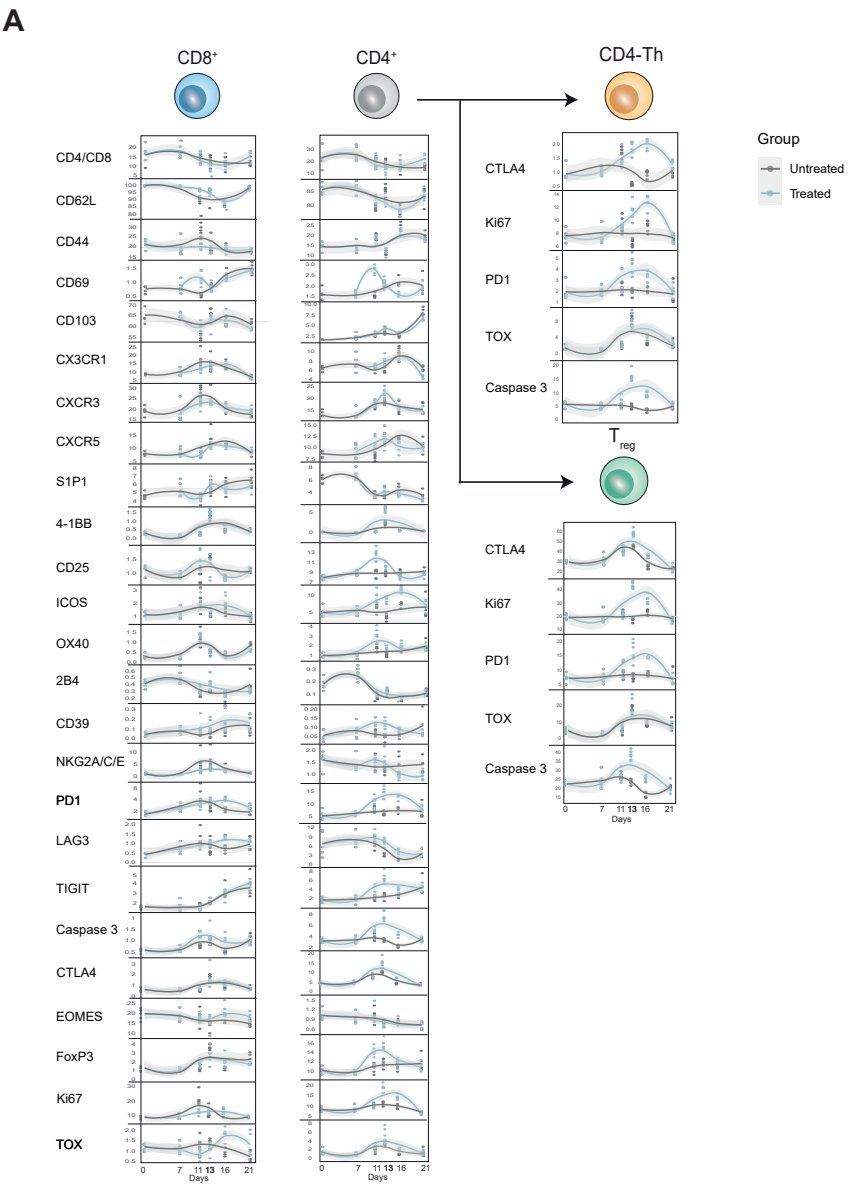

Figure S1: Comparison of CD8⁺ T cell and CD4⁺ T cell (CD4⁺ Th- and Treg) phenotype at different time points prior to or following checkpoint blockade, related to Figure 1

Protein expression (percentage positive) of co-stimulatory, co-inhibitory and transcription factors were compared between isotype-treated (grey) and anti-PD-L1-treated (blue) mice at each indicated time point (days post tumor inoculation) by flow cytometry, alternative to heatmaps illustrated in Figure 1D.

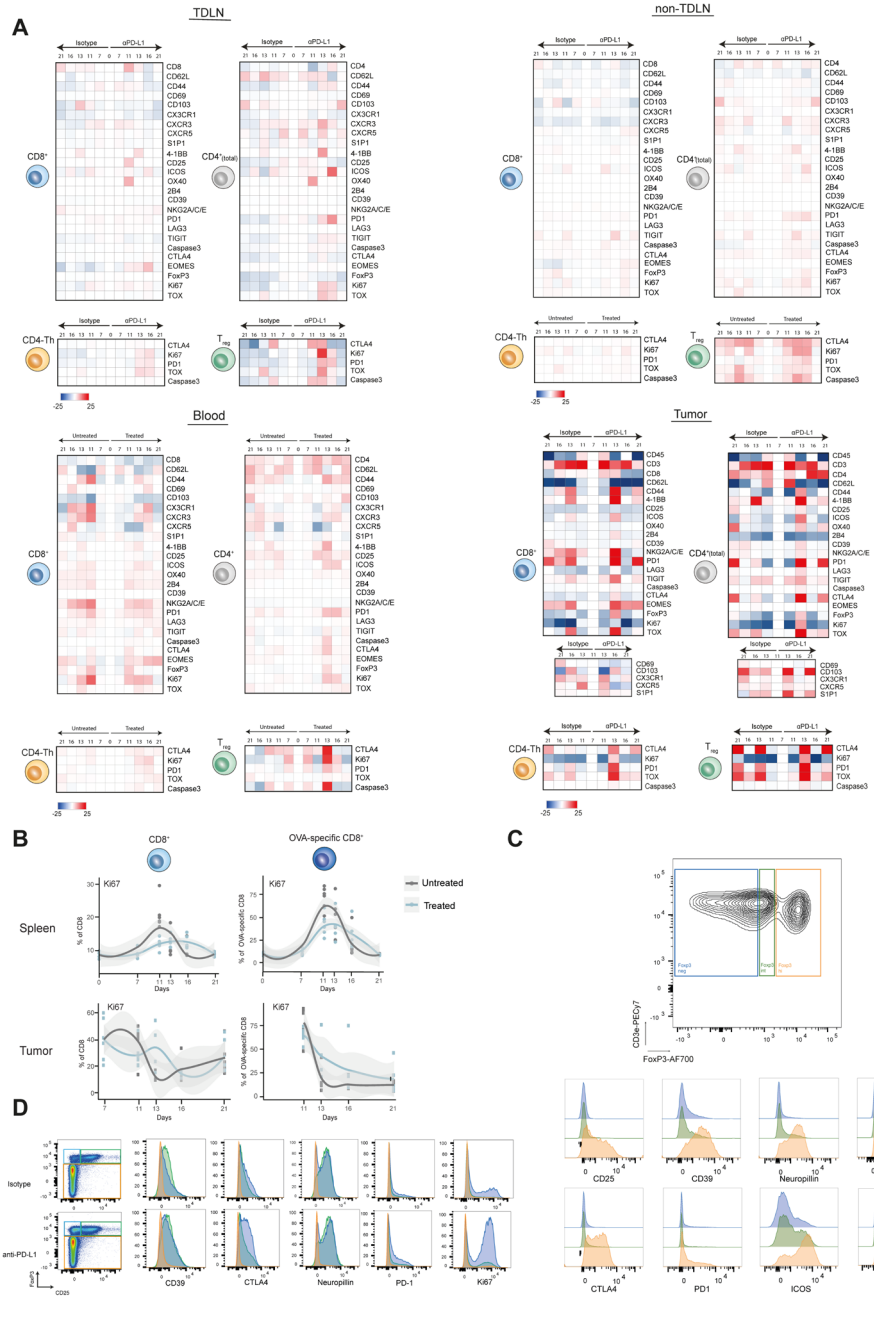
A
TDLN
non-TDLN
Blood
Tumor
Isotype
αPD-L1
Untreated
Treated
CD8+
CD4+(total)
CD4-Th
Treg
CD8
CD62L
CD44
CD69
CD103
CX3CR1
CXCR3
CXCR5
S1P1
4-1BB
CD25
ICOS
OX40
2B4
CD39
NKG2A/C/E
PD1
LAG3
TIGIT
Caspase3
CTLA4
EOMES
FoxP3
Ki67
TOX
CD45
CD3
CD4
B
CD8+
OVA-specific CD8+
Untreated
Treated
Spleen
Tumor
Ki67
% of CD8
% of OVA-specific CD8
Days
C
CD3e-PECy7
FoxP3-AF700
CD25
CD39
Neuropilin
Ki67
CTLA4
PD1
ICOS
OX40
D
Isotype
anti-PD-L1
Events
CD25
CD39
CTLA4
Neuropilin
PD-1
Ki67

◂Figure S2: Temporal analysis of T cells in anti-PD-L1-treated AE17-OVA model in TDLN, non-TDLN, blood and tumor, related to Figure 1

(A) Similar to Figure 1D, TDLNs, non-TDLNs, blood and tumors were harvested at different time points prior to and post anti-PD-L1 treatment i.p. at day 10. Heatmaps display the difference in percentage positive at the different time points compared with day 0 for all markers that were assessed by flow cytometry. (B) Ki67 protein expression was assessed for total $CD8^+$ T cells and OVA-specific $CD8^+$ T cells (stained by a SIINFKEL tetramer) at the different time points in spleen and tumor. (C) Treg related markers were assessed by flow cytometry for FoxP3 negative (blue), intermediate (green) and high (orange) subpopulations. (D) Treg related markers were assessed by flow cytometry for $FoxP3^-$ (orange), $FoxP3^+CD25^-$ (blue) and $FoxP3^+CD25^+$ (green) CD4 T cell subsets. TDLN = tumor-draining lymph node, i.p. = intraperitoneal.

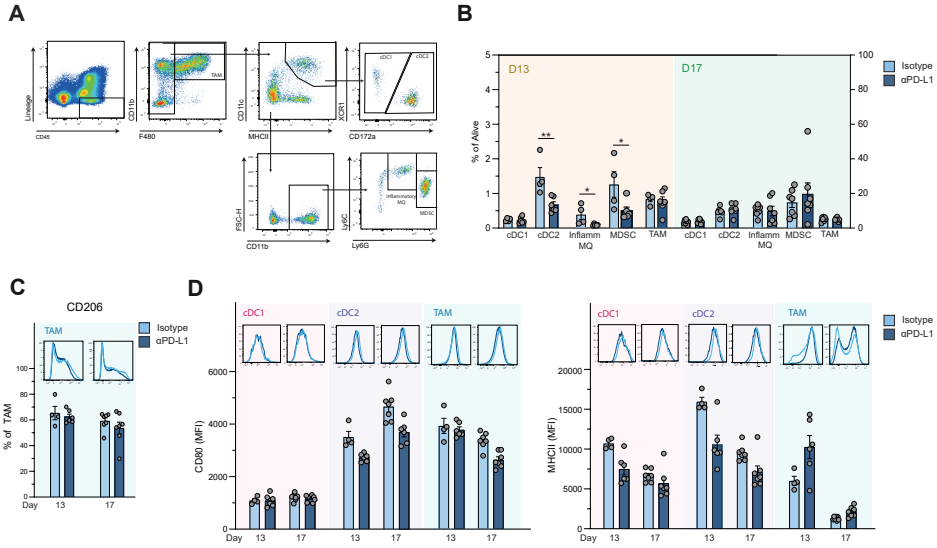

Figure S3: Evaluation of the effect of anti-PD-L1 treatment on myeloid cells in AE17-OVA bearing mice

(A) Gating strategy for the characterization of cDC1s, cDC2s, MDSCs and inflammatory MQs. (B) Bargraphs displaying the percentage of alive of the different cell types isolated from tumor material at day 13 (yellow) and 17 (green) following isotype or anti-PD-L1 treatment at day 10 (n = 4 to 6 mice per group). (C) Percentage CD206 positivity on TAMs (D) MFI of CD80 (left) and MHCII (right) on cDC1s (pink), cDC2s (purple) and TAMs (blue). Means and SEMs are shown and unpaired t tests were performed indicating statistical significance. * = $p < 0.05$, ** = $p < 0.01$. cDC = conventional dendritic cell, MDSC = myeloid-derived suppressor cell, MQ = macrophage, TAM = Tumor-associated macrophage, MFI = mean fluorescence intensity.

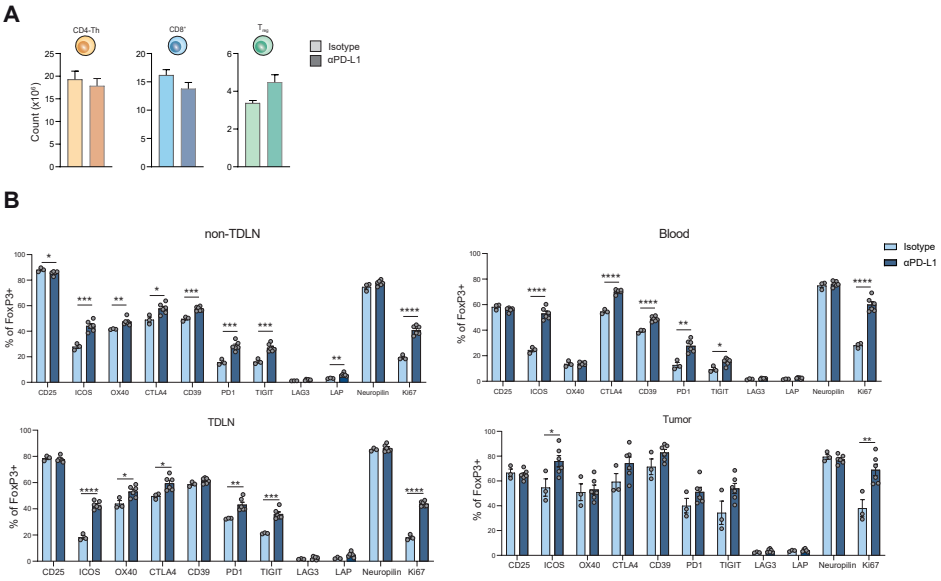

Figure S4: Comparison of Treg phenotype in non-TDLN, blood, TDLN and tumor of isotype- and anti-PD-L1 treated mice bearing AE17-OVA tumors, related to Figure 2

(A) Absolute counts of $CD4^+$ Th cells (orange), $CD8^+$ T cells (blue) and Tregs (green) in spleens at day 13, 3 days following isotype or anti-PD-L1 treatment. (B) Similar to Figure 2A, non-TDLNs, blood, TDLNs and tumors were isolated from AE17-OVA bearing mice 3 days post isotype or anti-PD-L1 treatment i.p. (d13) and Tregs were stained for markers associated with suppressive activity by flow cytometry. Means and SEMs are shown and unpaired t tests were performed indicating statistical significance. * = $p < 0.05$, ** = $p < 0.01$, *** = $p < 0.001$, **** = $p < 0.0001$. i.p = intraperitoneal, TDLN = tumor-draining lymph node, SEM = standard error of the mean.

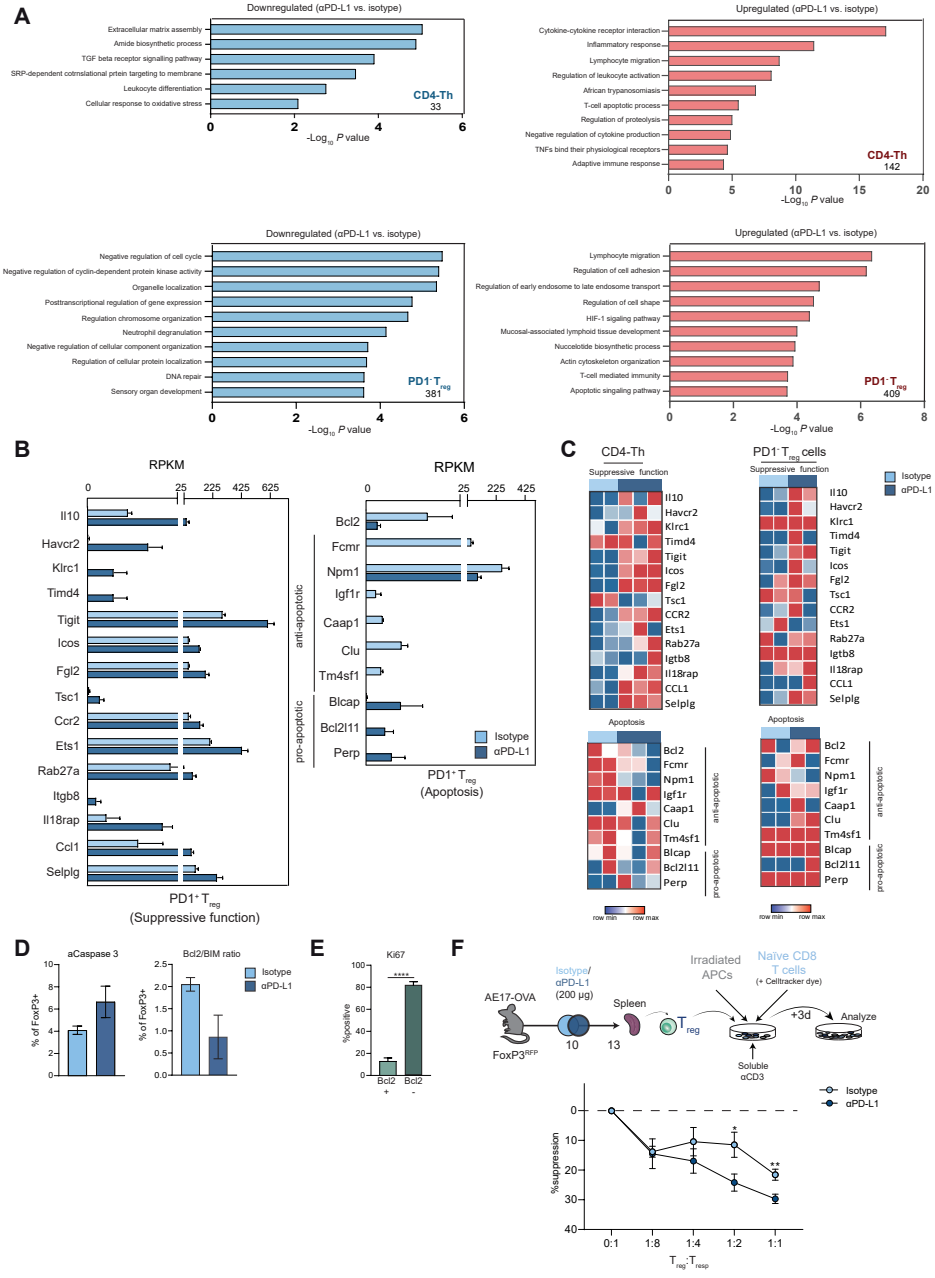
A
Downregulated (αPD-L1 vs. isotype)
Extracellular matrix assembly
Amide biosynthetic process
TGF beta receptor signalling pathway
SRP-dependent cotranslational prtein targeting to membrane
Leukocyte differentiation
Cellular response to oxidative stress
CD4-Th
33
-Log10 P value
Upregulated (αPD-L1 vs. isotype)
Cytokine-cytokine receptor interaction
Inflammatory response
Lymphocyte migration
Regulation of leukocyte activation
African trypanosomiasis
T-cell apoptotic process
Regulation of proteolysis
Negative regulation of cytokine production
TNFs bind their physiological receptors
Adaptive immune response
CD4-Th
142
-Log10 P value
Downregulated (αPD-L1 vs. isotype)
Negative regulation of cell cycle
Negative regulation of cyclin-dependent protein kinase activity
Organelle localization
Posttranscriptional regulation of gene expression
Regulation chromosome organization
Neutrophil degranulation
Negative regulation of cellular component organization
Regulation of cellular protein localization
DNA repair
Sensory organ development
PD1+ Treg
381
-Log10 P value
Upregulated (αPD-L1 vs. isotype)
Lymphocyte migration
Regulation of cell adhesion
Regulation of early endosome to late endosome transport
Regulation of cell shape
HIF-1 signaling pathway
Mucosal-associated lymphoid tissue development
Nucleotide biosynthetic process
Actin cytoskeleton organization
T-cell mediated immunity
Apoptotic singaling pathway
PD1+ Treg
409
-Log10 P value
B
RPKM
Il10
Havcr2
Klrc1
Timd4
Tigit
Icos
Fgl2
Tsc1
Ccr2
Ets1
Rab27a
Itgb8
Il18rap
Ccl1
Selplg
PD1+ Treg
(Suppressive function)
RPKM
Bcl2
Fcmr
Npm1
Igf1r
Caap1
Clu
Tm4sf1
Blcap
Bcl2l11
Perp
anti-apoptotic
pro-apoptotic
Isotype
αPD-L1
PD1+ Treg
(Apoptosis)
C
CD4-Th
PD1+ Treg cells
Suppressive function
Isotype
αPD-L1
Apoptosis
anti-apoptotic
pro-apoptotic
row min
row max
D
aCaspase 3
% of FoxP3+
Bcl2/BIM ratio
% of FoxP3+
Isotype
αPD-L1
E
Ki67
%positive
****
Bcl2 +
Bcl2 -
F
AE17-OVA
FoxP3RFP
Isotype/
αPD-L1
(200 µg)
10
13
Spleen
Treg
Irradiated
APCs
Naïve CD8
T cells
(+ Celltracker dye)
+3d
Analyze
Soluble
αCD3
Isotype
αPD-L1
%suppression
0:1
1:8
1:4
1:2
1:1
Treg:Tresp

◂Figure S5: Effects of anti-PD-L1 treatment on Treg gene expression and function in the AE17-OVA model, related to Figure 2

(A-C) Tregs and $CD4^+$ Th cells were purified based on CD4, CD25, PD-1 and RFP expression from tumors of $FoxP3^{RFP}$ mice on day 13, 3 days following treatment with either isotype or anti-PD-L1. (A) Similar to Figure 2B, pathway analysis was performed on downregulated (blue) and upregulated (red) DEGs in $CD4^+$ Th cells and PD-1^- Tregs. (B) Related to Figure 2C, RPKM values of genes differentially expressed in PD-1^+ Tregs related to suppressive function and apoptosis (shown as z-scores of RPKM levels with row min-max based on all three T cell subsets). (C) Gene expression of DEGs in $CD4^+$ Th cells and PD-1^- Tregs and displayed in heatmaps. (D) Expression of activated caspase 3 and Bcl2/BIM ratio in Tregs isolated from tumors at day 13, 3 days following treatment with isotype or anti-PD-L1. (E) Ki67 expression in $Bcl2^+$ and $Bcl2^-$ Tregs in tumor (F) Similar to Figure 2D, $CD25^+RFP^+CD4^+$ T cells were sorted from spleens and cultured for three days with labeled naive $CD8^+$ T cells, mitomycin-irradiated T cell depleted splenocytes (APCs) and soluble anti-CD3 for 3 days. Proliferation of naive $CD8^+$ T cells was assessed with different T_{reg}:T_{resp} ratios with Tregs from either isotype or anti-PD-L1 treated mice. Percent suppression was calculated as described in the method section. Means and SEMs are shown and unpaired t tests were performed indicating statistical significance. * = $p < 0.05$, ** = $p < 0.01$. DEG = differentially expressed genes, RPKM = reads per kilobase million, APC = antigen presenting cell.

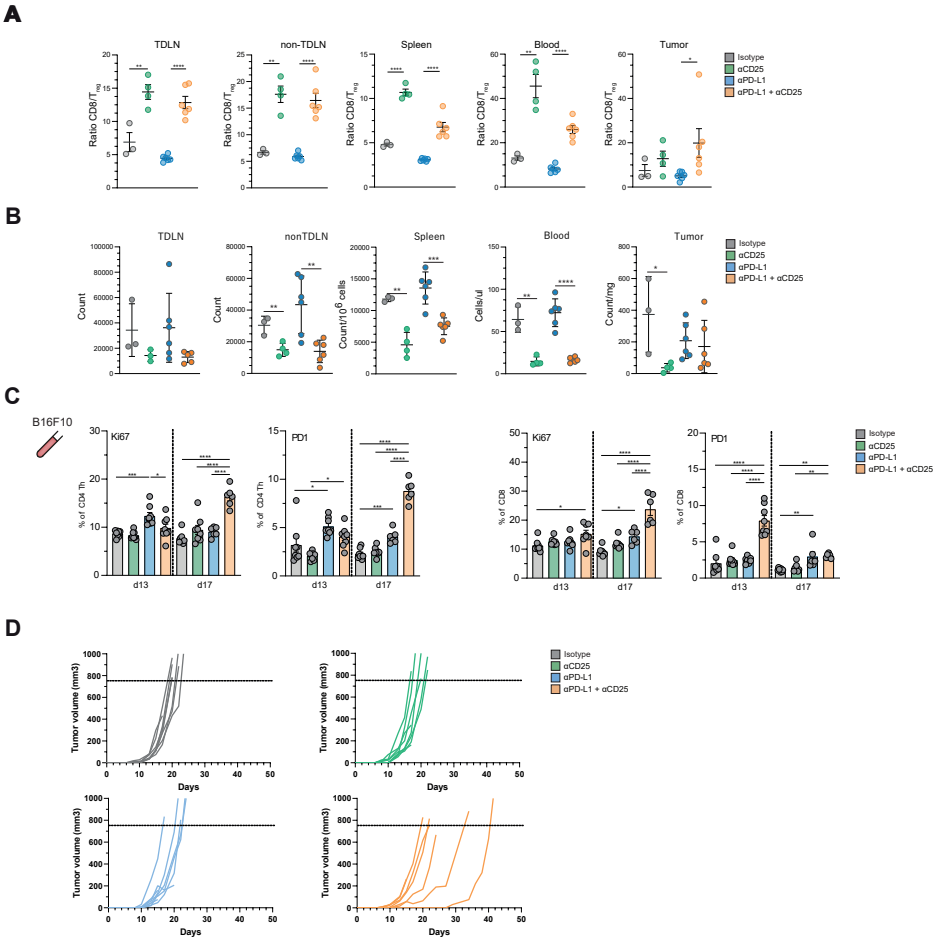

Figure S6: Evaluation of the effects T_{reg} depletion using anti-CD25 in combination with anti-PD-L1 in the AE17-OVA and B16F10 tumor model, related to Figure 4

(A-B) AE17-OVA bearing mice were treated with anti-CD25 mIgG2a at day 7 and 9 followed by anti-PD-L1 treatment at day 10. Mice were sacrificed at day 13 and TDLNs, non-TDLNs, spleens blood and tumors were harvested to assess the CD8/Treg ratio (A) and absolute Treg counts (B). (C-D) Mice bearing B16F10 tumors were treated with anti-CD25 mIgG2a at day 7 and 9 followed by anti-PD-L1 treatment at day 10, 13 and 17 and monitored for survival. (C) Peripheral blood was isolated at day 13 and 17 to assess the treatment effect on effector T cell proliferation (Ki67) and PD-1 expression. (D) Tumors were measured three times a week and displayed in growth curves. Mice were sacrificed when reaching a volume of >800 mm^3 (length x width x height x 0,52) or when severely ill. Means and SEMs are shown and unpaired t tests or one-way analysis of variance (ANOVA) were performed indicating statistical significance. * = $p < 0.05$, ** = $p < 0.01$, *** = $p < 0.001$, **** = $p < 0.0001$. i.p = intraperitoneal, TDLN = tumor-draining lymph node, SEM = standard error of the mean.

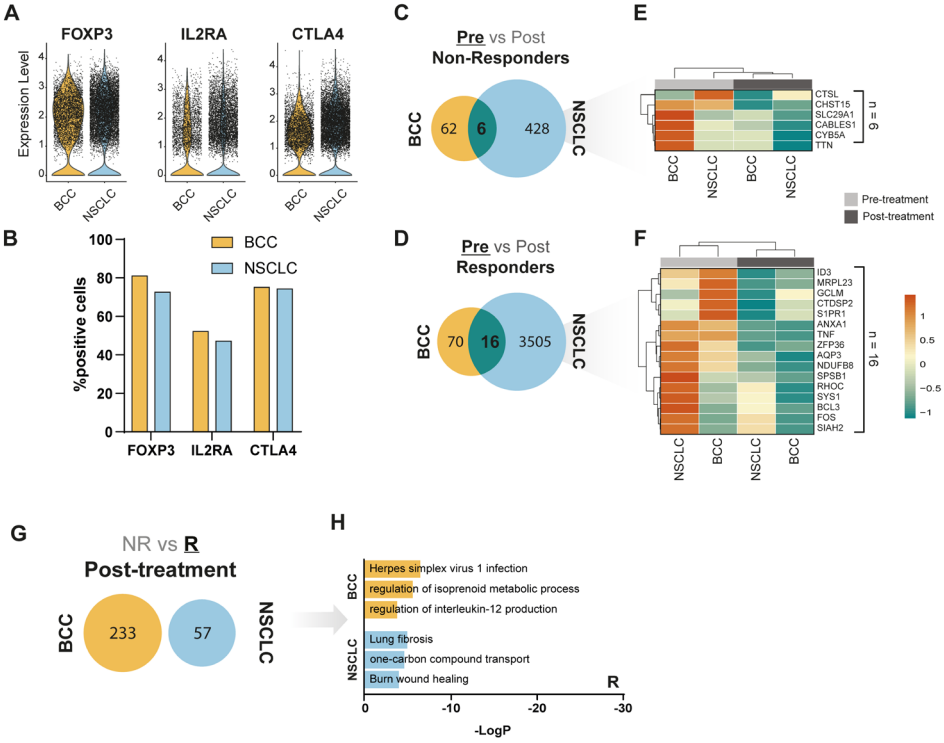

Figure S7: Transcriptional changes before and after anti-PD-1 therapy in BCC and NSCLC patients, related to Figure 5

(A) Violin plots showing the expression levels of Treg marker genes for the BCC and NSCLC datasets. (B) Percentage of cells expressing Treg marker genes of total Tregs for both the BCC and NSCLC datasets. (C) Venn diagram displaying overlap of genes upregulated pre-treatment (as compared with post-treatment samples) in non-responders of the BCC and NSCLC datasets. (D) Venn diagram displaying overlap of genes upregulated pre-treatment (as compared with post-treatment samples) in responders of the BCC and NSCLC datasets. (E) Heatmap of genes upregulated in both BCC and NSCLC non-responder patients pre-treatment, displayed as row Z-score. (F) Heatmap of genes upregulated in both BCC and NSCLC responder patients pre-treatment, displayed as row Z-score. (G) Venn diagram displaying overlap of genes upregulated in responders vs. nonresponders post-treatment in the BCC and NSCLC datasets. (H) Pathway enrichment analysis of genes upregulated in responders vs. nonresponders post-treatment in the BCC and NSCLC datasets. C-F) Adjusted P-value (FDR) < 0.05 and absolute log2fold change > 0.5.

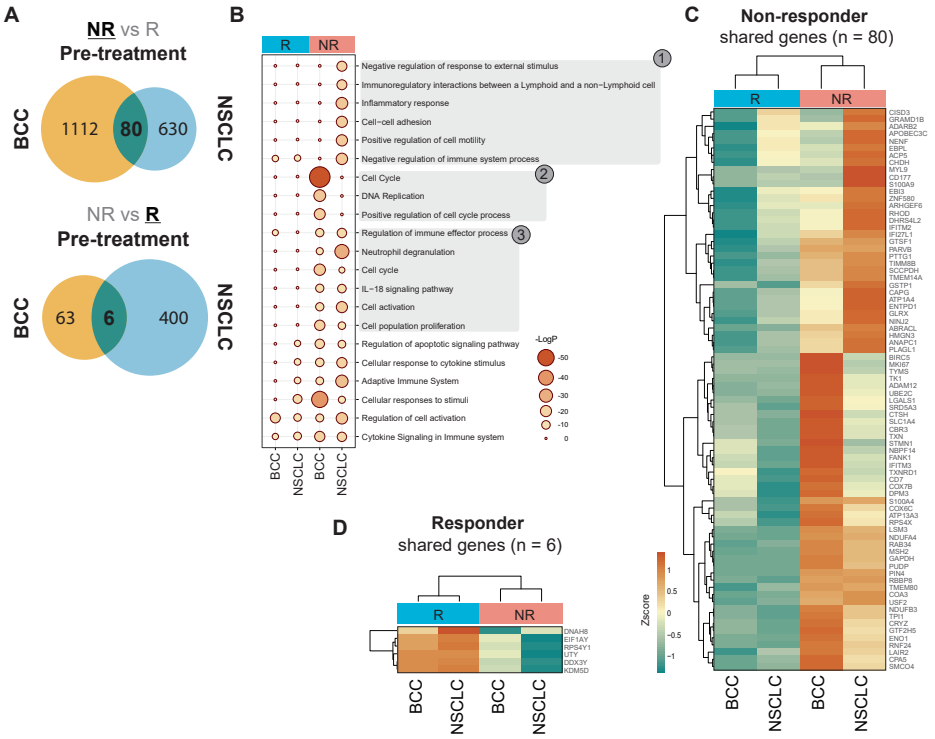

Figure S8: Differences between responders and nonresponders prior to treatment in BCC and NSCLC patients, related to Figure 5

(A) Venn diagrams displaying overlap in DEGs between BCC and NSCLC Tregs when comparing non-responders (NR) to responders (R). (B) Pathway enrichment analysis using pre-treatment DEGs upregulated in BCC and NSCLC Tregs from responders and nonresponders to anti-PD1 therapy. (C) Heatmap displaying scaled mean expression of genes upregulated in both BCC and NSCLC Tregs from nonresponders to anti-PD1 therapy. (D) Heatmap displaying the scaled mean expression of genes upregulated in both BCC and NSCLC Tregs from responders to anti-PD1 therapy. A-D) Adjusted P-value (FDR) < 0.05 and absolute log2fold change > 0.5. DEG = differentially expressed gene.

Figure S9: Evaluation of proliferation in Tregs, CD4⁺ Th cells and CD8⁺ T cells in patients with SCLC, NSCLC and mesothelioma at baseline and following anti-PD-1/ anti-PD-L1 treatment, related to Figure 6

Peripheral blood was isolated from patients with SCLC, NSCLC and mesothelioma at baseline (V1) and two weeks following start anti-PD-1/ anti-PD-L1 treatment (V2). (A-B) Graphs displaying the level of proliferation of PD-1⁻ Tregs in NSCLC (A) and mesothelioma (B). (C-D) Proliferation was assessed for PD-1⁻ and PD-1⁺ CD8 T cells (C) and PD-1⁻ and PD-1⁺ CD4⁺ Th cells (D) for SCLC patients. (E-F) For NSCLC, proliferation of PD-1⁻ and PD-1⁺ CD8 T cells (E) and PD-1⁻ and PD-1⁺ CD4⁺ Th cells (F) were assessed for nonresponding patients (orange) and responding patients (blue). (G-H) Proliferation of PD-1⁻ and PD-1⁺ CD8 T cells (G) and PD-1⁻ and PD-1⁺ CD4⁺ Th cells (H) was also assessed for nonresponding (orange) and responding (blue) mesothelioma patients. Means and SEMs are shown and unpaired t tests were performed indicating statistical significance. * = p < 0.05, ** = p < 0.01, *** = p < 0.001, **** = p < 0.0001. SCLC = small-cell lung cancer, NSCLC = non-small-cell lung cancer SEM = standard error of the mean.▸

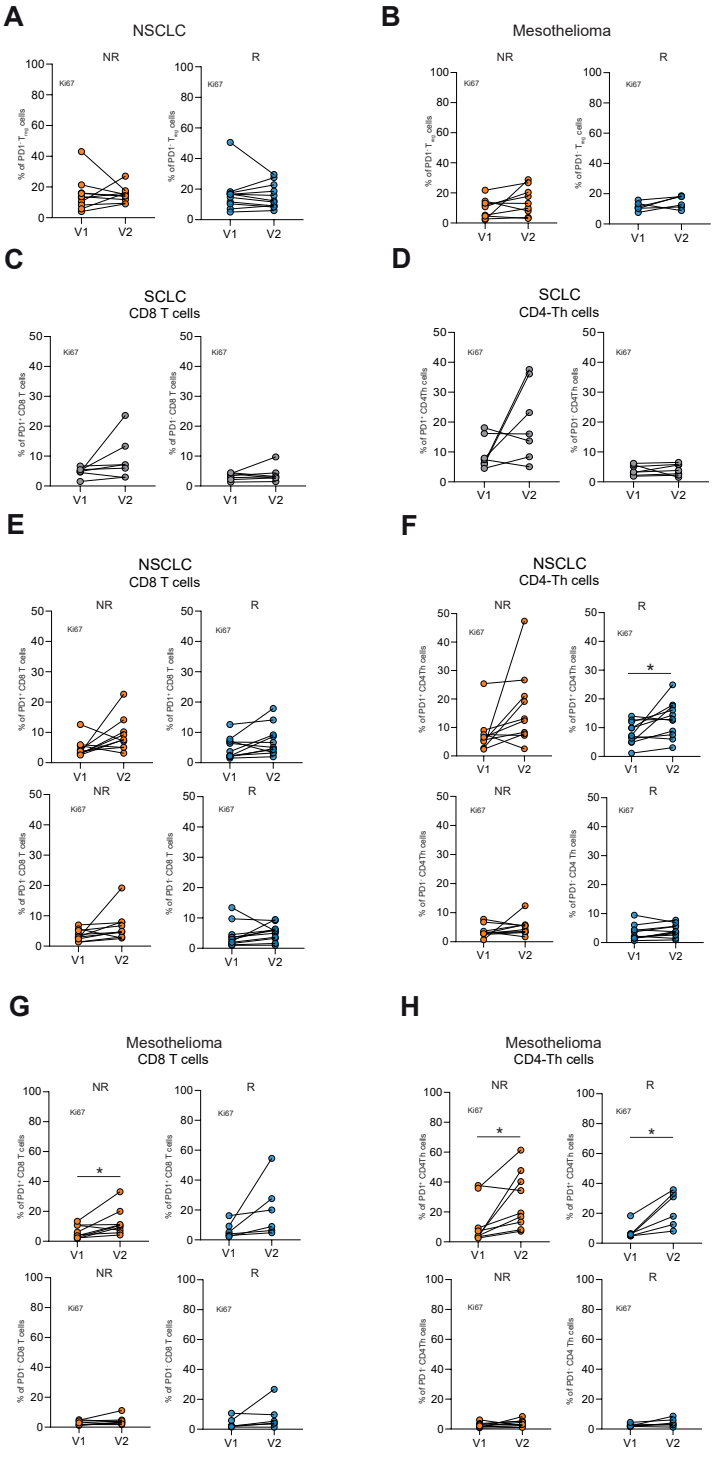
A
NSCLC
NR
R
Ki67
% of PD1+ T reg cells
V1
V2
B
Mesothelioma
C
SCLC
CD8 T cells
% of PD1+ CD8 T cells
D
SCLC
CD4-Th cells
% of PD1+ CD4Th cells
E
NSCLC
CD8 T cells
F
NSCLC
CD4-Th cells
% of PD1+ CD4 Th cells
G
Mesothelioma
CD8 T cells
H
Mesothelioma
CD4-Th cells
*

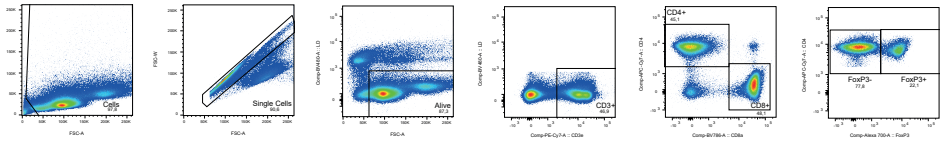

Figure S10: Gating strategy for the characterization of T cells in murine samples

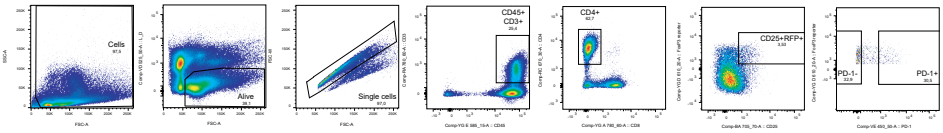

Figure S11: Gating strategy for the sorting of murine Tregs

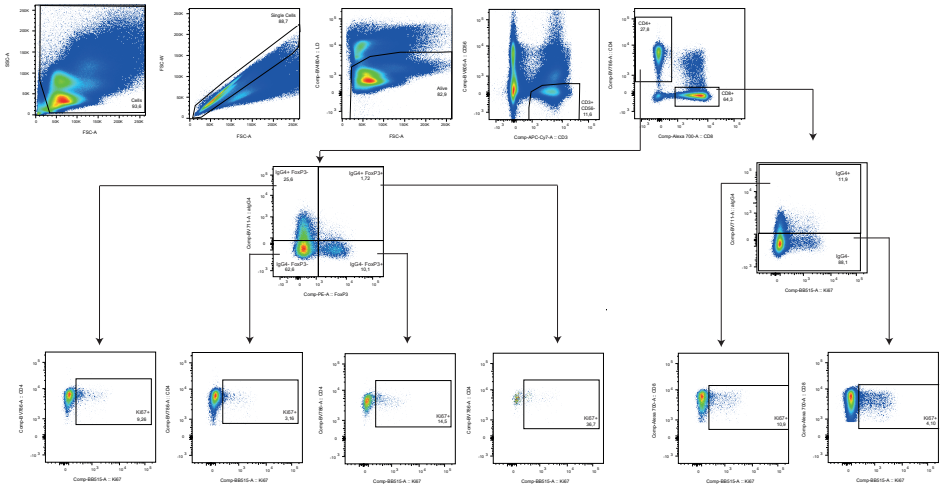

Figure S12: Gating strategy for the characterization of T cells in human peripheral blood

Table S1: NSCLC and BCC patient characteristics, related to Fig. 5

Characteristics		Yost et al. 2019			Liu et al. 2022		
		All patients (n = 11)	Responders (n = 6)	Nonresponders (n = 5)	All patients (n = 11)	Responders (n = 6)	Nonresponders (n = 5)
Patient characteristics							
Age		N/A	N/A	N/A	60 (48-73)	60 (48-73)	61 (57-64)
Sex	Male	N/A	N/A	N/A	8 (72.7)	5 (83.3)	3 (60.0)
	Female	N/A	N/A	N/A	3 (27.3)	1 (16.7)	2 (40.0)
Tumor characteristics							
Tumor type	BCC	11 (100)	6 (100)	5(100)	x	x	x
	NSCLC: LUAD	x	x	x	8 (72.7)	6 (100)	2 (40.0)
	NSCLC: LUSC	x	x	x	3 (27.3)	0	3 (60.0)
Biopsy site	Lymph node	x	x	x	4 (30.7)	2 (33.3)	2 (28.6)
	Right lung	x	x	x	5 (38.5)	3 (50.0)	2 (28.6)
	Left lung	x	x	x	3 (23.1)	1 (16.7)	2 (28.6)
	Liver	x	x	x	1 (7.7)	0	1 (14.3)
	Left arm	1 (9.1)	1 (16.7)	0	x	x	x
	Right arm	2 (18.2)	1 (16.7)	1 (20.0)	x	x	x
	Left ear	1 (9.1)	0	1 (20.0)	x	x	x
	Nose	1 (9.1)	1 (16.7)	0	x	x	x
	Knee	1 (9.1)	1 (16.7)	0	x	x	x
	Right calf	1 (9.1)	0	1 (20.0)	x	x	x
	Left forehead	1 (9.1)	1 (16.7)	0	x	x	x
	Right neck	1 (9.1)	0	1 (20.0)	x	x	x
	Left Cheek	2 (18.2)	1 (16.7)	1 (20.0)	x	x	x
Treatment							
Prior Treatment	Vismodegib	8 (72.7)	4 (66.7)	4 (80.0)	x	x	x
	Sonidegib	1 (9.1)	1 (16.7)	0	x	x	x
	None	2 (18.2)	1 (16.7)	1 (20.0)	11 (100)	6 (100)	5 (100)
Treatment	Pembrolizumab	8 (72.7)	3 (50.0)	5 (100)	11 (100)	6 (100)	5(100)
	Cemiplimab	3 (27.3)	3 (50.0)	0	x	x	x
Additional treatment	Ongoing Vismodegib treatment	3 (27.3)	1 (16.7)	2 (40.0)	x	x	x

Table S1: NSCLC and BCC patient characteristics, related to Fig. 5

Characteristics		Yost et al. 2019			Liu et al. 2022		
		All patients (n = 11)	Responders (n = 6)	Nonresponders (n = 5)	All patients (n = 11)	Responders (n = 6)	Nonresponders (n = 5)
Regulatory T-cells							
Cell numbers	Pre-treatment	2103	1347	756	4654	3038	1616
		(46.8)	(46.3)	(47.9)	(41.7)	(61.6)	(25.9)
	Post-treatment	2386	1564	822	6517	1896	4621
		(53.2)	(53.7)	(52.1)	(58.3)	(38.4)	(74.1)

Clinicopathological descriptives of all samples, in total and per response (responders and nonresponders)

Table S2. Patient characteristics of patients used in Figure 6.

Characteristics	SCLC	NSCLC	Mesothelioma
Patient characteristics			
n	7	21	15
Age	64 (52-78)	63 (45-73)	59 (49–82)
Sex			
Male	2 (28,6)	10 (47,6)	14 (93)
Female	5 (71,4)	11 (52,4)	1 (7)
Histology			
Adeno		15 (71,4)	0 (0)
Squamous		6 (28,6)	0 (0)
Epithelioid		0 (0)	12 (80)
Sarcomatoid		0 (0)	3 (20)
BOR (%)			
PD	0 (0)	10 (47,6)	5 (33,3)
SD	0 (0)	0 (0)	1 (6,7)
PR	7 (100)	11 (52,4)	9 (60)
Previous treatment			
0	0 (0)	5 (23,8)	0 (0)
1	0 (0)	5 (23,8)	15 (100)
2	0 (0)	2 (9,5)	0 (0)
3	0 (0)	4 (19)	0 (0)
4	0 (0)	1 (4,8)	0 (0)
5	0 (0)	1 (4,8)	0 (0)
6	0 (0)	1 (4,8)	0 (0)
7	0 (0)	1 (4,8)	0 (0)
8	0 (0)	1 (4,8)	0 (0)
anti-PD-1/PD-L1			
Platinum/etoposide /atezolizumab	7 (100)	0 (0)	0 (0)
Nivolumab	0 (0)	15 (71,4)	14 (93,3)
Pembrolizumab	0 (0)	6 (28,6)	1 (6,7)

0 = no treatment, 1 = Pemetrexed/platinum, 2 = Gemcitabine/platinum, 3 = Pemetrexed/platinum, radiotherapy, 4 = Etoposide/platinum, radiotherapy, 5 = Gemcitabine/platinum, radiotherapy, 6 = Etoposide/platinum, gemcitabine/platinum, radiotherapy, 7 = Pemetrexed/platinum, docetaxel, radiotherapy, 8 = Radiotherapy Clinicopathological descriptives of all samples (peripheral blood)

Part 2

Enhancing cancer vaccine efficacy through combined immunotherapy strategies

Chapter 5

Combination strategies to optimize efficacy of dendritic cell-based immunotherapy

Mandy van Gulijk, Floris Dammeijer, Joachim Aerts, Heleen Vroman

Frontiers of Immunology 2018 Dec 5:9:2759

Abstract

Dendritic cells (DCs) are antigen-presenting cells (APCs) that are essential for the activation of immune responses. In various malignancies, these immunostimulatory properties are exploited by DC therapy, aiming at the induction of effective anti-tumor immunity by vaccination with *ex vivo* antigen-loaded DCs. Depending on the type of DC therapy used, long-term clinical efficacy upon DC therapy remains restricted to a proportion of patients, likely due to lack of immunogenicity of tumor cells, presence of a stromal compartment, and the suppressive tumor microenvironment (TME) leading to the development of resistance. The efficacy of different types of DC therapy is dependent on the type of DC used and which type of antigen is used. In order to circumvent tumor-induced suppressive mechanisms and unleash the full potential of DC therapy, considerable efforts have been made to combine DC therapy with chemotherapy, radiotherapy or with immunomodulatory therapeutics, such as checkpoint inhibitors. These combination strategies could enhance tumor immunogenicity, stimulate endogenous DCs following immunogenic cell death, improve infiltration of cytotoxic T lymphocytes (CTLs) or specifically deplete immunosuppressive cells in the TME, such as regulatory T cells and myeloid-derived suppressor cells. In this review, different strategies of combining DC therapy with immunomodulatory treatments will be discussed. These strategies and insights will improve and guide DC-based combination immunotherapies with the aim of further improving patient prognosis and care.

Introduction

Dendritic cells (DCs) are the most potent antigen-presenting cells (APCs) and mediate a critical role in the interface between the innate and adaptive immune system. DCs can be subdivided in different subsets including conventional DCs (cDCs) and plasmacytoid DCs (pDCs) that arise in the bone marrow and reside in peripheral tissues in an immature state. In addition, monocytes are able to differentiate into monocyte-derived DCs (moDCs) upon inflammatory conditions [1-4]. Activation and maturation of DCs are induced upon exposure to environmental stimuli including damage-associated molecular patterns (DAMPs) and pathogen-associated molecular patterns (PAMPs), leading to enhanced expression of co-stimulatory molecules, cytokine production, reduced phagocytosing capacity and improved T- and B cell activation [5,6]. DC-mediated T cell activation is initiated by antigen presentation on major histocompatibility class (MHC) I and II and further guided by co-stimulation and secretion of cytokines [7-9]. In addition to T cell activation, DCs can activate natural killer (NK) cells by cell-cell contacts and secretion of pro-inflammatory cytokines such as type I interferons (IFNs) [10]. However, in a tumor setting, oncogenic mutations and factors secreted by cancer cells limit DC migration and maturation by inducing overexpression of signal transducer and activation of transcription 3 (STAT-3) [11-15], respectively. This leads to insufficient antigen presentation, T cell anergy and decreased T cell proliferation, thereby restricting effective anti-tumor immunity [16-18].

Therefore, administering mature *ex vivo*-activated DCs loaded with tumor antigens may circumvent suppressive tumor-derived signals, thereby inducing effective anti-tumor immunity upon vaccination. For the past two decades, DC therapy has been shown to be safe, well-tolerated and capable of inducing anti-tumor immunity [19]. However, response rates to DC therapy are limited, with objective responses rarely exceeding 15% [20]. Several mechanisms may contribute to the limited clinical efficacy besides suboptimal DC therapy design, including downregulation of tumor-associated antigens (TAAs) and MHC molecules by tumor cells, restricted migration of DCs to lymph nodes (LN) and the inherent immune suppressive tumor microenvironment (TME) [21-26]. The TME harbors a complex network of tumor tissue, stroma and immune cells including tumor-associated macrophages (TAMs), myeloid-derived suppressor cells (MDSCs) and regulatory T cells (Tregs). These suppressive cells inhibit activation, proliferation and effector functions of infiltrating immune cells by the expression of co-inhibitory molecules and secretion of immunosuppressive cytokines [27-29]. Conventional therapies, including chemotherapy and radiotherapy or more recently developed immunotherapies such as immune checkpoint inhibitors are able to counteract the immunosuppressive environment of the tumor. Therefore, combining these therapies with DC therapy could lead to synergistic effects and improve clinical responses. In this review, we will discuss current approaches of DC therapy, promising combinations with chemotherapy, radiotherapy and immune checkpoint inhibitors that are clinically applicable and future perspectives for novel combination therapies that can improve DC therapy efficacy.

Current approaches of DC therapy

In order to obtain a sufficient number of DCs for administration, DCs are commonly generated from isolated $CD14^+$ monocytes or from $CD34^+$ hematopoietic progenitors isolated from peripheral blood, bone marrow or cord blood [3,5]. Culturing purified $CD14^+$ monocytes with granulocyte-monocyte derived growth factor (GM-CSF) and interleukin (IL) 4 will lead to differentiation into immature moDCs [30]. Vaccination with these immature DCs loaded with tumor antigens characterizes first-generation DC therapy and resulted in poor clinical results with a tumor regression of 3.3% [31]. In second-generation DC therapy, DCs are additionally matured by 'maturation cocktails' including Toll-like receptor ligands and cytokines which improved clinical results with objective response rates of 8-15%. Sipuleucel-T, the only US FDA approved DC therapy for use in (prostate) cancer patients, can be positioned at the intersection between first- and second-generation DC therapy as maturation is not achieved by maturation cocktails but rather by the fusion of GM-CSF to prostate antigen [32]. In next generation DC therapy, naturally-occurring DC (nDCs) subsets are employed as nDCs are superior over mo-DCs in terms of functionality and production costs and time. In addition, different DC subsets also induce different tumor-specific immune responses, as vaccination with murine cDC1s induced a prominent $CD8^+$ T cell driven anti-tumor immune response beneficial in tumors with abundant Tregs whereas cDC2s induced a Th17-mediated anti-tumor immune response that were advantageous in tumors with tumor-associated macrophages [33,34]. Clinical trials using nDCs have shown that the usage of nDCs is safe, feasible and associated with promising efficacy which indicates that this should be further investigated [35,36].

DC loading

DCs can be loaded with different sources of tumor antigens, such as mRNA, peptides, proteins or whole tumor cell lysate [5,37]. While peptides bind directly to MHC molecules, proteins and tumor cells must be phagocytosed and processed before presentation on MHC molecules can occur. Furthermore, loading of DCs with tumor-associated peptides enables the induction of specific T cell responses, which minimizes the risk on side-effects and tolerance. However, for most tumor types, TAAs are still unidentified and can be circumvented by loading DCs with tumor lysate. Additionally, loading DCs with tumor lysate initiates a broad spectrum of immune responses which is not restricted to cytotoxic T lymphocyte (CTL) activation. This can improve DC therapy efficacy as objective clinical responses observed upon treatment with DCs loaded with tumor lysate (8.3%) are higher than treatment with DCs presenting defined antigens (3.6%) in a meta-analysis of 173 trials [38].

Route of administration

To induce effective anti-tumor immunity, migration of DCs to lymph nodes is essential. Therefore, various administration routes have been exploited (intradermally, intranodally, intravenously, subcutaneously and intratumorally), although to date the superior route of administration is not still not established. Also the percentages of DCs that migrate successfully towards the lymph nodes is

limited, with up to 4% of injected DCs reaching the lymph node after intradermal injection and 0-56% reaching the lymph node after intranodal injection [26]. The migratory capacity can be improved by preconditioning the injection site with a potent recall antigen, tetanus/dipteria toxoid, which improved overall survival (OS) and progression free survival (PFS) in glioblastoma patients [39]. In addition to improving migratory capacity, studies have also targeted apoptotic pathways by promoting Bcl-2 or inhibiting BAK/BAX signaling in DCs to increase the lifetime of DCs and thereby enhance bioavailability of the injected DCs which resulted in improved activation of T cells [40-43]. However, despite these attempts to improve DC therapy, combinatorial strategies are essential to prorogue suppressive mechanisms in the TME and to further potentiate the clinical efficacy of DC therapy.

Combination therapies to enhance DC therapy

Combination with chemotherapy

Chemotherapeutics are traditionally designed to eradicate and eliminate malignant cells to lower tumor burden. However, more recent insights indicate that chemotherapy also has off-target immunological effects depending on the type of chemotherapy, such as immunogenic cell death (ICD) of tumor cells, thereby enabling the induction of anti-tumor immunity [44]. ICD stimulates emission of DAMPs, including adenosine triphosphate (ATP), high mobility group box 1 (HMGB1) and calrecticulin (CALR), which initiates antigen uptake, maturation, activation, and recruitment of endogenous DCs in the tumor [45,46]. In addition, specific chemotherapeutics can directly deplete suppressive immune cells including Tregs and MDSCs [47-49]. Due to the effects on tumor burden and the immunosuppressive TME, chemotherapeutics could have synergistic effects when combined with DC therapy. For instance, tumor reduction by neo-adjuvant chemotherapy could improve DC therapy, as DC therapy is most effective in cases of low tumor burden [31]. In addition, depletion of immunosuppressive cells in the TME renders the TME more receptive for tumor-specific T cell infiltration upon DC therapy. Timing of chemotherapy administration may be crucial as potential synergistic effects of combination treatments depends on the interval and sequence of treatment administration [50]. For instance, chemotherapy applied prior to DC therapy with substantial intervals aims at tumor reduction whereas shorter intervals or concurrent combination therapy allow depletion of suppressive immune cells. In the following sections, combinations of well-studied chemotherapeutics with *ex vivo* antigen-loaded DCs will be discussed. A summary of the main characteristics of the studies is presented in Table S1.

Cyclophosphamide

Cyclophosphamide is an alkylating agent that has tumoricidal effects, thereby reducing tumor burden[51]. In addition, cyclophosphamide initiates ICD and transient lymphoablation upon high doses, which results in depletion of suppressive immune cells and stimulates anti-tumor T cell responses. In contrast, low-dose cyclophosphamide improves tumor-specific immunity by Treg depletion (Fig. 1) [47]. In

mesothelioma, melanoma and colon carcinoma murine models, administration of cyclophosphamide prior to DC therapy prolonged survival compared with mice treated with monotherapy. This is likely caused by a cyclophosphamide-induced decrease in Tregs, and subsequent increase in $CD3^+$ T cells, as observed in these studies [52,53]. Cyclophosphamide administration 3 days prior to DC therapy was shown to induce T cell responses to 3 melanoma gp100 antigen-derived peptides G154, G206-2M and G280-GV in 6 out of 7 melanoma patients post vaccination [54]. A reduction in Tregs was also observed in mesothelioma patients treated with concurrent combination of cyclophosphamide and DC therapy but remained unaffected in a study with melanoma patients [55,56]. These differences could be explained by differences in sampling time, as reduction in Tregs was evaluated after the first cyclophosphamide treatment in mesothelioma patients [55], whereas in melanoma patients, these levels were assessed after 4 and 6 cycles of DC therapy[56]. Combining DC therapy with cyclophosphamide also improves clinical efficacy, as patients with ovarian cancer that received cyclophosphamide concurrent with DC therapy and bevacizumab, a VEGF-a blocking antibody, exhibited significantly prolonged survival compared with patients not receiving cyclophosphamide [57]. These results were associated with reduced TGFβ levels, a cytokine that is abundantly produced by Tregs in ovarian cancer. Contradictory, combined DC therapy with cyclophosphamide resulted in poor clinical responses in patients with metastatic renal cell carcinoma. However, as the DCs administered in this study were of allogeneic origin, the lack of clinical efficacy could be explained by the nature of DCs administered[58]. These results indicate that Treg depletion upon cyclophosphamide treatment is able to synergistically augment DC therapy efficacy both in preclinical and clinical settings, depending on the tumor type and DCs applied.

Temozolomide

The alkylating agent temozolomide (TMZ) induces lymphoablation upon high dosages whereas at low doses it primarily targets Tregs (Fig. 1) [49]. As this compound effectively crosses the blood-brain barrier, TMZ is mainly used to treat glioblastoma and melanoma, as the brain is a frequent metastatic site for melanoma [59,60]. In patients with advanced melanoma, administration of one TMZ cycle prior to each DC therapy decreased circulating Tregs with 60.5% [61]. Simultaneous administration of TMZ and DC/glioma cell fusions in recurrent and newly-diagnosed glioma patients resulted in WT-1, gp100 and MAGE-A3-specific CTLs upon vaccination. In the newly-diagnosed patients, PFS and OS were improved compared with an international trial of TMZ monotherapy [62]. However, in recurrent glioblastoma patients, where DC therapy was followed by TMZ administration, combined treatment failed to improve 6-month PFS compared with a reference group with TMZ monotherapy [63]. This could be due to reduced CTL numbers caused by TMZ-induced lymphoablation, thereby counteracting the effects of DC therapy, as shown by a recent study [64]. Interestingly, this study also illustrated that, in contrast to CTL numbers, NK cells in peripheral blood remained constant after concurrent combinations with TMZ. However, whether the effects observed on NK cells were associated with depletion of Tregs remains elusive. Furthermore, this indicates that TMZ administration before or during DC therapy could enhance DC therapy efficacy, whereas DC therapy followed by TMZ may exert negative effects on DC-induced anti-tumor immunity.

Gemcitabine

Gemcitabine is able to improve anti-tumor immunity by depletion of MDSCs and Tregs (Fig. 1) [47,48,65]. Treatment of mice bearing pancreatic tumors with gemcitabine 2 days before and after DC therapy prolonged survival compared with untreated mice which was not observed for both monotherapies [66]. Concurrent treatment of DC therapy and gemcitabine in a murine pancreatic model delayed tumor growth and prolonged survival compared with both monotherapies. This could be dependent on MDSC numbers, as MDSC numbers were significantly reduced in spleens and tumors of mice treated with gemcitabine [67]. However, in pancreatic cancer patients, despite decreased PD-1$^+$CTL numbers in responders, the concurrent combination did not result in decreased MDSC and Treg numbers in responders versus non-responders [68]. These results indicate that gemcitabine may enhance DC therapy efficacy, however the mechanism of action warrants further investigation.

Other chemotherapy combinations

With the aim to reduce tumor burden, Hegmans et al. treated mesothelioma patients with premetrexed and cisplatin 12 weeks prior to DC therapy, which resulted in immunological responses in all patients against keyhole limpet hemocyanin (KLH), a protein used to assess T cell responses initiated by DC therapy [69]. As this trial has no control arm no conclusions on synergy can be made. Co-administration of oxiplatin, capecitabine and DC therapy in colon cancer patients induced proliferation of KLH-specific CD4$^+$T cells in all patients as well [70]. An effect on CD4$^+$ T cells was also observed in multiple myeloma patients wherein treatment with DCs and cytokine-induced killer cells (CIK) combined with bortezomib and dexamethasone improved CD4$^+$/CD8$^+$ T cell ratios compared with baseline and treatment with chemotherapy alone [71]. Specific anti-tumor immunity with CTLs directed against gp100, tyrosine and NY-ESO or WT1 was induced in respectively 67% or 44% of patients with stage IV melanoma upon combination with dacarbazine or carboplatin and paclitaxel [72,73]. However, combination with docetaxel failed to improve clinical responses in patients with esophageal cancer and did not resulted in improved PFS in patients with prostate cancer compared with docetaxel monotherapy [74,75]. These results indicate that combined treatment with chemotherapy and DC therapy is feasible and safe, however further research should be conducted providing insight into the potential synergistical effects.

Combination with radiotherapy

Ever since radiotherapy was found to affect non-radiated tumor lesions in a process called the abscopal effect, the immunomodulatory effects of this therapy have been more thoroughly appreciated. As radiotherapy induces ICD, one primary effect is the release of DAMPs and tumor-derived antigens which initiate the activation and migration of DCs to the LN where DCs subsequently cross-present these antigens to T cells and induce systemic anti-tumor immune responses (Fig. 1) [76-80]. The induction of systemic anti-tumor immunity was indeed observed when radiotherapy was combined with GM-CSF as it generated abscopal effects in some patients [81]. In addition, the combination with Flt-3 ligand in a Lewis lung carcinoma murine model reduced

metastases and prolonged survival [82]. However, in settings of compromised DC functionality, intratumoral injection of exogenously-prepared unloaded DCs followed by radiotherapy could be advantageous. Induction of systemic immunity was indeed observed in a squamous-cell carcinoma murine model, as combining radiotherapy with DC transfer increased the presence of CTLs in the tumor-draining LN (TDLN) compared with DC monotherapy [83]. In addition, reduced tumor burden and prolonged survival were observed compared with monotherapy [84-88]. In clinical trials with patients suffering from hepatocellular carcinoma and high-risk sarcoma, combining unloaded DCs with radiotherapy induced tumor-specific immunity in 70% and 52.9% of the cases, respectively [89,90]. Besides synergistic effects when combined with unloaded DCs, radiotherapy may also improve efficacy when combined with loaded DCs as it transforms irradiated tissue into an immunogenic niche by enhancing the expression of vascular endothelial cell adhesion protein 1 (VCAM-1) on endothelial cells, FAS, MHCI and natural killer group 2D (NKG2D) on tumor cells and increasing CXCL16 secretion, thereby promoting homing, infiltration and tumor killing by DC-induced lymphocytes (Fig. 1) [91-96]. In patients with stage I esophageal cancer, 1- and 2-year survival rates were significantly improved upon treatment with loaded DCs and radiotherapy as compared with radiotherapy alone. Addition of CIK to this combination failed to improve survival in patients with stage III/IV non-small-cell lung cancer [97,98]. These results indicate that combinatorial treatment has synergistic effects, but these depend on tumor type and stage, as improved efficacy is most prominent at early tumor stages.

Combination with immune checkpoint inhibitors

In cancer, tumor cells and immune cells often overexpress co-inhibitory molecules, such as PD-1/PD-L1 and CTLA-4, which suppress anti-tumor immunity. Checkpoint inhibitors targeting these co-inhibitory molecules improve existing anti-tumor immunity when administered as monotherapy [99,100]. Additionally, combinations with DC therapy may result in synergistic effects as expression of these co-inhibitory molecules could also limit durable DC therapy effects by inhibiting DC therapy induced T cells as well as DCs directly.

PD-1/PD-L blocking antibodies

The PD-1/PD-L-axis exerts negative effects on TME-infiltrating immune cells by inhibiting T cell effector functions, NK cells and inducing T cell exhaustion [101-104]. Additionally, PD-L1 expression on tumor cells also directly inhibits IFNγ-mediated cytotoxicity by a STAT3/caspase 7 dependent pathway [105]. Therapeutically targeting PD-1/PD-L1 could therefore render the TME more receptive for lymphocyte infiltration and sensitize tumor cells for cytotoxicity which could act synergistically upon combination with DC therapy (Fig. 1). Combining DC therapy with PD-1 blockade reduced Tregs, induced IFNγ secretion, while secretion of IL-10 by $CD4^+$T cells was decreased. In addition, cytotoxicity of CTLs improved when PD-1 was inhibited in a co-culture of tumor cells and T cells isolated from mice treated with DC/myeloma fusion [106]. *In vivo* investigation of DC therapy combined with PD-1 blockade reduced tumor volume of mice with melanoma [107] and prolonged survival in

murine models for glioblastoma [108] compared with monotherapy. These beneficial effects on anti-tumor immunity were also observed in a breast cancer murine model upon combinations with anti-PD-L1 antibodies [109]. Additionally, this study investigated the combination of specific blockade of PD-L1 on DCs by *in vitro* incubation with antagonistic monoclonal antibodies [109].

PD-L1/2 are both expressed on DCs and are associated with suppression of effector CTLs and $CD4^+$ T cells and induces Treg-expansion [110-117]. Conversely, the expression of PD-1 on DCs negatively affects DC survival [118]. This indicates that blockade of PD-1 or PD-L1 on DCs could enhance anti-tumor immunity *in vivo* via multiple ways. PD-L1 blockade on DCs improved maturation and proliferation of DCs during culture, inhibited tumor outgrowth and prolonged survival compared with mice treated with DCs and anti-PD-L1 inhibitors systemically [109]. These results underline the importance of PD-L1 expression on DCs in inhibiting anti-tumor immunity. Therefore, efforts are undertaken to establish DC-specific PD-L1 blockade, primarily by different RNA introducing techniques, such as small interference RNA (siRNA) or short hairpin RNA (shRNA). Preclinical data indicate that PD-L1 can effectively be silenced using these approaches without affecting viability, maturation or costimulatory molecule expression. In addition, silencing PD-L1 or PD-L2 specifically on DCs enhanced proliferation of tumor-specific CTLs and $CD4^+$ T cells, augmented production of IFNγ, tumor-necrosis factor alpha (TNFα), IL-2, IL-5 and IL-12 and promoted cytolysis of tumor cells *in vitro* [119-123]. These promising data provide incentive to further investigate the combination of systemic PD-(L)1 blockade with DC therapy and PD-L1 blockade on DCs.

CTLA-4

The antagonistic antibodies ipilimumab and tremelimumab are designed to target CTLA-4, an inhibitory pathway that inhibits activation of naïve T cells by preventing the binding of CD28 on T cells to CD80/CD86 on APCs, a mechanism widely exploited by Tregs[124,125]. In various murine models, ipilimumab was shown to induce antibody-dependent cell-mediated cytotoxicity (ADCC), thereby facilitating Treg depletion while tremelimumab inhibits effector functions of Tregs (Fig. 1) [126,127]. However, recent clinical data question the Treg-depleting capacity of ipilimumab, as treatment with ipilimumab did not deplete Tregs in the TME of patients with melanoma, prostate cancer and bladder cancer [128]. In a retrospective study with stage III melanoma patients that progressed after DC therapy, administration of ipilimumab induced tumor-specific T cell responses in 72% of the cases although this was not associated with improved OS [129]. Clinical and CTL responses were also not associated in a clinical trial with 16 melanoma patients treated with MART-1 peptide loaded DCs and tremelimumab [130]. However, most promising clinical results were obtained by a recent study, in which the overall response rate reached 38% in advanced melanoma patients treated with ipilimumab combined with DCs electroporated with CD40L, CD70 and constitutively activated TLR-4 encoding mRNA and one of 4 melanoma-associated antigens (MAGE-A3, MAGE-C2, tyrosinase, or gp100) fused to an HLA-class II targeting signal [131], thereby indicating that combining DC therapy with CTLA-4 targeting agents could lead to synergistic effects.

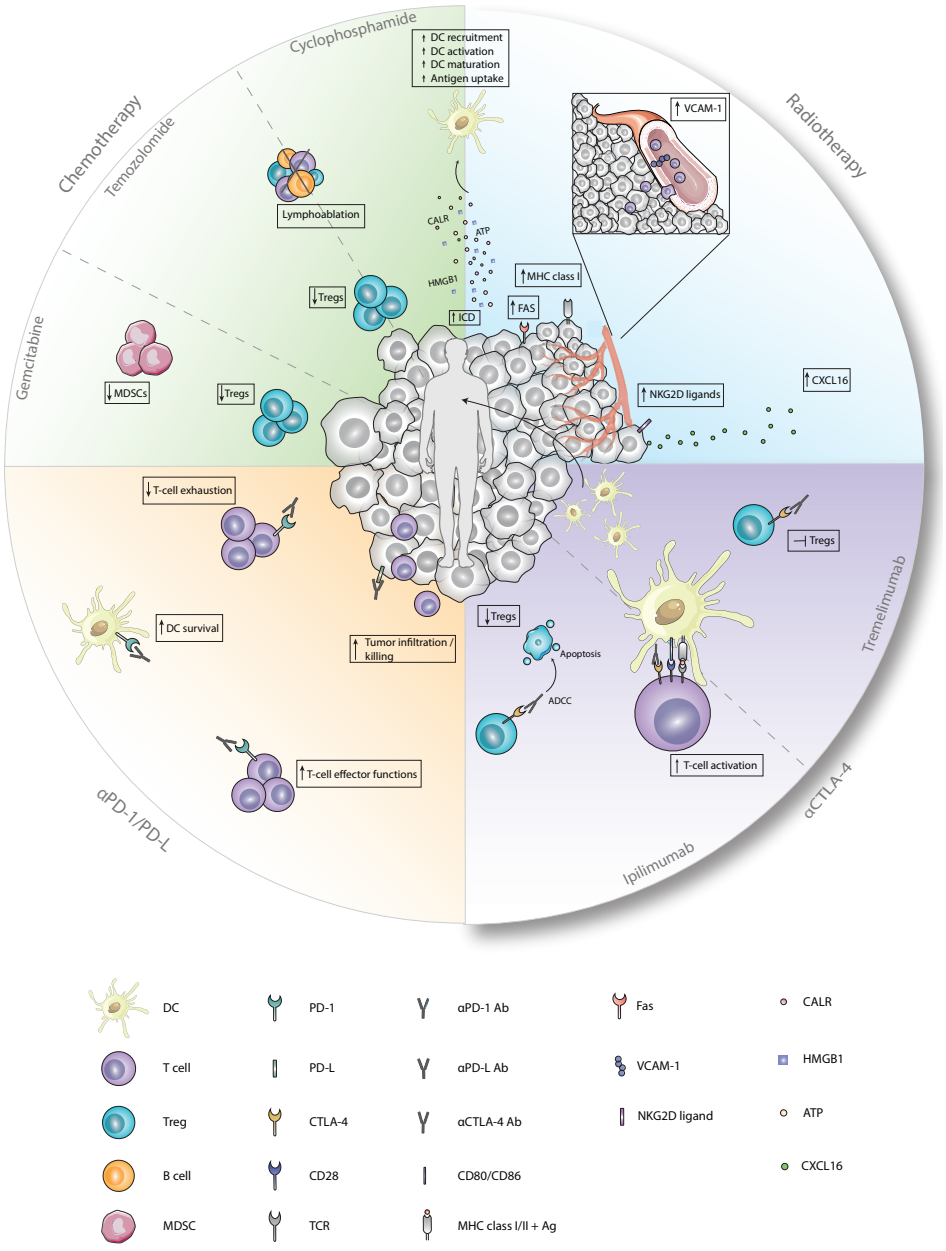
Chemotherapy
Cyclophosphamide
Temozolomide
Gemcitabine
Radiotherapy
αPD-1/PD-L
αCTLA-4
Tremelimumab
Ipilimumab
↑ DC recruitment
↑ DC activation
↑ DC maturation
↑ Antigen uptake
Lymphoablation
↓Tregs
↓MDSCs
↓Tregs
CALR
ATP
HMGB1
↑ ICD
↑MHC class I
↑FAS
↑ VCAM-1
↑ NKG2D ligands
↑CXCL16
↓T-cell exhaustion
↑DC survival
↑ Tumor infiltration / killing
↓Tregs
Apoptosis
ADCC
⊣Tregs
↑ T-cell activation
↑T-cell effector functions
DC
T cell
Treg
B cell
MDSC
PD-1
PD-L
CTLA-4
CD28
TCR
αPD-1 Ab
αPD-L Ab
αCTLA-4 Ab
CD80/CD86
MHC class I/II + Ag
Fas
VCAM-1
NKG2D ligand
CALR
HMGB1
ATP
CXCL16

◂Figure 1: Immunological effects of chemotherapy, radiotherapy and checkpoint inhibitors

Cyclophosphamide induces ICD which enhances the recruitment, activation, maturation and antigen uptake by DCs. In addition, cyclophosphamide and temozolomide deplete Tregs and induce lymphoablation upon treatment with low-dose or high-dose, respectively. Immunological functions of gemcitabine entail depletion of Tregs and MDSCs. Radiotherapy induces, besides ICD, enhanced expression of FAS, MHC class I and NKG2D ligands on tumor cells and enhanced expression of VCAM-1 on endothelial cells. Furthermore, secretion of CXCL16 by tumor cells is increased after radiotherapy. Antagonistic CTLA-4 antibodies enhance T cell activation by the preventing the binding of CD28 with CD80/86. Ipilimumab depletes Tregs by ADCC whereas tremelimumab inhibits functions of Tregs upon binding. Anti-PD1 antagonistic antibodies enhance T cell effector functions while preventing exhaustion of T cells. Blockade of PD-L1 on DCs improves survival while blockade on tumor cells results in improved tumor-cell infiltration and killing. Ab, antibody; Ag, antigen; ATP, adenosine triphosphate; CALR, calreticulin; CTLA-4 = cytotoxic T-lymphocyte-associated antigen, CXCL16 = chemokine ligand 16, DC = dendritic cell, Fas = first apoptosis signal, HMGB1 = high mobility group box 1, MDSC = myeloid-derived suppressor cell, MHC class I/II = major histocompatibility complex class I/II, NKG2D ligand = natural killer group 2 member D, PD-1 = programmed death 1; PD-L, programmed death ligand, TCR = T cell receptor, Treg = regulatory T cell, VCAM-1 = vascular endothelial cell adhesion protein 1.

Combination with other immunomodulating therapies

Recently also other immunomodulatory therapies were approved that enable depletion of specific immunosuppressive cell types, such as macrophages that are depleted upon antibody or tyrosine kinase inhibition of the M-CSF-receptor. In line, we have previously combined DC therapy with M-CSFR inhibitor treatment in murine tumor models and found improved survival compared with DC-monotherapy. In addition, numbers, proliferation and exhaustion state of CTLs were improved [132]. Similar results were obtained when combining DC therapy with a CD40-agonistic antibody, capable of converting macrophages to a proinflammatory phenotype and further stimulating the $CD40^+$ DCs [133]. Besides macrophages, selective depletion of Tregs could enhance anti-tumor immunity. Results in a preclinical melanoma mouse model showed that depletion of Tregs using anti-CD25 antibodies prior to DC therapy elicits long-lasting anti-tumor immunity, as most mice remained tumor-free after tumor rechallenge [134]. Further investigation into these combinations in different (pre)clinical models could lead to promising novel combination strategies.

Future perspectives

Despite the clinical success of DC therapy, clinical efficacy remains limited to a proportion of patients and integration of combinatorial approaches are therefore warranted to improve efficacy. Timing of these combinatorial approaches should be carefully considered as this will affect the potential synergistic mode of action. In addition, determining optimal combination therapies likely depends on multiple factors including patient's condition, tumor type, stage and composition of the TME. Therefore, characterization of tumor cells and immune cells present in the TME or peripheral blood of individual patients will help to select immunotherapies that most likely will work synergistically

with DC therapy. For example, treatment of tumors enriched with Tregs should entail combinations with Treg-depleting chemotherapeutics, whereas DC therapy should be combined with PD-L1 antagonistic antibodies in tumors with high PD-L1 expression. Furthermore, careful characterization of the TME and peripheral blood could provide novel insights for combination strategies.

Conclusion

Although combinations with DC therapy have demonstrated beneficial effects contributing to anti-tumor immunity, the potential for further improvement remains. A major focus should be on the careful characterization of tumor and peripheral blood of each individual patient as this will be needed to tailor treatments and enhance efficacy on a personalized level. In addition, more controlled clinical trials should be executed to directly compare efficacy with monotherapy. Timing of treatment administration should be taken into consideration in these studies as it could affect the efficacy of combination immunotherapies.

References

1. Guilliams, M.*, et al.* Unsupervised High-Dimensional Analysis Aligns Dendritic Cells across Tissues and Species. *Immunity* **45**, 669-684 (2016).
2. Guilliams, M.*, et al.* Dendritic cells, monocytes and macrophages: a unified nomenclature based on ontogeny. *Nat Rev Immunol* **14**, 571-578 (2014).
3. Sabado, R.L., Balan, S. & Bhardwaj, N. Dendritic cell-based immunotherapy. *Cell Res* **27**, 74-95 (2017).
4. Patel, V.I. & Metcalf, J.P. Identification and characterization of human dendritic cell subsets in the steady state: a review of our current knowledge. *J Investig Med* **64**, 833-847 (2016).
5. Constantino, J., Gomes, C., Falcao, A., Neves, B.M. & Cruz, M.T. Dendritic cell-based immunotherapy: a basic review and recent advances. *Immunol Res* **65**, 798-810 (2017).
6. Hopp, A.K., Rupp, A. & Lukacs-Kornek, V. Self-antigen presentation by dendritic cells in autoimmunity. *Front Immunol* **5**, 55 (2014).
7. Steinman, R.M. The dendritic cell system and its role in immunogenicity. *Annu Rev Immunol* **9**, 271-296 (1991).
8. Gardner, A. & Ruffell, B. Dendritic Cells and Cancer Immunity. *Trends Immunol* **37**, 855-865 (2016).
9. Bol, K.F., Schreibelt, G., Gerritsen, W.R., de Vries, I.J. & Figdor, C.G. Dendritic Cell-Based Immunotherapy: State of the Art and Beyond. *Clin Cancer Res* **22**, 1897-1906 (2016).
10. Munz, C.*, et al.* Mature myeloid dendritic cell subsets have distinct roles for activation and viability of circulating human natural killer cells. *Blood* **105**, 266-273 (2005).
11. Wellenstein, M.D. & de Visser, K.E. Cancer-Cell-Intrinsic Mechanisms Shaping the Tumor Immune Landscape. *Immunity* **48**, 399-416 (2018).
12. Peng, W.*, et al.* Loss of PTEN Promotes Resistance to T Cell-Mediated Immunotherapy. *Cancer Discov* **6**, 202-216 (2016).
13. Spranger, S., Bao, R. & Gajewski, T.F. Melanoma-intrinsic beta-catenin signalling prevents anti-tumour immunity. *Nature* **523**, 231-235 (2015).
14. Spranger, S.*, et al.* Density of immunogenic antigens does not explain the presence or absence of the T-cell-inflamed tumor microenvironment in melanoma. *Proc Natl Acad Sci U S A* **113**, E7759-E7768 (2016).
15. Nefedova, Y.*, et al.* Hyperactivation of STAT3 is involved in abnormal differentiation of dendritic cells in cancer. *J Immunol* **172**, 464-474 (2004).
16. Tang, M., Diao, J. & Cattral, M.S. Molecular mechanisms involved in dendritic cell dysfunction in cancer. *Cell Mol Life Sci* **74**, 761-776 (2017).
17. Pinzon-Charry, A., Maxwell, T. & Lopez, J.A. Dendritic cell dysfunction in cancer: a mechanism for immunosuppression. *Immunol Cell Biol* **83**, 451-461 (2005).
18. Chen, D.S. & Mellman, I. Oncology meets immunology: the cancer-immunity cycle. *Immunity* **39**, 1-10 (2013).
19. Constantino, J., Gomes, C., Falcao, A., Cruz, M.T. & Neves, B.M. Antitumor dendritic cell-based vaccines: lessons from 20 years of clinical trials and future perspectives. *Transl Res* **168**, 74-95 (2016).
20. Anguille, S., Smits, E.L., Lion, E., van Tendeloo, V.F. & Berneman, Z.N. Clinical use of dendritic cells for cancer therapy. *Lancet Oncol* **15**, e257-267 (2014).
21. Ghirelli, C. & Hagemann, T. Targeting immunosuppression for cancer therapy. *J Clin Invest* **123**, 2355-2357 (2013).
22. Blankenstein, T., Coulie, P.G., Gilboa, E. & Jaffee, E.M. The determinants of tumour immunogenicity. *Nat Rev Cancer* **12**, 307-313 (2012).
23. Vasaturo, A.*, et al.* Clinical Implications of Co-Inhibitory Molecule Expression in the Tumor Microenvironment for DC Vaccination: A Game of Stop and Go. *Front Immunol* **4**, 417 (2013).
24. Devaud, C., John, L.B., Westwood, J.A., Darcy, P.K. & Kershaw, M.H. Immune modulation of the tumor microenvironment for enhancing cancer immunotherapy. *Oncoimmunology* **2**, e25961 (2013).
25. Seyfizadeh, N., Muthuswamy, R., Mitchell, D.A., Nierkens, S. & Seyfizadeh, N. Migration of dendritic cells to the lymph nodes and its enhancement to drive anti-tumor responses. *Crit Rev Oncol Hematol* **107**, 100-110 (2016).
26. Verdijk, P.*, et al.* Limited amounts of dendritic cells migrate into the T-cell area of lymph nodes but have high immune activating potential in melanoma patients. *Clin Cancer Res* **15**, 2531-2540 (2009).
27. Mantovani, A., Marchesi, F., Malesci, A., Laghi, L. & Allavena, P. Tumour-associated macrophages as treatment targets in oncology. *Nat Rev Clin Oncol* **14**, 399-416 (2017).
28. Kumar, V., Patel, S., Tcyganov, E. & Gabrilovich, D.I. The Nature of Myeloid-Derived Suppressor Cells in the Tumor Microenvironment. *Trends Immunol* **37**, 208-220 (2016).
29. Tanaka, A. & Sakaguchi, S. Regulatory T cells in cancer immunotherapy. *Cell Res* **27**, 109-118 (2017).

30. Sallusto, F. & Lanzavecchia, A. Efficient presentation of soluble antigen by cultured human dendritic cells is maintained by granulocyte/macrophage colony-stimulating factor plus interleukin 4 and downregulated by tumor necrosis factor alpha. *J Exp Med* **179**, 1109-1118 (1994).
31. Garg, A.D., Coulie, P.G., Van den Eynde, B.J. & Agostinis, P. Integrating Next-Generation Dendritic Cell Vaccines into the Current Cancer Immunotherapy Landscape. *Trends Immunol* **38**, 577-593 (2017).
32. Kantoff, P.W.*, et al.* Sipuleucel-T immunotherapy for castration-resistant prostate cancer. *N Engl J Med* **363**, 411-422 (2010).
33. Laoui, D.*, et al.* The tumour microenvironment harbours ontogenically distinct dendritic cell populations with opposing effects on tumour immunity. *Nat Commun* **7**, 13720 (2016).
34. Broz, M.L.*, et al.* Dissecting the tumor myeloid compartment reveals rare activating antigen-presenting cells critical for T cell immunity. *Cancer Cell* **26**, 638-652 (2014).
35. Tel, J.*, et al.* Natural human plasmacytoid dendritic cells induce antigen-specific T-cell responses in melanoma patients. *Cancer Res* **73**, 1063-1075 (2013).
36. Prue, R.L.*, et al.* A phase I clinical trial of CD1c (BDCA-1)+ dendritic cells pulsed with HLA-A*0201 peptides for immunotherapy of metastatic hormone refractory prostate cancer. *J Immunother* **38**, 71-76 (2015).
37. Zhou, Y., Bosch, M.L. & Salgaller, M.L. Current methods for loading dendritic cells with tumor antigen for the induction of antitumor immunity. *J Immunother* **25**, 289-303 (2002).
38. Neller, M.A., Lopez, J.A. & Schmidt, C.W. Antigens for cancer immunotherapy. *Semin Immunol* **20**, 286-295 (2008).
39. Mitchell, D.A.*, et al.* Tetanus toxoid and CCL3 improve dendritic cell vaccines in mice and glioblastoma patients. *Nature* **519**, 366-369 (2015).
40. Hou, W.S. & Van Parijs, L. A Bcl-2-dependent molecular timer regulates the lifespan and immunogenicity of dendritic cells. *Nat Immunol* **5**, 583-589 (2004).
41. Min, S.*, et al.* Multiple tumor-associated microRNAs modulate the survival and longevity of dendritic cells by targeting YWHAZ and Bcl2 signaling pathways. *J Immunol* **190**, 2437-2446 (2013).
42. Chen, M., Huang, L., Shabier, Z. & Wang, J. Regulation of the lifespan in dendritic cell subsets. *Mol Immunol* **44**, 2558-2565 (2007).
43. Kang, T.H.*, et al.* Enhancing dendritic cell vaccine potency by combining a BAK/BAX siRNA-mediated antiapoptotic strategy to prolong dendritic cell life with an intracellular strategy to target antigen to lysosomal compartments. *Int J Cancer* **120**, 1696-1703 (2007).
44. Galluzzi, L., Buque, A., Kepp, O., Zitvogel, L. & Kroemer, G. Immunological Effects of Conventional Chemotherapy and Targeted Anticancer Agents. *Cancer Cell* **28**, 690-714 (2015).
45. Garg, A.D.*, et al.* Molecular and Translational Classifications of DAMPs in Immunogenic Cell Death. *Front Immunol* **6**, 588 (2015).
46. Galluzzi, L., Buque, A., Kepp, O., Zitvogel, L. & Kroemer, G. Immunogenic cell death in cancer and infectious disease. *Nat Rev Immunol* **17**, 97-111 (2017).
47. Zitvogel, L., Apetoh, L., Ghiringhelli, F. & Kroemer, G. Immunological aspects of cancer chemotherapy. *Nat Rev Immunol* **8**, 59-73 (2008).
48. Bracci, L., Schiavoni, G., Sistigu, A. & Belardelli, F. Immune-based mechanisms of cytotoxic chemotherapy: implications for the design of novel and rationale-based combined treatments against cancer. *Cell Death Differ* **21**, 15-25 (2014).
49. Karachi, A., Dastmalchi, F., Mitchell, D. & Rahman, M. Temozolomide for Immunomodulation in the Treatment of Glioblastoma. *Neuro Oncol* (2018).
50. Beyranvand Nejad, E., Welters, M.J., Arens, R. & van der Burg, S.H. The importance of correctly timing cancer immunotherapy. *Expert Opin Biol Ther* **17**, 87-103 (2017).
51. Emadi, A., Jones, R.J. & Brodsky, R.A. Cyclophosphamide and cancer: golden anniversary. *Nat Rev Clin Oncol* **6**, 638-647 (2009).
52. Veltman, J.D.*, et al.* Low-dose cyclophosphamide synergizes with dendritic cell-based immunotherapy in antitumor activity. *J Biomed Biotechnol* **2010**, 798467 (2010).
53. Liu, J.Y.*, et al.* Single administration of low dose cyclophosphamide augments the antitumor effect of dendritic cell vaccine. *Cancer Immunol Immunother* **56**, 1597-1604 (2007).
54. Carreno, B.M.*, et al.* IL-12p70-producing patient DC vaccine elicits Tc1-polarized immunity. *J Clin Invest* **123**, 3383-3394 (2013).
55. Cornelissen, R.*, et al.* Extended Tumor Control after Dendritic Cell Vaccination with Low-Dose Cyclophosphamide as Adjuvant Treatment in Patients with Malignant Pleural Mesothelioma. *Am J Respir Crit Care Med* **193**, 1023-1031 (2016).
56. Borch, T.H.*, et al.* mRNA-transfected dendritic cell vaccine in combination with metronomic cyclophosphamide as treatment for patients with advanced malignant melanoma. *Oncoimmunology* **5**, e1207842 (2016).

57. Tanyi, J.L., *et al.* Personalized cancer vaccine effectively mobilizes antitumor T cell immunity in ovarian cancer. *Sci Transl Med* **10**(2018).
58. Holtl, L., *et al.* Allogeneic dendritic cell vaccination against metastatic renal cell carcinoma with or without cyclophosphamide. *Cancer Immunol Immunother* **54**, 663-670 (2005).
59. Drean, A., *et al.* Blood-brain barrier, cytotoxic chemotherapies and glioblastoma. *Expert Rev Neurother* **16**, 1285-1300 (2016).
60. Quirt, I., Verma, S., Petrella, T., Bak, K. & Charette, M. Temozolomide for the treatment of metastatic melanoma: a systematic review. *Oncologist* **12**, 1114-1123 (2007).
61. Ridolfi, L., *et al.* Low-dose temozolomide before dendritic-cell vaccination reduces (specifically) CD4+CD25++Foxp3+ regulatory T-cells in advanced melanoma patients. *J Transl Med* **11**, 135 (2013).
62. Akasaki, Y., *et al.* Phase I/II trial of combination of temozolomide chemotherapy and immunotherapy with fusions of dendritic and glioma cells in patients with glioblastoma. *Cancer Immunol Immunother* **65**, 1499-1509 (2016).
63. Hunn, M.K., *et al.* Dendritic cell vaccination combined with temozolomide retreatment: results of a phase I trial in patients with recurrent glioblastoma multiforme. *J Neurooncol* **121**, 319-329 (2015).
64. Pellegatta, S., *et al.* Survival gain in glioblastoma patients treated with dendritic cell immunotherapy is associated with increased NK but not CD8(+) T cell activation in the presence of adjuvant temozolomide. *Oncoimmunology* **7**, e1412901 (2018).
65. Kershaw, M.H., Devaud, C., John, L.B., Westwood, J.A. & Darcy, P.K. Enhancing immunotherapy using chemotherapy and radiation to modify the tumor microenvironment. *Oncoimmunology* **2**, e25962 (2013).
66. Bauer, C., *et al.* Dendritic cell-based vaccination combined with gemcitabine increases survival in a murine pancreatic carcinoma model. *Gut* **56**, 1275-1282 (2007).
67. Ghansah, T., *et al.* Dendritic cell immunotherapy combined with gemcitabine chemotherapy enhances survival in a murine model of pancreatic carcinoma. *Cancer Immunol Immunother* **62**, 1083-1091 (2013).
68. Koido, S., *et al.* Treatment with chemotherapy and dendritic cells pulsed with multiple Wilms' tumor 1 (WT1)-specific MHC class I/II-restricted epitopes for pancreatic cancer. *Clin Cancer Res* **20**, 4228-4239 (2014).
69. Hegmans, J.P., *et al.* Consolidative dendritic cell-based immunotherapy elicits cytotoxicity against malignant mesothelioma. *Am J Respir Crit Care Med* **181**, 1383-1390 (2010).
70. Lesterhuis, W.J., *et al.* A pilot study on the immunogenicity of dendritic cell vaccination during adjuvant oxaliplatin/capecitabine chemotherapy in colon cancer patients. *Br J Cancer* **103**, 1415-1421 (2010).
71. Zhao, X., *et al.* Immunomodulatory effect of DC/CIK combined with chemotherapy in multiple myeloma and the clinical efficacy. *Int J Clin Exp Pathol* **8**, 13146-13155 (2015).
72. Rozera, C., *et al.* Intratumoral injection of IFN-alpha dendritic cells after dacarbazine activates anti-tumor immunity: results from a phase I trial in advanced melanoma. *J Transl Med* **13**, 139 (2015).
73. Fukuda, K., *et al.* Peptide-pulsed dendritic cell vaccine in combination with carboplatin and paclitaxel chemotherapy for stage IV melanoma. *Melanoma Res* **27**, 326-334 (2017).
74. Kongsted, P., *et al.* Dendritic cell vaccination in combination with docetaxel for patients with metastatic castration-resistant prostate cancer: A randomized phase II study. *Cytotherapy* **19**, 500-513 (2017).
75. Matsuda, T., *et al.* Pilot study of WT1 peptide-pulsed dendritic cell vaccination with docetaxel in esophageal cancer. *Oncol Lett* **16**, 1348-1356 (2018).
76. Demaria, S. & Formenti, S.C. Role of T lymphocytes in tumor response to radiotherapy. *Front Oncol* **2**, 95 (2012).
77. Bhattacharyya, T., Purushothaman, K., Puthiyottil, S.S., Bhattacharjee, A. & Muttah, G. Immunological interactions in radiotherapy-opening a new window of opportunity. *Ann Transl Med* **4**, 51 (2016).
78. Brix, N., Tiefenthaller, A., Anders, H., Belka, C. & Lauber, K. Abscopal, immunological effects of radiotherapy: Narrowing the gap between clinical and preclinical experiences. *Immunol Rev* **280**, 249-279 (2017).
79. Teitz-Tennenbaum, S., *et al.* Mechanisms involved in radiation enhancement of intratumoral dendritic cell therapy. *J Immunother* **31**, 345-358 (2008).
80. de la Cruz-Merino, L., *et al.* Radiation for Awakening the Dormant Immune System, a Promising Challenge to be Explored. *Front Immunol* **5**, 102 (2014).
81. Golden, E.B., *et al.* Local radiotherapy and granulocyte-macrophage colony-stimulating factor to generate abscopal responses in patients with metastatic solid tumours: a proof-of-principle trial. *Lancet Oncol* **16**, 795-803 (2015).
82. Chakravarty, P.K., *et al.* Flt3-ligand administration after radiation therapy prolongs survival in a murine model of metastatic lung cancer. *Cancer Res* **59**, 6028-6032 (1999).
83. Akutsu, Y., *et al.* Combination of direct intratumoral administration of dendritic cells and irradiation induces strong systemic antitumor effect mediated by GRP94/gp96 against squamous cell carcinoma in mice. *Int J Oncol* **31**, 509-515 (2007).

84. Teitz-Tennenbaum, S.*, et al.* Radiotherapy potentiates the therapeutic efficacy of intratumoral dendritic cell administration. *Cancer Res* **63**, 8466-8475 (2003).
85. Huang, J.*, et al.* Radiation-induced apoptosis along with local and systemic cytokine elaboration is associated with DC plus radiotherapy-mediated renal cell tumor regression. *Clin Immunol* **123**, 298-310 (2007).
86. Teitz-Tennenbaum, S.*, et al.* Radiotherapy combined with intratumoral dendritic cell vaccination enhances the therapeutic efficacy of adoptive T-cell transfer. *J Immunother* **32**, 602-612 (2009).
87. Lee, T.H.*, et al.* Enhanced antitumor effect of dendritic cell based immunotherapy after intratumoral injection of radionuclide Ho-166 against B16 melanoma. *Immunol Lett* **106**, 19-26 (2006).
88. Tatsuta, K.*, et al.* Complete elimination of established neuroblastoma by synergistic action of gamma-irradiation and DCs treated with rSeV expressing interferon-beta gene. *Gene Ther* **16**, 240-251 (2009).
89. Chi, K.H.*, et al.* Combination of conformal radiotherapy and intratumoral injection of adoptive dendritic cell immunotherapy in refractory hepatoma. *J Immunother* **28**, 129-135 (2005).
90. Finkelstein, S.E.*, et al.* Combination of external beam radiotherapy (EBRT) with intratumoral injection of dendritic cells as neo-adjuvant treatment of high-risk soft tissue sarcoma patients. *Int J Radiat Oncol Biol Phys* **82**, 924-932 (2012).
91. Lugade, A.A.*, et al.* Local radiation therapy of B16 melanoma tumors increases the generation of tumor antigen-specific effector cells that traffic to the tumor. *J Immunol* **174**, 7516-7523 (2005).
92. Lugade, A.A.*, et al.* Radiation-induced IFN-gamma production within the tumor microenvironment influences antitumor immunity. *J Immunol* **180**, 3132-3139 (2008).
93. Chakraborty, M.*, et al.* Irradiation of tumor cells up-regulates Fas and enhances CTL lytic activity and CTL adoptive immunotherapy. *J Immunol* **170**, 6338-6347 (2003).
94. Reits, E.A.*, et al.* Radiation modulates the peptide repertoire, enhances MHC class I expression, and induces successful antitumor immunotherapy. *J Exp Med* **203**, 1259-1271 (2006).
95. Matsumura, S.*, et al.* Radiation-induced CXCL16 release by breast cancer cells attracts effector T cells. *J Immunol* **181**, 3099-3107 (2008).
96. Kim, J.Y.*, et al.* Increase of NKG2D ligands and sensitivity to NK cell-mediated cytotoxicity of tumor cells by heat shock and ionizing radiation. *Exp Mol Med* **38**, 474-484 (2006).
97. Wang, C.*, et al.* A Dendritic Cell Vaccine Combined With Radiotherapy Activates the Specific Immune Response in Patients With Esophageal Cancer. *J Immunother* **40**, 71-76 (2017).
98. Zhang, L.*, et al.* Feasibility study of DCs/CIKs combined with thoracic radiotherapy for patients with locally advanced or metastatic non-small-cell lung cancer. *Radiat Oncol* **11**, 60 (2016).
99. Leach, D.R., Krummel, M.F. & Allison, J.P. Enhancement of antitumor immunity by CTLA-4 blockade. *Science* **271**, 1734-1736 (1996).
100. Hirano, F.*, et al.* Blockade of B7-H1 and PD-1 by monoclonal antibodies potentiates cancer therapeutic immunity. *Cancer Res* **65**, 1089-1096 (2005).
101. Baumeister, S.H., Freeman, G.J., Dranoff, G. & Sharpe, A.H. Coinhibitory Pathways in Immunotherapy for Cancer. *Annu Rev Immunol* **34**, 539-573 (2016).
102. Zarour, H.M. Reversing T-cell Dysfunction and Exhaustion in Cancer. *Clin Cancer Res* **22**, 1856-1864 (2016).
103. Liu, Y.*, et al.* Increased expression of programmed cell death protein 1 on NK cells inhibits NK-cell-mediated anti-tumor function and indicates poor prognosis in digestive cancers. *Oncogene* **36**, 6143-6153 (2017).
104. Bardhan, K., Anagnostou, T. & Boussiotis, V.A. The PD1:PD-L1/2 Pathway from Discovery to Clinical Implementation. *Front Immunol* **7**, 550 (2016).
105. Gato-Canas, M.*, et al.* PDL1 Signals through Conserved Sequence Motifs to Overcome Interferon-Mediated Cytotoxicity. *Cell Rep* **20**, 1818-1829 (2017).
106. Rosenblatt, J.*, et al.* PD-1 blockade by CT-011, anti-PD-1 antibody, enhances ex vivo T-cell responses to autologous dendritic cell/myeloma fusion vaccine. *J Immunother* **34**, 409-418 (2011).
107. Nagaoka, K.*, et al.* Dendritic cell vaccine induces antigen-specific CD8(+) T cells that are metabolically distinct from those of peptide vaccine and is well-combined with PD-1 checkpoint blockade. *Oncoimmunology* **7**, e1395124 (2018).
108. Antonios, J.P.*, et al.* PD-1 blockade enhances the vaccination-induced immune response in glioma. *JCI Insight* **1**(2016).
109. Ge, Y., Xi, H., Ju, S. & Zhang, X. Blockade of PD-1/PD-L1 immune checkpoint during DC vaccination induces potent protective immunity against breast cancer in hu-SCID mice. *Cancer Lett* **336**, 253-259 (2013).
110. Curiel, T.J.*, et al.* Blockade of B7-H1 improves myeloid dendritic cell-mediated antitumor immunity. *Nat Med* **9**, 562-567 (2003).
111. Ge, W.*, et al.* B7-H1 up-regulation on dendritic-like leukemia cells suppresses T cell immune function through modulation of IL-10/IL-12 production and generation of Tregs. *Leuk Res* **33**, 948-957 (2009).

112. Gibbons, R.M., *et al.* B7-H1 signaling is integrated during CD8(+) T cell priming and restrains effector differentiation. *Cancer Immunol Immunother* **63**, 859-867 (2014).
113. Sponaas, A.M., *et al.* PDL1 Expression on Plasma and Dendritic Cells in Myeloma Bone Marrow Suggests Benefit of Targeted anti PD1-PDL1 Therapy. *PLoS One* **10**, e0139867 (2015).
114. Pulko, V., *et al.* TLR3-stimulated dendritic cells up-regulate B7-H1 expression and influence the magnitude of CD8 T cell responses to tumor vaccination. *J Immunol* **183**, 3634-3641 (2009).
115. Schneider, T., *et al.* Non-small cell lung cancer induces an immunosuppressive phenotype of dendritic cells in tumor microenvironment by upregulating B7-H3. *J Thorac Oncol* **6**, 1162-1168 (2011).
116. Song, S., *et al.* Dendritic cells with an increased PD-L1 by TGF-beta induce T cell anergy for the cytotoxicity of hepatocellular carcinoma cells. *Int Immunopharmacol* **20**, 117-123 (2014).
117. Francisco, L.M., *et al.* PD-L1 regulates the development, maintenance, and function of induced regulatory T cells. *J Exp Med* **206**, 3015-3029 (2009).
118. Park, S.J., *et al.* Negative role of inducible PD-1 on survival of activated dendritic cells. *J Leukoc Biol* **95**, 621-629 (2014).
119. Wang, S., *et al.* Silencing B7-H1 enhances the anti-tumor effect of bladder cancer antigen-loaded dendritic cell vaccine in vitro. *Onco Targets Ther* **7**, 1389-1396 (2014).
120. Van den Bergh, J.M.J., *et al.* Monocyte-Derived Dendritic Cells with Silenced PD-1 Ligands and Transpresenting Interleukin-15 Stimulate Strong Tumor-Reactive T-cell Expansion. *Cancer Immunol Res* **5**, 710-715 (2017).
121. Hobo, W., *et al.* Improving dendritic cell vaccine immunogenicity by silencing PD-1 ligands using siRNA-lipid nanoparticles combined with antigen mRNA electroporation. *Cancer Immunol Immunother* **62**, 285-297 (2013).
122. Daneshmandi, S., Pourfathollah, A.A., Karimi, M.H. & Emadi-Baygi, M. PDL-1/PDL-2 blockade in mice dendritic cells by RNAi techniques to induce antitumor immunity. *Immunotherapy* **7**, 1145-1158 (2015).
123. Roeven, M.W., *et al.* Efficient nontoxic delivery of PD-L1 and PD-L2 siRNA into dendritic cell vaccines using the cationic lipid SAINT-18. *J Immunother* **38**, 145-154 (2015).
124. Chambers, C.A., Kuhns, M.S., Egen, J.G. & Allison, J.P. CTLA-4-mediated inhibition in regulation of T cell responses: mechanisms and manipulation in tumor immunotherapy. *Annu Rev Immunol* **19**, 565-594 (2001).
125. Blank, C.U. & Enk, A. Therapeutic use of anti-CTLA-4 antibodies. *Int Immunol* **27**, 3-10 (2015).
126. Romano, E., *et al.* Ipilimumab-dependent cell-mediated cytotoxicity of regulatory T cells ex vivo by nonclassical monocytes in melanoma patients. *Proc Natl Acad Sci U S A* **112**, 6140-6145 (2015).
127. Ramagopal, U.A., *et al.* Structural basis for cancer immunotherapy by the first-in-class checkpoint inhibitor ipilimumab. *Proc Natl Acad Sci U S A* **114**, E4223-E4232 (2017).
128. Sharma, A., *et al.* Anti-CTLA-4 immunotherapy does not deplete FOXP3+ regulatory T cells (Tregs) in human cancers. *Clin Cancer Res* (2018).
129. Boudewijns, S., *et al.* Ipilimumab administered to metastatic melanoma patients who progressed after dendritic cell vaccination. *Oncoimmunology* **5**, e1201625 (2016).
130. Ribas, A., *et al.* Dendritic cell vaccination combined with CTLA4 blockade in patients with metastatic melanoma. *Clin Cancer Res* **15**, 6267-6276 (2009).
131. Wilgenhof, S., *et al.* Phase II Study of Autologous Monocyte-Derived mRNA Electroporated Dendritic Cells (TriMixDC-MEL) Plus Ipilimumab in Patients With Pretreated Advanced Melanoma. *J Clin Oncol* **34**, 1330-1338 (2016).
132. Dammeijer, F., *et al.* Depletion of Tumor-Associated Macrophages with a CSF-1R Kinase Inhibitor Enhances Antitumor Immunity and Survival Induced by DC Immunotherapy. *Cancer Immunol Res* **5**, 535-546 (2017).
133. Lievense, L., *et al.* Combination therapy with a CD40-agonist and dendritic cell immunotherapy has synergistic effects in a murine mesothelioma model. *Journal of Thoracic Oncology* **10**, S253 (2015).
134. Prasad, S.J., *et al.* Dendritic cells loaded with stressed tumor cells elicit long-lasting protective tumor immunity in mice depleted of CD4+CD25+ regulatory T cells. *J Immunol* **174**, 90-98 (2005).

Supplementary data

Table 1. Study characteristics of (pre)clinical studies.

	Type of CTX	Cancer Type	n[a]	Comparison group	Treatment schedule
Preclinical	Cyclophosphamide	Mesothelioma (AB1)	6	Untreated CTX + DC-Tx + CTX DC-Tx + CTX	CTX: day 3-10[b] DC-Tx: day 12[b]
		Melanoma (B16)	10	Untreated CTX DC-Tx	CTX: day 5[b] DC-Tx: day 9 and 23[b]
		Colon carcinoma (CT26)	10	Untreated CTX DC-Tx	CTX: day 5[b] DC-Tx: day 9 and 23[b]
	Gemcitabine	Pancreatic cancer (Panc02)	6-8	Untreated CTX DC-Tx	CTX 2 days prior and after DC-Tx for 5 weeks
		Pancreatic cancer (Panc02)	8	Untreated CTX DC-Tx	CTX: every 3-4 days until day 42 (start day 3) DC-Tx: day 3, 7 and 10[b]
Clinical	Cyclophosphamide	Melanoma	7		CTX: 3 days prior to first DC-tx. DC-tx: 6 vaccinations with 3-week intervals
		Mesothelioma	10		7x CTX followed by 1x DC-Tx 4 days after CTX. Cycle repeated 3x

Type of DC vaccine	Dosage CTX	Immunological response CTX[c]	Immunological response combination treatment[c,d]	Clinical response	Ref.
Tumor lysate-loaded mature BM-derived DCs	0,13 mg/ml (drinking water)	Tregs		Prolonged survival compared with untreated	52
Tumor lysate-loaded mature BM-derived DCs	50 mg/kg body weight			Prolonged survival compared with monotherapy and untreated	53
Tumor lysate-loaded mature BM-derived DCs	50 mg/kg body weight	Tregs	IFNγ secreting lymphocytes	Prolonged survival compared with monotherapy and untreated	53
BM-derived mature DCs loaded with Panc02 cells	25 and 50 mg/kg body weight			Prolonged survival compared with untreated (for both dosages)	66
Unloaded immature BM-derived DCs	120 mg/kg body weight	MDSCs	IFNγ secreting lymphocytes $CD8^+$ T cells in tumor tissue	Prolonged survival compared with monotherapy and untreated	67
gp100 antigen derived peptide-loaded mature autologous DCs	300 mg/m^2		T cell immunity against gp100-derived antigens 6/7 Positive correlation DC derived IL-12p70 levels and time to progression		54
Tumor lysate-loaded mature autologous DCs	2x50 mg	Tregs		Disease control in 8 patients	55

Table 1. Continued

	Type of CTX	Cancer Type	n[a]	Comparison group	Treatment schedule
Clinical (Continued)		Melanoma	22		7x CTX followed by 1x DC-Tx. Cycle repeated 6x
		Ovarian cancer	22	DC-tx (+ bevacizumab) (n=10)	CTX one day prior to each DC-Tx + bevacuzimab given 1x each 3 weeks Repeated 4-5x
		Renal cell carcinoma	22	DC-tx (n=12)	CTX: 3 and 4 days prior to each DC-Tx DC-Tx: 3 vaccinations with monthly intervals

Type of DC vaccine	Dosage CTX	Immunological response CTX[c]	Immunological response combination treatment[c,d]	Clinical response	Ref.
Mature autologous DCs transfected with p53, survivin and hTERT	50 mg		Tregs and MDSCs unchanged IFNγ Immune response 6/17	PD: n=13 OS: 10.4 mo SD: n=9 PFS: 3.1 mo	56
Tumor-lysate loaded mature autologous DCs	200 mg/m^2		Vaccine-specific T cells IFNγ serum levels TGFβ serum levels compared with no CTX	Improved OS compared with no treatment with CTX	57
Tumor lysate-loaded mature allogeneic DCs	300 mg/m^2		No proliferative or cytokine immune responses	No CTX CTX PD: n=9 PD: n=4 SD: n=2 SD: n=1 MR: n=0 MR: n=2 LFU: n=1 LFU: n=3 OS: 20.3 mo OS: 23.2 mo	58

Table 1. Continued

	Type of CTX	Cancer Type	n[a]	Comparison group	Treatment schedule
Clinical (Continued)	Temozolomide	Melanoma	21		14x CTX followed by 1x DC-tx. Cycle repeated 6x
		Glioblastoma	32		CTX: 5 days/28 in each cycle DC-Tx: 3x starting 2 weeks after CTX. Repeated 3x
		Glioblastoma	14		CTX: 5 days/28 starting one week after 3rd DC-Tx Cycle repeated up to 6x DC-Tx: 3x each cycle with 2 –week intervals.
		Glioblastoma	24		CTX: 5 days/28 starting after 3rd DC-Tx. Cycle repeated 6x DC-Tx: 1-4: two-week intervals, 5-6: monthly intervals, 7: 8 weeks after 6th DC-Tx
	Gemcitabine	Pancreatic cancer	10		CTX: day 1,8 and 15 of a 28-day cycle DC-Tx: Starting one week after first CTX cycle. Given 3x biweekly
	Premetrexed and cisplatin	Mesothelioma	10		CTX: 4x each 3 weeks DC-Tx: 3x each 2 weeks starting 12 weeks after last CTX
	Oxiplatin and capecitabine	Colon cancer	7		CTX: 1x oxiplatin followed by 14x capecitabine. Cycle repeated 8 times DC-Tx: 3x during first cycle of CTX

Type of DC vaccine	Dosage CTX	Immunological response CTX[c]	Immunological response combination treatment[c,d]	Clinical response	Ref.
Tumor lysate-loaded mature autologous DCs	75 mg/m^2		Tregs	PD: n=10 OS: 10 mo SD: n=6 PR: n=1 NT: n=3	61
DCs fused with glioma cells	150-200 mg/m^2		WT-1, gp100 and MAGE-A3 specific immune responses 4/4	Recurrent Initial OS: 18.0 mo OS: 30.5 mo PFS: 10.3 mo PFS: 18.3 mo	62
Tumor cell-loaded mature autologous DCs	150-200 mg/m^2			PD: n=4 OS: 23 mo SD then PD: n=3 PFS_{6mo}: 22% PR then PD: n=2 NT: n=4	63
Tumor lysate-loaded mature autologous DCs	75 mg/m^2		Positive correlation activation NK cells and PFS	OS: 20.1 mo PFS 10.5 mo	64
I, II or I/II-WT1 restricted peptide-loaded mature DCs	1000 mg/m^2			PD: n=3 SD: n=7	68
Tumor lysate-loaded mature autologous DCs	Preme-trexed: 500 mg/m^2 Cisplatin: 75 mg/m^2		KLH-specific antibodies 10/10	PD: n=6 SD: n=1 PR: n=3	69
CEA peptide-loaded mature autologous DCs	Oxiplatin: 130 mg/m^2 Capecit-abine: 2000 mg/m^2		CEA-specific T cell response 4/7 Proliferative KLH-specific $CD4^+$ T cell response 7/7		70

Table 1. Continued

	Type of CTX	Cancer Type	n[a]	Comparison group	Treatment schedule
Clinical (Continued)	Bortezomib and dexamethasone	Multiple myeloma	50	CTX (n=24)	Bortezomib: day 1,4,8 and 11 Dexamethasone: day 1-2, 4-5, 8-9, 11-12 DC-Tx: 6x day 15-20 Cycle lasted 28 days. Repeated 3x
	Dacarbazine	Melanoma	6		CTX: 6x at 3-week intervals DC-Tx: 6x one day after CTX
	Carboplatin and paclitaxel	Melanoma	9		CTX: day 1 of each cycle DC-Tx: day 8 and 22 of each cycle Cycle lasted 28 days Repeated 3x
	Docetaxel	Prostate cancer	40	CTX (n=19)	CTX: 1x each 3 weeks. Repeated 10x DC-Tx: 2x in cycle 1-5 and 1x cycle 5-10
		Esophageal cancer	10		CTX: day 1 of each cycle DC-Tx: day 15 and 22 of each cycle Cycle lasted 4 weeks. Repeated 3x

AUC = area under curve, BM-derived DCs = bone marrow-derived DCs, CEA = carcinoembryonic antigen, CTX = chemotherapy, CIK = cytokine-induced killer cells, DC = dendritic cell, DC-Tx = Dendritic cell therapy, gp100 = glycoprotein 100, hTERT = human telomerase reverse transcriptase, IFN = interferon, IFNγ = interferon gamma, IL = interleukin, KLH = keyhole limpet hemocyanin, LFU = lost to follow-up, MAGE = melanoma-associated antigen, MDSC = myeloid-derived suppressor cell, MR = mixed response, NK cells = natural killer cells, NT = not treated, OS = overall survival,

Type of DC vaccine	Dosage CTX	Immunological response CTX[c]	Immunological response combination treatment[c,d]	Clinical response	Ref.
Autologous DCs/ CIK	Bortezomib: 1.0-1.3 mg/ m^2 Dexame-thasone: 20 mg		CD4/CD8 ratio IL-2 and IFNγ in PB IL-4, IL-5 and TGFβ in PB compared with CTX	Improved quality of life compared with no DC-Tx	71
Autologous IFN-DCs	1000 mg/m^2		Tyrosinase, NY-ESO-1 and gp100-specific immune response 2/3	PD: n=2 SD: n=3 NT: n=1	72
WT1, gp100, tyrosinase and MAGE-A2/A3 peptide-loaded mature DCs	Carboplatin: AUC5 Paclitaxel: 175 mg/m^2		WT1-specific immune response 4/9	PD: n=4 OS: 12 mo SD: n=4 PFS: 2.3 mo PR: n=1	73
Mature autologous DCs transfected with PSA, PAP, survivin and hTERT	75 mg/m^2	MDSCs and Tregs unchanged	MDSCs (positive correlation with PFS) Tregs unchanged	PFS without DC-Tx: 5.5 mo PFS with DC-Tx: 5.7 mo	74
WT-1 peptide-loaded matured DCs	50 mg/m^2		WT1-specific immune response 5/8	PD: n=9 SD: n=1 OS: 5 mo	75

PAP = prostatic acid phosphatase, PB = peripheral blood, PD = progressive disease, PFS = progression-free survival, PR = partial response, PSA, = prostate-specific antigen, SD = stable disease, TGF-β = transforming growth factor beta, Tregs = regulatory T cells, WT = wilms tumor gene. [a], for preclinical studies n is number mice per group, for clinical studies n is the total number patients; [b], days after tumor inoculation; [c], compared with baseline unless indicated otherwise; [d], immunological responses measured after combination treatment.

Chapter 6

Combination of PD-1/PD-L1 checkpoint inhibition and dendritic cell therapy in mice models and in patients with mesothelioma

Mandy van Gulijk, Bob Belderbos, Daphne Dumoulin, Robin Cornelissen, Koen Bezemer, Larissa Klaase, Floris Dammeijer, Joachim Aerts

International Journal of Cancer 2023 Apr 1;152(7):1438-1443

Abstract

Immunotherapy with anti-PD1/PD-L1 is effective in only a subgroup of patients with malignant pleural mesothelioma (MPM). We investigated the efficacy of a combination of anti-PD1/PD-L1 and dendritic cell (DC) therapy to optimally induce effective anti-tumor immunity in MPM in both humans and mice. Data of nine MPM patients treated with DC therapy and sequential anti-PD1 treatment were collected and analyzed for progression-free survival (PFS) and overall survival (OS). Survival and T cell responses were monitored in AC29 mesothelioma-bearing mice treated concurrently with the combination therapy; additionally, the role of the tumor-draining lymph node (TDLN) was investigated. The combination therapy resulted in a median OS and PFS of 17.7 and 8.0 months, respectively. Grade 3-4 treatment-related adverse events had not been reported. Survival of the mesothelioma-bearing mice treated with the combination therapy was longer than that of untreated mice, and coincided with improved T cell activation in peripheral blood and less T cell exhaustion in end stage tumors. Comparable results were obtained when solely the TDLN was targeted. We concluded that this combination therapy is safe and shows promising OS and PFS. The murine data support that anti-PD-L1 treatment may reinvigorate the T cell responses induced by DC therapy, which may primarily be the result of TDLN targeting.

Introduction

The median survival after diagnosis for patients with malignant pleural mesothelioma (MPM) remains between 13 and 18 months [1,2]. Therefore, novel therapeutic strategies that effectively induce anti-tumor responses are warranted. PD-1 checkpoint inhibition has shown remarkable responses in multiple cancer types. Anti-PD-1 therapy induces responses in 9-29% of MPM patients and as second line treatment it has been associated with a median progression-free survival (PFS) of 2.5 months and median overall survival (OS) of 10.7 months [1,3-5]. In combination with ipilimumab (anti-CTLA-4), response rates were even higher and more durable. Still, the majority of patients failed to respond which could be due to lack of T cell infiltration before treatment [2,6].

Dendritic cell (DC) therapy has been shown to be safe, feasible and able to induce radiological responses in MPM coinciding with enhanced intratumoral T cell infiltration [7-9]. As DC therapy-induced infiltrating T cells may in turn become exhausted through PD-1/PD-L1 signaling, we investigated the efficacy of adjuvant anti-PD-1 immunotherapy in DC-treated MPM patients. Additionally, as PD-L1 is expressed on DCs, the effects of concurrently combining DC- and anti-PD-L1 therapy were analyzed in a MPM murine model.

Material and methods

Patient data collection

Data were collected of nine patients with histologically proven MPM treated in second or third line with CI therapy after progression on treatment with autologous monocyte-derived DCs (moDCs) loaded with allogeneic (n = 8) or autologous (n = 1) tumor lysate (NCT02395679, NCT01241682). Five patients had received first line chemotherapy prior to DC therapy.

Patient treatment

Intravenous anti-PD-1 treatment, consisting of nivolumab (3 mg/kg every 2 weeks) or pembrolizumab (2 mg/kg every 3 weeks) was administered, irrespectively of PD-L1 expression. One patient received nivolumab and ipilimumab at dosages described in the INITIATE trial [10].

Patient response evaluation

Radiological tumor evaluation was done 6 weeks after start of treatment and every 4 to 12 weeks thereafter; the interval depended on the previous CT evaluation. The tumor response was assessed using the modified Response Evaluation Criteria in Solid Tumors (mRECIST) for mesothelioma (final data check November 19th, 2021) [11]. OS was defined as the time from start of CI therapy until death. PFS was determined from the time of start of CI therapy until radiological

progression or death of any cause. The overall response rate was defined as the percentage of patients with a partial response (PR) or complete response. Disease control rate was defined as the percentage of patients without progressive disease as best overall response (BOR).

***In vivo* experiment in murine AC29 tumor model**

Female 8- to -12-week-old CBA/J mice and C57BL/6 mice were purchased from Envigo and housed under specific pathogen-free conditions in individually ventilated cages at the animal care facility of the Erasmus University Medical Center (Erasmus MC), Rotterdam. For tumor inoculation, mice were intraperitoneally (i.p.) injected with 10^6 AC29 mesothelioma tumor cells (RRID:CVCL_4407) in 300 µl PBS, as described previously [12]. Mice with established i.p. tumors were killed at indicated time points for immune cell profiling or when profoundly ill according to the body condition score for therapy efficacy experiments. Mice were randomly assigned to experimental groups. For bone marrow derived dendritic cells (BMDC)-transfer, AC29 tumor lysate was produced and DCs were cultured as previously described [13]. Briefly, tumor lysate was produced by disrupting frozen tumor cells by four cycles of freeze-thaw cycles with liquid nitrogen followed by sonication. BMDCs were generated using recombinant murine GM-CSF (provided by B. Lambrecht VIB, Ghent) in DC-culture medium followed by loading with tumor lysate and activation with CpG (Invitrogen) on day 9 and injection at day 10. Where applicable, DCs were labeled at day 10 with carboxyfluorescein succinimidyl ester (CFSE) according to the manufacturer's instructions (Thermo Fisher). Dependent on treatment arm, mice were treated with either 200 µg isotype (clone 2A3, BioXCell) or 200 µg anti-PD-L1 antibody (clone MIH5, provided by L. Boon, Bioceros B.V., Utrecht, the Netherlands) in 300 µl PBS in the peritoneal cavity. In case of intrapleural injection, 200 µL PBS was injected in the pleural cavity of mice that were under short-term anesthesia. All experiments were performed with mycoplasma-free cells.

Preparation of single cell suspensions from mouse tissues

Single-cell suspensions were generated from isolated inguinal lymph node (non-tumor draining lymph node (non-TDLN), mediastinal lymph node (TDLN), blood and tumor tissue of mice from each group as previously reported [13]. In brief, 30 µl blood was collected in EDTA tubes (Microvette CB300, Sarstedt) and erythrocytes were lysed using osmotic lysis buffer (8.3% NH_4Cl, 1% $KHCO_3$, and 0.04% Na_2EDTA in Milli-Q). Tumors were collected and dissociated using a validated tumor dissociation system (Miltenyi Biotec) according to protocol.

Statistical analysis

Median OS and PFS were estimated using a Kaplan-Meier curve in combination with a log-rank (Mantel-cox) test. Survival data were plotted as Kaplan-Meier survival curves, using the log-rank test to determine statistical significance. A P-value of 0.05 or below was considered to indicate statistical significance. All reported p-values were two tailed. Statistical analyses were performed using R 3.6.0 (R Foundation for Statistical Computing) or Graphpad Prism 8.0.

Results

We identified strong PD-L1 upregulation on *in vitro* matured patient-derived moDCs used for vaccination (Fig 1A). Vaccination of mice with DCs induced $CD8^+$ T cell (CTL) infiltration, which coincided with increased PD-L1 expression by tumor cells, likely due to increased IFNγ production by CTLs (Fig. 1B-C). Due to the upregulation of PD-1 on CTLs and PD-L1 on both tumor cells and exogenous DCs, we investigated whether checkpoint blockade could re-induce T cell mediated immunity and responses in patients. We assessed nine MPM patients receiving pembrolizumab (n = 2) or nivolumab (n = 7; one patient combined with ipilimumab) upon progression after DC therapy (Fig. 1C). The median PFS following start checkpoint blockade was 8.0 months and the median OS was 17.7 months (Fig. 1E). Three patients exhibited partial responses, five stable disease, and one progressive disease; thus, the objective response rate was 33% (Fig. 1D). At 6 months, five patients (55.6%) showed disease control. Application of the Common Terminology Criteria for Adverse Events (CTCAE 5.0) did not reveal any grade 3/4 adverse events.

Similar to the PD-L1 upregulation on patient-derived moDCs, we identified increased PD-L1 expression on both transferred and endogenous DCs in the TDLNs of tumor-bearing mice (Fig. 2A). Therefore, we wondered whether concurrent treatment with DC therapy and checkpoint blockade could enhance anti-tumor immunity. To investigate this, we concurrently treated mesothelioma-bearing mice with DC therapy and anti-PD-L1, enabling us to assess PD-1 expression on T cells following treatment. This combination treatment resulted in longer survival compared with untreated mice (Fig. 2B-C). This was accompanied by synergistic and rapid CD69 upregulation (early activation marker) on T cells in peripheral blood, followed by increased proliferation (assessed by Ki67), which was most prominent for $CD4^+$ Th-cells (Fig. 2D, S1A). Moreover, the expression of the exhaustion-program driver TOX on tumor-infiltrating CTLs was most profoundly decreased following combination treatment, indicating a less-exhausted T cell phenotype. This phenotype was confirmed by a decreased percentage of cells positive for PD-1, TIM3 and CD39, and lower TOX expression within this triple-positive cell subset (Fig. 2E, S2B).

We have previously shown a critical role for PD-L1-expressing DCs in suppressing anti-tumor T cells in TDLNs of mesothelioma-bearing mice [12]. This potentially suggest that TDLNs may be important in mediating the efficacy of PD-L1 blockade combined with DC therapy. To investigate whether the efficacy in mice resulted from PD-L1 blockade in TDLNs or in tumors, we targeted PD-L1 specifically and solely in TDLNs using an established method in which anti-PDL1 is administered at a low dose in the pleural cavity [12]. Blocking PD-L1 solely in TDLNs mimicked systemic anti-PD-L1 treatment for survival (Fig. 2C) and for alterations in immune phenotype (Fig. 2D-E). This implies that the efficacy of concurrent combination treatment may primarily depend on blocking the PD-1/PD-L1 axis in the TDLN, thereby resulting in improved T cell priming by DCs. These findings could indicate the importance of optimizing T cell priming in TDLNs for maximum anti-tumor T cell capacity and provide a preclinical rationale for concurrent treatment in MPM patients.

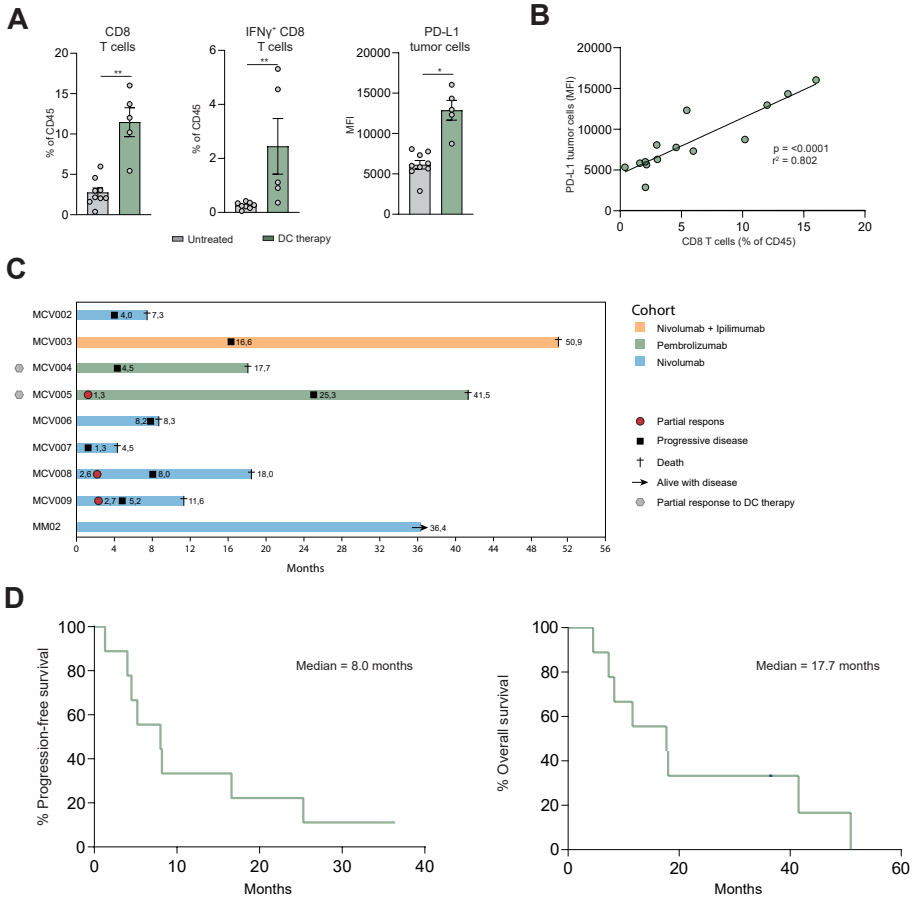

Figure 1: Rationale and clinical responses to treatment with checkpoint blockade upon progression to DC therapy

(A) MFI of PD-L1 on immature and mature patient-derived DCs cultured *in vitro* for therapy. (B) $CD8^+$ T cell infiltration, IFNγ production and PD-L1 expression on tumor cells was assessed in AC29 bearing female CBA/J mice untreated (n = 9) or treated with DC therapy (n = 5) on day 15. (C) Correlation of PD-L1 expression on tumor cells and $CD8^+$ T cell levels and a Pearson correlation coefficient was calculated (r^2) (n = 14). (D) Swimmer plot of patients treated with checkpoint blockade upon progression to DC therapy. Overall survival of patients since date of first vaccination is represented by the filled bars. Start and end of RECIST responses are depicted by the red circles and black squares, respectively. First evaluation of response was after 6 weeks for all patients. (E) Kaplan-Meier curves showing progression-free survival (left) and overall survival (right) for all patients. Means and SEMs are shown and Mann-Whitney U tests were performed indicating statistical significance. * = $p < 0.05$, ** = $p < 0.01$.

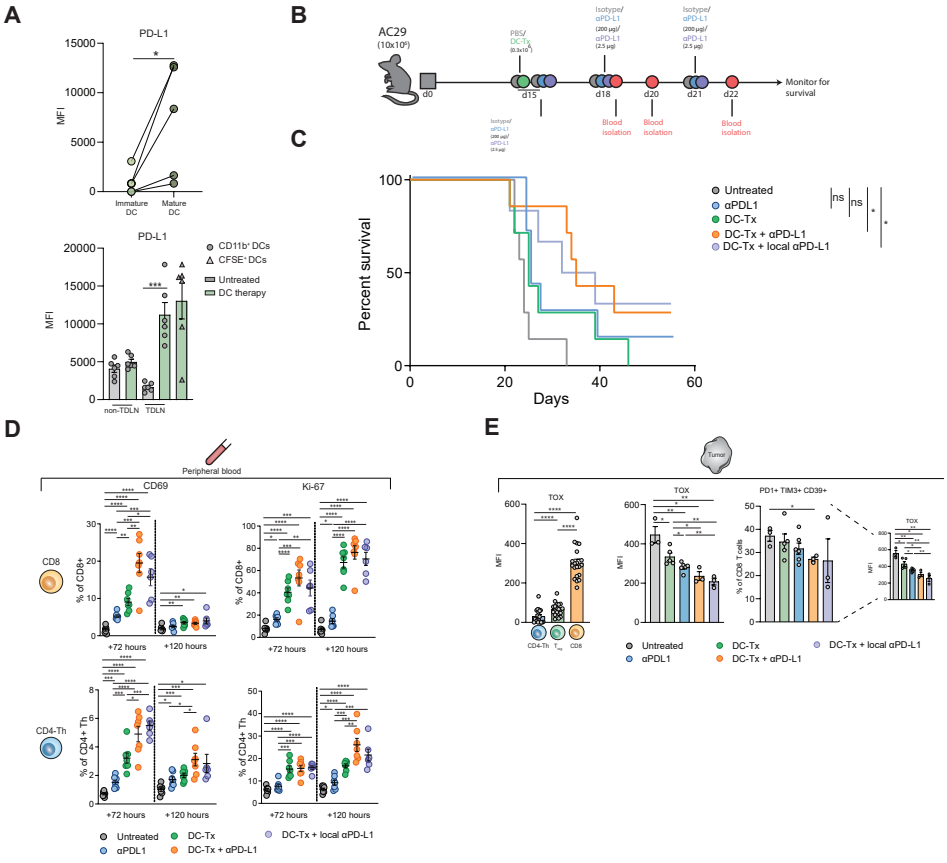

Figure 2: Concurrent treatment with anti-PD-L1 and DC therapy results in improved survival and anti-tumor immunity

(A) MFI of PD-L1 on injected CFSE labeled DCs and endogenous DCs in non-TDLN and TDLN of AC29 mesothelioma bearing CBA/J mice (n = 6 per group; total n = 12) 24 hours after DC therapy. (B) Mice bearing AC29 tumors (n = 7 per group; total n = 35) were treated with DC therapy or PBS at day 15. At day 15, 18 and 21, mice were also treated with either isotype, low-dose anti-PD-L1 (2.5 μg) or systemic dose (200 μg). (C) Mice were monitored for survival which is depicted in a Kaplan-Meier curve. (D) From the experiment in B, blood was isolated at day 18 and 20 and expression of early-activation marker CD69 and proliferation marker Ki67 were determined for $CD8^+$ T cells and CD4-Th cells. (E) Expression of TOX on $CD4^+$ Th cells, Tregs and $CD8^+$ T cells and the percentage of triple-positive ($PD\text{-}1^+$ $TIM3^+$ $CD39^+$) and their TOX expression level was determined in end-stage tumor material from experiment in B. Means and SEMs are shown and paired- and unpaired t tests were performed indicating statistical significance. * = $p < 0.05$, ** = $p < 0.01$, *** = $p < 0.001$, **** = $p < 0.0001$. MFI = median fluorescence intensity, non-TDLN = non-tumor draining lymph node, TDLN = tumor-draining lymph node, CD4-Th = CD4 T helper, SEM = standard error of the mean.

Discussion

In this study, we have shown that anti-PD-1 following DC therapy is safe and feasible in MPM patients. The response rate (33%), PFS (8.0 months) and OS (17.7 months) are promising when compared with anti-PD-1 monotherapy. Still, the potential bias in patient selection calls for caution in the interpretation of these findings. To support the potential synergy, combining DC therapy with concurrent blockade of the PD-1/PD-L1 axis reinvigorated T cells and prolonged survival in the mesothelioma-bearing mice. This synergistic effect of concurrent treatment may be the result of the high PD-L1 expression on DCs *in vivo* and on moDCs given as DC therapy. The data suggest that this effect could be primarily derived from the TDLN, as TDLN-specific blockade of PD-L1 resulted in comparable immune-stimulating effects as did systemic anti-PD-L1 treatment. By releasing progenitor-exhausted tumor-specific T cells, PD-L1 blockade on DCs in the TDLN has been shown to induce effective tumor immunity [12,14]. As we observed a less-exhausted tumor-infiltrating CTL phenotype in combination therapy-treated mice, these results could indicate that concurrent treatment may eventually result in more efficient T cell priming in the TDLN by DCs. Since we treated MPM patients sequentially with PD-1 blockade, our data indicate that clinical responses might even be further improved by concurrent treatment.

Limitations of our study include the lack of pre-and post-treatment biopsies in MPM patients treated with DC therapy. This precluded investigation of the PD-L1 upregulation that we observed in mice. Furthermore, due to rapid tumor growth, we could not include a murine treatment arm of DC- and anti-PD-L1 therapy administered sequentially. Lastly, while MPM patients were treated with PD-1 blocking agents, mesothelioma-bearing mice were treated with antibodies blocking its ligand, PD-L1. Although both antibodies block the same axis, it has recently been demonstrated that anti-PD-1 and anti-PD-L1 may have different immune modulating effects due to *cis* interactions with CD80 on antigen-presenting cells which could potentially influence efficacy of the combination treatment [15]. Whether anti-PD-L1 leads to suboptimal anti-tumor immunity, compared with anti-PD-1, needs to be further investigated in our models.

In conclusion, our data from both patients and mice indicate that the combination of DC therapy and anti-PD-1/PD-L1 could be a promising treatment for MPM, as it was found feasible and safe, and did show clinical efficacy.

References

1. Yap, T.A., Aerts, J.G., Popat, S. & Fennell, D.A. Novel insights into mesothelioma biology and implications for therapy. *Nat Rev Cancer* **17**, 475-488 (2017).
2. Baas, P*., et al.* First-line nivolumab plus ipilimumab in unresectable malignant pleural mesothelioma (CheckMate 743): a multicentre, randomised, open-label, phase 3 trial. *Lancet* **397**, 375-386 (2021).
3. Popat, S*., et al.* A multicentre randomised phase III trial comparing pembrolizumab versus single-agent chemotherapy for advanced pre-treated malignant pleural mesothelioma: the European Thoracic Oncology Platform (ETOP 9-15) PROMISE-meso trial. *Ann Oncol* **31**, 1734-1745 (2020).
4. Fennell, D.A*., et al.* Nivolumab versus placebo in patients with relapsed malignant mesothelioma (CONFIRM): a multicentre, double-blind, randomised, phase 3 trial. *Lancet Oncol* (2021).
5. Cantini, L*., et al.* Nivolumab in pre-treated malignant pleural mesothelioma: real-world data from the Dutch expanded access program. *Transl Lung Cancer Res* **9**, 1169-1179 (2020).
6. Ahmadzada, T*., et al.* Retrospective Evaluation of the Use of Pembrolizumab in Malignant Mesothelioma in a Real-World Australian Population. *JTO Clin Res Rep* **1**, 100075 (2020).
7. Aerts, J*., et al.* Autologous Dendritic Cells Pulsed with Allogeneic Tumor Cell Lysate in Mesothelioma: From Mouse to Human. *Clin Cancer Res* **24**, 766-776 (2018).
8. Hegmans, J.P*., et al.* Consolidative dendritic cell-based immunotherapy elicits cytotoxicity against malignant mesothelioma. *Am J Respir Crit Care Med* **181**, 1383-1390 (2010).
9. Cornelissen, R*., et al.* Extended Tumor Control after Dendritic Cell Vaccination with Low-Dose Cyclophosphamide as Adjuvant Treatment in Patients with Malignant Pleural Mesothelioma. *Am J Respir Crit Care Med* **193**, 1023-1031 (2016).
10. Disselhorst, M.J*., et al.* Ipilimumab and nivolumab in the treatment of recurrent malignant pleural mesothelioma (INITIATE): results of a prospective, single-arm, phase 2 trial. *Lancet Respir Med* **7**, 260-270 (2019).
11. Armato, S.G., 3rd & Nowak, A.K. Revised Modified Response Evaluation Criteria in Solid Tumors for Assessment of Response in Malignant Pleural Mesothelioma (Version 1.1). *J Thorac Oncol* **13**, 1012-1021 (2018).
12. Dammeijer, F*., et al.* The PD-1/PD-L1-Checkpoint Restrains T cell Immunity in Tumor-Draining Lymph Nodes. *Cancer Cell* **38**, 685-700 e688 (2020).
13. Dammeijer, F*., et al.* Depletion of Tumor-Associated Macrophages with a CSF-1R Kinase Inhibitor Enhances Antitumor Immunity and Survival Induced by DC Immunotherapy. *Cancer Immunol Res* **5**, 535-546 (2017).
14. Peng, Q*., et al.* PD-L1 on dendritic cells attenuates T cell activation and regulates response to immune checkpoint blockade. *Nat Commun* **11**, 4835 (2020).
15. Zhao, Y*., et al.* PD-L1:CD80 Cis-Heterodimer Triggers the Co-stimulatory Receptor CD28 While Repressing the Inhibitory PD-1 and CTLA-4 Pathways. *Immunity* **51**, 1059-1073 e1059 (2019).

Supplementary data

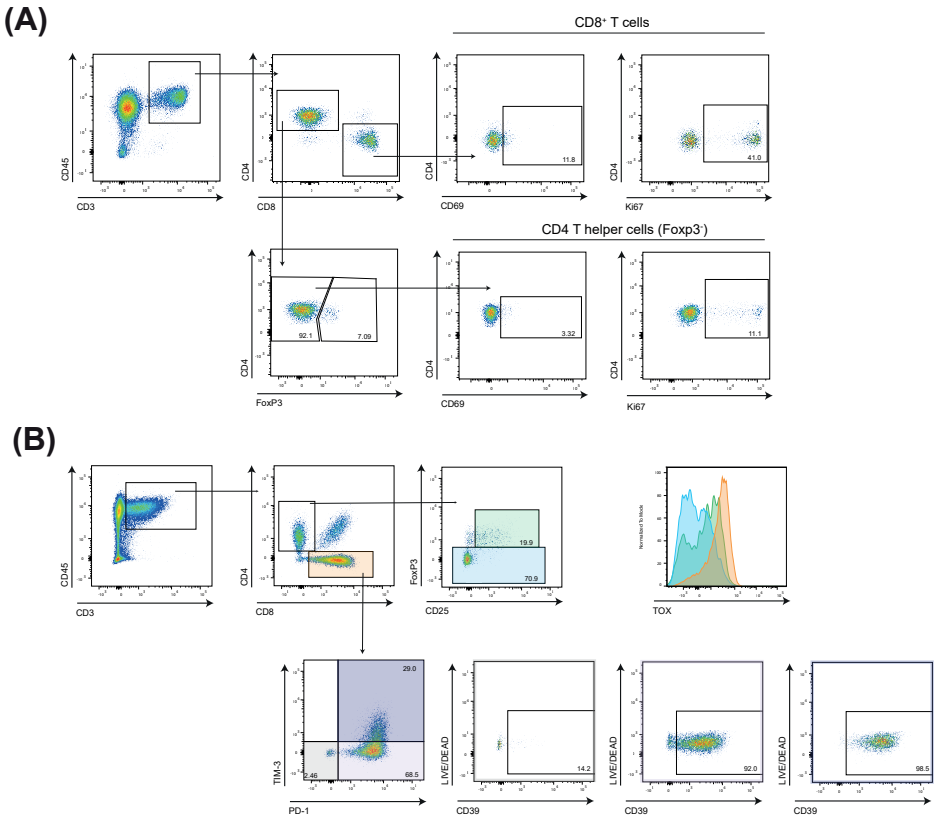

Figure S1: **Characterization of T cells in peripheral blood and tumor in AC29 bearing mice treated with DC therapy and/or anti-PDL1**

(A) Gating strategy of T cells ($CD8^+$ T cells and $CD4^+$ T helper cells) and related expression levels of CD69 of Ki67 in peripheral blood isolated 72- and 120 hours following start treatment, related to Figure 2D. (B) Gating strategy for the characterization of end stage tumor infiltrating T cells ($CD8^+$ T cells, $CD4^+$ T helper cells and regulatory T cells) and related expression levels of TOX. For $CD8^+$ T cells, gating for triple-positive cells was accomplished by first gating on TIM3 and PD-1 ($PD\text{-}1^-$ $TIM3^-$ (grey)/ $PD\text{-}1^+$ $TIM3^-$ (light purple)/$PD\text{-}1^+$ $TIM3^+$ (dark purple)), followed by CD39 in each subset, related to Figure 2E.

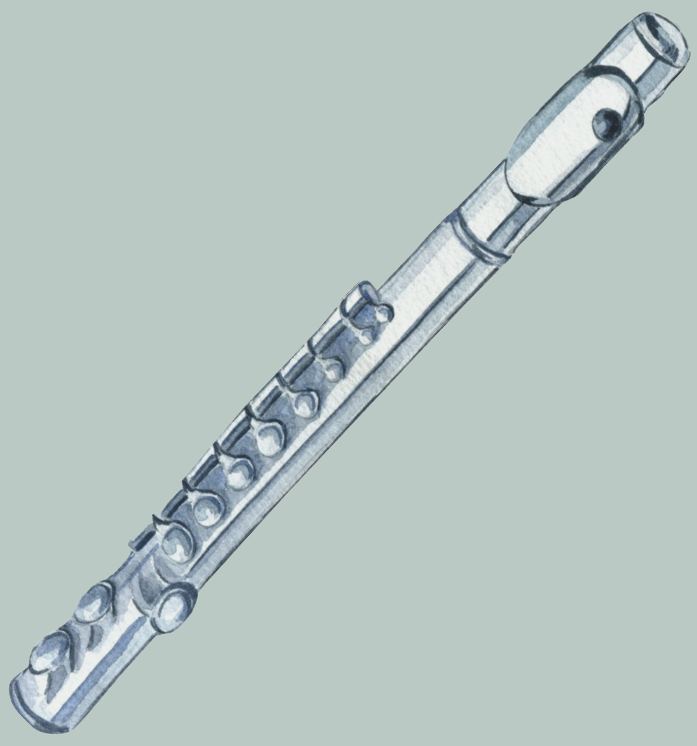

Chapter 7

Low-dose JAK3-inhibition improves anti-tumor T cell immunity and immunotherapy efficacy

Floris Dammeijer, Mandy van Gulijk, Larissa Klaase, Menno van Nimwegen, Rachid Bouzid, Robin Hoogenboom, Maria E Joosse, Rudi W Hendriks, Thorbald van Hall, Joachim Aerts

Molecular Cancer Therapeutics 2022 Sep 6;21(9):1393-1405

Abstract

Terminal T cell exhaustion poses a significant barrier to effective anti-cancer immunotherapy efficacy with current drugs aimed at reversing exhaustion being limited. Recent investigations into the molecular drivers of T cell exhaustion have led to the identification of chronic IL-2 receptor (IL-2R) – STAT5 pathway signaling in mediating T cell exhaustion. We targeted the key downstream IL-2R-intermediate Janus kinase (JAK) 3 using a clinically relevant highly specific JAK3-inhibitor (JAK3i; PF-06651600) that potently inhibited STAT5-phosphorylation *in vitro*. Whereas pulsed high-dose JAK3i administration inhibited anti-tumor T cell effector function, low-dose chronic JAK3i significantly improved T cell responses and decreased tumor load in mouse models of solid cancer. Low-dose JAK3i combined with cellular and peptide vaccine strategies further decreased tumor load compared with both monotherapies alone. Collectively, these results identify JAK3 as a novel and promising target for combination immunotherapy.

Introduction

Cancer immunotherapy induces durable anti-tumor immune and clinical responses but only in a minority of patients and tumor types for reasons still incompletely understood [1-3]. T cell exhaustion is a major mechanism underlying cancer immunotherapy resistance and current treatment strategies aimed at the prevention or reversal of exhaustion are lacking [4]. T cell exhaustion arises through chronic antigen stimulation of the T cell receptor (TCR) in a suppressive tumor microenvironment (TME), decreasing T cell functionality and persistence [5,6]. Attempts have been made to prevent T cell exhaustion by inhibiting key downstream TCR-signaling pathways (e.g. MAPK/ERK, mTOR), yielding varying clinical and preclinical results [7-11]. Possible redundancy between different signaling pathways and the existence of exhaustion mechanisms other than chronic TCR-activation could be involved in T cell exhaustion and immunotherapy resistance.

Besides excessive TCR stimulation, continuous IL-2 receptor (IL-2R)-induced signal transducer and activator of transcription 5 (STAT5)-phosphorylation in T cells has recently been linked to exhaustion in chronic viral infection and cancer, with IL-2^{hi} cancers exhibiting poor prognosis [12,13]. Despite that IL-2 is required for initial T cell expansion and survival, excess IL-2 during T cell priming skews toward a short-lived T cell effector fate at the expense of memory precursor T cells [14,15]. Whether temporal downstream IL-2R-inhibition improves antitumor immunity is currently unknown. The IL-2R may be a particularly attractive target as activation of the receptor culminates in MAPK-, mTOR- as well as STAT5-signaling, thereby allowing for concomitant targeting of multiple exhaustion-related pathways.

Binding of IL-2 to the high affinity IL-2R consisting of α, β and γ chains (CD25, CD122 and CD132, respectively) activates a downstream cascade initiated by Janus-kinase (JAK) family members JAK1 and JAK3 that in turn phosphorylate STAT5 leading to dimerization and target gene transcription [16,17]. In contrast with JAK1 associating with various type I and II cytokine receptors, JAK3 is located downstream of the common-gamma chain cytokine receptor family, including IL-2R, IL-4R, IL-7R and IL-15R. With the recent development of specific JAK inhibitors, interrogation of these downstream cytokine-receptors pathways has become feasible with minimal off-target activity [18]. This allowed us to investigate JAK3 as novel immunotherapeutic target downstream of the IL-2R using the highly specific JAK3-inhibitor (JAK3i) PF-06651600 (further referred to as PF-06) that was initially developed for treatment of autoimmune disease [19,20]. In this report, we demonstrate that this JAK3i effectively inhibits IL-2-mediated STAT5-phosporylation in T cells and when administered at high dose diminishes anti-tumor T cell immunity. In contrast, at low-dose, PF-06 improves T cell responses and decreases tumor load in solid tumor mouse models. Moreover, JAK3i potentiated cellular- and peptide-vaccine immunotherapies, improving therapeutic efficacy and reducing the exhausted T cell phenotype. These important potential improvements of current immunotherapy warrant further investigation into the clinical use of low-dose JAK3i in patients with solid tumor.

Materials and Methods

Phosphoflow analysis

Wildtype C57BL/6 mice were euthanized by cervical dislocation and the spleens were isolated and mashed over a 100-µm filter establishing a cell suspension in RPMI 1640 containing 2% FCS. A total of $2x10^6$ splenocytes were incubated for 3 hours at 37°C with vehicle (same amount of DMSO as highest concentration of inhibitor as negative control) or acalabrutinib (10µM, 1µM and 0.1µM in DMSO) or Ibrutinib (10µM, 1µM and 0.1µM in DMSO) or PF-06651600 (10µM, 1µM and 0.1µM in deionized water (MilliQ), all obtained from Sigma-Aldrich). The cells were stimulated with anti-CD3/CD28 biotin in case of the stimulated samples or RPMI1640 2% FCS for unstimulated samples. Afterwards, the cells were washed with RPMI1640 2% FCS and stained with streptavidin PerCP Cy5.5 to establish receptor cross-linking. After washing, the samples were stimulated at 37°C for 1 minute for $pZAP70_{Y319}$ (pZAP70) and $pSLP76_{Y128}$ (pSLP76), 5 minutes for $pITK_{Y180}$ ($pITK_{180}$) 120 minutes for IkB and $pS6_{S240/244}$ (pS6). Ten minutes before the end of the stimulation a live/death marker was added. At the end of the stimulation, Fix/Perm was added and incubated at 37°C for 10 minutes followed by transfer on ice and wash with permeabilization buffer. After permeabilization, the samples were stained for 30 minutes with extracellular surface markers using a monoclonal antibody (mAb) staining mix including Fc-receptor blocking antibodies (anti-CD16/32; Bioceros). After wash, the samples were stained for one of each of the following phosphoflow targets; pZAP70, pSLP76, pITK180 and pS6. In case of the unlabeled anti-pS6 antibody, a third staining step containing a PE-labeled anti-Rabbit antibody was necessary. For pIkB a different staining protocol was used by which cells were fixed with paraformaldehyde incubated for 10 minutes at room temperature followed by permeabilization using 0.5% saponin in FACS. Cells were then stained with surface markers and anti-pIkB followed by acquisition for flow cytometry.

IL-2 stimulation and pSTAT5 phosphoflow

A total of $24x10^6$ splenocytes were divided over 12 wells of a 24-well plate and anti-CD3/CD28 Dynabeads (Thermofisher) were added in a 1:1 ratio for 72 hours in TCM to induce IL-2R expression as assessed by upregulation of CD25. Dynabeads were extracted by magnet retrieval and $2x10^6$ cells were incubated for 3 hours at 37°C with vehicle (same amount of DMSO as highest concentration of inhibitor as negative control) or Acalabrutinib (10µM, 1µM and 0.1µM in DMSO) or Ibrutinib (10µM, 1µM and 0.1µM in DMSO) or PF-06651600 (10µM, 1µM and 0.1µM in deionized water). After 3 hours, a 500.000/50µL cell suspension was activated for 15 minutes with 10ng/mL IL-2 (R&D Systems) at 37°C. Ten minutes before the re-stimulation end time, a live/death marker was added (eBioscience) followed by cell fixation using BD Cytofix and incubated for 10 minutes at 37°C. After the cells were fixed, the cells were washed with MACS buffer (PBS containing 5mM EDTA and 1% BSA) and permeabilized with 150µL permbuffer III (BD) and the cells were incubated for 30 minutes at -20°C. After 30 minutes the cells were washed with MACS buffer and stained with surface markers containing CD25, CD8, CD4, PD-1, CD44, B220 and CD3 and Fc-block for 30 minutes at 4°C followed by wash with MACS buffer and pSTAT5 staining for 30 minutes at room temperature.

Bone marrow derived macrophage cultures

Bone marrow cells were isolated from the femurs and tibias of naïve CBA/J (Janvier, Hannover, Germany), or C57BL/6 mice (Envigo, Zeist, The Netherlands) mice under sterile conditions. In short, all muscle tissues are removed with gauze from the bones and placed in a 60-mm dish with 70% alcohol for 1 minute, washed twice with PBS and transferred into a fresh dish with RPMI 1640. Bones were crushed using a pestle and mortar and subsequently passed through nylon mesh to remove small pieces of bone and debris followed by erythrocyte lysis using ammonium chloride. Bone marrow cells were resuspended in RPMI supplemented with 10% FCS, 2.5ml gentamicin (10mg/ml) (Gibco, Breda, the Netherlands), 50 μM β-mercaptoethanol (SigmaAldrich) and 10 ng/ml M-CSF (R&D systems, Oxon, UK) to establish macrophage-TCM. $2x10^5$ cells were plated per well in a 24-well Nunc plate with Upcell surface coating, allowing for harvest of cells at low temperatures following a 7-day culture period. Fresh TCM was added on day 3 of culture, and polarizing cytokines with or without a range drug concentrations on day 6 for the final 24-hour remainder of the culture period. M1 macrophages were generated by adding LPS (50ng/ml) and IFNγ (50ng/ml), or IL-4 (10ng/ml) with or without IL-10 (10ng/ml) or IL-13 (10ng/ml) in case of M2 macrophages. Besides the inhibition of JAK3 using the specific JAK3-inhibitor (PF06651600, Sigma Aldrich), cells were alternatively treated with trimeric CD40L (Immunex, 1μg/ml), with a JAK1/JAK3 dual inhibitor (Tofacitinib, Sigma-Aldrich) or associated diluents as negative controls. At the end of the culture, the plates were put on ice and cell suspensions were harvested and prepared for flow cytometry analysis.

Monocyte derived macrophage cultures

Venous blood from adult healthy individuals was collected in EDTA tubes and peripheral blood mononuclear cells (PBMCs) were isolated using a Ficoll-Hypaque gradient according to standard protocol (Axis-Shield Diagnostics, Dundee, UK). Written informed consent was obtained from the donors and studies were conducted in agreement with the Declaration of Helsinki, according to the ICH Harmonized Tripartite Guideline on Good Clinical Practice and in accordance with recognized ethical guidelines approved by our local institutional review board. Monocytes were extracted with magnetic-activated cell sorting (MACS) using anti-CD14 antibody coated microbeads (Milteny Biotec) according to the manufacturer's protocol. Following the MACS-procedure, cells were stained for flow cytometry to guarantee sufficient purity (>98%). Monocytes were then suspended in TCM consisting of RPMI 1640 + Glutamax, 10% normal healthy AB serum and human macrophage colony-stimulating factor (20ng/mL, R&D Systems). Cells were cultured similarly to murine macrophages, with the exception of being an 8-day culture with macrophage polarization occurring in the final 48 hours of culture. Polarization to the M1 or M2 phenotype occurred in the presence of LPS (100ng/mL, Sigma-Aldrich) and IFNγ (20ng/mL, R&D Systems) for M1 or IL-4 (20ng/mL, R&D Systems) with or without IL-13 (20 ng/mL, R&D Systems) for M2 for 2 days.

Bone marrow derived DC- OT-I and tumor-cell co-culture

Bone marrow derived dendritic cells (BMDC) were cultured from n = 3 wild-type C57BL/6 donor mice (female, 8 weeks) similarly to BMDMs but GM-CSF instead of M-CSF was used as a growth factor for 9 days of culture in normal tissue-culture coated 6-well plates (Sarstedt), followed by 24 hours of simulation with OVA-protein (150µg/ml) and CpG in the presence of JAK3i (PF06651600, Sigma Aldrich) as reported previously and analyzed using flow cytometry [21]. Next, OT-I cells were sorted from spleens and lymph nodes of female OT-I mice bred in house using a $CD3^+$ negative selection kit (EasySep; StemCell) followed by cell labeling using CellTrace Far Red proliferation dye (Invitrogen) according to manufacturer protocols. Labeling efficacy and OT-I purity were checked using flow cytometry before co-culture. A total of $5.0x10^3$ non-JAK3i pre-treated SIINFEKL-peptide (500ng/ml) loaded BMDCs were co-cultured with $2.5x10^4$ naïve labeled and purified OT-I T cells in 96-well flat-bottom plates using T cell medium (IMDM supplemented with 10% FBS, β-mercapto-ethanol and gentamicin) and JAK3i in a 1:5 (DC-T-cell) ratio for 72 hours and harvested or for subsequent co-culture with AE17-OVA tumor cells for 24 hours (ratio: 1:1) followed by for flow cytometry analysis.

Human T cell cultures

PBMCs from healthy donors were labelled with CellTrace Violet (ThermoFisher Scientific) and were stimulated with anti-CD3/CD28 Dynabeads at 0.5 bead per mononuclear cell with or without recombinant human IL-2 (1, 10 or 100 IU/ml, R&D Systems) for the indicated time-points. In some conditions, Tofacitinib (200µM or 1000µM) or PF-06651600 (200µM or 1000µM) was added to the culture. Cells were cultured in IMDM (ThermoFisher Scientific) supplemented with heat inactivated FCS, Glutamax (ThermoFisher Scientific), 2-mercaptoethanol, penicillin and streptomycin. Cytokine concentrations in cell supernatants were analyzed using an ELISA set for IFNγ (eBioscience) according to the manufacturer's instructions. In case of murine T cell cultures, proliferation-dye pre-stained wild-type C57BL/6 T cells were stimulated with anti-CD3/CD28 Dynabeads at 1:1 ratio with various concentrations of PF06651600 (negative control=H_2O) or Tofacitinib (negative control=DMSO) and assessed for proliferation, activation (CD69, CD25) and cytokine (TNFα, IFNγ) production 24 hours later using (intracellular) flow cytometry.

***In vivo* murine tumor models and experiments**

Female 8- to 10-week-old C57BL/6 mice (Envigo, Zeist, The Netherlands) and CBA/J mice (Janvier, Hannover, Germany) were housed under specific pathogen-free conditions at the animal care facility of the Erasmus MC, Rotterdam. Experiments were approved by the local and central Ethical Committee for Animal Welfare and complied to the Guidelines for the Welfare of Animals in Experimental Neoplasia by the United Kingdom Coordinating Committee on Cancer Research (UKCCCR) and by the Code of Practice of the Dutch Veterinarian Inspection. The AE17 cell and AC29 mesothelioma cell lines were kindly provided by Bruce W.S. Robinson of the Queen Elizabeth II Medical Centre, Nedlands, Australia who previously authenticated these cells as being mesothelioma cells. At every 8–10 passages, cell lines were tested for mycoplasma contamination by PCR and remained negative. Tumor

cells were cultured in RPMI 1640 medium containing 25mM HEPES, Glutamax, 50g/ml gentamicin, and 5% FBS (all obtained from Gibco) in a humidified atmosphere and at 5% CO2, in air. For culture, either culture flasks or CellSTACKs (Corning Life Sciences) were used to reach appropriate tumor cell frequencies for injection. AE17 and AC29 cells were passaged once or twice a week to a new flask by treatment with 0.05% trypsin, 0.53n mmol/L EDTA in PBS (all Gibco). At the start of the experiment, CBA/J or C57BL/6 mice were intraperitoneally or subcutaneously injected with either 10^7 AC29 cells or $0.5x10^6$ AE17 cells, respectively, dissolved in PBS, or with PBS as control. Mice were scored using the body condition score, killed when body condition score was below 2 and scored as a death in the survival analysis. For DC therapy experiments, BMDC were generated from wildtype CBA/J mice and loaded with AC29 tumor cell lysate *in vitro* as described previously[22]. On day 10 following i.p. tumor inoculation, $2\text{-}3x10^6$ DCs pre-loaded with AC29 tumor lysate and stimulated with CpGwere injected i.p [21]. For SLP-vaccination studies in the TC-1 tumor model, TC-1 cells were cultured in 500 ml IMDM medium, 8% FBS (40 ml) and pen/strep plus L-glutamin and following cell harvest were injected in the flank of wildtype C57BL/6 mice. When tumors were established on day 8, mice received subcutaneous PBS or the SLP HPV16 E743–77 (GQAEPDRAHYNIVTFCCKCDSTLRLCVQSTHVDIR) emulsified at a 1:1 ratio with Incomplete Freunds Adjuvant (IFA; Difco) in the contralateral flank. In case of subcutaneous tumor models, tumors were measured twice weekly using an electronic micro-caliper and mice were euthanized when tumors grew beyond $100mm^2$ or became ulcerated.

***In vivo* treatment with PF-06651600**

Mice were treated with a range of PF-06651600 concentrations dissolved in pre-warmed deionized water (Milli-Q) with all tested concentrations ranging within the solubility spectrum (5mg/ml). Mice were treated with the JAK3-inhibitor or the diluent (deionized water) via oral gavage, twice daily with intervals of 12 hours, as reported by the manufacturer for a maximum of 14 days. Alternatively, PF-06651600 was administered in drinking water ad libitum, assuming that 8-week-old female mice with an average weight of 20 g drink approximately 5 ml of water per 24 hours (meaning that for the 5 mg/kg dose in drinking water, 10 mg of PF-06651600 was dissolved in 1 L of deionized water, amounting to a ~25µM). Drinking water was refreshed every week and bottles were covered with aluminum foil.

Preparation of Single Cell Suspensions from Tissues

Single cell suspensions were generated from the spleens, blood and tumors of mice from each group. All tissues were either weighed in a microbalance in case of tumors and spleens, or volume determined for blood. Briefly, spleens were aseptically removed and mechanically dispersed over a 100-µm nylon mesh cell strainer (BD Biosciences) followed by erythrocyte lysis using osmotic lysis buffer (8.3% NH4Cl, 1% KHCO3, and 0.04% Na2EDTA in deionized water). Blood was collected in EDTA tubes (Microvette CB300, Sarstedt) and subsequently lysed. Tumors were collected, and dissociated using a validated tumor dissociation system (Miltenyi Biotec). Cells suspensions were filtered through a 100-µm nylon mesh cell strainer (BD Biosciences) and counted in trypane blue with a hemocytometer using the Burker-Turk method.

Immunomonitoring using Flow Cytometry

For measurements of cytokine production in lymphoid cells by flow cytometry, cells were restimulated for 4 hours at 37°C using PMA and ionomycin supplemented with GolgiStop (BD Biosciences). For assessing cytokine production by myeloid cells, cells were subjected to 4 hours incubation with Golgistop. For cell surface marker staining, cells were washed with FACS-wash (0.05% NaN3, 2% BSA in PBS) and Fc II/III receptor blocking was performed using anti-mouse 2.4G2 antibody (1 : 200; kindly provided by L. Boon, Bioceros, Utrecht, The Netherlands). After the blocking procedure, antibodies (all derived from BD Biosciences, Biolegend or Thermofisher Scientific, titrated to optimal dilutions and used according to the manufacturer's protocol) for cell surface staining were added into each sample and placed on ice for 30 minutes. Cells were washed in FACS-wash followed by a PBS wash, and then stained for viability using fixable LIVE/DEAD aqua cell stain (Thermo-Fisher Scientific, 1:200). After two additional washes with FACS-wash, cells were either measured or in case of intracellular staining; fixed, permeabilized and stained using Fix/Perm buffer (in case of nuclear protein staining, eBioscience) or 4% PFA and 0.5% saponin (in case of cytokine/granzyme-B stainings, Sigma-Aldrich). Antibodies were stained for 30 minutes in case of the PFA/Saponin protocol and 60 minutes for the intranuclear staining protocol, on ice in the dark. A fixed number of counting beads (Polysciences Inc.) was added before data acquisition to determine the absolute amount of cells. Data were acquired using an LSR II flow cytometer (BD) equipped with three lasers and FACSDiva software (BD) and analyzed by FlowJo (Tree Star Inc., USA) software V10.1.

Tumor cell apoptosis assay

A total of $0.2x10^6$ cells from various murine and human cancer-derived cell lines were cultured in aforementioned appropriate culture conditions in 6-wells plates for 48 hours in the presence of absence of different JAK3i (PF-06651600) concentrations. Following culture, cells were harvested and stained for cell death and apoptosis using the 7-AAD/Annexin V staining kit, according to the manufacturer's protocol (Biolegend).

Statistical Analysis

Data are expressed as means with SEM. Comparisons between groups were made using one-way ANOVA tests where experimental treatment groups were compared with vehicle, or the Wilcoxon signed rank test in case of paired samples. When correlations were depicted, Spearman's rank correlation test was performed to test for statistical significance. A two-tailed value of $p < 0.05$ was considered statistically significant. Survival data were plotted as Kaplan-Meier survival curves, using the log-rank test to determine statistical significance. Data was analyzed using Graphpad Prism software (Graphpad, V5.01).

Results

PF-06 is a potent inhibitor of IL-2 mediated STAT5-phosphorylation in T cells

Chronic phosphorylation of STAT5 by JAK1/3 in T cells has been recently found to underlie ineffective anti-tumor immunity providing a rational for JAK3i in solid tumors [12]. Because JAKs are involved in many pro- and anti-tumor cytokine receptor pathways, off-target specificity of early generation JAK3i could potentially antagonize beneficial outcomes of JAK3-specific inhibition at the expense of increased toxicity [18]. To evaluate whether the novel compound PF-06 specifically inhibits STAT5-phosphorylation and to which degree, wildtype naive and pre-activated $CD25^+$ murine T cells were simulated *in vitro* using anti-CD3/CD28 or IL-2, respectively, and analyzed using Phosphoflow [23]. The broad kinase inhibitor Ibrutinib was applied as a positive control since kinomescan data identified multiple kinases, including JAK3 as targets [24]. The selective BTK-inhibitor Acalabrutinib was used as a negative control in our studies as BTK is not expressed by T cells [24,25]. Only PF-06 specifically inhibited IL-2-mediated pSTAT5 in both $CD8^+$ and $CD4^+$ T cells (Fig. 1) while leaving other quintessential T cell signaling pathways (e.g. downstream TCR and NF-κB unaltered (Fig. 2, S1). As CD25 expression among $CD25^+$ T cells varied, we compared pSTAT5 levels at baseline and in response to JAK3i in CD25-high, intermediate and low-expressing T cells. CD25-high expressing cells displayed increased STAT5-phosphorylation at baseline but also in response to low-dose JAK3i *in vitro* suggesting increased sensitivity to IL-2 in CD25-high expressing cells (Fig. S2A). Regulatory T cells (Tregs) constitutively express CD25 as a means to scavenge IL-2 thereby inhibiting effector T cell proliferation [26]. To investigate how Tregs respond to IL-2 and JAK3i, we assessed pSTAT5-phosphorylation status in $CD44^+$ $CD25^{hi}$ $CD4^+$ T cells, a population enriched for Tregs in the naïve spleen (Fig. S2B). As expected, pSTAT5-expression was nearly twice as high in Tregs compared with non-Tregs, with pSTAT5 being completely inhibited only at higher micromolar levels of PF-06 *in vitro* (Fig. S2B). We concluded that the specific JAK3i PF-06 efficiently prevented STAT5 phosphorylation in mouse T cells in a low micromolar range.

PF-06 inhibits T cell proliferation and effector function at high concentrations *in vitro*

To investigate how decreased IL-2-mediated STAT5-phosphorylation translates to T cell proliferation over time, we stimulated dye-labeled T cells *in vitro* using anti-CD3/CD28 Dynabeads alone or in the context of JAK3i. Head-to-head comparison between PF-06 and the less specific JAK1/3i Tofacitinib showed both drugs to inhibit T cell proliferation, activation and effector cytokine production but only at high (>1.0 μM) drug concentrations in mouse (Fig. S3) and human (Fig. S4A-C) T cells. Interestingly, whereas Tofacitinib more potently inhibited T cell proliferation and cytokine expression in humans compared with PF-06, the opposite was true for mice (Fig. S3-4). In contrast to Tofacitinib, however, PF-06 only modestly inhibited cellular activation and IFNy production in healthy-control derived T cells at the micromolar range (Fig. S4C). These findings show PF-06 to be a potent inhibitor of IL-2-mediated pSTAT5 in T cells, with T cell functions being inhibited only at higher drug concentrations providing a window for STAT5 modulation.

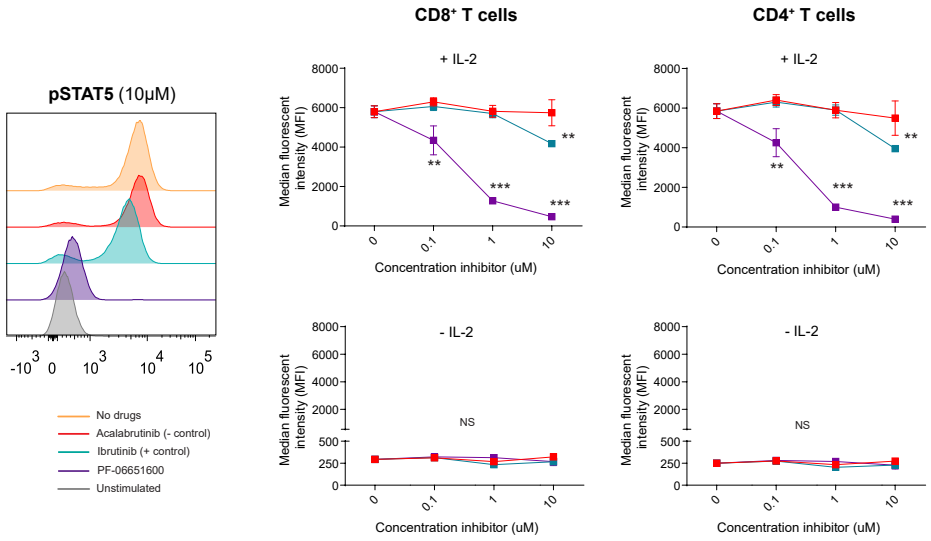

Figure 1: The JAK3-inhibitor PF-06651600 potently inhibits STAT5-phosphorylation in response to IL-2 in T cells

(A) Pre-activated IL-2Rα (CD25) expressing murine T cells were stimulated with IL-2 after pre-incubation alone (orange), with the specific JAK3i; PF-06651600 (purple), aspecific JAK3i; Ibrutinib (turquoise) or negative control; Acalabrutinib (red) using Phosphoflow. Histograms are shown displaying the effects of the different inhibitors on pSTAT5-expression at 10μM (left panel, $CD8^+$) and quantified expression of pSTAT5 in $CD8^+$ and $CD4^+$ T cells stimulated or unstimulated with IL-2 (right panels). MFI = median fluorescence intensity, * = $p < 0.05$, ** = $p < 0.01$, *** = $p < 0.001$. Means and SEM are shown, n = 5 per condition.

JAK3i decreases tumor progression depending on the dose and mode of administration

To assess the effects of PF-06 *in vivo* and its anti-tumor efficacy, we treated AE17 and AC29 immune competent mesothelioma tumor-bearing mice with PF-06 administered by oral gavage twice-daily as described by others [19]. Using this treatment scheme, tumor progression was unaltered in these tumor models compared with vehicle treatment (Fig. 3A). The lack of response was accompanied by a reduction in T cell proliferation monitored in peripheral blood (PB), and decreased activation, proliferation and effector function at the tumor site (Fig. 3B), indicative of suppressed anti-tumor immunity. We postulated that peak PF-06 concentrations following oral administration would approach immune suppressive drug concentrations reminiscent of aforementioned *in vitro* studies (Fig. S3), and that low-grade and stable dosing of JAK3i in drinking water would ameliorate this issue. Therefore, we repeated the *in vivo* experiment dissolving PF-06 in drinking water aiming for tonic inhibition of the IL-2R/JAK3/STAT5-axis throughout the anti-tumor immune response. In contrast with oral gavage, continuous low-dose JAK3i suppressed tumor growth with approximately 25 μmol/L being established as the optimal dose (Fig. 4A). Changes in tumor burden were paralleled by increased T cell frequencies and a more activated and proliferative T cell compartment as evidenced by increased Ki67

and PD-1 expression (Fig. 4B, Fig. S5). B and NK cells on the other hand were not, or only marginally affected by JAK3i treatment (Fig. S5). These data show that JAK3i, if provided as a steady continuous administration, impedes tumor progression coinciding with increased T cell activation. In contrast to *in vitro*, macrophage polarization is not altered by JAK3i *in vivo*

As JAK3 associates with cytokine receptors on other immune cells, treatment efficacy could potentially be explained by inhibition of alternative pathways, including IL-4/IL-4R signaling. Indeed, BMDMs stimulated *in vitro* with IL-4 upregulated the M2 markers CD206, arginase and PD-L1 that could be antagonized by JAK3i (Fig. S6A). This effect could not be rescued by addition of excess IL-13, another M2-inducing cytokine sharing the IL-4R-alpha subunit, or IL-10 (Fig. S6B) [27,28]. In contrast with the JAK1/3i Tofacitinib, PF-06 did not alter pro-inflammatory (M1) macrophage differentiation as evaluated by iNOS and MHCII expression (Fig. S6C). Similar findings were obtained using human monocyte-derived macrophages (MoDM) (Fig. S7). Tumor-associated macrophage and conventional DC frequency and phenotype, however, were largely unaltered by JAK3i in all our investigated models, indicating that IL-4 plays an inferior or redundant role in *in vivo* myeloid cell polarization (Fig. S6D-E). On the same line, JAK3i did not directly affect solid tumor-cell apoptosis *in vitro* (Fig. S8A) or *in vivo* (Fig. S8B), except in case of the JAK3-mutated T cell lymphoma cell line Hu-78 (Fig. S8A). We concluded that T cells are the most likely direct targets of JAK3i.

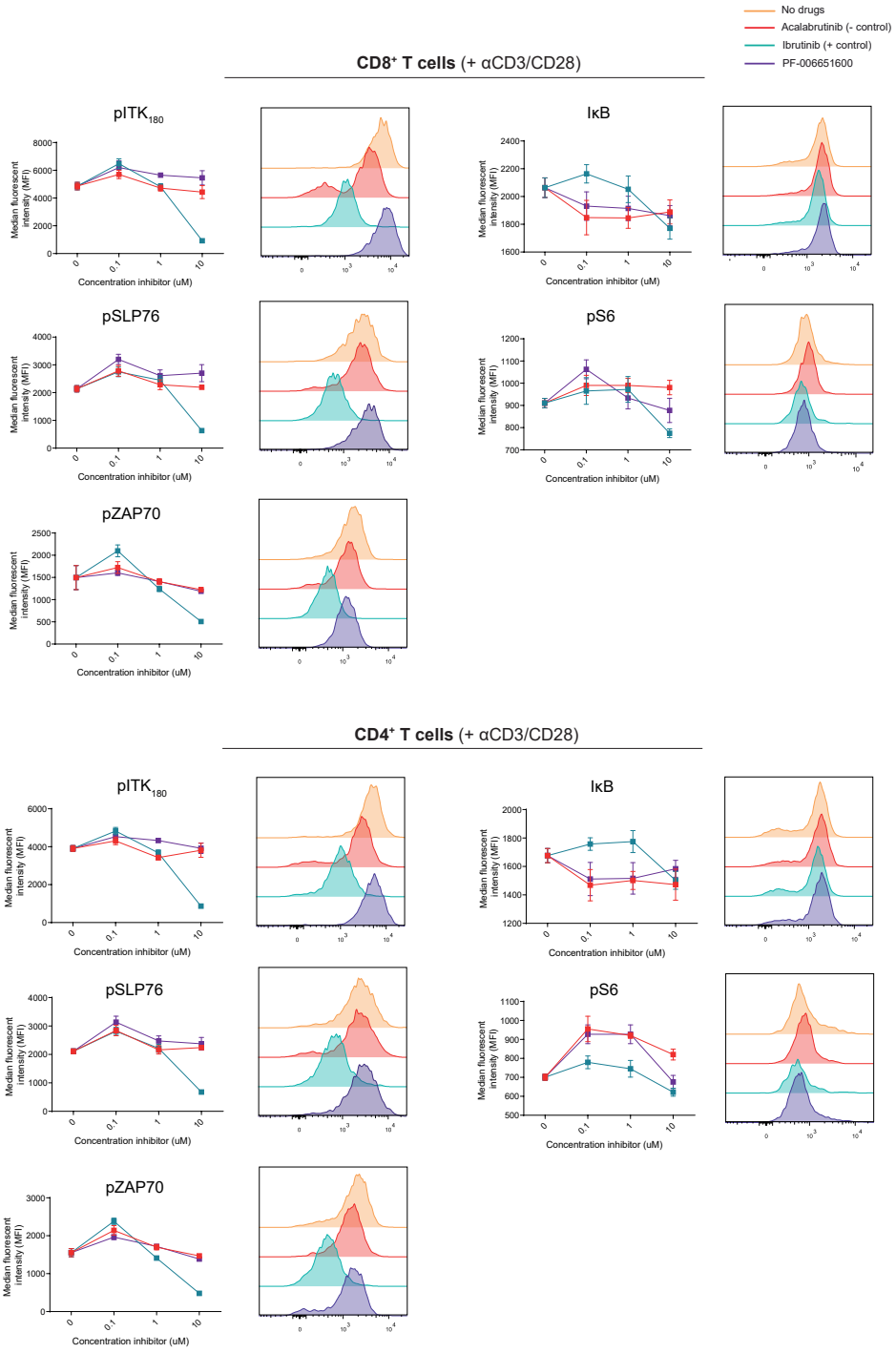
No drugs
Acalabrutinib (- control)
Ibrutinib (+ control)
PF-006651600
CD8+ T cells (+ αCD3/CD28)
pITK180
IκB
pSLP76
pS6
pZAP70
CD4+ T cells (+ αCD3/CD28)
pITK180
IκB
pSLP76
pS6
pZAP70
Median fluorescent intensity (MFI)
Concentration inhibitor (uM)

◂Figure 2: PF-06651600 does not inhibit other T cell signaling pathways

In order to determine off-target efficacy of PF-06 on other crucial T cell signaling pathways we assessed phosphorylation of proteins downstream of the T cell receptor (TCR) (pZAP70, pSLP76, pITK180), PI3K-Akt (pS6), NF- kB (IKB) or MAPK-ERK (pERK) pathways following anti-CD3/CD28 stimulation with or without inhibitors using Phosphoflow. Results for both $CD8^+$ (upper panels) and $CD4^+$ T cells (lower panels) are shown as histograms (10μM drug concentration) and line graphs. MFI = median fluorescence intensity, means and SEM are shown, n = 5 per condition.

Although JAK3i as monotherapy is capable of inhibiting tumor progression, combining JAK3i with existing immunotherapies could further enhance efficacy of both modalities. Cellular and peptide cancer vaccines are safe and efficacious in inducing anti-tumor T cell responses in solid advanced cancer, but durable responses are obtained in a small minority of patients possibly due to the eventual exhaustion of vaccine-elicited T cell responses [21,29-33]. To improve vaccine-induced T cells and treatment efficacy, we treated AC29-bearing mice, at late stage, with tumor-lysate loaded BMDCs in the presence or absence of JAK3i (Fig. 5A). We found JAK3i-DC-combination immunotherapy to effectively reduce tumor load compared with both monotherapies alone (Fig. 5B). Similarly, we combined JAK3i with a SLP vaccine in the aggressive TC-1 solid tumor model showing similar combination immunotherapy efficacy, improving response rates, and reducing heterogeneity in tumor responses observed (Fig. 5C-E). Further investigations into the immunological mechanisms underlying combination immunotherapy efficacy in end-stage tumors revealed JAK3i to spare $CD8^+$ T cell proliferation and boost TIL activation as indicated by increased CD25 and PD-1- but not CTLA-4 expression (Fig. 6A). In line with an activated rather than exhausted TIL phenotype was a specific increase in single PD-1-expressing TILs ($PD\text{-}1^+$ $CTLA\text{-}4^-$) rather than inhibitory receptor double-positive TILs known to be exhausted [34,35]. Recently, the surface molecule CD39 was reported to mark activated, (pre-)exhausted and tumor-specific $CD8^+$ and $CD4^+$ T cells in the TME and this marker was significantly upregulated in combination immunotherapy-treated TILs compared with TILs derived from untreated- or JAK3i-only treated mice [36,37]. Besides surface molecules, combination immunotherapy-treated TILs displayed highest levels of IFNγ and granzyme-B (Fig. 6A). These findings were not limited to $CD8^+$ T cells, as $CD4^+$ T-helper cells were similarly altered in the TME (Fig. 6B). These findings provide a preclinical rationale for JAK3i-combination immunotherapy and inclusion of anti-PD-1 ICI to further increase anti-tumor responses.

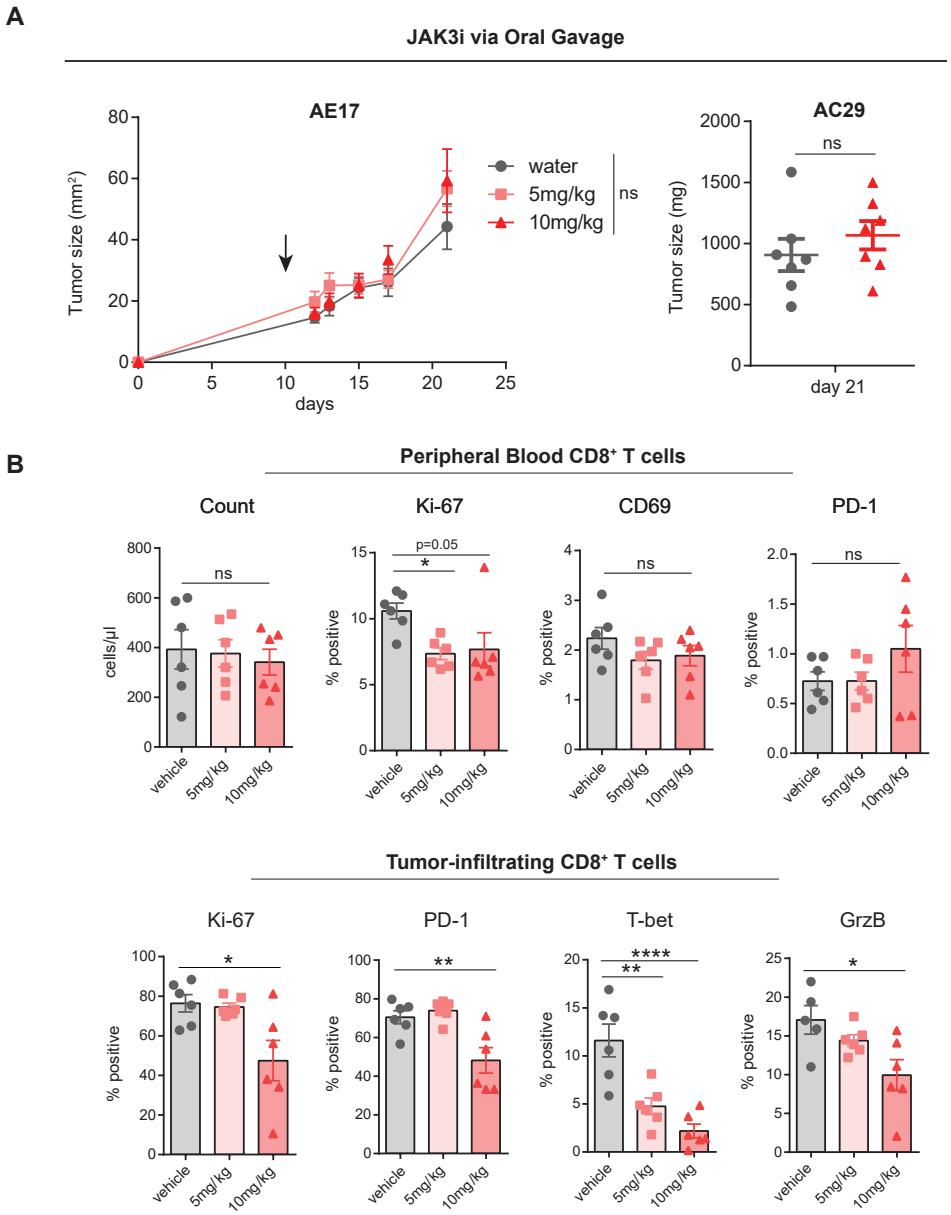

Figure 3: Twice-daily high-dose JAK3i via oral gavage does not impact tumor growth and inhibits T cell immunity

(A) AE17 subcutaneous and AC29 intraperitoneal tumor-bearing mice were treated with the JAK3i; PF-06651600 via twice-daily oral gavage starting on day 10 and tumor burden was assessed on day 21. (B) CD8⁺ T cells in peripheral blood on day 15 or in the tumor at end-stage (C) were assessed for proliferation (Ki67) and activation status using multicolor flow cytometry. Means and SEM are shown with n = 6 mice per condition. JAK3i = JAK3-inhibitor, Ns = non-significant, * = $p < 0.05$, ** = $p < 0.01$, GrzB = granzyme-B.

A

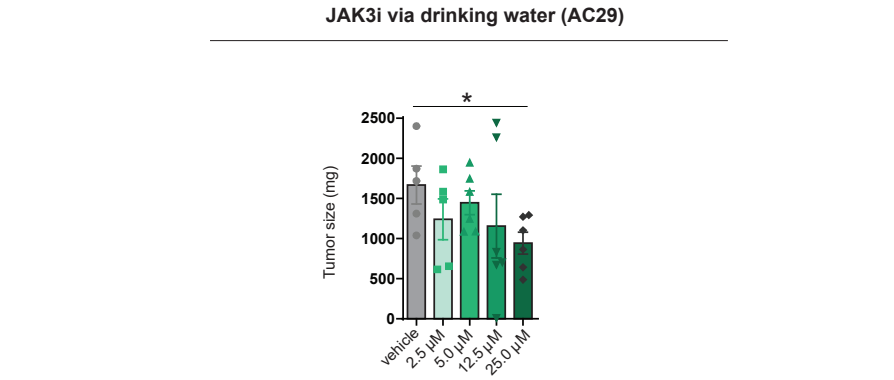
JAK3i via drinking water (AC29)
Tumor size (mg)
2500
2000
1500
1000
500
0
*
vehicle
2.5 µM
5.0 µM
12.5 µM
25.0 µM

B

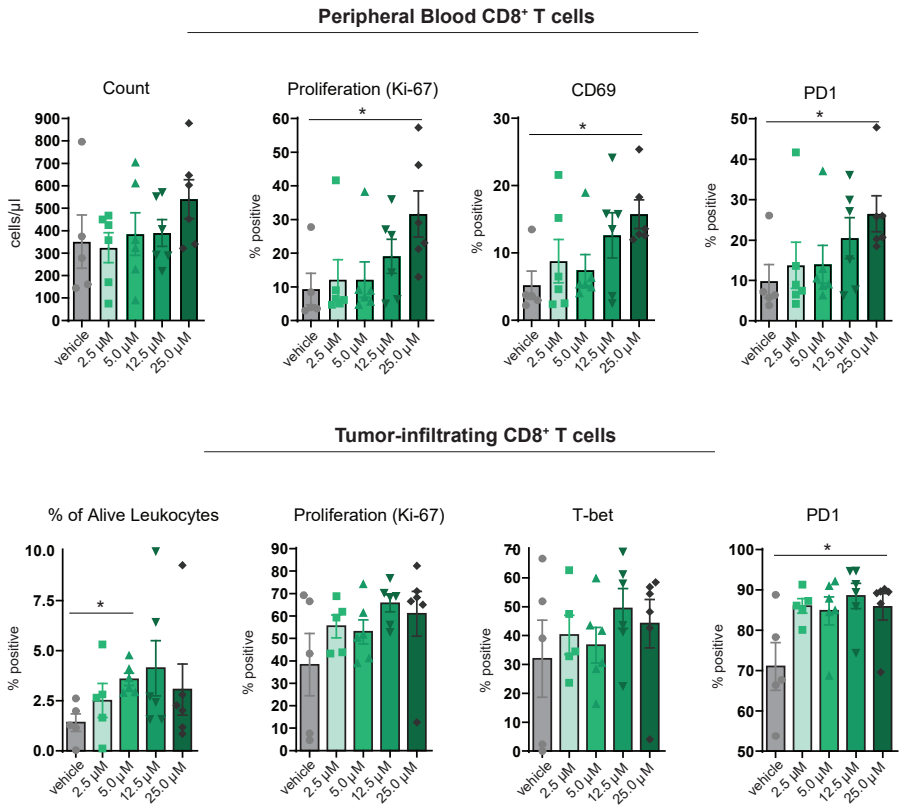
Peripheral Blood CD8⁺ T cells
Count
cells/µl
Proliferation (Ki-67)
% positive
CD69
% positive
PD1
% positive
Tumor-infiltrating CD8⁺ T cells
% of Alive Leukocytes
% positive
Proliferation (Ki-67)
% positive
T-bet
% positive
PD1
% positive
vehicle
2.5 µM
5.0 µM
12.5 µM
25.0 µM

◂Figure 4: Continuous low-dose JAK3i at 5.0mg/kg significantly decreases tumor weight in AC29-bearing mice and improves anti-tumor T cell immunity

(A) AC29 intraperitoneal tumor-bearing mice were treated with the JAK3i; PF-06651600 dissolved in drinking water at various pre-specified doses and tumor weight was monitored. (B) $CD8^+$ T cells in peripheral blood on day 15 or in the tumor at the end of the experiment (day 20) were assessed for proliferation (Ki67) and activation status using multicolor flow cytometry. Means and SEM are shown with n = 6 mice per condition. JAK3i = JAK3-inhibitor, ns = non-significant, * = $p < 0.05$.

JAK3i modulates DC-mediated T cell priming resulting in decreased sensitivity to exhaustion

We previously observed that continuous low-dose JAK3i as monotherapy, or in combination with vaccines, increased T cell proliferation early after treatment. This suggests that T cell priming could be modulated by fine-tuning JAK3-activity. To investigate this, we first assessed whether JAK3i directly affected DC-phenotype *in vitro* by treating GM-CSF cultured BMDCs with increasing concentrations of JAK3i during activation with the TLR9-ligand CpG (Fig. 7A). We found that DC-viability, co-stimulatory- and homing (CCR) receptor expression were unaltered by JAK3i and MHC class I and II expression was only marginally increased at high concentrations, similar to macrophages (Fig. S9, S6-7). Next, OVA-peptide loaded DCs were co-cultured with sorted naïve OT-I T cells in the presence or absence of JAK3i and T cell proliferation and phenotype were assessed. Even at the highest concentration, we found that JAK3i did not impair T cell expansion or activation capacity (determined by proliferation dye dilution and CD44, PD-1-expression, respectively). However, activated-induced apoptosis and exhaustion (as measured by TOX and CD39 expression) were decreased, suggesting sustainable T cell activation (Fig. 7B). CD25 expression was dose-dependently decreased by JAK3i confirming the role of IL2R-JAK3-STAT5 signaling in amplifying CD25 and thus high-affinity IL2R-expression[38]. Furthermore, 0.1 µmol/L JAK3i cultured T cells demonstrated increased AE17-OVA killing capacity *in vitro*, albeit not statistically significant, whereas at higher concentrations effector function decreased (Fig. 7C). The improved T cell phenotype observed during priming persisted during the effector phase of the immune response (Fig. S9B). These findings indicate that fine-tuning JAK3-activity during priming yields a superior T cell phenotype that could underlie improved anti-tumor efficacy *in vivo*.

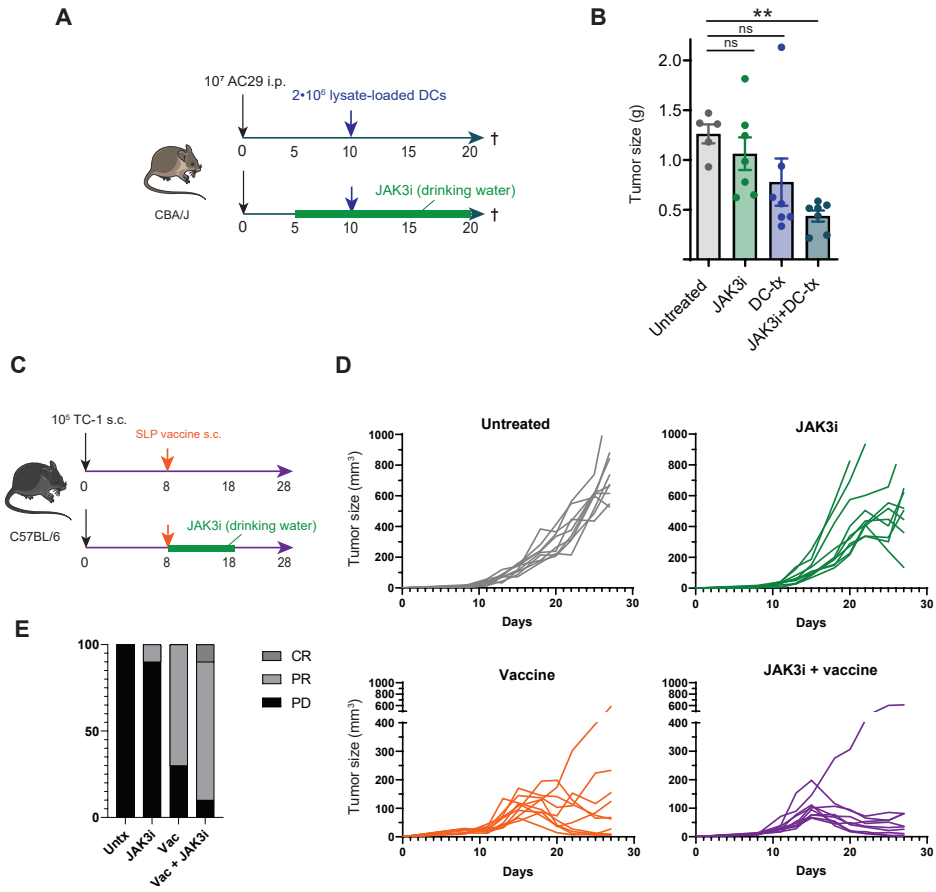

Figure 5: JAK3i increases cellular and peptide vaccine efficacy

(A-B) intraperitoneal (i.p.) AC29 and subcutaneous (s.c.) TC-1 bearing mice (C) were treated with dendritic cell (DC) therapy or a synthetic-long peptide (SLP) vaccine, respectively, alone or in combination with JAK3i (PF-06651600) at indicated time points. Tumor weight was monitored at end-stage in case of AC29 tumors, and individual tumor-size was monitored 3/week in case of TC-1 (D). (E) tumor responses were graded as complete response (CR) defined as a complete eradication of tumor (being non-palpable), partial response (PR) being >30% decrease in tumor volume compared with maximum initial tumor size and progressive disease less than 30% regression and eventual tumor progression. Means and SEM are shown with n = 6 to 10 mice per condition. JAK3i = JAK3-inhibitor, Vac = SLP-vaccine, ns = non-significant, * = $p < 0.05$, ** = $p < 0.01$

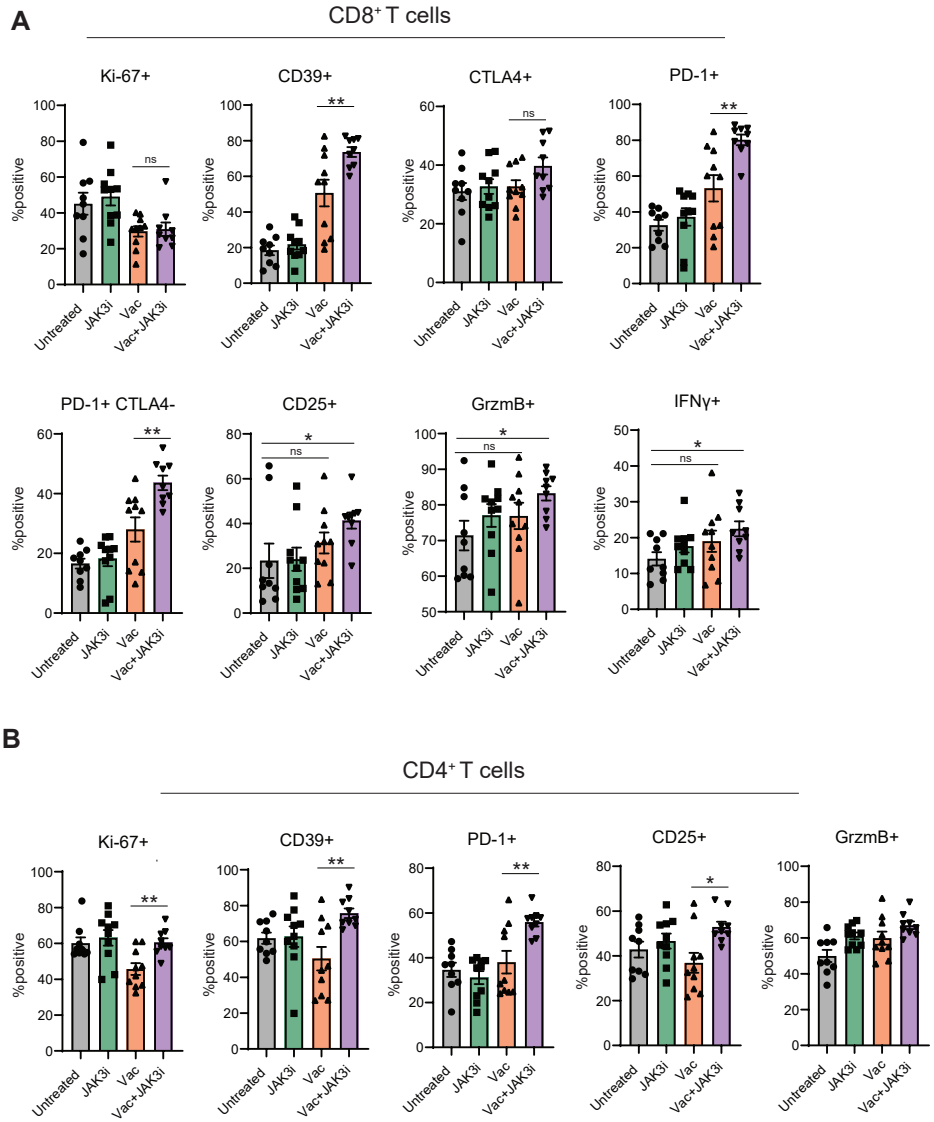

Figure 6: JAK3i improves peptide-vaccine induced CD8⁺ and CD4⁺ T cell immunity in the tumor microenvironment

CD8⁺ (A) and CD4⁺ T-helper cell (B) proliferation (Ki67), and surface expression of co-inhibitory checkpoints or activation markers was assessed in end-stage tumors of the experiment described in Fig. 4C. Means and SEM are shown with n = 9 to 10 mice per condition. JAK3i = JAK3-inhibitor, Vac = SLP-vaccine, GrzmB = granzyme-B, IFNγ = interferon-gamma, ns = non-significant, * = p< 0.05, ** = p < 0.01, *** = p < 0.001, **** = p <0.0001.

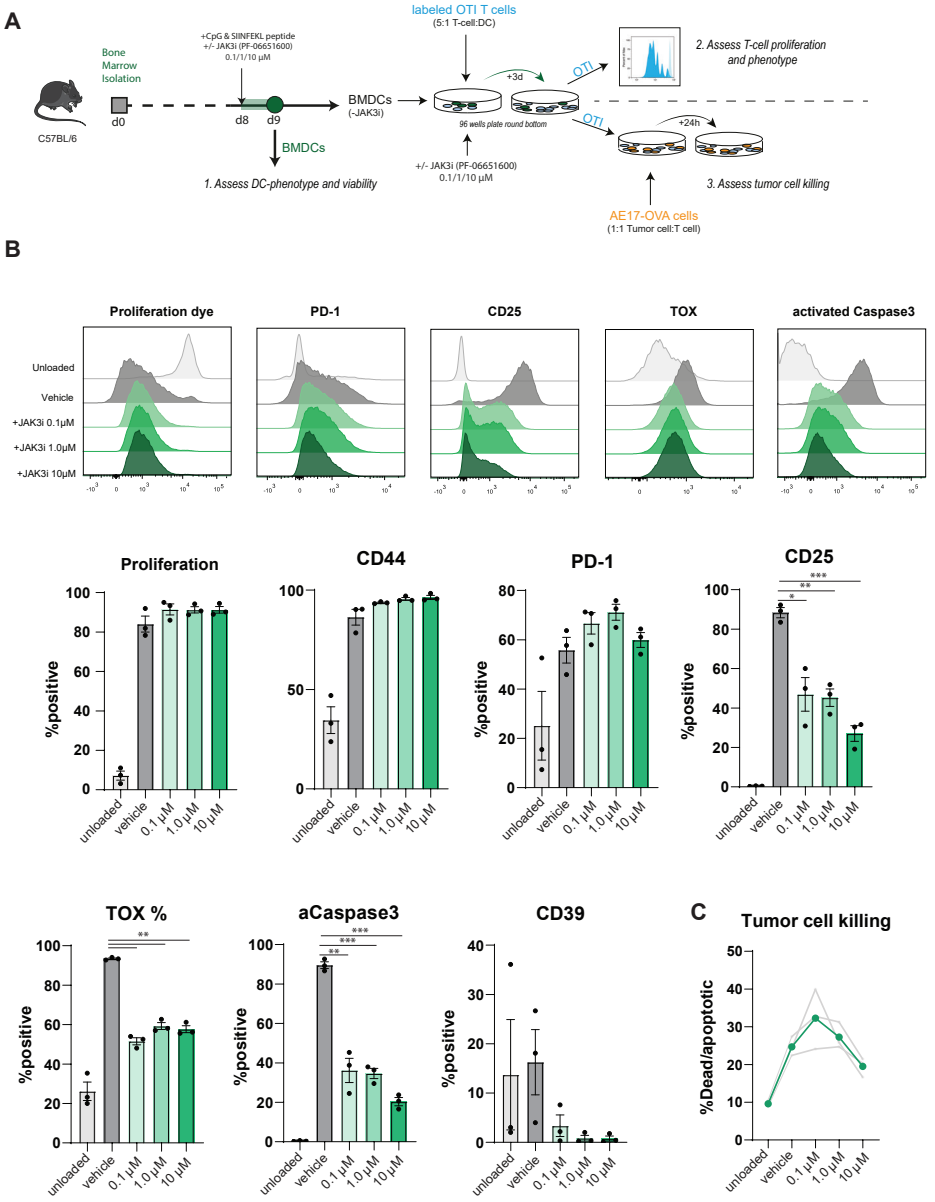

Figure 7: JAK3i does not impede expansion following DC-mediated priming but rather limits T cell exhaustion and apoptosis *in vitro*

(A) Experimental setup of the *in vitro* OT-I T cell-DC/tumor-cell co-culture system (B), Histograms showing T cell phenotype after 72 hours of co-culture with OVA-peptide loaded DCs in the presence of increasing concentrations of JAK3i ((PF-06651600). (C) Primed JAK3i-cultured OT-I cells were mixed with AE17-OVA tumor cells for 24 hours and tumor killing (dead + apoptotic tumor cells) was assessed. Ns = non-significant, * = $p < 0.05$, ** = $p < 0.01$, *** = $p < 0.001$, **** = $p < 0.0001$.

Discussion

In this study, we found low-dose JAK3i to decrease pSTAT5 expression while preserving T cell proliferation *in vitro* and to improve T cell phenotype and tumor load in solid tumor models as monotherapy, and in combination with cellular and peptide-vaccine approaches. JAK3i-cancer vaccine combination immunotherapy could be a particularly potent anti-cancer strategy with cellular and peptide vaccines inducing novel polyfunctional T cell clones that are preserved and further boosted by JAK3i. This approach differs from current treatments primarily aimed at amplifying existing and often dysfunctional anti-tumor T cell responses that are only short-term effective in a proportion of patients with cancer [1,39]. Of note, in a recently described screening assay for T cell exhaustion reversing compounds, two JAK3i were identified to effectively counter T cell exhaustion *in vitro* similar to our findings, further solidifying a role for JAK3 in mediating T cell dysfunction [4]. Whether *in vivo* anti-tumor efficacy of JAK3i is driven solely by effects of JAK3i on T cells or whether other immune cells are involved remains to be further investigated.

With the discovery of more specific JAK3i (e.g. PF-06 and decernotinib [40]), JAK3 can be specifically targeted limiting unwanted action and toxicity as described for more broad kinase inhibitors such as Tofacitinib and Ibrutinib [18,41,42]. Specific, small molecule inhibitors hold significant advantages compared with antibody-mediated therapies including route of administration (oral vs. i.v.), lack of anti-drug antibody formation and the possibility of timely and graded target inhibition which may be key in case of pleiotropic targets such as the IL-2R [43]. IL-2-IL-2R interaction may be essential or deleterious for T cell effector function and pool size, depending on the strength, duration and moment of interaction in the anti-tumor immune response [12,16]. Especially in the setting of vaccination, too early or strong blockade of IL-2R signaling following T cell priming could suppress proper T cell expansion thereby limiting therapy efficacy. Although we did not assess early T cell expansion in PB of mice following DC- or SLP-vaccination, the effects of JAK3i monotherapy in PB and the effects on tumor progression indicate that graded JAK3i improves, rather than hampers T cell activity. Further exploration of JAK3i timing and dosing could further inform about optimal treatment conditions in solid tumor treatment.

Recently, Liu and colleagues demonstrated that chronic IL-2-mediated JAK1/3-pSTAT5 signaling in the TME-induced T cell exhaustion via generation of tryptophan metabolites triggering the aryl hydrocarbon receptor (AhR) in T cells [12]. As the authors did not therapeutically target this pathway *in vivo*, our findings with JAK3i complement their findings as JAK3i using PF-06 potently and specifically inhibited STAT5-phosphorylation in T cells and improved T cell phenotype *in vivo*. Interestingly, Liu and colleagues found that an IL-2^{hi} gene signature in multiple solid cancer types but also AML was associated with poor patient survival, indicating that IL-2R targeting compounds may act on a wide variety of tumor types, including solid- and non-solid cancer types [12]. Whether our JAK3i acts by limiting pSTAT5 mediated tryptophan metabolism and subsequent AhR-stimulation remains

to be investigated. JAK3 is located downstream of several (common γ-chain) cytokine receptors besides the IL-2R which may in part explain our *in vivo* efficacy. Although we found a strong effect of JAK3i on IL-4 mediated alternative macrophage polarization *in vitro*, we could not detect this *in vivo* questioning the role of this Th2-related cytokine in the TME. IL-4-mediated M2-polarization and T cell suppression can be induced, however, following radiotherapy limiting its immunogenic effect on $CD8^+$ T cells as documented in a mammary tumor model [44]. IL-15 and IL-7 are two other important cytokines signaling through JAK3-associated receptors whose downstream inhibition could play a role in our tumor models. In contrast with IL-2 that is dynamically upregulated following TCR-stimulation by cognate antigen, IL-7/IL-15 are involved in maintaining survival of naïve and memory T cells during homeostatic conditions [45]. Liu and colleagues found IL-15 to be unable to exert the same exhausted profile in $CD8^+$ T cells, even though both IL-2 and IL-15 signal through STAT5 [12]. Besides their known effects on $CD8^+$ T cells, common γ-chain cytokines including IL-2 can skew Th-phenotypes, particularly IL-2 mediated Th1-induction [45]. Although we could not detect changes in IFNγ production by Th-cells following JAK3i *in vivo* modulation through Th-subclass differentiation remains a possibility. The same accounts for Treg that constitutively express high levels of the IL-2R and rely on IL-2 for their expansion, survival but not for their suppressive function [26,45,46]. Interestingly, although effector T cell phenotype was altered by JAK3i, we did not observe changes in Treg frequencies or proliferation at the applied JAK3i dose, possibly due to high intrinsic IL-2R expression compensating for decreased downstream signaling in the context of JAK3i (Fig S2B).

We have shown JAK3 to be a novel and effective target for cancer immunotherapy, improving T cell phenotype and anti-tumor function depending on the mode of targeting. Our findings lay the groundwork for further efficacy testing in human cancer as monotherapy but more promising in combination with existing immunotherapies.

References

1. Galon, J. & Bruni, D. Approaches to treat immune hot, altered and cold tumours with combination immunotherapies. *Nat Rev Drug Discov* **18**, 197-218 (2019).
2. Waldman, A.D., Fritz, J.M. & Lenardo, M.J. A guide to cancer immunotherapy: from T cell basic science to clinical practice. *Nature reviews. Immunology* **20**, 651-668 (2020).
3. Dammeijer, F., Lau, S.P., van Eijck, C.H.J., van der Burg, S.H. & Aerts, J. Rationally combining immunotherapies to improve efficacy of immune checkpoint blockade in solid tumors. *Cytokine & growth factor reviews* (2017).
4. Marro, B.S.*, et al.* Discovery of Small Molecules for the Reversal of T Cell Exhaustion. *Cell reports* **29**, 3293-3302.e3293 (2019).
5. McLane, L.M., Abdel-Hakeem, M.S. & Wherry, E.J. CD8 T Cell Exhaustion During Chronic Viral Infection and Cancer. *Annual review of immunology* **37**, 457-495 (2019).
6. Schietinger, A.*, et al.* Tumor-Specific T Cell Dysfunction Is a Dynamic Antigen-Driven Differentiation Program Initiated Early during Tumorigenesis. *Immunity* **45**, 389-401 (2016).
7. Moore, E.C.*, et al.* Enhanced Tumor Control with Combination mTOR and PD-L1 Inhibition in Syngeneic Oral Cavity Cancers. *Cancer immunology research* **4**, 611-620 (2016).
8. Eng, C.*, et al.* Atezolizumab with or without cobimetinib versus regorafenib in previously treated metastatic colorectal cancer (IMblaze370): a multicentre, open-label, phase 3, randomised, controlled trial. *The Lancet Oncology* **20**, 849-861 (2019).
9. Verma, V.*, et al.* MEK inhibition reprograms CD8+ T lymphocytes into memory stem cells with potent antitumor effects. *Nature immunology* **22**, 53-66 (2021).
10. Ebert, P.J.R.*, et al.* MAP Kinase Inhibition Promotes T Cell and Anti-tumor Activity in Combination with PD-L1 Checkpoint Blockade. *Immunity* **44**, 609-621 (2016).
11. Diken, M.*, et al.* mTOR inhibition improves antitumor effects of vaccination with antigen-encoding RNA. *Cancer immunology research* **1**, 386-392 (2013).
12. Liu, Y.*, et al.* IL-2 regulates tumor-reactive CD8+ T cell exhaustion by activating the aryl hydrocarbon receptor. *Nature immunology* (2021).
13. Beltra, J.-C.*, et al.* IL2Rβ-dependent signals drive terminal exhaustion and suppress memory development during chronic viral infection. *Proceedings of the National Academy of Sciences* **113**, E5444-E5453 (2016).
14. Kalia, V.*, et al.* Prolonged interleukin-2Ralpha expression on virus-specific CD8+ T cells favors terminal-effector differentiation in vivo. *Immunity* **32**, 91-103 (2010).
15. Boyman, O. & Sprent, J. The role of interleukin-2 during homeostasis and activation of the immune system. *Nature reviews. Immunology* **12**, 180-190 (2012).
16. Liao, W., Lin, J.X. & Leonard, W.J. Interleukin-2 at the crossroads of effector responses, tolerance, and immunotherapy. *Immunity* **38**, 13-25 (2013).
17. O'Shea, J.J.*, et al.* The JAK-STAT Pathway: Impact on Human Disease and Therapeutic Intervention. *Annual review of medicine* **66**, 311-328 (2015).
18. Schwartz, D.M.*, et al.* JAK inhibition as a therapeutic strategy for immune and inflammatory diseases. *Nat Rev Drug Discov* **16**, 843-862 (2017).
19. Telliez, J.B.*, et al.* Discovery of a JAK3-Selective Inhibitor: Functional Differentiation of JAK3-Selective Inhibition over pan-JAK or JAK1-Selective Inhibition. *ACS chemical biology* **11**, 3442-3451 (2016).
20. Thorarensen, A.*, et al.* Design of a Janus Kinase 3 (JAK3) Specific Inhibitor 1-((2S,5R)-5-((7H-Pyrrolo[2,3-d]pyrimidin-4-yl) amino)-2-methylpiperidin-1-yl)prop-2-en-1-one (PF-06651600) Allowing for the Interrogation of JAK3 Signaling in Humans. *Journal of medicinal chemistry* **60**, 1971-1993 (2017).
21. Dammeijer, F.*, et al.* Depletion of Tumor-Associated Macrophages with a CSF-1R Kinase Inhibitor Enhances Antitumor Immunity and Survival Induced by DC Immunotherapy. *Cancer immunology research* **5**, 535-546 (2017).
22. Dammeijer, F.*, et al.* Depletion of tumor-associated macrophages with a CSF-1R kinase inhibitor enhances antitumor immunity and survival induced by DC immunotherapy. *Cancer immunology research* (2017).
23. Schulz, K.R., Danna, E.A., Krutzik, P.O. & Nolan, G.P. Single-cell phospho-protein analysis by flow cytometry. *Current protocols in immunology* **Chapter 8**, Unit 8.17 (2007).
24. Herman, S.E.M.*, et al.* The Bruton Tyrosine Kinase (BTK) Inhibitor Acalabrutinib Demonstrates Potent On-Target Effects and Efficacy in Two Mouse Models of Chronic Lymphocytic Leukemia. *Clinical cancer research : an official journal of the American Association for Cancer Research* **23**, 2831-2841 (2017).

25. Pal Singh, S., Dammeijer, F. & Hendriks, R.W. Role of Bruton's tyrosine kinase in B cells and malignancies. *Molecular cancer* **17**, 57 (2018).
26. Pandiyan, P., Zheng, L., Ishihara, S., Reed, J. & Lenardo, M.J. CD4+CD25+Foxp3+ regulatory T cells induce cytokine deprivation–mediated apoptosis of effector CD4+ T cells. *Nature immunology* **8**, 1353-1362 (2007).
27. LaPorte, S.L.*, et al.* Molecular and Structural Basis of Cytokine Receptor Pleiotropy in the Interleukin-4/13 System. *Cell* **132**, 259-272 (2008).
28. Bosurgi, L.*, et al.* Macrophage function in tissue repair and remodeling requires IL-4 or IL-13 with apoptotic cells. *Science* **356**, 1072-1076 (2017).
29. Dammeijer, F.*, et al.* The Efficacy of Tumor Vaccines and Cellular Immunotherapies in Non-Small Cell Lung Cancer: A Systematic Review and Meta-Analysis. *Journal of clinical oncology : official journal of the American Society of Clinical Oncology* (2016).
30. Hegmans, J.P.*, et al.* Consolidative dendritic cell-based immunotherapy elicits cytotoxicity against malignant mesothelioma. *American journal of respiratory and critical care medicine* **181**, 1383-1390 (2010).
31. Aerts, J.*, et al.* Autologous Dendritic Cells Pulsed with Allogeneic Tumor Cell Lysate in Mesothelioma: From Mouse to Human. *Clinical cancer research : an official journal of the American Association for Cancer Research* **24**, 766-776 (2018).
32. van Poelgeest, M.I.E.*, et al.* HPV16 synthetic long peptide (HPV16-SLP) vaccination therapy of patients with advanced or recurrent HPV16-induced gynecological carcinoma, a phase II trial. *Journal of translational medicine* **11**, 88-88 (2013).
33. Ott, P.A.*, et al.* An immunogenic personal neoantigen vaccine for patients with melanoma. *Nature* **547**, 217-221 (2017).
34. Duraiswamy, J., Kaluza, K.M., Freeman, G.J. & Coukos, G. Dual blockade of PD-1 and CTLA-4 combined with tumor vaccine effectively restores T-cell rejection function in tumors. *Cancer research* **73**, 3591-3603 (2013).
35. Fourcade, J.*, et al.* Upregulation of Tim-3 and PD-1 expression is associated with tumor antigen-specific CD8+ T cell dysfunction in melanoma patients. *The Journal of experimental medicine* **207**, 2175-2186 (2010).
36. Kortekaas, K.E.*, et al.* CD39 Identifies the CD4⁺ Tumor-Specific T-cell Population in Human Cancer. *Cancer immunology research* **8**, 1311 (2020).
37. Duhen, T.*, et al.* Co-expression of CD39 and CD103 identifies tumor-reactive CD8 T cells in human solid tumors. *Nature communications* **9**, 2724-2724 (2018).
38. Kim, H.P., Kelly, J. & Leonard, W.J. The basis for IL-2-induced IL-2 receptor alpha chain gene regulation: importance of two widely separated IL-2 response elements. *Immunity* **15**, 159-172 (2001).
39. Pai, C.S.*, et al.* Clonal Deletion of Tumor-Specific T Cells by Interferon-gamma Confers Therapeutic Resistance to Combination Immune Checkpoint Blockade. *Immunity* **50**, 477-492.e478 (2019).
40. Farmer, L.J.*, et al.* Discovery of VX-509 (Decernotinib): A Potent and Selective Janus Kinase 3 Inhibitor for the Treatment of Autoimmune Diseases. *Journal of medicinal chemistry* **58**, 7195-7216 (2015).
41. Eberl, H.C.*, et al.* Chemical proteomics reveals target selectivity of clinical Jak inhibitors in human primary cells. *Scientific reports* **9**, 14159 (2019).
42. Dunbar, A., Joosse, M.E., de Boer, F., Eefting, M. & Rijnders, B.J.A. Invasive fungal infections in patients treated with Bruton's tyrosine kinase inhibitors. *The Netherlands journal of medicine* **78**, 294-296 (2020).
43. Oo, C. & Kalbag, S.S. Leveraging the attributes of biologics and small molecules, and releasing the bottlenecks: a new wave of revolution in drug development. *Expert Review of Clinical Pharmacology* **9**, 747-749 (2016).
44. Shiao, S.L.*, et al.* TH2-Polarized CD4(+) T Cells and Macrophages Limit Efficacy of Radiotherapy. *Cancer immunology research* **3**, 518-525 (2015).
45. Lin, J.X. & Leonard, W.J. The Common Cytokine Receptor γ Chain Family of Cytokines. *Cold Spring Harbor perspectives in biology* **10**(2018).
46. Fontenot, J.D., Rasmussen, J.P., Gavin, M.A. & Rudensky, A.Y. A function for interleukin 2 in Foxp3-expressing regulatory T cells. *Nature immunology* **6**, 1142-1151 (2005).

Supplementary data

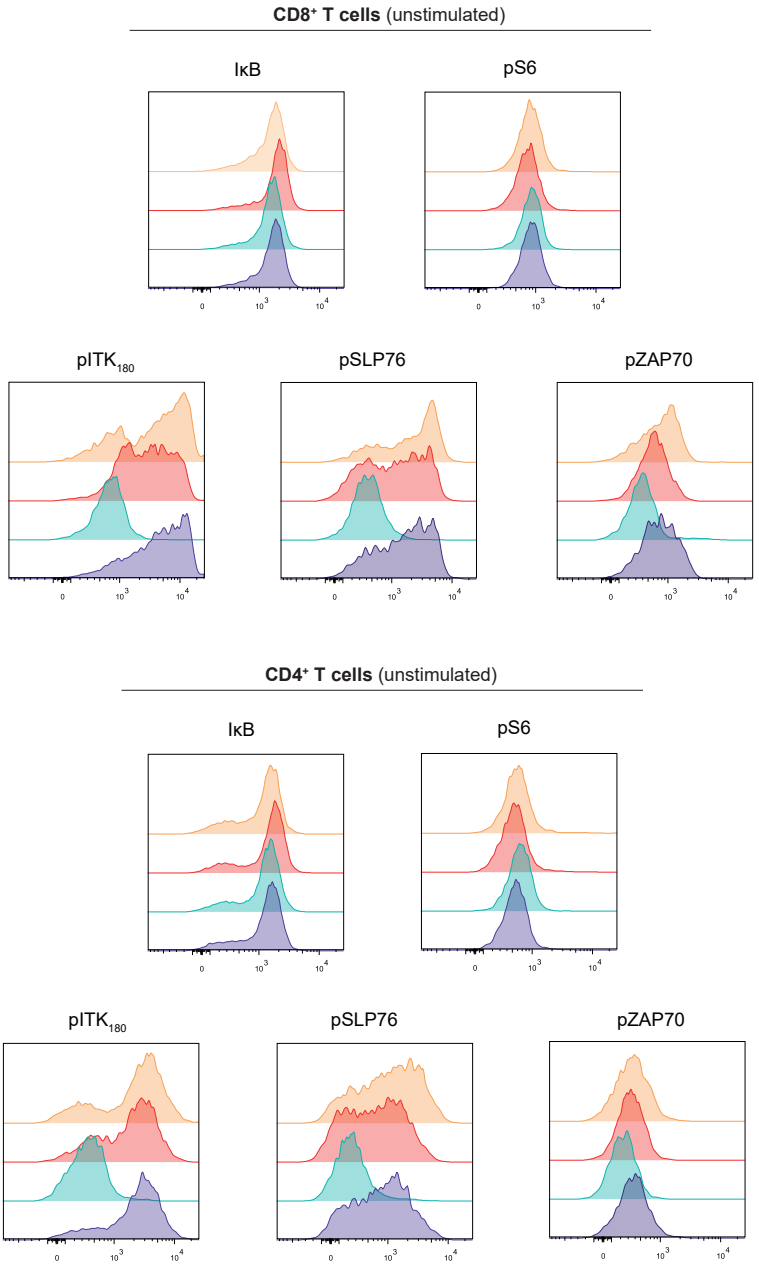

Figure S1: The effects of the different inhibitors used in Figs 1-2 on phospho-targets in different T cell signaling pathways in the unstimulated setting, for both $CD8^+$ (upper panels) and $CD4^+$ T cells (lower panels) at the 10 µmol/L concentration.

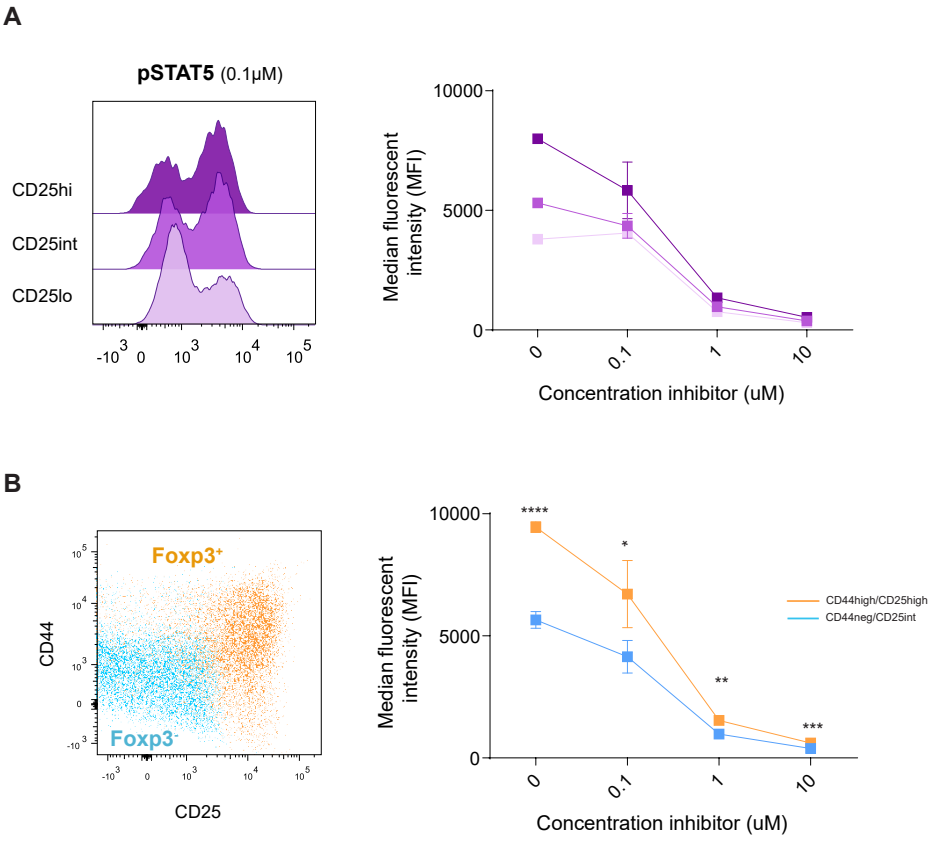

Figure S2: (A) CD25^{+} CD4^{+} T cells were subdivided into CD25 high/intermediate and low-expressing cells and pSTAT5 expression was assessed for the different subsets. (B) Alternatively, as FoxP3 could not be included in the Phosphoflow analysis for technical reasons, CD44^{+} CD25^{hi} (enriching for FoxP3-positivity, left panel) was chosen as a surrogate for FoxP3^{+} cells and compared with CD44$^{+/-}$ CD25^{int} cells (right panel). * = $p < 0.05$, ** = $p < 0.01$, *** = $p < 0.001$, **** = $p < 0.0001$, Means and SEM are shown, n = 5 mice per condition.

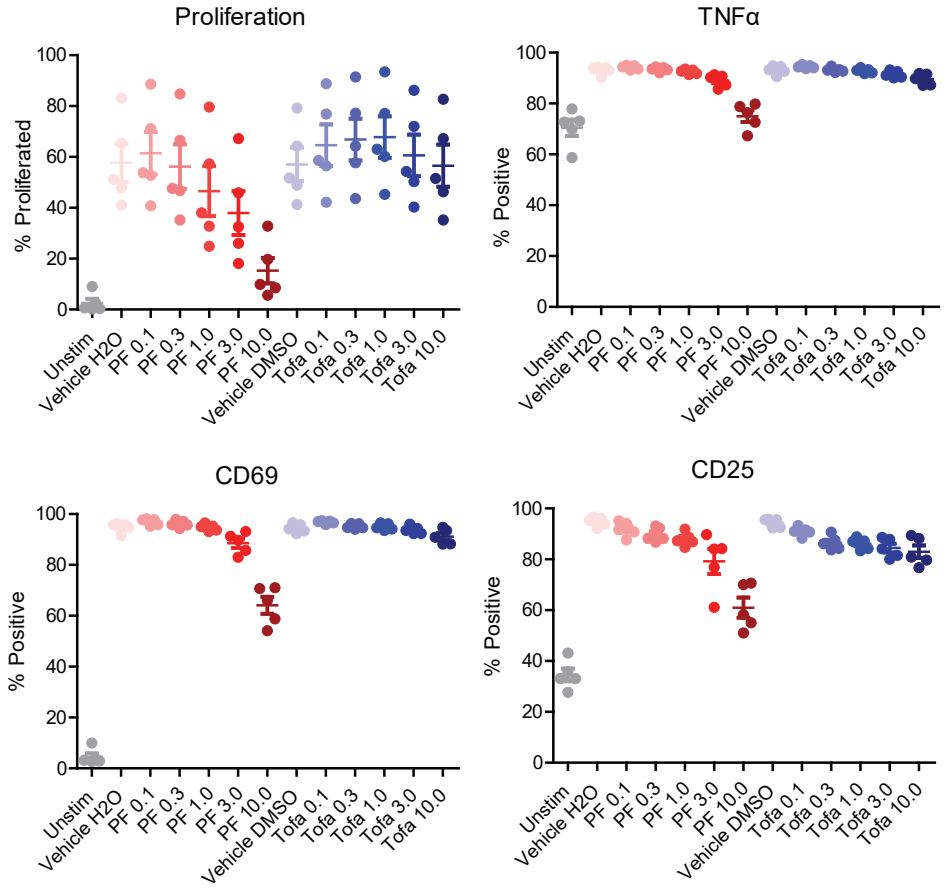

Figure S3: Murine wildtype proliferation-dye labeled T cells were stimulated with anti-CD3/CD28 beads in the absence or presence of ascending concentrations of either PF-06651600 (PF) or Tofacitinib (Tofa, both as µmol/L) and proliferation (A), activation (B) and cytokine production (C) were assessed by multicolor flow cytometry. Means and SEM are shown with n = 5 mice per condition IFNγ = interferon gamma, TNFα = tumor-necrosis factor alpha.

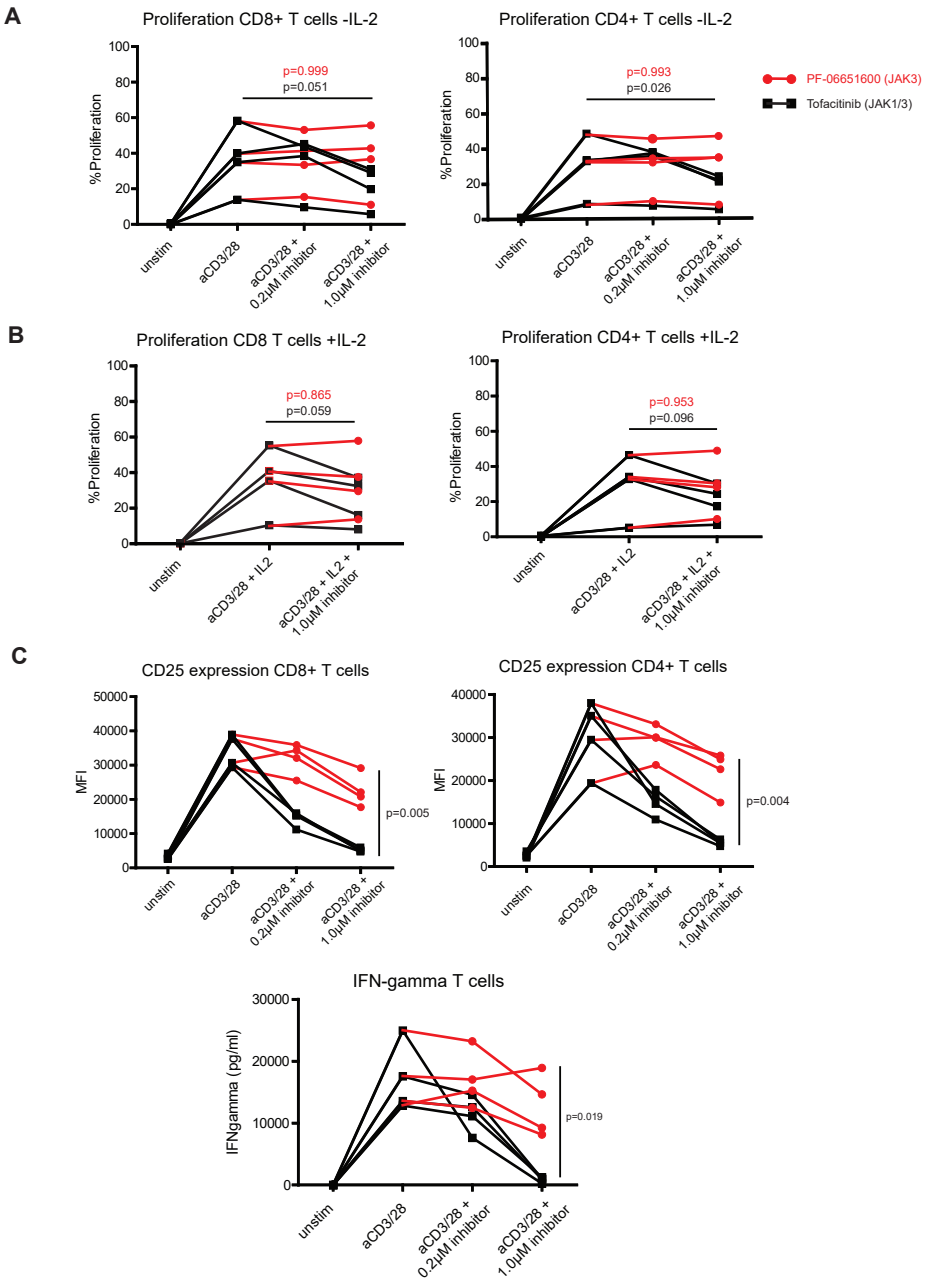

Figure S4: healthy donor-derived T cells were stimulated with anti-CD3/CD28 beads in PF-06651600 or Tofacitinib containing medium without (A) or with (B) exogenous IL-2 added to the culture system. (C) $CD4^+$ and $CD8^+$ T cell activation as assessed by CD25-upregulation was quantified by flow cytometry, in addition to IFNy levels in the supernatant using ELISA (D). Means and SEM are shown with n = 4 healthy controls per condition, IL-2 = interleukin 2, MFI = median fluorescence intensity.

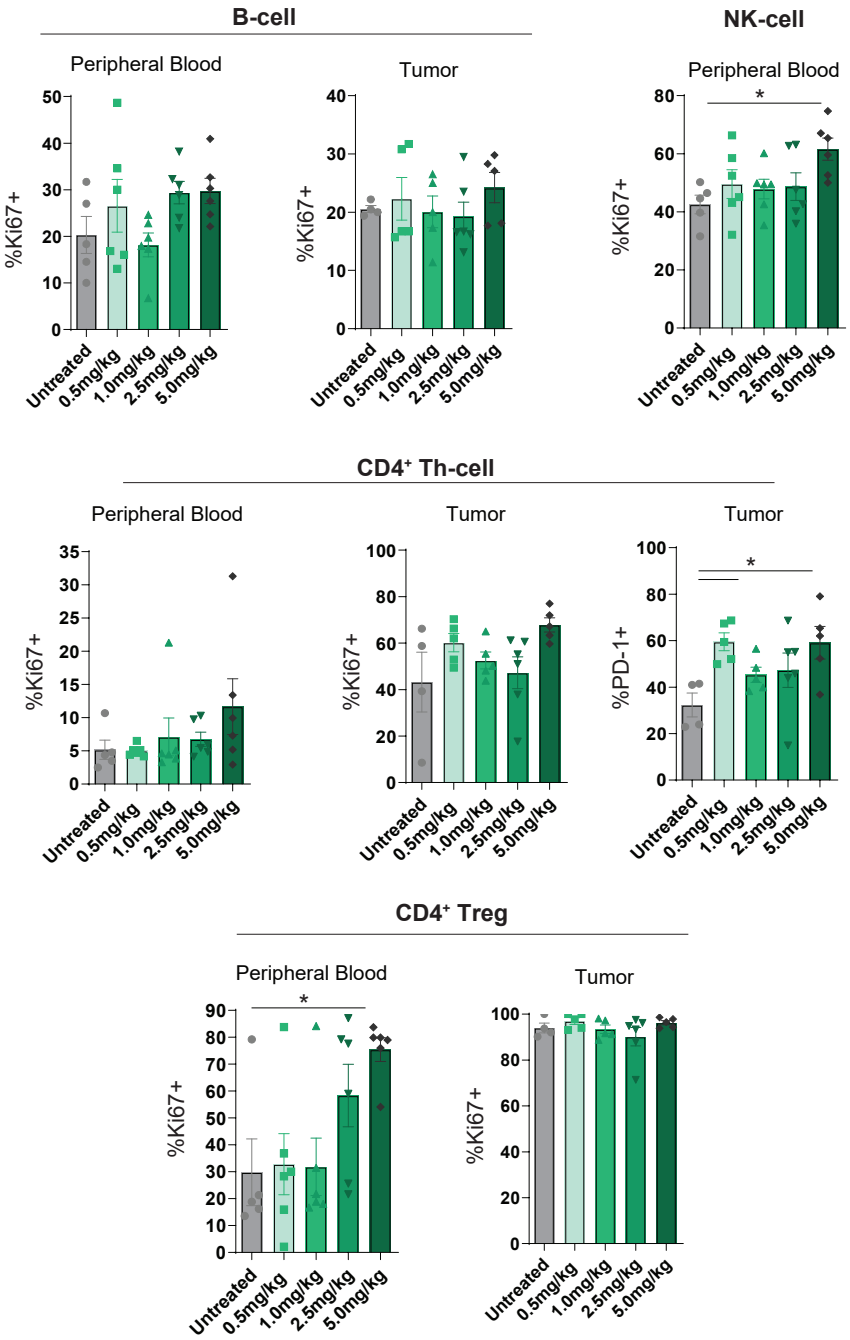

Figure S5: B-, NK- CD4⁺ Th- and Treg data relating to the experiment in Figure 4. Means and SEM are shown.

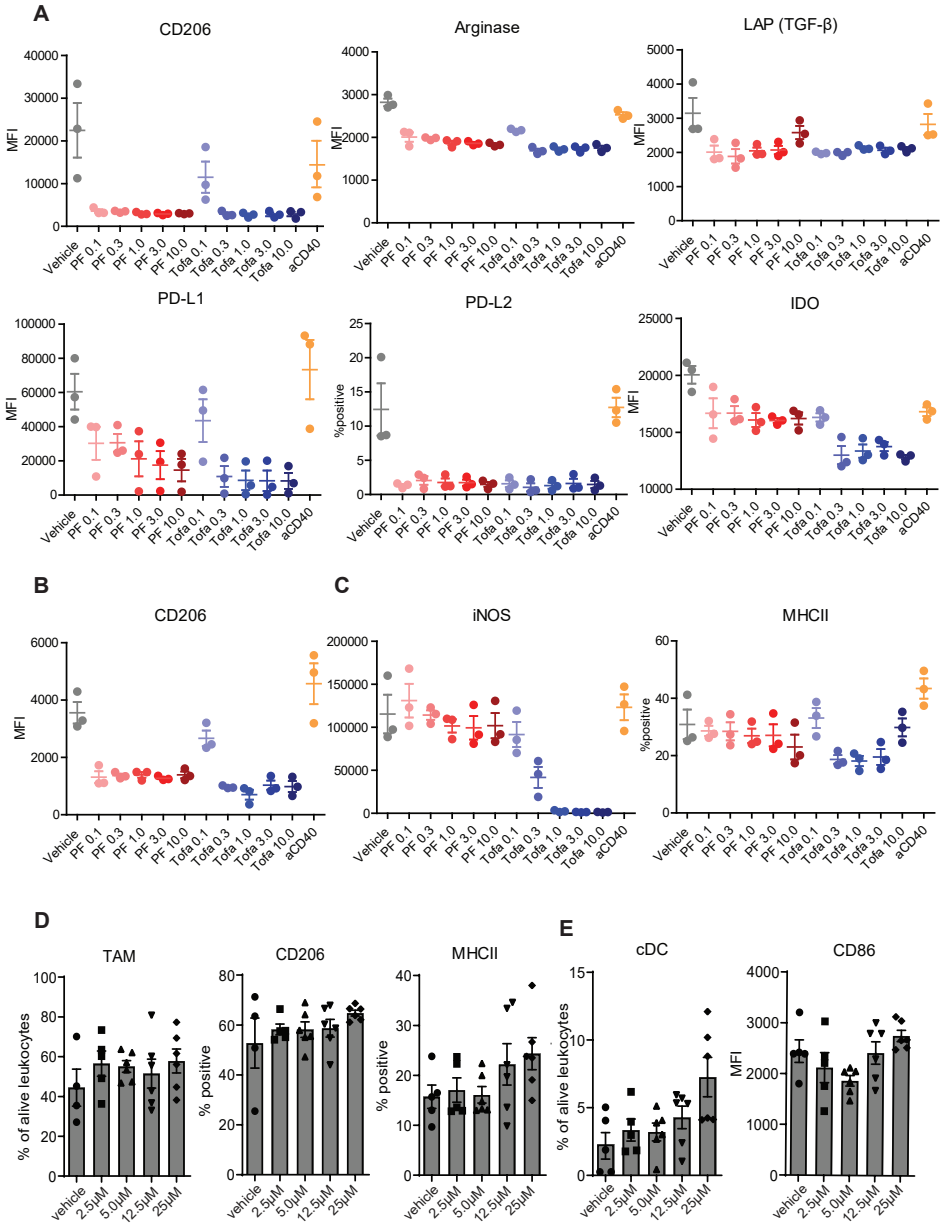

Figure S6: M-CSF generated murine bone-marrow derived macrophages were skewed to the M2 phenotype using IL-4 (A) or IL-4+IL-13 (B), or to a pro-inflammatory M1 phenotype using LPS and IFNγ (C) in the presence of PF-06651600 (PF) or Tofacitinib (Tofa) and surface markers were assessed using flow cytometry. a trimeric CD40-agonist (aCD40) was used as a prototypic M1-skewing compound serving as a positive control. (D) tumor-associated macrophages (TAM) and conventional dendritic cells (cDC) in end-stage tumors from the experiment in Figure 4 were analyzed for frequency and phenotype. MFI = median fluorescence intensity. Means and SEM are shown.

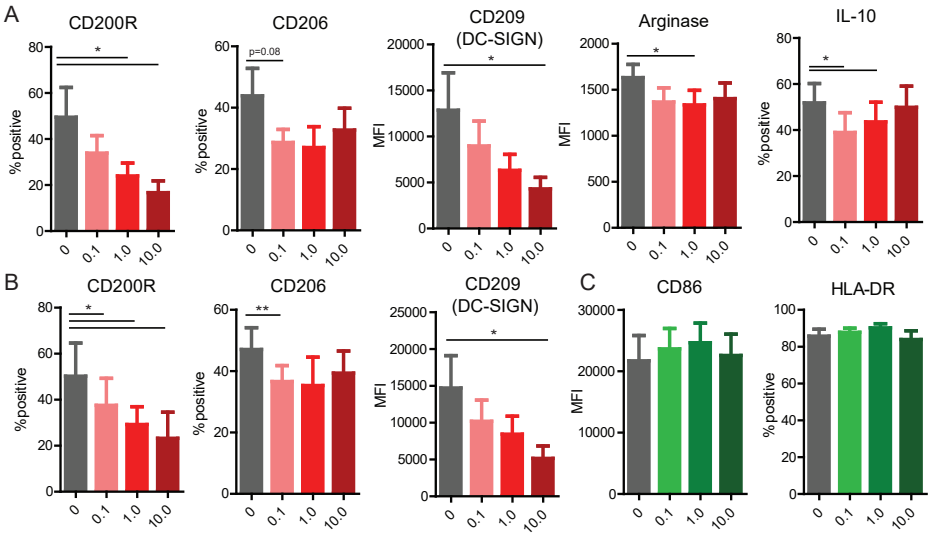

Figure S7: M-CSF generated monocyte-derived macrophages from healthy donors were skewed to M2-macrophages using IL-4 (A), IL-4+IL-13 (B) or to a pro-inflammatory M1 phenotype using LPS and IFNγ (C) in the presence of various JAK3i (PF-06651600) concentrations (as µM). MFI = median fluorescence intensity. Means and SEM are shown. * = $p < 0.05$, ** = $p < 0.01$.

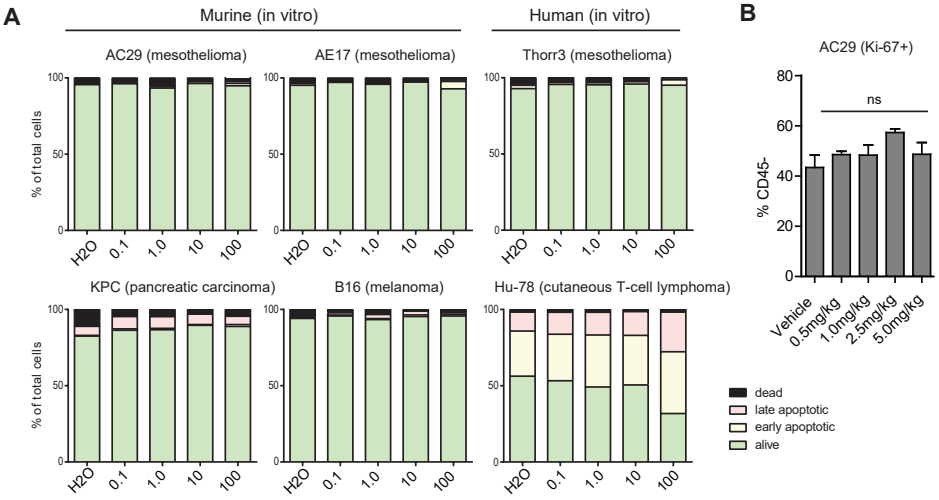

Figure S8: (A) various murine and human tumor cell lines were cultured in the absence or presence of increasing concentrations of JAK3i (PF-06651600) followed by flow-cytometric apoptosis and cell death detection. The T-cell lymphoma cell line Hu78 was used as a positive control as JAK3 is constitutively active and hence responsive to JAK3i. (B) $CD45^-$ (tumor) cells from the experiment in Figure 4 were assessed for proliferation (Ki67) at various doses of PF-06651600 *in vivo*. Ns = non-significant.

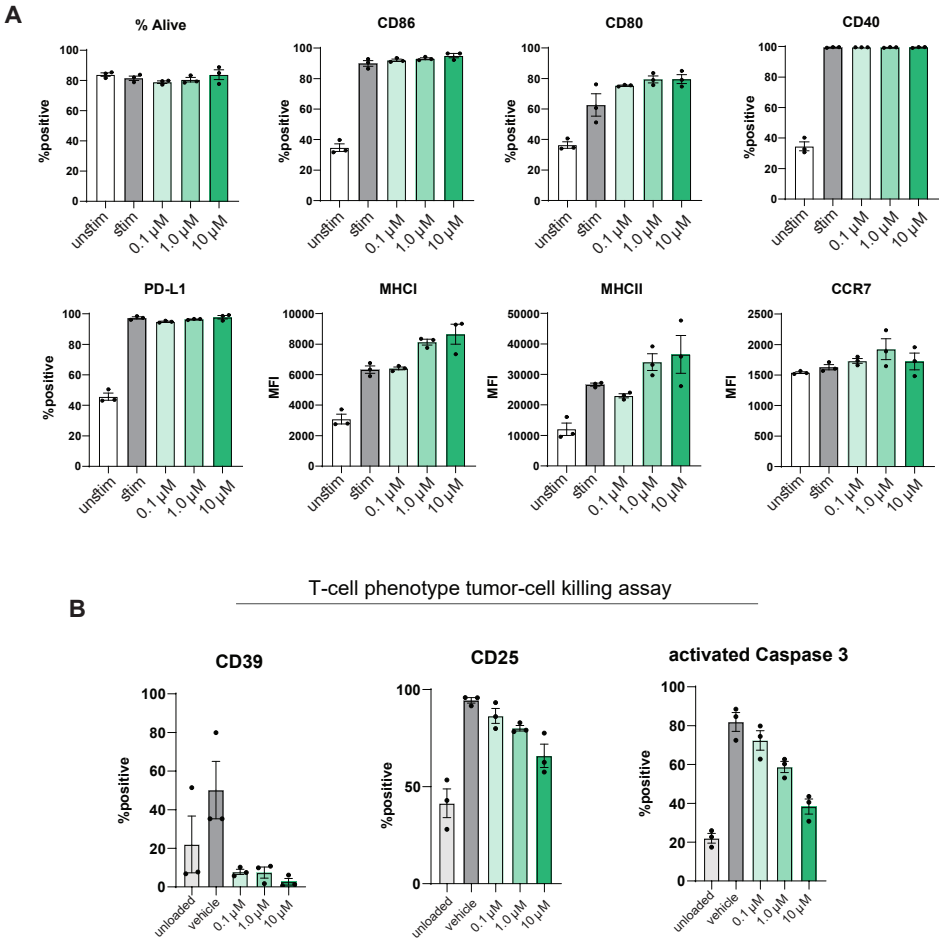

Figure S9: (A) bone-marrow derived DCs (BMDCs) were loaded- and stimulated, respectively, with OVA protein and CpG in the presence or absence of increasing doses of JAK3i (PF-06651600) followed by flow-cytometry analysis. (B) T cell phenotypical analysis following 24-hour co-culture with AE17-OVA tumor cells, related to the experiment performed in Figure 7C. Means and SEMs are shown with n = 3 OT-I donor mice.

Chapter 8

General discussion

General discussion

Immunotherapy has caused a paradigm shift in the treatment of patients with cancer [1]. However, durable clinical responses are limited to a subset of patients and tumor types [2-4]. To understand this limited efficacy, extensive research has focused on the tumor microenvironment (TME), but these efforts have not yet succeeded in substantial improvements in therapeutic efficacy. The significance of coordinating regulation across various tissues is becoming apparent, highlighting the roles of the spleen, bone marrow, gut microbiome, and the tumor-draining lymph node (TDLN) in establishing systemic anti-tumor immunity. Therefore, to effectively reach a wider population of patients, our palette of immunotherapy research should extend beyond the tumor site. Understanding the dynamic coordination between cell types and their location in orchestrating anti-tumor immunity could provide novel insights in the requirements for an effective response to immunotherapy [5-8]. Therefore, the aim of this thesis was to acquire in-depth understanding of mechanisms underlying the effectiveness and resistance of different immunotherapy strategies – immune checkpoint blockade (ICB) and dendritic cell (DC) therapy - by adopting a wider perspective of the systemic anti-tumor immune response. More specifically, in **Part A** of this thesis, we identified novel modes of action and resistance of antibodies blocking programmed cell death protein 1 (PD-1) or its ligand PD-L1. In **Chapter 2**, we identified the TDLN as an important site in dictating the efficacy of anti-PD-L1 therapy and the level of PD-1/PD-L1 interactions in the TDLN were indicated to be of predictive value in melanoma patients. The importance of TDLN biology in orchestrating effective anti-tumor immunity was further underlined in **Chapter 3**, where we found that differences in TDLN immune contexture could underlie effective anti-tumor immunity as an immunosuppressive environment in the TDLN was related to disease recurrence in melanoma patients. Besides a deeper understanding of the mechanisms of action, we also aimed to unravel novel mechanisms responsible for therapy resistance in **Chapter 4**. Here we identified the systemic activation of regulatory T cells (Tregs) by anti-PD-1/PD-L1, causing therapy resistance in the process. In **Part B** of this thesis, we focused on identifying systemic immunological mechanisms that could be targeted to improve the efficacy of DC therapy as discussed in **Chapter 5**. Combination of DC therapy with anti-PD-1/PD-L1 in **Chapter 6** was safe and feasible in mesothelioma patients and resulted in increased T cell activation and therapeutic efficacy in preclinical tumor models. In **Chapter 7**, chronic and low-dose inhibition of IL-2 receptor-STAT5 signaling using a janus kinase 3 (JAK3) inhibitor resulted in improved T cell responses and decreased tumor load when combined with DC therapy and peptide vaccination. How do these findings relate to our current understanding of systemic anti-tumor immunity and how can these findings give direction to future research and immunotherapy development?

The central role of the TDLN in systemic anti-tumor immunity and immunotherapy efficacy

The first step to initiate a functional anti-tumor T cell response is the release of cancer cell antigens that are presented by antigen-presenting cells (APCs), primarily migratory and resident DCs, to T cells with a cognate T cell receptor (TCR). This process of priming and activating T cells is predominantly

localized within the TDLN. Subsequently, primed tumor-reactive T cells migrate to the tumor site, where they carry out their effector functions [9,10]. In the context of cancer, these processes are often hampered as TDLN contexture and priming capacity are impaired due to drainage of tumor-derived suppressive molecules and cell subsets [11]. This could imply that enhancing the functionality of immune processes in TDLNs could be advantageous for bolstering systemic anti-tumor immunity and immunotherapy efficacy.

The role of the TDLN in the context of PD-1/PD-L1 blocking antibodies

In **Chapter 2**, we demonstrated that therapeutic efficacy of checkpoint targeting therapy, at least in part, arises from the disruption of the PD-1/PD-L1 axis in the TDLN. How do these findings align with the prevailing knowledge about the orchestration of anti-tumor immunity in the context of PD-1/PD-L1 blockade? A long-held view was that PD-1 primarily acts on TCR signaling in tumor-infiltrating T cells [12,13]. However, this view was challenged by findings that PD-1 also significantly impacts CD28-B7 mediated co-stimulation, thereby suggesting that B7-expressing myeloid cells in the vicinity of PD-1$^+$ T cells could be important in dictating efficacy following anti-PD-1/PD-L1 [14,15]. This was further supported by observations that PD-L1 expression on host cells, and not on tumor cells, is essential in mediating anti-PD-1/PD-L1 efficacy [16-18]. Our data not only corroborate these findings by demonstrating close interactions between DCs that express high levels of PD-L1 and B7 molecules and PD-1$^+$ tumor-reactive T cells, but they also add to these findings by showing that these interactions occur in the TDLN. Thereby, even more prominently, our findings oppose the commonly-held view that the key target of inhibitors blocking PD-1 or PD-L1 is solely contained at the tumor site. Specific inhibition of the PD-1/PD-L1 axis in the TDLN resulted in delayed tumor growth with concomitant increase of tumor-infiltrating T cells, including the progenitor-exhausted T cell population (Tpex cells) that are described to be preferentially reinvigorated following anti-PD-1/PD-L1 [19-24]. Tumor infiltration of T cells activated in the TDLN could also explain the emergence of novel T cell clones from extratumoral sources in patients responding to anti-PD-1/PD-L1 [25-28]. Seminal discoveries finding clonal overlap of Tpex cells in the TDLN and more terminally exhausted T cells (Tex) cells in the tumor further supports a model where the TDLN acts as a functional reservoir for anti-tumor immunity by continuously seeding the tumor with Tpex cells which then further differentiate into exhausted states [29-32]. Our findings together with these studies highlight the importance of the TDLN in dictating efficacy of PD-1/PD-L1 blockade. What are the remaining questions that need to be addressed to acquire a better understanding of TDLN biology in the context of PD-1/PD-L1 blockade to improve efficacy?

First, in-depth insight is required into the modes of action by which DCs impact T cell priming and phenotype through PD-1/PD-L1 interactions and how this translates to improved anti-tumor immunity upon blockade. In **Chapter 2,** we identified that the frequency of PD-1/PD-L1 interactions associated with recurrence in melanoma patients and that these interactions were primarily observed between cDCs and T cells. In combination with observations that anti-PD-L1

efficacy is independent from TDLN-macrophages, our findings highlight cDCs as prime candidates for mediating response to anti-PD-L1 in the TDLN. The important role for DCs in the PD-1/PD-L1 axis is further supported by data showing that PD-L1 expression on DCs is a key regulator in restricting $CD8^+$ T cell responses [29,33-35]. Recent studies by Spitzer's group provided more detailed insights by demonstrating that anti-PD-L1 treatment in patients with head- and neck cancer increased the frequency of DCs in the vicinity of Tpex cells and more-differentiated Tex-int cells in the TDLN [29]. How this is mediated remains to be elucidated. Antibodies blocking PD-1 or PD-L1 could potentially improve migration of DCs to the TDLN or alter their spatial organization within the TDLN. In addition to pinpointing these underlying mechanisms, it is essential to provide formal evidence regarding which subset of PD-L1-expressing cDCs exert the most significant role in limiting $CD8^+$ T cell responses. Our findings showed that cDC2s were more dominant in the TDLN, expressed higher levels of PD-L1 compared with cDC1 and co-localized with $CD8^+$ T cells. This notable finding does not align with the well-established paradigm where cDC1s are specialized in priming $CD8^+$ T cells, and cDC2s are dedicated to the activation of $CD4^+$ T cells. However, this paradigm underwent a shift in light of recent data suggesting that cDC2s could efficiently impact $CD8^+$ T cells besides their well-established function in activating $CD4^+$ T cells [36,37]. Therefore, specific depletion of cDC subsets in the TDLN together with spatial analyses, could shed further light on the role of cDCs in expanding tumor-reactive T cells following anti-PD-1/PD-L1. In addition, in-depth insights into these PD-1/PD-L1-specific interactions in the TDLN could also offer novel avenues for predicting disease outcome by using TDLN biopsies or even peripheral blood as Text-int cells were reported to be increased in this compartment following anti-PD-L1 treatment [29]. This will need to be investigated in larger cohorts with responding and nonresponding patients.

As DCs in the TDLN are important candidates in dictating efficacy following PD-1 or PD-L1 blockade, the TDLN could also act as an important effector site of DC therapy in the context of anti-PD-1/PD-L1. Therefore, the relative contribution of the TDLN in determining the therapeutic potential of DC therapy combined with anti-PD-1/PD-L1 should be further established. In **Chapter 6,** we identified strong PD-L1 upregulation on DCs used for vaccination in both murine and human setting. Concurrent administration of DC therapy and anti-PD-L1 increased T cell activation and prolonged survival. Interestingly, TDLN-specific blockade of PD-L1 in combination with DC therapy resulted in near comparable levels of T cell activation and survival, suggesting that improved efficacy is in part derived from improved T cell priming in the TDLN. Future studies should decipher whether this TDLN-derived effect can be explained by distinct effects of DC therapy and anti-PD-L1 on T cell responses or by the improvement of the priming potential of DCs used for vaccination in the context of anti-PD-L1. Experiments using PD-L1 knockout DCs for vaccination could shed further light on the mechanisms responsible for improved therapeutic efficacy. These findings could subsequently provide a preclinical foundation for the potential refinement of DC culture protocols and the adjustment of timing and dosing for DC therapy within the context of

PD-1/PD-L1 blockade in clinical setting. Furthermore, whether comparable PD-L1 upregulation occurs with other DC-targeting therapies, such as peptide vaccines, remains to be determined. This could provide mechanistic insights in the synergy of peptide vaccines and anti-PD-1 blockade, as has been recently reported [38,39].

Our findings in **Chapter 2 and 6** highlight the TDLN as an important orchestrator of anti-tumor immunity following PD-L1 blockade. However, systemic administration of anti-PD-L1 antibodies outperformed local TDLN dosing which could imply the additional requirement of responses in the TME for optimal efficacy [40]. For example, the abundance of tissue-resident memory T cells in human tumors also associated with improved overall survival and contributes to therapeutic efficacy following neoadjuvant ICB [41-44]. However, it is important to note that our approach of TDLN-specific blockade of PD-L1 was incomplete, with only 30-40% of cDCs bound by anti-PD-L1 antibodies. Therefore, an alternative explanation for the outperformance by systemic anti-PD-L1 treatment could be superior antibody binding efficacy. Hence, it remains to be determined what the exact magnitude of PD-1/PD-L1 inhibition on TDLN T cells is and how this relates to targeting of PD-1$^+$ T cells in the TME. It could well be that efficacy of anti-PD-1/PD-L1 depends on a concerted effort by PD-1$^+$ T cells in TME inducing a local inflammatory response that potentiates T cell priming in the TDLN, egress of primed T cells from the TDLN and/or their migration to the TME.

In these chapters we have primarily focused on melanoma, NSCLC and mesothelioma. Could our findings on PD-1/PD-L1 interaction in TDLNs be extrapolated to other cancer types as well? In C**hapter 2,** we show that in nearly all preclinical models analyzed, PD-1 and PD-L1 are increasingly expressed on TDLNs compared with non-TDLNs. Only in the KPC pancreatic cancer cell line lacking OVA, we could not discern any PD-1/PD-L1 axis activity which could be due to lack of immunogenicity in this model. Therefore, it is to be expected in the patient setting that similar immunogenic tumor types harbor PD-1/PD-L1 and likely also other immune checkpoint activity in TDLNs and that in more immunologically naïve tumors such as most pancreatic cancers, an immune-sensitizing approach (e.g. with peptide or cellular vaccines) is needed to induce this activity. This will be of importance for further studies investigating the utility of TDLN-composition (and PD-1/PD-L1 in particular) as biomarkers and novel therapeutic targets.

The TDLN as therapeutic opportunity beyond the PD-1/PD-L1 axis

The role of the TDLN as effector site in establishing anti-tumor immunity receives increasing interest and could represent an untapped target for immunotherapies beyond the PD-1/PD-L1 axis. This increasing interest is partly fueled by observations that the process of tumor-specific T cell differentiation starts in the TDLN, with the TDLN functioning as a reservoir by maintaining the tumor-specific T cells in a stem-like state [32,45]. Stimulation of this reservoir could therefore benefit the strength of anti-tumor T-cell immunity. However, how this pool is maintained in the TDLN and 'protected' from differentiation to a dysfunctional state remains incompletely understood. This may

entail continuous differentiation of Tpex cells from naïve T cells followed by their rapid egress as well as maintenance of the pool due to the self-renewal capacity of Tpex cells that are protected from further differentiation to a more exhausted state by spatial or molecular cues within the TDLN. One such protective mode could be the prevention of persistent antigen exposure in TDLN residing tumor-reactive T cells. TCR signaling transcripts were found to be lower in TDLN-residing T cells compared with intratumoral T cells [32]. As chronic TCR signaling is described to be a driving factor for differentiation into a terminally exhausted state once infiltrated in the tumor, reduced TCR signaling in the TDLN could potentially prevent this terminal differentiation [46,47]. The extent to which the abovementioned mechanism contribute to the maintenance of this T cell pool in the TDLN and the specific mechanisms through which this occurs needs to be determined. Besides understanding how tumor-reactive T cells, including Tpex cells, are generated, maintained and depart from the TDLN, it is vital to understand how perturbations of these processes contribute to failed anti-tumor immunity. For example, it was shown that cDC numbers and their immunostimulatory phenotype decreased in the TDLN upon tumor progression. Boosting this cell type by administration of Ftl3L and anti-CD40 resulted in improved anti-tumor immunity [45]. DC functionality was also impaired in immunosuppressive cellular niches surrounding Tpex cells in metastatic TDLNs with increased IDO, PD-L1, CD39 and TIM-3 expression, indicating a tolerogenic DC state [29,35,48]. It will be important to determine to which extent impaired DC functionality and other TDLN-based perturbations contribute to TME-composition and failed anti-tumor immunity.

Understanding the molecular mechanisms through which tumor progression influences DC dysfunction and hinders T cell activation, including Tpex cells, in the TDLN could potentially offer novel avenues to improve DC therapy efficacy. While vaccination using DCs can initiate potent anti-tumor immune responses, these responses are often not effective enough to achieve clinical benefit. On one hand, this could be explained by the lack of DCs reaching the TDLN following administration of DCs to more easily accessible sites (e.g. intradermal and intravenous injection) [49-51]. Recent observations indicated that the TDLN harbors tumor-reactive functional resident memory T cells that predicted survival in patients with melanoma[52]. Due to the residency of these tumor-reactive T cells in the TDLN, enhancing the proportion of administered DCs capable of reaching the TDLN might consequently provide therapeutic benefit. The therapeutic potential of local immune modulation by enhancing the proportion of DCs in the TDLN is already shown by the administration of GM-CSF and CpG around the melanoma excision site [53-55]. Local immunosuppressive mechanisms could, on the other hand, intervene with DC-mediated T cell priming. Tregs congregate around DCs to downregulate B7 molecule expression which was rescued in Treg-depleted hosts [56,57]. Next to downregulation of B7 molecules, recent data highlight the role of Tregs in impairing T cell activation by restraining cDC1 functionality, which was dependent on MHCII [58]. Therefore, anti-tumor efficacy of DC therapy may be further boosted by restraining the immunosuppressive counterpart. In addition to modulating these immunosuppressive mechanisms, engaging a broader range of adaptive immunity may offer an alternative strategy to propel therapeutic efficacy. Thus far, DC

therapy has been shown to predominantly elicit a CD4$^+$ T helper response [50]. The relevance of CD4$^+$ T cells in anti-tumor immunity is becoming more apparent as they can exert cytolytic mechanisms and modulate the TME [59,60]. Perhaps more important is the role of CD4$^+$ T cells in providing help to CD8$^+$ T cells. In this process, antigen-specific interactions of CD4$^+$ T cells with DCs, including CD40/CD40L interactions, optimize the capacity of DCs to functionally prime CD8$^+$ T cells resulting in improved memory formation, migratory potential and enhanced activity and expansion [61]. Therefore, it is important that, next to stimulating CD4$^+$ T cell responses, the same DC has the capacity to elicit strong CD8$^+$ T cell immunity. Research efforts should be focused on methods, including antigen-delivery tools, which can promote this presentation capacity of exogenous *in vitro* stimulated DCs.

In order to further explore the immunosuppressive mechanisms in the TDLN, digital spatial profiling (DSP) was performed on TDLNs from patients with stage III melanoma either with or without disease recurrence. In **Chapter 3**, we revealed increased expression of suppressive proteins including CTLA-4, IDO1, PD-L1 and FOXP3 as well as increased frequencies of PD-L1$^+$ DCs in patients with disease recurrence, which is consistent with our findings in **Chapter 2** and findings by others [29]. Intriguingly, these differences were found at sites distant from the TDLN metastasis while immune compositions in peritumoral regions were similar between patients with and without disease recurrence. This suggests that risk on recurrence is dictated by regions in the TDLN that are spatially distant from metastasis and aligns with recent findings showing that the suppressive TDLN-environment not only enables LN metastasis but also colonization to distant tissues [62]. It remains to be formally determined on single-cell level which cell types in the TDLN are primarily involved and how interactions with other immune cells and/or stromal cells dictate disease progression. The increased expression of CTLA-4, IDO1, PD-L1 and FOXP3 in patients with disease recurrence may suggest a role for TDLN-residing Tregs in impeding systemic anti-tumor immunity. Tregs are central regulators of immune homeostasis by safe-guarding self-tolerance. Treg accumulation in the TDLN is associated with metastatic spread to those lymph nodes which was recently suggested to be explained by local suppression of natural killer cells, thereby facilitating metastasis [63,64]. Depletion of Tregs from TDLN cell suspensions resulted in improved IFNy production by CD8$^+$ T cells upon co-culture which could potentially be due to improved cDC1 functionality [65,58]. In the clinical setting, local administration of anti-CTLA-4 at the primary excision site of patients with melanoma resulted in a systemic reduction of Tregs, including in the TDLN, and was associated with bolstered activation of migratory cDCs [66]. Together with our findings, this could suggest a prominent role for Tregs in the TDLN in curtailing anti-tumor immunity by creating an immunosuppressive TDLN milieu. However, to date, it remains a technical challenge to explicitly probe the impact of Tregs in the TDLN. The importance of overcoming this technical challenge is further underlined as it has been shown that tumor-residing Tregs could impact CD4$^+$ T cell priming by inducing a tolerogenic cDC2 phenotype in the TDLN [67]. Therefore, specific ablation of the Treg population in the TDLN by using transgenic murine tumors models could shed further light on the relevance of TDLN-residing Tregs in impeding systemic anti-tumor immunity.

Targeting regulatory T cells to improve therapeutic efficacy of antibodies blocking PD-1 or PD-L1

In **Chapter 4**, we unveiled that PD-L1 blockade systemically increased the suppressive ability of Tregs in both nonresponsive mice and patients, thereby playing a critical role in resistance to anti-PD-L1 treatment. How do these findings relate to our current understanding of the role of Tregs in limiting anti-PD-1/PD-L1 efficacy? Other studies have previously reported that anti-PD-1 treatment can enhance the suppressive capabilities of Tregs [68-70]. Notably, a group led by Nishikawa suggested that this phenomenon could be a driving factor in a subset of patients experiencing hyperprogressive disease, which is characterized by rapid tumor progression [71]. Supporting this concept, additional preclinical data showed that creating a TME dominated by Tregs through $CD8^+$ T cell depletion, using near-infrared photoimmunotherapy (NIR-PIT), resulted in hyperprogressive disease upon subsequent anti-PD-1 therapy [72]. Furthermore, they demonstrated that the level of PD-1 expression on Tregs relative to $CD8^+$ T cells within the tumor tissue could predict whether patients with gastric cancer and non-small cell lung cancer (NSCLC) would respond to anti-PD-1 therapy [73]. Our own findings complement these existing studies by revealing that Tregs are not solely associated with the rare occurrence of hyperprogressive disease but are also likely involved in the much more common problem of therapy resistance. What is particularly interesting is that while above-mentioned studies mainly focused on the effect of anti-PD-1/PD-L1 antibodies on tumor-residing Tregs, we found that the effects of anti-PD-1/PD-L1 extended beyond the tumor site and affected the macroenvironment, including the TDLN. As already mentioned, TDLN-residing Tregs are able to curb T cell priming, facilitate LN metastasis and are potentially involved in mediating disease recurrence in patients with melanoma, as demonstrated in **Chapter 3.** Amplifying the suppressive function of Tregs by antibodies blocking PD-1 or PD-L1 could therefore not only impact anti-tumor immunity at the tumor site but also influence TDLN immune contexture and T cell priming. Systemic Treg activation was also found in mice bearing breast cancer as combined treatment with anti-CTLA-4 and anti-PD-1 amplified Treg activity in multiple tissues, including the TDLN. Treg depletion, in turn, resulted in sustained T cell activation in the circulation together with decreased metastasis formation and was suggested to be the result of improved T cell priming in Treg-depleted TDLNs [74]. Whether resistance to PD-1 or PD-L1 blockade is mediated through amplification of effector functions of tumor-residing Tregs or by restricted priming in the TDLN remains to be investigated using abovementioned transgenic murine models. Understanding the primary tissue involved and the mechanisms underlying the enhanced suppressive capacity of Tregs following anti-PD-1/PD-L1 therapy is critical as it can guide the identification of potential Treg-directed targets for intervention.

How to counteract ICB-mediated activation of Tregs to reinforce therapeutic benefit?

Due to the function of Tregs in impairing effective anti-tumor immunity, various Treg-directed targets, including anti-CD25, were used for intervention to either deplete this suppressive subset or attenuate their suppressive function. However, the clinical success of these approaches has been limited, and they often give rise to immune-related adverse effects like pneumonitis and colitis [75-78]. Emerging studies are uncovering context-specific functional reprogramming of Tregs in tissues,

including the tumor. Confining alterations specifically to tumor tissue could potentially prevent impacting Tregs at other sites, thereby rationally minimizing the risk on autoimmunity. For example, recent data highlighted the activator protein-1 (AP-1) transcription factor Basic Leucine Zipper ATF-Like Transcription Factor (BATF) and chemokine receptor CCR8 to be viable candidates as their expression is mainly conserved to highly immunosuppressive Tregs residing in tumor tissue [57,79-84]. Alternatively, tumor-residing Tregs are described to be able to adapt to the challenging metabolic landscape in the TME, including alterations in lactate and lipid signaling. Targeting metabolic checkpoints could therefore potentially dampen Treg functioning specifically at the tumor site [85-89]. In the context of ICB-mediated activation of Tregs, it remains to be determined which signaling entities are the drivers of the increased suppressive capacity of Tregs following treatment, whether these entities are shared between different tumor types, and, as already mentioned, whether the tumor site is the primary effector location of this effect. Limited data available suggested an important yet conflicting role for the PI3K-AKT signaling pathway in mediating enhanced suppressive capacity of Tregs, with some groups reporting enhanced activity of this pathway while others demonstrated reduced PI3K-AKT signaling [70,73]. Instead of focusing on a limited set of molecules or pathways, future research should focus on getting a complete understanding of Treg-intrinsic alterations induced by PD-1 or PD-L1 blocking antibodies using unbiased systems approaches and comprehensive (epi)genetic tools. Of note, recent data suggested that in some cases PD-1 blockade reduces Treg activity and tumor development. However, this PD-1 inactivation was induced prior to tumor inoculation, thereby suggesting that Treg activation by tumor antigens may cause cell-intrinsic rewiring that results in an altered response to PD-1 or PD-L1 blockade [90]. These factors should be taken into account when investigating the intrinsic changes in Tregs following PD-1 or PD-L1 blockade. These findings could pave the way to the identification of targetable modalities that could prevent or neutralize inadvertent activating Treg-directed effects by anti-PD-1/PD-L1 therapy. By employing these strategies, only the subset of Tregs that are influenced by PD-1 or PD-L1 blockade would be selectively targeted, thereby potentially minimizing the risk of side effects.

Concluding remarks and prospects

Cancer immunotherapy has made an unprecedented impact on the treatment landscape of patients with cancer but durable clinical success is limited to a subset of patients. Knowledge on the modes of action of immunotherapies as well as on factors that thwart effective anti-tumor immunity could offer avenues for improving efficacy of existing immunotherapies and propel the development of novel immunotherapeutic strategies. This thesis provides novel insights in modes responsible for induction and suppression of anti-tumor immunity following immunotherapy. Importantly, these insights move away from the traditional tumor-based view to a more systemic holistic view, where coordinated regulation across multiple tissues is required for sculpting effective anti-tumor immunity. As we and others have identified the TDLN as a central regulator of anti-tumor immunity and efficacy of PD-1/PD-L1 blockade, future research will be directed to further in-depth characterization of the immune landscape in TDLNs in the context of the PD-1/PD-L1 axis and beyond. More specifically,

this research will entail detailed understanding of DC and T cell interactions on spatial and molecular level and the means by which these TDLN-based interactions dictate the quality of anti-tumor T cell immunity and TME composition. In parallel, it will be indispensable to pinpoint immunosuppressive mechanisms responsible for impeding these interactions and how this contributes to anti-tumor immunity and LN metastasis. To achieve this understanding on detailed level, it is important to exploit sequencing and imaging tools that enable (spatial) insights at single-cell resolution. This detailed understanding could, in turn, aid in further optimization of existing immunotherapies, including antibodies blocking PD-1 or PD-L1 and DC therapy, and could potentially offer novel therapeutic targets. As we identified the value of PD-1/PD-L1 interactions in the TDLN in predicting disease recurrence, focusing on the TDLN and/or the resultant effect in peripheral blood could also be valuable for the purpose of biomarker finding [29]. In addition to pinpointing the TDLN as an important anatomical site of action for antibodies blocking PD-1 or PD-L1, our research has uncovered that PD-L1 blockade can inadvertently systemically activate Tregs which leads to therapy resistance by curbing anti-tumor immunity. Future research will provide more insights into the extent to which ICB-mediated Treg activation influences the obstruction of either the priming phase in the TDLN or effector phase at the tumor site and their relative contribution to therapy resistance. These insights will aid in uncovering potential therapeutic targets in Tregs activated by PD-1 or PD-L1 blockade. Such targets can be harnessed to mitigate or counteract the activation of these suppressive Tregs, with the ultimate goal of maximizing anti-tumor immunity while minimizing the potential for adverse side effects. The findings by us and other groups underlining the importance of Tregs in (primary and secondary) therapy resistance in multiple murine and human tumors indicate that patients with different types of tumor treated with anti-PD-1/PD-L1 blocking antibodies could benefit from Treg-directed therapies. However, in-depth characterization of the macroenvironment is warranted to identify the importance of Tregs in different tumor types to maximize efficacy and prevent unnecessary toxicity.

Due to increasing ethical, societal and political pressures, a movement is directed from preclinical murine experiments towards studying anti-tumor immunity in patient-derived materials, including organoids and *ex vivo* tumor platforms [91-93]. Although these patient-derived approaches directly provide clinical relevance and have enabled more mechanistic understanding of human tumors, these methods also face important challenges. In light of the increasing relevance of systemic anti-tumor immunity, longitudinal multi-tissue analyses are required to get a full glimpse of (therapy-induced) anti-tumor immunity and its mechanistic underpinnings. These options are often limited using these platforms and also obscure the coordinated dynamics between tissues, such as T cell infiltration and recirculation. Despite the obvious pitfalls, preclinical tumor immunology models remain an irreplaceable cornerstone as it allows longitudinal interrogation of multiple tissues. In addition, (transgenic) murine models enables experimental validation for establishing causal relationships. This is becoming increasingly important in the current era where multidimensional analysis platforms such as scRNA-seq and ATAC-seq are widely applied. Findings are often descriptive

and it remains a great challenge to prevent the obscuring of experimental error and biological complexity in the deluge of –omics data. Therefore, a collaborative effort between clinicians, biomedical scientists and bioinformaticians in combination with the use of appropriate models and techniques will be indispensable to provide precise mechanistic understanding of cancer immunotherapies and ultimately improve clinical outcome for affected individuals.

References

1. Waldman, A.D., Fritz, J.M. & Lenardo, M.J. A guide to cancer immunotherapy: from T cell basic science to clinical practice. *Nat Rev Immunol* **20**, 651-668 (2020).
2. O'Donnell, J.S., Teng, M.W.L. & Smyth, M.J. Cancer immunoediting and resistance to T cell-based immunotherapy. *Nat Rev Clin Oncol* **16**, 151-167 (2019).
3. Sharma, P., Hu-Lieskovan, S., Wargo, J.A. & Ribas, A. Primary, Adaptive, and Acquired Resistance to Cancer Immunotherapy. *Cell* **168**, 707-723 (2017).
4. Vesely, M.D., Zhang, T. & Chen, L. Resistance Mechanisms to Anti-PD Cancer Immunotherapy. *Annu Rev Immunol* **40**, 45-74 (2022).
5. Spitzer, M.H*., et al.* Systemic Immunity Is Required for Effective Cancer Immunotherapy. *Cell* **168**, 487-502 e415 (2017).
6. Allen, B.M*., et al.* Systemic dysfunction and plasticity of the immune macroenvironment in cancer models. *Nat Med* **26**, 1125-1134 (2020).
7. Park, E.M*., et al.* Targeting the gut and tumor microbiota in cancer. *Nat Med* **28**, 690-703 (2022).
8. Helmink, B.A., Khan, M.A.W., Hermann, A., Gopalakrishnan, V. & Wargo, J.A. The microbiome, cancer, and cancer therapy. *Nat Med* **25**, 377-388 (2019).
9. Chen, D.S. & Mellman, I. Oncology meets immunology: the cancer-immunity cycle. *Immunity* **39**, 1-10 (2013).
10. Mellman, I., Chen, D.S., Powles, T. & Turley, S.J. The cancer-immunity cycle: Indication, genotype, and immunotype. *Immunity* **56**, 2188-2205 (2023).
11. Cochran, A.J*., et al.* Tumour-induced immune modulation of sentinel lymph nodes. *Nat Rev Immunol* **6**, 659-670 (2006).
12. Yokosuka, T*., et al.* Programmed cell death 1 forms negative costimulatory microclusters that directly inhibit T cell receptor signaling by recruiting phosphatase SHP2. *J Exp Med* **209**, 1201-1217 (2012).
13. Mizuno, R*., et al.* PD-1 Primarily Targets TCR Signal in the Inhibition of Functional T Cell Activation. *Front Immunol* **10**, 630 (2019).
14. Hui, E*., et al.* T cell costimulatory receptor CD28 is a primary target for PD-1-mediated inhibition. *Science* **355**, 1428-1433 (2017).
15. Kamphorst, A.O*., et al.* Rescue of exhausted CD8 T cells by PD-1-targeted therapies is CD28-dependent. *Science* **355**, 1423-1427 (2017).
16. Lau, J*., et al.* Tumour and host cell PD-L1 is required to mediate suppression of anti-tumour immunity in mice. *Nat Commun* **8**, 14572 (2017).
17. Kleinovink, J.W*., et al.* PD-L1 expression on malignant cells is no prerequisite for checkpoint therapy. *Oncoimmunology* **6**, e1294299 (2017).
18. Tang, H*., et al.* PD-L1 on host cells is essential for PD-L1 blockade-mediated tumor regression. *J Clin Invest* **128**, 580-588 (2018).
19. He, R*., et al.* Follicular CXCR5- expressing CD8(+) T cells curtail chronic viral infection. *Nature* **537**, 412-428 (2016).
20. Im, S.J*., et al.* Defining CD8+ T cells that provide the proliferative burst after PD-1 therapy. *Nature* **537**, 417-421 (2016).
21. Kurtulus, S*., et al.* Checkpoint Blockade Immunotherapy Induces Dynamic Changes in PD-1(-)CD8(+) Tumor-Infiltrating T Cells. *Immunity* **50**, 181-194 e186 (2019).
22. Miller, B.C*., et al.* Subsets of exhausted CD8(+) T cells differentially mediate tumor control and respond to checkpoint blockade. *Nat Immunol* **20**, 326-336 (2019).
23. Sade-Feldman, M*., et al.* Defining T Cell States Associated with Response to Checkpoint Immunotherapy in Melanoma. *Cell* **175**, 998-1013 e1020 (2018).
24. Siddiqui, I*., et al.* Intratumoral Tcf1(+)PD-1(+)CD8(+) T Cells with Stem-like Properties Promote Tumor Control in Response to Vaccination and Checkpoint Blockade Immunotherapy. *Immunity* **50**, 195-211 e110 (2019).
25. Valpione, S*., et al.* Immune-awakening revealed by peripheral T cell dynamics after one cycle of immunotherapy. *Nat Cancer* **1**, 210-221 (2020).
26. Wu, T.D*., et al.* Peripheral T cell expansion predicts tumour infiltration and clinical response. *Nature* **579**, 274-278 (2020).
27. Yost, K.E*., et al.* Clonal replacement of tumor-specific T cells following PD-1 blockade. *Nat Med* **25**, 1251-1259 (2019).
28. Liu, B*., et al.* Temporal single-cell tracing reveals clonal revival and expansion of precursor exhausted T cells during anti-PD-1 therapy in lung cancer. *Nat Cancer* **3**, 108-121 (2022).
29. Rahim, M.K*., et al.* Dynamic CD8(+) T cell responses to cancer immunotherapy in human regional lymph nodes are disrupted in metastatic lymph nodes. *Cell* **186**, 1127-1143 e1118 (2023).
30. Prokhnevska, N*., et al.* CD8(+) T cell activation in cancer comprises an initial activation phase in lymph nodes followed by effector differentiation within the tumor. *Immunity* **56**, 107-124 e105 (2023).

31. Pai, J.A., *et al.* Lineage tracing reveals clonal progenitors and long-term persistence of tumor-specific T cells during immune checkpoint blockade. *Cancer Cell* **41**, 776-790 e777 (2023).
32. Connolly, K.A., *et al.* A reservoir of stem-like CD8(+) T cells in the tumor-draining lymph node preserves the ongoing antitumor immune response. *Sci Immunol* **6**, eabg7836 (2021).
33. Oh, S.A., *et al.* PD-L1 expression by dendritic cells is a key regulator of T-cell immunity in cancer. *Nat Cancer* **1**, 681-691 (2020).
34. Peng, Q., *et al.* PD-L1 on dendritic cells attenuates T cell activation and regulates response to immune checkpoint blockade. *Nat Commun* **11**, 4835 (2020).
35. Maier, B., *et al.* A conserved dendritic-cell regulatory program limits antitumour immunity. *Nature* **580**, 257-262 (2020).
36. Bosteels, C., *et al.* Inflammatory Type 2 cDCs Acquire Features of cDC1s and Macrophages to Orchestrate Immunity to Respiratory Virus Infection. *Immunity* **52**, 1039-1056 e1039 (2020).
37. Ruhland, M.K., *et al.* Visualizing Synaptic Transfer of Tumor Antigens among Dendritic Cells. *Cancer Cell* **37**, 786-799 e785 (2020).
38. Massarelli, E., *et al.* Combining Immune Checkpoint Blockade and Tumor-Specific Vaccine for Patients With Incurable Human Papillomavirus 16-Related Cancer: A Phase 2 Clinical Trial. *JAMA Oncol* **5**, 67-73 (2019).
39. Weber, J.S., *et al.* Individualised neoantigen therapy mRNA-4157 (V940) plus pembrolizumab versus pembrolizumab monotherapy in resected melanoma (KEYNOTE-942): a randomised, phase 2b study. *Lancet* **403**, 632-644 (2024).
40. Nagasaki, J., *et al.* PD-1 blockade therapy promotes infiltration of tumor-attacking exhausted T cell clonotypes. *Cell Rep* **38**, 110331 (2022).
41. Ganesan, A.P., *et al.* Tissue-resident memory features are linked to the magnitude of cytotoxic T cell responses in human lung cancer. *Nat Immunol* **18**, 940-950 (2017).
42. Duhen, T., *et al.* Co-expression of CD39 and CD103 identifies tumor-reactive CD8 T cells in human solid tumors. *Nat Commun* **9**, 2724 (2018).
43. Anadon, C.M., *et al.* Ovarian cancer immunogenicity is governed by a narrow subset of progenitor tissue-resident memory T cells. *Cancer Cell* **40**, 545-557 e513 (2022).
44. Luoma, A.M., *et al.* Tissue-resident memory and circulating T cells are early responders to pre-surgical cancer immunotherapy. *Cell* **185**, 2918-2935 e2929 (2022).
45. Schenkel, J.M., *et al.* Conventional type I dendritic cells maintain a reservoir of proliferative tumor-antigen specific TCF-1(+) CD8(+) T cells in tumor-draining lymph nodes. *Immunity* **54**, 2338-2353 e2336 (2021).
46. Schietinger, A., *et al.* Tumor-Specific T Cell Dysfunction Is a Dynamic Antigen-Driven Differentiation Program Initiated Early during Tumorigenesis. *Immunity* **45**, 389-401 (2016).
47. Blank, C.U., *et al.* Defining 'T cell exhaustion'. *Nat Rev Immunol* **19**, 665-674 (2019).
48. Magen, A., *et al.* Intratumoral dendritic cell-CD4(+) T helper cell niches enable CD8(+) T cell differentiation following PD-1 blockade in hepatocellular carcinoma. *Nat Med* **29**, 1389-1399 (2023).
49. Belderbos, R.A., *et al.* A multicenter, randomized, phase II/III study of dendritic cells loaded with allogeneic tumor cell lysate (MesoPher) in subjects with mesothelioma as maintenance therapy after chemotherapy: DENdritic cell Immunotherapy for Mesothelioma (DENIM) trial. *Transl Lung Cancer Res* **8**, 280-285 (2019).
50. Lau, S.P., *et al.* Autologous dendritic cells pulsed with allogeneic tumour cell lysate induce tumour-reactive T-cell responses in patients with pancreatic cancer: A phase I study. *Eur J Cancer* **169**, 20-31 (2022).
51. Verdijk, P., *et al.* Limited amounts of dendritic cells migrate into the T-cell area of lymph nodes but have high immune activating potential in melanoma patients. *Clin Cancer Res* **15**, 2531-2540 (2009).
52. Molodtsov, A.K., *et al.* Resident memory CD8(+) T cells in regional lymph nodes mediate immunity to metastatic melanoma. *Immunity* **54**, 2117-2132 e2117 (2021).
53. Sluijter, B.J., *et al.* Arming the Melanoma Sentinel Lymph Node through Local Administration of CpG-B and GM-CSF: Recruitment and Activation of BDCA3/CD141(+) Dendritic Cells and Enhanced Cross-Presentation. *Cancer Immunol Res* **3**, 495-505 (2015).
54. van den Hout, M.F., *et al.* Local delivery of CpG-B and GM-CSF induces concerted activation of effector and regulatory T cells in the human melanoma sentinel lymph node. *Cancer Immunol Immunother* **65**, 405-415 (2016).
55. Koster, B.D., *et al.* In the mix: the potential benefits of adding GM-CSF to CpG-B in the local treatment of patients with early-stage melanoma. *Oncoimmunology* **9**, 1708066 (2020).
56. Onishi, Y., Fehervari, Z., Yamaguchi, T. & Sakaguchi, S. Foxp3+ natural regulatory T cells preferentially form aggregates on dendritic cells in vitro and actively inhibit their maturation. *Proc Natl Acad Sci U S A* **105**, 10113-10118 (2008).
57. Kidani, Y., *et al.* CCR8-targeted specific depletion of clonally expanded Tregs in tumor tissues evokes potent tumor immunity with long-lasting memory. *Proc Natl Acad Sci U S A* **119**(2022).

58. Zagorulya, M.*, et al.* Tissue-specific abundance of interferon-gamma drives regulatory T cells to restrain DC1-mediated priming of cytotoxic T cells against lung cancer. *Immunity* **56**, 386-405 e310 (2023).
59. Cachot, A.*, et al.* Tumor-specific cytolytic CD4 T cells mediate immunity against human cancer. *Sci Adv* **7**(2021).
60. Oh, D.Y.*, et al.* Intratumoral CD4(+) T Cells Mediate Anti-tumor Cytotoxicity in Human Bladder Cancer. *Cell* **181**, 1612-1625 e1613 (2020).
61. Borst, J., Ahrends, T., Babala, N., Melief, C.J.M. & Kastenmuller, W. CD4(+) T cell help in cancer immunology and immunotherapy. *Nat Rev Immunol* **18**, 635-647 (2018).
62. Reticker-Flynn, N.E.*, et al.* Lymph node colonization induces tumor-immune tolerance to promote distant metastasis. *Cell* **185**, 1924-1942 e1923 (2022).
63. Nunez, N.G.*, et al.* Tumor invasion in draining lymph nodes is associated with Treg accumulation in breast cancer patients. *Nat Commun* **11**, 3272 (2020).
64. Kos, K.*, et al.* Tumor-educated T(regs) drive organ-specific metastasis in breast cancer by impairing NK cells in the lymph node niche. *Cell Rep* **38**, 110447 (2022).
65. Deng, L.*, et al.* Accumulation of foxp3+ T regulatory cells in draining lymph nodes correlates with disease progression and immune suppression in colorectal cancer patients. *Clin Cancer Res* **16**, 4105-4112 (2010).
66. van Pul, K.M.*, et al.* Local delivery of low-dose anti-CTLA-4 to the melanoma lymphatic basin leads to systemic T(reg) reduction and effector T cell activation. *Sci Immunol* **7**, eabn8097 (2022).
67. Binnewies, M.*, et al.* Unleashing Type-2 Dendritic Cells to Drive Protective Antitumor CD4(+) T Cell Immunity. *Cell* **177**, 556-571 e516 (2019).
68. Vick, S.C., Kolupaev, O.V., Perou, C.M. & Serody, J.S. Anti-PD-1 Checkpoint Therapy Can Promote the Function and Survival of Regulatory T Cells. *J Immunol* **207**, 2598-2607 (2021).
69. Perry, J.A.*, et al.* PD-L1-PD-1 interactions limit effector regulatory T cell populations at homeostasis and during infection. *Nat Immunol* **23**, 743-756 (2022).
70. Tan, C.L.*, et al.* PD-1 restraint of regulatory T cell suppressive activity is critical for immune tolerance. *J Exp Med* **218**(2021).
71. Kamada, T.*, et al.* PD-1(+) regulatory T cells amplified by PD-1 blockade promote hyperprogression of cancer. *Proc Natl Acad Sci U S A* **116**, 9999-10008 (2019).
72. Wakiyama, H.*, et al.* Treg-Dominant Tumor Microenvironment Is Responsible for Hyperprogressive Disease after PD-1 Blockade Therapy. *Cancer Immunol Res* **10**, 1386-1397 (2022).
73. Kumagai, S.*, et al.* The PD-1 expression balance between effector and regulatory T cells predicts the clinical efficacy of PD-1 blockade therapies. *Nat Immunol* **21**, 1346-1358 (2020).
74. Blomberg, O.S.*, et al.* Neoadjuvant immune checkpoint blockade triggers persistent and systemic T(reg) activation which blunts therapeutic efficacy against metastatic spread of breast tumors. *Oncoimmunology* **12**, 2201147 (2023).
75. Kurose, K.*, et al.* Phase Ia Study of FoxP3+ CD4 Treg Depletion by Infusion of a Humanized Anti-CCR4 Antibody, KW-0761, in Cancer Patients. *Clin Cancer Res* **21**, 4327-4336 (2015).
76. Rech, A.J.*, et al.* CD25 blockade depletes and selectively reprograms regulatory T cells in concert with immunotherapy in cancer patients. *Sci Transl Med* **4**, 134ra162 (2012).
77. Zappasodi, R.*, et al.* Rational design of anti-GITR-based combination immunotherapy. *Nat Med* **25**, 759-766 (2019).
78. Diab, A.*, et al.* A Phase I, Open-Label, Dose-Escalation Study of the OX40 Agonist Ivuxolimab in Patients with Locally Advanced or Metastatic Cancers. *Clin Cancer Res* **28**, 71-83 (2022).
79. Itahashi, K.*, et al.* BATF epigenetically and transcriptionally controls the activation program of regulatory T cells in human tumors. *Sci Immunol* **7**, eabk0957 (2022).
80. Shan, F.*, et al.* Integrated BATF transcriptional network regulates suppressive intratumoral regulatory T cells. *Sci Immunol* **8**, eadf6717 (2023).
81. Dykema, A.G.*, et al.* Lung tumor-infiltrating T(reg) have divergent transcriptional profiles and function linked to checkpoint blockade response. *Sci Immunol* **8**, eadg1487 (2023).
82. Van Damme, H.*, et al.* Therapeutic depletion of CCR8(+) tumor-infiltrating regulatory T cells elicits antitumor immunity and synergizes with anti-PD-1 therapy. *J Immunother Cancer* **9**(2021).
83. Campbell, J.R.*, et al.* Fc-Optimized Anti-CCR8 Antibody Depletes Regulatory T Cells in Human Tumor Models. *Cancer Res* **81**, 2983-2994 (2021).
84. Weaver, J.D.*, et al.* Differential expression of CCR8 in tumors versus normal tissue allows specific depletion of tumor-infiltrating T regulatory cells by GS-1811, a novel Fc-optimized anti-CCR8 antibody. *Oncoimmunology* **11**, 2141007 (2022).
85. Watson, M.J.*, et al.* Metabolic support of tumour-infiltrating regulatory T cells by lactic acid. *Nature* **591**, 645-651 (2021).
86. Kumagai, S.*, et al.* Lactic acid promotes PD-1 expression in regulatory T cells in highly glycolytic tumor microenvironments. *Cancer Cell* **40**, 201-218 e209 (2022).
87. Lim, S.A.*, et al.* Lipid signalling enforces functional specialization of T(reg) cells in tumours. *Nature* **591**, 306-311 (2021).

88. Cantini, L.*, et al.* High-intensity statins are associated with improved clinical activity of PD-1 inhibitors in malignant pleural mesothelioma and advanced non-small cell lung cancer patients. *Eur J Cancer* **144**, 41-48 (2021).
89. Cantini, L., Pecci, F., Dammeijer, F., Aerts, J. & Berardi, R. Re: Comments on 'High-intensity statins are associated with improved clinical activity of programmed cell death protein 1 inhibitors in malignant pleural mesothelioma and advanced non-small cell lung cancer patients'. *Eur J Cancer* **153**, 267-269 (2021).
90. Kim, M.J.*, et al.* Deletion of PD-1 destabilizes the lineage identity and metabolic fitness of tumor-infiltrating regulatory T cells. *Nat Immunol* **24**, 148-161 (2023).
91. Cattaneo, C.M.*, et al.* Tumor organoid-T-cell coculture systems. *Nat Protoc* **15**, 15-39 (2020).
92. Voabil, P.*, et al.* An ex vivo tumor fragment platform to dissect response to PD-1 blockade in cancer. *Nat Med* **27**, 1250-1261 (2021).
93. Thommen, D.S. Tumour avatars to model patients' responses to immunotherapy. *Nat Rev Cancer* **22**, 660 (2022).

Encore

Encore 1

English Summary

English Summary

Cancer is one of the leading causes of death and the global burden of cancer is predicted to increase to approximately 30 million new cases by 2040. The development of cancer is characterized by genomic instability causing mutations and structural alterations in genes, which eventually results in uncontrolled cell growth. To target these rapidly growing and dividing tumor cells, the most recommended conventional treatment strategies encompass chemotherapy, radiotherapy or targeted therapies, such as tyrosine kinase inhibitors. Since the last decade, a different type of therapy, termed immunotherapy, has created a monumental breakthrough in cancer treatment. Instead of directly targeting rapidly growing and dividing tumor cells, immunotherapy modulates components of the immune system to install effective immunosurveillance. The immune system surveys the body for tumor cells as it does for infections with pathogens like bacteria and viruses. Due to the fundamental role of the immune system in controlling the development of cancer, tumor cells acquire different mechanisms to hijack and suppress the immune system to prevent their elimination. For example, tumor cells can hide from the immune system or can create a suppressive local environment that prevents immune cells from entering the tumor site or their functioning. The success of immunotherapy relies on overcoming these barriers and to effectively activate the immune system. Indeed, immunotherapy has achieved impressive clinical responses in multiple types of cancer, however, only a fraction of patients responds durably to treatment. To improve the understanding of the interplay between immune cells and cancer and enhance the fraction of responding patients, extensive research has focused on the tumor site and the local interactions with the immune system. Despite these efforts, it is increasingly recognized that the disease extends beyond tumor cells and their local immune environment as the immune landscape undergoes alterations more globally and affects functional and compositional immune-related changes in lymph nodes, bone marrow, spleen, and gut. Therefore, to more effectively combat cancer, it is of paramount importance to understand the systemic requirements for an effective immune response. Having a more holistic vision encompassing the tumor macroenvironment could offer avenues for improving the efficacy of existing immunotherapies and pave the way for the development of novel immunotherapies.

Novel perspectives on the mode of action and mechanisms of resistance to immune checkpoint blockade

T cells play a central role in the immune system as they are responsible for recognizing and attacking foreign invaders, including tumor cells as they differ slightly from healthy cells. The activation of T cells is a highly regulated process to ensure effective immune responses while preventing the attack on the body's own cells. Following T cell activation, the expression of programmed cell death protein 1 (PD-1) is upregulated on the cell surface of T cells. The main physiological function of PD-1 is to dampen T cell activation by sending inhibitory signals when binding to its ligand protein PD-L1, thereby functioning as an immune checkpoint. In the context of cancer, tumor

cells exploit PD-1/PD-L1 signaling to dampen T cell activation, thereby promoting the survival of tumor cells. Immune checkpoint blockers (ICB) as immunotherapy prevent the binding of PD-1 with their partner proteins. This releases the molecular brakes in T cells, allowing them to kill tumor cells. The introduction of ICB has been an important achievement in cancer treatment. Despite the success of ICB for multiple types of cancer, the majority of patients, however, does not durably respond to treatment. **Part A** of this thesis delves into novel perspectives on the mechanism of action and resistance associated with ICB. Due to the PD-L1 expression on tumor cells, the longstanding paradigm is that the efficacy of ICB is attributed to its impact on T cells at the tumor site. However, the value of using PD-L1 expression on tumor cells as a predictive biomarker for ICB appeared limited for the majority of tumor types and the therapeutic relevance of PD-L1 at other sites remains unknown. In **Chapter 2**, we studied whether tumor-draining lymph nodes (TDLNs) are involved in ICB efficacy. TDLNs have a central role in anti-tumor immunity as T cells are activated to tumor antigens in TDLNs followed by migration to the tumor site to kill tumor cells. The PD-1/PD-L1 axis appeared to be greatly present in the TDLN with high levels of PD-1 on T cells directed to tumor antigens together with abundant PD-L1 expression. In order to study whether PD-1 to PD-L1 binding in the TDLN is important in determining therapy response, we developed a system in mouse tumor models to prevent these interactions in the TDLN using ICB without affecting other sites. This selective approach enhanced the immune response to tumor cells by activating T cells in the TDLN that subsequently migrate to the tumor, indicating that the TDLN is an important target for ICB. This response was no longer observed when migration of T cells from the TDLN to the tumor was prevented, further underlining the importance of TDLN in ICB efficacy. As clinical translation of our findings, we revealed that the level of PD-1 to PD-L1 binding in the TDLN is also important in determining whether patients with melanoma were likely to have metastasis in the future (e.g. disease recurrence). To further establish the role of the TDLN in the process of disease recurrence beyond the PD-1/PD-L1 axis, we studied in **Chapter 3** more in detail how the immune composition of the TDLN correlates to disease recurrence. We revealed that patients with disease recurrence have increased expression of suppressive proteins in the TDLN compared with patients without disease recurrence. Using a novel imaging technique, we discovered that these differences were found at sites distant from the metastasis in the TDLN while the regions close to the tumor cells were rather similar.

The ultimate goal of ICB is to release the break from T cells, thereby allowing T cells to more effectively kill tumor cells. Yet, not all T cells are focused on eliminating tumor cells. A subset of T cells, regulatory T cells (Tregs), suppresses the immune system and provides protection to tumor cells. As PD-1 is also highly expressed on this subset, ICB could potentially impact this Treg subset which could have a negative impact on therapeutic outcome. In **Chapter 4**, we examined the impact of ICB on the function of Tregs and their involvement in mediating therapy resistance. Tregs demonstrated an increased capacity to suppress the immune system after ICB, especially notable in mouse tumor models that are not responding to ICB. To investigate the contribution of Treg

activation to therapy resistance, we selectively depleted this suppressive subset in combination with ICB. Indeed, Treg depletion reversed therapy resistance by sensitizing mice with mesothelioma to the effects of ICB. These observations extended beyond the murine setting, as we noted that Tregs in tumor tissue and peripheral blood of patients treated with ICB were more activated, particularly in patients not responding to therapy. This underscores that ICB can also have negative effects on the immune system by activating Tregs and suggests that patients not responding to ICB might benefit from Treg-directed therapies.

Enhancing cancer vaccine efficacy through combined immunotherapy strategies

In addition to ICB, cancer vaccines are another promising type of immunotherapy, intending to educate the immune system to recognize and eliminate tumor cells. Dendritic cells (DCs) play an essential role in the mechanism of these vaccines as DCs possess the capability to capture and present various antigens, including those derived from tumors. Through antigen presentation, DCs instruct T cells to eliminate potential harmful non-self particles and cells, establishing them as central regulators of immune responses. However, the quantity and/or functionality of DCs are often compromised in the context of cancer, leading to weakened immune responses directed against tumor cells. Cancer vaccines are designed to enhance the activation of T cells by DCs and can be categorized into different classes, such as peptide vaccines and cellular vaccines. A type of cellular vaccine is DC therapy, where DCs are produced from patient's blood, loaded with tumor antigens and then reintroduced into the patient. Although cancer vaccines are able to induce effective anti-tumor T cell responses, the majority of treated patients does not respond clinically or only temporarily. In **Part B** of this thesis, we investigated whether the efficacy of cancer vaccines can be enhanced through combination with therapies that neutralize mechanisms that may diminish the effectiveness of cancer vaccines which are reviewed in **Chapter 5**. T cells activated by cancer vaccines need to infiltrate the tumor site to effectively eliminate tumor cells and their effectiveness can be hampered by the abundance of PD-L1 at the tumor site. To overcome this hurdle, we explored ICB with DC therapy in mouse models and patients with mesothelioma in **Chapter 6.** In patients with mesothelioma, ICB treatment after DC therapy resulted in promising survival responses. Combining ICB with DC therapy significantly improved survival and enhanced T cell activation in mice with mesothelioma compared with DC therapy alone. Notably, this improvement was, in part, associated with the TDLN, as blockade between PD-1 and PD-L1 specifically in the TDLN using aforementioned strategy produced outcomes nearly as effective as systemic ICB treatment.

In addition to the PD-1/PD-L1 axis, targeting other pathways that hinder optimal T cell activation could enhance the efficacy of cancer vaccines. Janus kinase 3 (JAK3) plays a crucial role in signaling pathways responding to various cytokines in immune cells like macrophages and T cells. In **Chapter 7**, we investigated the impact of a specific JAK3 inhibitor on macrophages and T cells and its therapeutic potential when combined with peptide vaccination and DC therapy. Prolonged JAK3 inhibition positively influenced T cells by improving their activation within tumors. Notably,

combining JAK3 inhibition with a peptide vaccine and DC therapy further enhanced these responses in mouse models and resulted in reduced tumor weight. These results identify the inhibition of JAK3 as an promising approach for combination immunotherapy although the potential benefit of this approach remains to be investigated in patients.

The results of this thesis are put into perspective in **Chapter 8**. Together, the results presented in this thesis provide novel and important insights in the mode of action and mechanisms of resistance to immunotherapies, with a focus on ICB (anti-PD-1/PD-L1) and cancer vaccines (DC therapy). Importantly, these findings highlight that the effectiveness of immune responses directed at tumor cells is shaped by the intricate interactions among multiple tissues, rather than being exclusively dictated by conditions at the tumor site. These insights could offer novel avenues for improving existing strategies and could pave the way for the emergence of novel immunotherapies. To propel these developments, future research should be directed to more in-depth characterization of the role of tissues beyond the tumor site in establishing anti-tumor immunity, with a focus on the TDLN. In parallel, finding selective therapeutic targets in Tregs to mitigate the activating effect of ICB on Tregs could be pivotal to optimize ICB efficacy in a subset of patients. Achieving these goals requires robust collaboration among biomedical scientists, clinicians, and bioinformaticians. This collaborative effort is essential for advancing the percentage of patients who can benefit optimally from immunotherapy.

Encore 2

Nederlandse Samenvatting

Nederlandse Samenvatting

Kanker is een van de belangrijkste doodsoorzaken en het aantal nieuwe gevallen van patiënten met kanker zal wereldwijd stijgen tot ongeveer 30 miljoen in 2040. De ontwikkeling van kanker wordt gekenmerkt door veranderingen in het genoom, wat uiteindelijk leidt tot ongecontroleerde celgroei. Om deze snelgroeiende en delende tumorcellen aan te pakken bestaan de meest aanbevolen conventionele behandelingen uit chemotherapie, radiotherapie of gerichte therapieën, zoals tyrosinekinaseremmers. Sinds het afgelopen decennium heeft een ander type behandeling, genaamd immuuntherapie, een doorbraak gecreëerd in de behandeling van kanker. In plaats van zich primair te richten op snelgroeiende en delende tumorcellen, richt immuuntherapie zich op het moduleren en activeren van het immuunsysteem. Het immuunsysteem patrouilleert het lichaam op de aanwezigheid van tumorcellen zoals het dat doet voor bacteriële en virale infecties. Gezien de fundamentele rol van het immuunsysteem bij het onderdrukken van de ontwikkeling van kanker hebben tumorcellen verschillende manieren ontwikkeld om het immuunsysteem te omzeilen. Zo kunnen tumorcellen zich camoufleren voor het immuunsysteem of een omgeving creëren die voorkomt dat immuun cellen de tumor binnendringen of hun functie goed kunnen uitvoeren. Het succes van immuuntherapie hangt af van het dusdanig activeren van het immuunsysteem, waardoor het in staat is deze barrières te overwinnen. De introductie van immuuntherapie heeft geresulteerd in indrukwekkende klinische reacties bij meerdere soorten kanker, maar slechts een fractie van de behandelde patiënten reageert duurzaam op de behandeling. Veel onderzoek is gericht op het begrijpen van wat er zich afspeelt in de tumor en de lokale interacties met het immuunsysteem, met als doel het aantal patiënten dat effectief reageert op immuuntherapie te vergroten. Ondanks deze inspanningen wordt steeds meer erkend dat kanker niet alleen de tumorcellen en hun lokale omgeving beïnvloedt. Zo ondergaat het immuunsysteem systemische veranderingen tijdens de groei van de tumor en wordt de samenstelling en functie van andere organen, zoals de milt, darm, beenmerg en lymfeklieren ook beïnvloed. Om die reden is het van groot belang om een meer holistische visie te ontwikkelen, zodat er een beter begrip ontstaat over de totstandkoming van een effectieve immuunrespons tegen de tumor. Dit zou bestaande immunotherapieën kunnen verbeteren en de ontwikkeling van nieuwe soorten immuuntherapie kunnen bevorderen.

Nieuwe inzichten in de werkingswijze van ICB antistoffen

T cellen spelen een centrale rol in het immuunsysteem doordat ze verantwoordelijk zijn voor het herkennen en aanvallen van lichaamsvreemde stoffen, waaronder tumorcellen, aangezien deze enigszins verschillen van gezonde cellen. De activering van T cellen is een sterk gereguleerd proces om een effectieve immuunreactie te kunnen genereren zonder dat het lichaamseigen cellen gaat aanvallen. Na activatie van T cellen wordt de expressie van het eiwit PD-1 op het celoppervlak verhoogd om zo de T cel activatie weer te dempen. Deze dempende functie van PD-1 komt tot stand wanneer deze bindt aan zijn bindingpartner PD-L1. In de context van kanker maken tumorcellen misbruik van deze interactie door aanzienlijke hoeveelheden PD-L1 tot expressie te brengen. Dit

vermindert de activatie van T cellen, waardoor tumorcellen kunnen overleven. Een veelvoorkomende vorm van immuuntherapie is het gebruik van antilichamen, bekend als ICB antilichamen, die de binding tussen PD-1 en PD-L1 voorkomen. Hierdoor wordt de moleculaire rem opgeheven in de T cellen, waardoor ze beter in staat zijn in het doden van tumorcellen. De introductie van deze ICB antistoffen is een belangrijke stap geweest in de behandeling van patiënten met kanker. Ondanks het succes van deze therapie voor meerdere soorten kanker reageert de meerderheid van de patiënten niet duurzaam op de behandeling. **Deel A** van dit proefschrift richt zich op nieuwe inzichten in de werkingswijze en locaties van ICB antilichamen, evenals de mechanismen die verantwoordelijk zijn voor resistentie tegen deze therapie. Vanwege de hoge expressie van PD-L1 op tumorcellen werd lange tijd aangenomen dat de effectiviteit van ICB antistoffen uitsluitend wordt toegeschreven aan de impact op T cellen in de tumor. Echter, deze PD-L1 expressie op tumorcellen blijkt van beperkte waarde bij het voorspellen of een patiënt gaat reageren op ICB antistoffen. Dit suggereert dat PD-L1 expressie op andere cellen of andere locaties dan de tumor ook van belang is in het bewerkstelligen van een immuunreactie na behandeling. In **Hoofdstuk 2** hebben we onderzocht of lymfeklieren die zich dicht in de buurt van de tumor bevinden (tumor-drainerende lymfeklieren) betrokken zijn bij de werkzaamheid van ICB antistoffen. Tumor-drainerende lymfeklieren spelen een centrale rol bij de immuunreactie tegen tumoren, aangezien hier de eerste stap wordt gezet in de activatie van T cellen tegen de tumor. Onze resultaten lieten zien dat er een hoge expressie was van zowel PD-1 als PD-L1 in de tumor-drainerende lymfeklieren, met een hoge expressie van PD-1 op T cellen gericht tegen de tumor, samen met een hoge PD-L1 expressie. Om te onderzoeken of bindingen tussen PD-1 en PD-L1 in deze lymfeklieren van belang zijn voor de respons op ICB antistoffen ontwikkelden we een systeem waarbij de binding tussen PD-1 en PD-L1 werd verbroken in de tumor-drainerende lymfeklier zonder andere weefsels te beïnvloeden, zoals de tumor zelf. Deze selectieve therapie resulteerde in een toename van geactiveerde T cellen in de tumor-drainerende lymfeklieren, die vervolgens naar de tumor migreerden en daar in grotere aantallen aanwezig waren. Wanneer de T cellen in de tumor-drainerende lymfeklier niet meer in staat waren uit de lymfeklier naar de tumor te migreren werd het effect van ICB antistoffen op de tumor teniet gedaan. Dit impliceert dat de tumor-drainerende lymfeklier een belangrijk doelwit is voor ICB antistoffen. Deze resultaten bleken ook van waarde in klinische setting aangezien in patiënten met huidkanker een hoge hoeveelheid bindingen tussen PD-1 en PD-L1 in de tumor-drainerende lymfeklier gecorreleerd was met de ontwikkeling van uitzaaiingen. In patiënten die geen uitzaaiingen ontwikkelden waren deze bindingen in mindere mate aanwezig. Om de rol van de tumor-drainerende lymfeklier in het proces van uitzaaiing verder te onderbouwen, hebben we in **Hoofdstuk 3** de samenstelling van het immuunsysteem in de tumor drainerende lymfeklier op een gedetailleerde niveau bestudeerd en de correlatie ervan met het ontwikkelen van uitzaaiingen onderzocht. We zagen in patiënten die uitzaaiingen ontwikkelden een verhoogde expressie van eiwitten die het immuunsysteem afremmen in de tumor-drainerende lymfeklieren in vergelijking met patiënten zonder deze ontwikkeling. Met behulp van een nieuwe techniek ontdekten we dat deze verschillen werden gevonden op locaties op afstand van de tumorcellen in de tumor-drainerende lymfeklier. De regio's dicht bij de tumorcellen waren echter meer vergelijkbaar.

Zoals eerder benoemd, is het uiteindelijke doel van ICB antistoffen om de T cellen zodanig te activeren dat ze tumorcellen effectiever kunnen aanvallen. Echter zijn niet alle T cellen gespecialiseerd in het elimineren van tumorcellen. Een deel van T cellen, de regulatoire T cellen (Tregs), heeft juist als functie om het immuunsysteem te onderdrukken en biedt daarmee bescherming aan tumorcellen. Aangezien PD-1 ook sterk tot expressie komt op deze subset, zouden ICB antistoffen ook mogelijk invloed kunnen hebben op Tregs, wat de therapeutische respons negatief kan beïnvloeden. In **Hoofdstuk 4** onderzochten we het effect van ICB antistoffen op de functie van Tregs en hun rol bij het ontstaan van resistentie tegen ICB antistoffen. Na therapie zagen we dat Tregs beter in staat waren het immuunsysteem af te remmen, met name in muismodellen die niet reageerden op de behandeling met ICB antistoffen. Ook in patiënten bleek dat Tregs in de tumor en bloed actiever waren na behandeling met ICB antistoffen, vooral bij patiënten die niet reageerden op de behandeling. Wanneer deze Tregs therapeutisch werden verwijderd uit muizen met mesothelioom zagen we dat de behandeling met ICB antistoffen wel effectief was. Deze resultaten benadrukken dat ICB antistoffen ook een nadelig effect kunnen hebben middels de activatie van Tregs, wat vervolgens resulteert in een slechte respons op de behandeling met ICB antistoffen. Patiënten met een beperkte respons op ICB antistoffen zouden mogelijk baat kunnen hebben bij nieuwe behandelingen die gericht zijn op Tregs om het activerende effect van ICB antistoffen op Tregs te voorkomen.

Effectiviteit van tumor vaccins verhogen door middel van combinatietherapieën

Een andere soort immuuntherapie die veelbelovend is, is het gebruik van tumor vaccins. Deze vaccins zijn gericht op trainen van immuuncellen om kankercellen aan te vallen. Dendritische cellen (DCs) spelen een essentiële rol in de werking van deze vaccins, aangezien DCs de capaciteit hebben om eiwitten afkomstig van tumorcellen op te nemen en te presenteren aan het immuunsysteem. Door deze presentatie van eiwitten aan T cellen zijn DCs in staat om T cellen te activeren en hen te informeren over hoe de tumor eruitziet, wat uiteindelijk resulteert in de eliminatie van tumorcellen. DCs hebben daardoor een centrale rol in het bewerkstellen van een immuunreactie tegen de tumor maar de kwaliteit en/of functionaliteit van deze DCs is vaak aangetast in de context van kanker. Tumor vaccins zijn ontworpen om de activatie van T cellen door DCs te verbeteren en kunnen worden ingedeeld in verschillende klassen, zoals peptide vaccins en cellulaire vaccins. Onder cellulaire vaccins valt onder andere DC therapie, waarbij DCs worden geproduceerd uit het bloed van de patiënt, geladen met tumordeeltjes en vervolgens opnieuw in de patiënt worden geïntroduceerd. Hoewel tumor vaccins in staat zijn om effectieve en langdurige T cel reacties op te wekken tegen de tumor, reageert de meerderheid van behandelde patiënten niet of slechts tijdelijk. In **Deel B** van dit proefschrift hebben we onderzocht of de effectiviteit van tumor vaccins kan worden verhoogd door middel van combinatie met therapieën die gericht zijn op het neutraliseren van mechanismen die de effectiviteit van tumor vaccins kunnen verminderen zoals besproken in **Hoofdstuk 5.** Om tumorcellen effectief aan te kunnen vallen moeten T cellen, die in lymfeklieren geactiveerd zijn door DCs, in staat zijn om hun functie uit te oefenen wanneer ze de tumor binnendringen. Deze functie

kan echter belemmerd worden door de eerdergenoemde expressie van PD-L1 op tumorcellen. Om deze potentiële belemmering aan te pakken, onderzochten we de blokkade van de PD-1/PD-L1-as met behulp van ICB antistoffen in combinatie met DC therapie in **Hoofdstuk 6.** Het gebruik van ICB antistoffen na DC therapie in patiënten met mesothelioom resulteerde in veelbelovende klinische responsen. Het combineren van ICB antistoffen met DC therapie verbeterde de overleving aanzienlijk en verhoogde de activatie van T cellen in muizen met mesothelioom in vergelijking met DC therapie alleen. Deze verbetering bleek geassocieerd te zijn met de tumor-drainerende lymfeklier, aangezien het blokkeren van PD-1 en PD-L1 interacties enkel in de tumor-drainerende lymfeklieren bijna net zo effectief was als systemische behandeling met ICB antistoffen. Naast PD-1 en PD-L1 interacties kunnen andere mechanismen ook betrokken zijn het belemmeren van optimale T cel activatie en daarmee de effectiviteit van tumor vaccins. Janus kinase 3 (JAK3) wordt tot expressie gebracht in immuun cellen zoals macrofagen en T cellen. In **Hoofdstuk 7** onderzochten we de impact van een specifieke JAK3-remmer op macrofagen en T cellen en het therapeutische potentieel ervan bij gecombineerd gebruik met peptide vaccins en DC therapie. Langdurige JAK3-remming had een positieve invloed op T cellen door hun activatie in tumoren te verhogen. Dit effect werd verder versterkt bij het combineren van JAK3-remming met een peptide vaccin en DC therapie, wat resulteerde in verminderd tumorgewicht in muismodellen. Deze resultaten wijzen op de remming van JAK3 als een veelbelovende benadering, hoewel het potentiële voordeel van deze aanpak nog nader onderzocht moet worden.

In **Hoofdstuk 8** worden de resultaten van dit proefschrift in perspectief geplaatst, wat nieuwe inzichten biedt in de werking van immuuntherapie, evenals de mechanismen die resistentie tegen immuuntherapie kunnen veroorzaken. Deze inzichten benadrukken dat de kwaliteit van immuunreacties tegen de tumor niet alleen wordt bepaald door effecten in de tumor zelf, maar ook door processen in organen verder gelegen van de tumor. In toekomstig onderzoek zal het belangrijk zijn om de rol van het immuunsysteem in het tot stand brengen van anti-tumor immuniteit in weefsels buiten de tumor verder in kaart te brengen, met een focus op de tumor-drainerende lymfeklier. Tegelijkertijd kan het vinden van een therapeutische target in Tregs van belang zijn voor patiënten die slecht reageren op behandeling met ICB antistoffen. Uiteindelijk zouden deze inspanningen mogelijkheden kunnen bieden om bestaande immunotherapieën te verbeteren en bij te dragen aan de ontwikkeling van nieuwe vormen van immuuntherapie. Voor deze vooruitgang is een effectieve samenwerking tussen biomedische wetenschappers, clinici en bioinformatici noodzakelijk, met als doel het vergroten van het percentage patiënten dat effectief kan worden behandeld met immuuntherapie.

Encore 3

Dankwoord

Dankwoord

En zo komt deze fantastische en uitdagende periode bijna tot een einde. Ondanks dat mijn naam op dit proefschrift staat, is dit werk een reflectie van de inspanning van velen. Veel bijzondere mensen hebben hun bijdrage geleverd aan dit proefschrift, ieder op hun eigen manier. Graag zou ik een aantal personen specifiek willen uitlichten zonder wiens inspanning dit proefschrift niet tot stand zou zijn gekomen.

Promotieteam

Graag wil ik mijn promotoren en copromotor bedanken voor hun bijdrage aan dit boekje en mijn ontwikkeling als wetenschapper. **Prof.dr. Aerts,** beste **Joachim.** Vanaf het allereerste moment dat ik onder jouw vleugels begon als PhD student heb ik de vrijheid gekregen om me te ontwikkelen als onafhankelijke wetenschapper. Door de jaren heen heb jij me gestimuleerd en losgelaten om alle uitdagende proeven uit te voeren die nodig waren voor de meest creatieve onderzoeksvragen. Deze vrije aanpak is echter nooit gepaard gegaan met het gevoel dat ik er alleen voor sta aangezien ik altijd binnen no time bij je terecht kan voor de meest uiteenlopende vragen en gesprekken. Waar ik af en toe kan twijfelen aan mijn eigen kwaliteiten, heb jij altijd het volste vertrouwen in mij. De combinatie van het loslaten en dit vertrouwen heeft mij veel gebracht in mijn ontwikkeling als wetenschapper en persoon. Ik hoop dat onze samenwerking nog vele jaren zal blijven continueren als preklinische Postdoc in de THORR groep. **Prof.dr. Van Hall,** beste **Thorbald,** waar Joachim altijd hamerde op de klinische relevantie, focuste jij je meer op de biologische relevantie. Jullie vormden voor mij dan ook het perfecte promotor duo. Bij jou kon ik altijd terecht voor de meest gedetailleerde immunologische vraagstukken en wist jij altijd een kritische en terechte toevoeging te leveren aan proefopzetten. Tegelijkertijd heb ik veel geleerd van jouw gave om een verhaal pakkend en bondig op te schrijven. Jouw diepgaande kennis en ervaring hebben een grote bijdrage geleverd aan de successen die we hebben behaald als team, waarvoor veel dank. Beste **Floris**, van stagebegeleider naar copromotor! De combinatie van je talent, ontembare energie en enthousiasme, creativiteit en de kunst om ieder (wetenschappelijk) verhaal net iets aantrekkelijker te maken, maakt jou een wetenschapper pur sang. In de afgelopen jaren heb ik hier veel van kunnen leren en ik ben dan ook trots op onze samenwerking. Voor mij wordt deze samenwerking gekenmerkt door humor, hard werken en tegenstrijdigheden welke de drijfveer vormen van ons succes als team. Met jou als de optimistische en chaotische creatieveling en met mij als de realistische en georganiseerde perfectionist zijn we in staat om diepgang en kwaliteit te leveren aan ieder project. Je bent er altijd voor me, ook buiten wetenschappelijke context. Ik waardeer je ontzettend als persoon en wetenschapper en ik hoop dat we nog lang kunnen samenwerken! Tevens wil ik graag de leden van de kleine commissie bedanken voor het kritisch lezen en becommentariëren van mijn proefschrift, dank **Prof.dr. Reno Debets, Prof. dr. Karin de Visser** en **Prof.dr. Tanja de Gruijl.** Graag wil ik ook de leden van mijn promotiecommissie bedanken voor het doorlezen van mijn proefschrift en de bereidwilligheid om deel te nemen aan mijn verdediging. Ik hoop dat het een mooie discussie gaat worden!

Prof.dr. Hendriks, beste **Rudi.** Jouw passie voor wetenschap gecombineerd met je kritische blik werkt aanstekelijk en heeft mij vaak aan het denken gezet hoe we het onderzoek kwalitatief nog naar een hoger niveau konden tillen. Dank voor alle inspiratie, waardevolle input en dat ik al deze jaren op de afdeling heb mogen werken.

Paranimfen

Collega's komen en gaan, maar soms ontmoet je collega's waarmee de band uitgroeit tot een vriendschap. Het is dan ook van onschatbare waarde dat deze personen met je kunnen toeleven naar dit bijzondere moment en naast je staan als paranimfen tijdens de verdediging. Lieve **Denise**, jij bent een van de belangrijkste steunpilaren geweest tijdens mijn promotie. Jij wist vaak bij mij de scherpe randjes eraf te halen door een luisterend oor te bieden tijdens momenten van zorgen en frustratie. Tegelijkertijd was je ook de liefste persoon met wie ik elke overwinning, hoe klein ook, kon vieren. Ik ben dankbaar dat onze band niet is verzwakt toen je het lab verliet en dat we tot op de dag van vandaag nog steeds onze successen samen vieren, genieten van heerlijke diners en neerploffen op de bank voor een slechte serie of een goed gesprek. Je hebt een hart van goud en ik ben heel trots op hoe jij je de afgelopen tijd hebt ontwikkeld. Ik hoop dat ik nog lang kan genieten van jou als vriendin! Lieve **Marcella**, vanaf het allereerste moment zijn wij twee handen op één buik geweest. Wij spreken dezelfde taal, al zijn woorden vaak niet eens nodig en begrijpen we elkaars gedachten met slechts een simpele blik. Doordat wij zo op één lijn zitten, zijn de congressen - en de daaropvolgende vakanties - in Frankrijk, Canada en Amerika de hoogtepunten van mijn promotie die ik met niemand anders had willen meemaken. Ik bewonder hoe je iedere uitdaging (en vaak meerdere tegelijk) vol aanpakt en tegelijkertijd met beide benen op de grond kan blijven staan. Ik ben dan ook ontzettend blij dat jij niet alleen tijdens mijn verdediging naast mij staat, maar ook tijdens alle andere successen en uitdagingen in de afgelopen tijd. Ik hoop dat onze band zo blijft en dat we samen nog veel mooie momenten mee gaan maken!

De THORR groep

De afdeling Longziekten, en met name de THORR groep, is voor mij vele jaren de plek geweest waar ik meer tijd heb doorgebracht dan waar dan ook. Het is dan ook geëvolueerd tot mijn wetenschappelijke thuisbasis: waar ik 7 jaar geleden begon als masterstudent, loop ik nu door de gangen als Postdoc. Het is dan ook een voorrecht om omringd te zijn met fijne collega's. Beste **Heleen**, jij was de eerste persoon met wie ik in contact kwam van de afdeling Longziekten. Dank voor je ondersteuning tijdens de eerste periode van mijn wetenschappelijke carrière, eerst als masterstudent en daarna als beginnend PhD student. Ik heb veel van je mogen leren. **Anneloes,** wat ontzettend fijn dat je mij zo hebt kunnen helpen met alle - voor mij onnavolgbare - bioinformatische analyses die een grote bijdrage hebben geleverd aan dit proefschrift. Je bent een ware wizard en ik vond het top om met je samen te werken! **Vivian,** ondanks dat onze persoonlijkheden zich bevinden aan ieder uiteinde van het spectrum, vind ik het heerlijk om je als collega te hebben. Je humor, enthousiasme en levensvisie zorgen voor een goede sfeer op het lab. Ik hoop dat ik je nog vaak al

mompelend in de vensterbank zal aantreffen tijdens een zonnige dag. Never change! Ciao **Luca**! Our relationship has evolved from three conversations a year to a friendship that I hope will endure in the years to come (no need to be too flattered now..). You are the perfect example of how to embrace life as one big crazy adventure, and I am grateful for all the great moments we have shared! **Bob** en **Joanne,** wij zijn rond dezelfde tijd begonnen in de THORR groep als PhD knurften. Naast het bespreken van de tragedie van een promotietraject kon ik altijd bij jullie terecht met klinische vraagstukken en zonder jullie bijdrage was dit proefschrift er niet geweest. Daarnaast heb ik veel met jullie kunnen lachen bij ons op kantoor en tijdens congressen. Veel succes met het afronden van jullie boekje! **Christianne,** je bent sinds kort begonnen bij ons op het lab als Postdoc en ik ben stiekem al fan van je geworden. Het is heerlijk om iemand in de groep te hebben die dezelfde 'no-nonsense' mentaliteit heeft. Op naar mooie samenwerkingen! **Sai Ping,** jouw bijzondere benadering van de wetenschap en het leven in het algemeen zorgden vaak voor de unieke combinatie van een lach en ongeloof. Succes met je klinische carrière! Gedurende mijn promotietraject heb ik een aantal studenten mogen begeleiden. **Robin, Alexis, Tim** en **Sabine**, jullie hebben allemaal op jullie eigen manier een bijdrage geleverd aan dit proefschrift. Dank! Ik wens jullie allemaal heel veel succes met jullie studie en toekomstige (wetenschappelijke) carrière. Sinds ruim een jaar heb ik ook de eer om een aantal PhD studenten te mogen begeleiden. Beste **Mike**, voor jou is echt niets te gek. Je was nog niet eens geregistreerd in Hora Finita of je had al tot 's avonds laat rebuttal experimenten uitgevoerd in Gent samen met mij, Floris en Sjoerd. Deze bereidwilligheid, gecombineerd met je leergierigheid, behulpzaamheid en je gevoel voor humor maken jou een ideale teamplayer en beloven veel goeds voor jouw wetenschappelijke carrière. Je bent een topper! Dear **Leila**, I admire your courage to start your PhD and rebuild your life in this foreign and cold country. With your motivation and enthusiasm, I hope that your time as a PhD student will be a great experience. I am looking forward to unravel the mysteries of DC therapy with you. We are in this together!

Dit proefschrift is zeker ook een reflectie van de kwaliteit van de analisten die onderdeel zijn/waren van de THORR groep. Beste **Menno**, jij hebt de gave om aan alles wat je doet een extra dimensie toe te voegen. Jouw schurende opmerkingen, abstracte humor en filosofische denkwijze maakten veel gesprekken los over de zin van het leven, in de breedste zin van het woord. Het is werkelijk nooit saai met jou en tegelijkertijd ben je een meester in het brengen van rust op chaotische dagen. Ik hoop dat ik nog lang met jou mag samenwerken! Lieve **Melanie**, terwijl ik dit schrijf, verschijnt er een grote glimlach op mijn gezicht. Wat kijk ik met een hoop plezier terug op onze tijd samen op het lab! Als een geschenk van boven kwam jij als analist terecht in onze groep toen ik net begon aan mijn promotietraject. Het feit dat wij door iedereen 'Mandelie' werden genoemd, geeft maar aan hoe onafscheidelijk wij waren. Je blijft me altijd verbazen met je wijsheid en positieve instelling en ik ben dan ook ontzettend blij dat je nog steeds in mijn leven bent als vriendin! **Larissa**, ondanks dat we je mailden met 'Davey' in de aanhef begon je vol enthousiasme bij ons in de groep als analist. Je was er een uit duizenden; er zijn maar weinig mensen die zo hard en met zulke precisie kunnen werken, wat resulteerde in een blind vertrouwen. We hebben samen kostelijk kunnen lachen om onder

andere het mini stikstofvat (en het bijbehorende personeel), de fiets tatoeage en het wijntje te veel tijdens een rebuttalexperiment. Bedankt voor alle mooie momenten! **Nina,** ik heb nog niet veel met je samen mogen werken maar ik kan altijd genieten van je enthousiasme en je sprankelende energie. Tegelijkertijd weet je wat hard werken is en ik hoop dat je nog lang bij ons blijft.

De afdeling Longziekten

De THORR groep is slechts een onderdeel van de gehele afdeling Longziekten en ook zij hebben een grote bijdrage geleverd aan dit poefschrift door hun ondersteuning en/of door het zijn van lotgenoten. **Ralph**, ik vraag me soms af hoe je het allemaal doet. Binnen no time heb je een grote en succesvolle onderzoeksgroep weten op te zetten. Vaak gaat zulk succes ten koste van persoonlijk contact, maar in jouw geval is niets minder waar. **Marjolein,** als labmama heeft jij mij vaak voorzien van goed advies, technische ondersteuning en een terechte kritische blik. Zonder jou was het lab nog een veel grotere chaos geweest. De deur staat altijd bij je open voor (last minute) vragen en ik wil je bedanken voor al je hulp en geduld. **Mieke, Lianne** en **Simone**, mijn gym bae's. Het is een wekelijkse routine geworden die hopelijk nog lang stand houdt. Dit is niet alleen vanwege het sportieve element, maar ook omdat deze momenten vaak gekenmerkt worden door hilarische gesprekken waar iedereen in de kleedkamer van kan meegenieten. Ook buiten de fitnessruimte vinden wij elkaar voor een 'wine and dine' avondje (laten we het daar maar op houden..). Op naar nog veel leuke momenten samen! **Stefan**, wij zijn echt lotgenoten aangezien wij ongeveer tegelijkertijd zijn begonnen aan de pracht en tragedie van een PhD en die nu doorzetten als Postdoc. Dank voor alle hilarische momenten, de knuffels en voor het creëren van een fijne sfeer in onze PhD groep. **Lieke**, ook jij brengt een hoop gezelligheid met je mee zowel op het lab, tijdens PhD weekenden als tijdens borrels. Je hebt nog even te gaan maar ik ben er van overtuigd dat je een mooi boekje gaat krijgen! **Bernard,** in de afgelopen jaren heb je enkele iconische memes gecreëerd, wat een positieve weerspiegeling is van je persoonlijkheid. Momenteel ben je druk bezig met het afronden van je promotieonderzoek, en dat lijkt net zo snel te gaan als het eten van brood. Heel veel succes met de laatste loodjes! **Odilia, Esmee, Niels, Anne** en **Thomas** en alle anderen op het lab, dank voor alle gezelligheid! **Jennifer, Ingrid, alle 'Pheravengers', Karolina, Margreet** en **Orisia,** dank voor alle ondersteuning en leuke momenten door de jaren heen. **Jasper**, dank voor alle leuke gesprekken, je uitgebreide kennis en voor het bewaren van je geduld tijdens de miljoenen vragen die ik op je afvuurde. **Jelle**, mede door jouw gevoel voor humor en je kwaliteit om bijzondere vragen te stellen is jouw aanwezigheid op het lab een memorabele periode geweest. Met niemand anders had ik dan ook het iconische PhD weekend willen organiseren. Ik vind het ontzettend tof dat jij, samen met **Paula**, bij mijn verdediging aanwezig kunt zijn! **Lisette**, jouw tijd op het lab herinner ik me als kort maar krachtig. Op de meest positieve manier heb jij wat stof (letterlijk) doen opwaaien en bracht je een hoop gezelligheid met je mee. Dank voor alle leuke momenten! **Pauline, Irma, Peter, Simar, Madelief, Mirjam** en **Alex,** ik wens jullie heel veel succes en plezier met jullie nieuwe/huidige werk.

Beste **Sjoerd,** in Amsterdam of Gent; onze samenwerking blijkt altijd te blijven continueren. Ondanks onze gave om de meest monstrueuze experimenten op te zetten, was jij altijd bereid om ons te helpen vol overgave, enthousiasme en hier en daar wat chaos. Dank voor de fijne samenwerking, voor het brengen van diepgang in onze artikelen en voor alle goede filosofische gesprekken!

Vrienden en familie

Liefste **Levensnectar meiden**, waar veel vriendschappen uit elkaar groeien na de middelbare schoolperiode, zijn wij juist naar elkaar toe gegroeid. Al meer dan 17 jaar (!) zijn jullie in mijn leven en in al die jaren hebben we zo veel fantastische momenten met elkaar mogen beleven. Tegelijkertijd zijn jullie bij uitstek degenen die weer een glimlach op mijn gezicht weten te toveren tijdens mindere periodes. Met jullie is simpelweg alles leuker en ik zou niet weten wat ik zonder jullie zou moeten. **Anne,** onze vriendschap heeft een vlucht genomen sinds wij beiden aan de Boezemsingel wonen. Deze vriendschap betekent ontzettend veel voor me, meer dan ik misschien laat blijken. Wat ben je een fantastische vriendin en wat kijk ik uit naar alle avonturen die we samen nog gaan beleven! **Merel**, wat ben ik dankbaar hoe onze vriendschap de afgelopen tijd is gegroeid. Je bent een prachtig persoon, van binnen en van buiten. **Elise,** met bewondering kijk ik naar jou als je op het podium staat en, hoe langer ik erover nadenk, hoe meer paralellen ik zie met hoe jij door het leven danst: met kracht, elegantie en passie. Samen met Bas ga je een fantastische toekomst tegemoet! **Elze**, met je gevoel voor humor, belangstelling en je scherpe opmerkingen weet jij ieder moment samen mooier te maken. Ik weet zeker dat je passie en toewijding je ontzettend ver gaan brengen en ik kan niet wachten op het moment dat jij je proefschrift mag verdedigen! **Inge,** wat heb ik bewondering voor de manier waarop jij je eigen weg kan kiezen en je niet snel laat afleiden door wie of wat dan ook. Ik geniet van je nuchterheid, je gekkigheid en de gave om van kleine dingen te genieten.

Lieve **Evelien,** als er iemand een voorbeeld is van een powervrouw dan ben jij het wel. Als een grote zus voorzie jij mij vaak van goed advies in een voorverwarmde auto op dat aftandse parkeerterrein na een uurtje calorieën verbranden in de dansschool. Wat doe je het allemaal goed; ik kan niet anders zeggen dan dat ik trots op je ben!

Lianne, amies. ik denk dat wij allebei niet hadden kunnen bedenken dat wij nu zo close zouden zijn maar wat ben ik dankbaar dat ik nu kan spreken van een echte vriendschap. Spontaan naar Barcelona, bezoekje aan de Veluwse bron en iedere zondagochtend staan we als twee Rotterdamse yuppen op de yogamat, gevolgd door avocado toast en een goed gesprek. Je wijsheid, gevoel voor humor, oprechtheid en 'let's go' mentaliteit maken je een mooi mens en een fijne vriendin.

Lieve **Gijs**, ons decennium durende tijdperk samen gevuld met je ongelimiteerde steun en liefde moet hier zeker benoemd worden. Deze steun en de liefde hebben een grote bijdrage geleverd aan de totstandkoming van dit proefschrift en - nog belangrijker - aan de vorming van de persoon die ik vandaag de dag ben. Ik zal onze fantastische tijd samen nooit vergeten.

Els en **André**, vaak heb ik jullie mijn tweede ouders genoemd. In goede en mindere tijden zijn jullie er altijd geweest voor ons gezin en mede door jullie heb ik de stap gemaakt om Biomedische Wetenschappen te gaan studeren. Els, wat had ik je graag met een grote glimlach in het publiek willen zien tijdens mijn verdediging. We missen je.

Lieve **oma**, bij elk bezoek kreeg ik steevast de vraag of ik nou nog steeds bezig ben met hetzelfde onderzoek, maar ook hoe trots je bent op wat ik doe. Een van je wensen was dan ook dat je dit proefschrift door mij overhandigd zou krijgen en dat we het samen kunnen vieren. Wat ben ik dankbaar dat die wens, een gedeelde wens, in vervulling is gebracht.

Lieve **Remco** en **Lisanne**. **Lisanne**, al meer dan 15 jaar maak jij deel uit van onze familie als mijn schoonzus(je). Ik zie ons nog zitten aan de keukentafel, waar jij mij bijles gaf in scheikunde. Dit geeft ook meteen weer hoe betrokken en lief jij bent als persoon. Ik weet dan ook zeker dat je een fantastische moeder gaat worden en ik kan niet wachten om tante te worden van jullie kleine wonder! **Remco**, mijn grote broer. Wij lijken misschien in veel opzichten niet op elkaar maar ik vind het mooi om te zien dat we steeds meer naar elkaar toe groeien naarmate de jaren verstrijken. In de afgelopen jaren is gebleken dat je er altijd voor me zult zijn en dit is volledig wederzijds. Ik vind het bewonderingswaardig hoe jij in het leven staat en stiekem kan ik daar af en toe een beetje jaloers op zijn. Ik ben ontzettend trots op je!

Lieve **papa** en **mama**, de waarde van jullie steun en liefde is met geen pen te beschrijven. Jullie staan soms achter me om mij een duwtje in de juiste richting te geven, soms voor me om mij te behoeden voor een foute keuze, maar bovenal staan jullie naast me en geven jullie onvoorwaardelijke steun bij elke stap die ik maak. De omslag van dit proefschrift is dan ook een ode aan jullie; als harmonieus team hebben jullie er altijd voor gezorgd dat ik de beste versie van mezelf kan zijn, op werkgebied en daarbuiten. Jullie zijn mijn vangnet, mijn grootste fans, mijn thuis en tegelijkertijd zie ik jullie als mijn beste vrienden. Meer kan ik als dochter niet wensen en ik ben dan ook ongelooflijk trots om jullie mijn ouders te mogen noemen. Ik houd zielsveel van jullie.

Encore 4

List of Publications

List of Publications

PD-L1 checkpoint blockade promotes regulatory T-cell activity that underlies therapy resistance
van Gulijk M, van Krimpen A, Schetters S, Eterman M, van Elsas M, Mankor J, Klaase L, de Bruijn M, van Nimwegen M, van Tienhoven T, van Ijcken W, Boon L, van der Schoot J, Verdoes M, Scheeren F, van der Burg S, Lambrecht B, Stadhouders R, Dammeijer F, Aerts J, van Hall T. *Science Immunology.* 2023 May 19;8(83):eabn6173. doi: 10.1126/sciimmunol.abn6173

Combination of PD-1/PD-L1 checkpoint inhibition and dendritic cell therapy in mice models and in patients with mesothelioma
van Gulijk M *, Belderbos B*, Dumoulin D, Cornelissen R, Bezemer K, Klaase L., Dammeijer F, Aerts J. *International Journal of Cancer.* 2023 Sep 14. doi: 10.1002/ijc.34293

Immune suppression in the tumor-draining lymph node corresponds with distant disease recurrence in patients with melanoma
van Krimpen A, **van Gulijk M**, Gerretsen VIV, Mulder EEAP, van den Bosch TPP, von der Thüsen J, Grünhagen DJ, Verhoef C, Mustafa D, Aerts JG, Stadhouders R, Dammeijer F. *Cancer Cell*. 2022 Jul 6:S1535-6108(22)00273-2. doi: 10.1016/j.ccell.2022.06.009.

Low-dose JAK3-inhibition improves anti-tumor T-cell immunity and immunotherapy efficacy
Dammeijer F, **van Gulijk M**, Klaase L, van Nimwegen M, Bouzid R, Hoogenboom R, Joosse ME, Hendriks RW, van Hall T, Aerts JG. *Molecular Cancer Therapeutics*. 2022 Jun 23:molcanther.0943.2021. doi: 10.1158/1535-7163.MCT-21-0943

NKG2A is a late immune checkpoint on CD8 T cells and marks repeated stimulation and cell division
Borst L, Sluijter M, Sturm G, Charoentong P, Santegoets SJ, **van Gulijk M**, van Elsas MJ, Groeneveldt C, van Montfoort N, Finotello F, Trajanoski Z, Kiełbasa SM, van der Burg SH, van Hall T. *International Journal of Cancer.* 2022 Feb 15;150(4):688-704. doi: 10.1002/ijc.33859.

Immune monitoring in mesothelioma patients identifies novel immune-modulatory functions of gemcitabine associating with clinical response
Dammeijer F*, De Gooijer CJ*, **van Gulijk M**, Lukkes M, Klaase L, Lievense LA, Waasdorp C, Jebbink M, Bootsma GP, Stigt JA, Biesma B, Kaijen-Lambers MEH, Mankor J, Vroman H, Cornelissen R, Baas P, van der Noort V, Burgers JA, Aerts JG. *EBioMedicine*. 2021 Feb;64:103160. doi: 10.1016/j.ebiom.2020.103160 *Not included in this thesis*

The PD-1/PD-L1-checkpoint restrains T cell immunity in tumor-draining lymph nodes
van Gulijk M*, Dammeijer F*, Mulder EE, Lukkes M, Klaase L, van den Bosch T, van Nimwegen M, Lau SP, Latupeirissa K, Schetters S, van Kooyk Y, Boon L, Moyaart A, Mueller YM, Katsikis PD, Eggermont AM, Vroman H, Stadhouders R, Hendriks RW, Thüsen JV, Grünhagen DJ, Verhoef C, van Hall T, Aerts JG. *Cancer Cell*. 2020 Nov 9;38(5):685-700.e8. doi: 10.1016/j.ccell.2020.09.001

Dendritic cell vaccination and CD40-agonist combination therapy licenses T cell-dependent antitumor immunity in a pancreatic carcinoma murine model
Lau SP, van Montfoort N, Kinderman P, Lukkes M, Klaase L, van Nimwegen M, **van Gulijk M**, Dumas J, Mustafa DAM, Lievense SLA, Groeneveldt C, Stadhouders R, Li Y, Stubbs A, Marijt KA, Vroman H, van der Burg SH, Aerts J, van Hall T, Dammeijer F, van Eijck CHJ. *Journal of Immunotherapy of Cancer*. 2020 Jul;8(2):e000772. doi: 10.1136/jitc-2020-000772

Combination strategies to optimize efficacy of dendritic cell-based immunotherapy
Van Gulijk M, Dammeijer F, Aerts JGJV, Vroman, H. *Frontiers in Immunology.* 2018 Dec 5;9:2759. doi: 10.3389/fimmu.2018.02759

* Shared first authors

Encore 5

About the Author

About the Author

Mandy van Gulijk was born on the 17th of March, 1995 in Vlaardingen. She completed her secondary school education (Athenaeum) at Reviuslyceum Maassluis in 2013. In the same year, she started with the bachelor Biomedical Sciences at the medical faculty of Leiden University. Here, she performed her first internship at the department of Gastroenterology and Hepatology, where she studied the role of mesenchymal stromal cells in Inflammatory Bowel Disease under supervision of dr. Marieke Barnhoorn, dr. Luuk Hawinkels and prof. dr. Hein Verspaget. After completing her bachelor, Mandy proceeded with the master Biomedical Sciences and decided to specialize in immunology. As part of her master program, she performed an internship at the Transplantation Laboratory at Erasmus Medical Center under supervision of dr. Nicole van Besouw and prof.dr. Carla Baan to investigate the role donor-specific memory B cells in kidney transplant recipients. Her interest in tumor immunology was sparked in the second year of her master which led to the decision to perform her final internship at the Department of Pulmonary Medicine at Erasmus Medical Center, Thoracic Oncology Research Group (group leader prof.dr. Joachim Aerts) to study the role of myeloid cells in modulating anti-tumor immunity. Having successfully graduated in 2018 with honors (cum laude), Mandy started her academic career as PhD candidate at the Department of Pulmonary Medicine of which the results are presented in this thesis. In 2022, she transitioned into the role of a postdoctoral researcher at the same department.

PhD Portfolio

Summary of PhD training, teaching activities and funding

Name	Mandy van Gulijk
Department	Dept. of Pulmonary Medicine, Erasmus Medical Center Rotterdam
Research School	Molecular Medicine Postgraduate School
PhD period	2018-2024
Promotors	Prof. J.G. Aerts, Prof. T. van Hall
Co-promotor	Dr. F. Dammeijer

1. PhD training	**Year**	**Workload (ECTS)**
Courses		
• The advanced course on Applications in flow cytometry	2018	0.5
• Basic and Translational Oncology	2018	1.8
• Advanced Immunology Course	2019	4.5
• Research Integrity	2019	0.3
• The Basic course on R	2019	1.8
• Biomedical English Writing Course	2021	2.5
Presentations & Conferences		
• Annual Cancer Immunology & Immunotherapy Conference CICON (AACR/CIMT/CRI/EATI) NYC, USA | *Poster Presentation*	2018	1.2
• Annual Cancer Immunology & Immunotherapy Conference CICON (AACR/CIMT/CRI/EATI) Paris, France | *Poster Presentation*	2019	1.2
• NVVI Annual Meeting, Noordwijkerhout, NL – Poster Presentation	2019	0.6
• Annual Molmed Day, Rotterdam, NL | *Oral Presentation*	2020	0.3
• Biomedical Science PhD day, Rotterdam, NL | *Poster Presentation*	2022	0.3
• NVVI Annual Meeting, Noordwijkerhout, NL | *Poster Presentation*	2022	0.6
• VIB congress, Leuven, BE | *Oral Presentation*	2022	0.6
• Annual Cancer Immunology & Immunotherapy Conference CICON (AACR/CIMT/CRI/EATI) NYC, USA | *Poster Presentation*	2022	1.2
• Keystone Meeting – Cancer Immunotherapy: Mechanisms of Response versus Resistance – Banff, Canada | *Poster Presentation*	2023	1.5
• 16th International Conference of the International Mesothelioma Interest Group, Lille, France | *Oral Presentation*	2023	2.0
• IASLC 2023 Hot Topic Meeting In Basic & Translational Science: Resistance to IO in NSCLC, Brussels, BE | *Oral Presentation*	2023	1.2

2. Teaching	Year	Workload (ECTS)
Supervising students		
• **Supervisor of Life Science Student: 5-month internship R. Hoogenboom,** project entitled: JAK3: a future target for immunotherapy	2019	2.2
• **Supervisor of Chemistry and Bio-industries student: 2-month internship A. Fontaine,** project entitled: Assessment of the efficacy of gemcitabine used as a second-line treatment on T cell subsets in peripheral blood of mesothelioma patients	2019	1.5
• **Supervisor of Master student Biomedical Sciences: 9-month internship T. van Tienhoven,** project entitled: The role of regulatory T cells in the resistance to checkpoint inhibitors in a mesothelioma mouse model	2020 - 2021	5.0
• **Supervisor of Master student Biomedical Sciences: 9-month internship S. Nooren,** project entitled: The role of immunotherapy-medicated activation of regulatory T cells in therapy resistance	2021 - 2022	5.0
• **Co-promotor PhD student M. Eterman** on the subject of identifying novel resistance mechanisms to immune checkpoint blockade	2022 -	5.0
• **Co-promotor PhD student L. Pisheh** on the subject of identifying novel mechanisms to improve the efficacy of dendritic cell therapy	2023 -	5.0
• **Co-organizer annual ACE symposium**	2023 -	1.0
Total ECTS		**46.8**

3. Funding	Year	Amount
• **Mesothelioma Applied Research Grant** Research grant awarded for project 'Identifying novel Treg targets to sensitize mesothelioma to ICB'	2022	€100.000
• **Team Westland** Research grant awarded for project: Asbestkanker gevoelig maken voor immuntherapie	2022	€90.000
Total funding		**€190.000**

Encore 6

About the Cover

About the Cover

Ballet, a mesmerizing art form filled with intricate narratives and fluid movements, thrives on the enigmatic bond between dancers and music. A wise ballet instructor once mused, “Music pulsates at the core of ballet; it steers our steps and injects vitality in our gestures”. Within the captivating domain of ballet, music therefore acts as an artist’s brushstroke, adding richness and vibrancy and establishing a platform for dancers to fully embody their roles. Comprising a diverse group of musicians, each with their unique skills and instruments, an orchestra is a marvel of teamwork and collaboration. Musicians must play their parts precisely when required and rely on impeccable timing and coordination. Each musician has clearly defined roles and each role should be filled; if the piano player is missing, the flute cannot substitute its sound. As such, a combination of individual excellence and teamwork creates a powerful synergy that drives success. Imagine the immune system as the ballerina. Imagine multiple tissues as the musicians of the orchestra that coordinately regulate the optimal performance of this immune system. Only when all components and tissues are able to individually excel in their performance and work together as a team, the immune system is able to successfully attack the tumor, just like a symphony is required for a ballerina to flourish. At the same time, the instruments symbolize different types of immunotherapy. The creation of music is like an enigmatic puzzle that must be pieced together with precision to bring a ballet to life and this creation is different for each ballet production. The right type of immunotherapy, and combinations thereof, should be carefully selected to fully bring the immune system to life and this can differ for different tumor types, or even for individual patients. A collaborative effort is required among biomedical scientists, clinicians and bioinformaticians to compose these immunotherapy strategies. It takes an orchestra, not a soloist, to cure cancer.